IOWA STATE UNIVERSITY
Digital Repository

Graduate Theses and Dissertations

Iowa State University Capstones, Theses and Dissertations

2017

A novel approach to measure, understand, and assess the thermal environment in grow-finish swine facilities

Brett Carlos Ramirez
Iowa State University

Follow this and additional works at: https://lib.dr.iastate.edu/etd

 Part of the Agriculture Commons, and the Bioresource and Agricultural Engineering Commons

Recommended Citation
Ramirez, Brett Carlos, "A novel approach to measure, understand, and assess the thermal environment in grow-finish swine facilities" (2017). *Graduate Theses and Dissertations*. 16201.
https://lib.dr.iastate.edu/etd/16201

This Dissertation is brought to you for free and open access by the Iowa State University Capstones, Theses and Dissertations at Iowa State University Digital Repository. It has been accepted for inclusion in Graduate Theses and Dissertations by an authorized administrator of Iowa State University Digital Repository. For more information, please contact digirep@iastate.edu.

A novel approach to measure, understand, and assess the thermal environment in grow-finish swine facilities

by

Brett Carlos Ramirez

A dissertation submitted to the graduate faculty

in partial fulfillment of the requirements for the degree of

DOCTOR OF PHILOSOPHY

Major: Agricultural and Biosystems Engineering

Program of Study Committee:
Steven J. Hoff, Major Professor
Jay D. Harmon
Hongwei Xin
John F. Patience
Philip M. Dixon

The student author and the program of study committee are solely responsible for the content of this dissertation. The Graduate College will ensure this dissertation is globally accessible and will not permit alterations after a degree is conferred.

Iowa State University

Ames, Iowa

2017

Copyright © Brett Carlos Ramirez, 2017. All rights reserved.

TABLE OF CONTENTS

LIST OF FIGURES

LIST OF TABLES

ACKNOWLEDGMENTS

I would truly like to thank everyone who has aided in developing my success as not only a student, researcher, and engineer, but also a person during my graduate career at Iowa State University (ISU). Through everyone's support, guidance, and inspiration I was able to achieve goals beyond my expectations and accomplish many great achievements. I would sincerely like to thank my major professor, Dr. Steven Hoff, for providing me with this outstanding opportunity and for all his insightful guidance and wisdom. A mentor I will truly cherish forever. In addition, I was privileged to be mentored by Dr. Jay Harmon who provided invaluable knowledge and philosophical perspectives along the way. The direction, feedback, and encouragement from my passionate and enthusiastic committee members Drs. Xin, Patience, and Dixon, allowed me to further enhance my skills and thrive in my efforts. Without them, I would not be where I am today.

Words cannot express my gratitude to the endless list of people in the Air Dispersion Lab and Departments of Agricultural and Biosystems Engineering and Animal Science at ISU. Everyone has contributed to the success of this dissertation by donating time, effort, and assistance.

I would also like to thank all those in the Center for Communication Excellence at ISU for their support and comradery. My experience as a disciplinary writing consultant, an opportunity created my department, was phenomenal and truly made me a better scholarly communicator.

I would not have been able to do this without the support, encouragement, and quiet patience of my wonderful girlfriend – Shelby. Her unyielding passion and care allowed me to find the inspiration and motivation to succeed not only in completing this dissertation, but also in life.

To close, I would like to thank my family and friends for their unconditional support and inspiration in all aspects of my life.

I undoubtedly owe my success to all these people.

ABSTRACT

The thermal environment (TE) inside swine production systems substantially affects animal performance as well as facility natural resource usage; hence, our measurement, understanding, and assessment of the TE must be advanced to sustainably meet the animal-protein demand of the growing global population. The TE describes the parameters that influence heat exchange between an animal and its surroundings, with maximum animal performance achieved when minimal thermoregulatory effort is required. Instrumentation and analysis techniques connecting the impact of the TE on total heat loss and subsequently, to animal performance in intensive housing systems are limited. Therefore, the goals of this dissertation research were to create a novel measurement system for quantifying the TE, develop a mechanistic model to understand the interaction between pigs and their TE, and lastly, establish the methodology to assess the TE for improved management strategies. This dissertation describes the design, validation, and implementation of an innovative TE sensor array (TESA) featuring dry-bulb and black globe temperature, airspeed, and relative humidity measurements. A low-cost omnidirectional thermal anemometer was engineered and calibrated with documented measurement uncertainty for reliable airspeed measurements. These measured parameters were needed as inputs to estimate the convective, radiative, and evaporative modes of heat loss in the developed model, which simulated the cascade of behavioral and physiological thermoregulatory responses of group-housed, grow-finish pigs as a function of the TE. Model results were used to generate a new thermal index for assessing different combinations of the TE and predicting the subsequent impact on animal performance. This index was applied to spatially and temporally analyze data collected from a network of 44 TESAs deployed symmetrically in two rooms of a commercial swine facility. TESA adds a new level of measurement precision greatly needed in modern facilities and goes beyond solely measuring dry-

bulb temperature. The testing and calibration of TESA demonstrates the functional performance capabilities of the instrument and sets the standard for animal production sensor development. The mechanistic model provides reasonable agreement with previously published results and can be used to inexpensively explore different combinations of the TE on swine performance. Overall, this dissertation will help the swine industry by providing new technology and methods to quantify the impact of TE on performance for improved housing system management and control decisions. This dissertation will advance the corpus of knowledge required to provide food security for the growing global population through economically and sustainably housed pigs.

CHAPTER 1. GENERAL INTRODUCTION

This general introduction and literature review focuses on the exchange of thermal energy (heat) between pigs and their surroundings as well as characterizes their thermoregulatory responses to different thermal environment (TE) conditions to better understand how to measure and evaluate the TE in swine housing systems. The chapter concludes with the research objectives and organization of this dissertation.

Literature review

The global population is projected to increase from 7.6 billion in 2017 to 9.8 billion people in 2050 (UN, 2017) and will require a secure animal-based protein supply that is raised safely, efficiently, and without adverse environmental impact. Global animal production accounts for approximately 40% of gross agriculture production, with demand for animal products in developing countries anticipated to double by 2030 (Alexandratos & Bruinsma, 2012). The intensification of swine and poultry production is essential to meet this increasing demand of the growing and more affluent population. Modern intensification of animal production over the last century has been achieved by building larger production units with advanced technology, higher animal densities, increasing mechanization and efficiency in processing, using specialized feeds, and extensive use of pharmaceutical supplements (Gilbert et al., 2015; Kittawornrat & Zimmerman, 2011). Even though intensification has resulted in the increased availability of cost-effective animal products, there are remaining environmental, health, and social concerns (Mench, James, Pajor, & Thompson, 2008). Intensive animal production systems are still in their early stages and must continue to be advanced to satisfy growing global population demand, while simultaneously, providing economic and effective strategies for environment sustainability.

The United States is the third largest pork producer in the world, behind China and the European Union (USDA FAS, 2017). In Iowa, the national leader in both total market hog inventory (19.2 million, ~31% of total U.S.; USDA NASS, 2017) and value-added economy (~12.2 billion USD; IPPA, 2017), the majority of these market pigs are housed in intensive production systems (~61% of operations having >1000 head; USDA NASS, 2014). These production systems provide a controlled TE that mitigates exposure to extreme and rapid fluctuations in ambient conditions, feed and water that are formulated and monitored, protection from predators and parasites, and a means for workers to efficiently interact with the pigs (Curtis, 1983). However, this high animal density can make pigs vulnerable and more susceptible to pathogens, be exposed to poor air quality, and potentially create well-being concerns. Failure to provide the optimum TE (e.g., heat stress), even within these climate controlled facilities, has major economic implications. St-Pierre, Cobanov, & Schnitkey (2003) estimate economic losses of about $300 million per year for the U.S. pork industry and herd productivity is predicted to diminish for about 40% of the year (Hostetler, 2015). Hence, quality and control of the indoor environment are critical components of intensive swine production and require improvement to ensure that these systems, which house the vast majority of pigs, provide conditions for efficient feed conversion, limited exposure to pathogens, and optimal natural resource usage.

The indoor environment is primarily controlled by either mechanical (i.e., fan-driven airflow) or natural (i.e., wind/buoyancy-driven airflow) ventilation systems to provide fresh air, and remove noxious gases, moisture, and heat generated by the animals (Albright, 1990). Fresh air enters a room through planned inlets (opening size often adjusted mechanically) as a result of a pressure gradient created by either density differences (natural) or by fans or wind. The thermal component of the indoor environment is managed by a combination of ventilation, heating, and cooling

systems. Liquid propane fueled forced air furnaces and radiant brooders commonly provide supplemental heat. Conversely, for cooling, evaporative pads to reduce incoming air temperature and low-pressure sprinklers to directly wet the pigs are used. While a typical room in a swine facility houses between 1,000 to 2,000 head with 30 to 60 animals per pen, and can vary in dimensions and layout, the design, placement, and operation of these systems contrast considerably (NPB, 2009). All these systems must seamlessly integrate together to achieve the optimum TE for maximum animal performance. Essentially, the TE must be capable of dissipating metabolically generated heat and avoid invoking performance penalties due to thermal stress. Due to the economic and performance implications, it is imperative to understand the impact the TE has on swine performance and universally assess the TE in the diverse array of facilities and systems.

Heat transfer

Swine are homoeothermic animals that maintain a narrow core body temperature range (approximately 39°C) via a cascade of thermoregulatory mechanisms (physiological and behavioral). Since energy must be conserved from one form to another (first law of thermodynamics), heat loss to the environment must equal the total energy product of metabolism (ASHRAE, 2013; Curtis, 1983; DeShazer, 2009), if normal core body temperature is to be maintained.

Thermal environment

The TE describes the parameters that influence thermal (heat) exchange between an animal and its surroundings (ASHRAE, 2013; DeShazer, 2009). Heat loss is partitioned into sensible (conduction, convection, and radiation) and latent (evaporation) modes. Sensible modes are driven by a temperature gradient and latent modes by a water vapor pressure gradient between an animal outer surface (skin or pelage) and its surroundings. Animal characteristics, for instance,

configuration, surface area, and surface temperature effect all modes of heat loss, while additionally; the animal's surface emissivity only impacts radiation. Environmental characteristics each uniquely impact the different modes of heat loss, such as surrounding surface temperatures (conduction and radiation), dry-bulb temperature (convection), air velocity (convection and evaporation), vapor pressure (evaporation), emissivity and orientation of surrounding objects (radiation), and lastly, heat capacity and thermal resistance of contact object (conduction). The TE can be complicated to describe and understand, but is an essential component of the thermal balance between an animal and its surroundings.

Conduction

Thermal conduction is the transmission of thermal energy through a continuous, non-moving medium, dependent on the specific thermal properties of the medium (ASHRAE, 2013). Heat transfer occurs from an area of higher temperature to an area of lower temperature, as stated by the second law of thermodynamics. The surface areas, thermal conductivity, and temperature of each solid in contact govern conductive flux.

For animals, conductive energy exchange is dependent on the animal's skin temperature, surface area in contact, and thermal conductivity of the contact material (DeShazer, 2009). Animals have several stationary orientations, such as lying, standing, leaning, eating, etc. The predominate orientation that influences conductive energy exchange is lying, while conduction is assumed negligible, when the animal is standing or travelling. A lying animal is exchanging energy with the surface (often times the floor, bedding, etc.) in which the animal's surface is contacting. Swine spend approximately 22 of 24 h lying down (Kelly, Bond, & Garrett, 1964); thus, energy exchange via conduction can be an important factor managing the TE. An animal's surface area is a function of body weight (Kelley, Curtis, Marzan, Karara, & Anderson, 1973); for example,

growing-finishing pigs have approximately 20% of their body surface in contact with the floor surface area (Kelly et al., 1964). Conduction is driven primarily by the temperature gradient between the animal's skin temperature and floor temperature; hence, monitoring and managing floor temperature can be a critical component in TE evaluation. The rate in which heat is transmitted is also influenced by the thermal conductivity of the material. Heat will transfer slower through a material with a low thermal conductivity, and vice versa for a material with a high thermal conductivity. The thermal conductivity for many construction materials has been summarized extensively in ASHRAE (2013).

Heat transfer rates by conduction from swine to a surface have not been extensively studied in the last four decades. Conductive heat transfer from swine to the floor, while important, lacks data, cohesiveness, and mutual understanding throughout the literature. It is agreed that conductive heat transfer is non-negligible. Data obtained through controlled environment studies provide insight to partitioned energy exchange, for ideal conditions without other factors; but lacks applicably to modern production systems, as the number of variables (e.g., airspeed, radiation, other animals, etc.) substantially increases. Additionally, other factors, such as animal activity, presence of other animals, and body weight, need to be accounted for if a calorimeter study was to be scaled to a modern production system. In extreme hot and cold climates, control of conductive heat transfer through floor heating or cooling may be desirable; however, accurate sizing and implementation of a system may be cost prohibitive and challenging. Prediction equations and models may be more suitable for estimating conductive heat transfer in a modern production system since they can account for the high number of variables, but maybe with less accuracy. Floor temperature assessment may be a supplemental evaluation if animal activity or behavior suggest potential discomfort when other TE measurements indicate a comfortable TE.

Convection

Thermal convection is sub-categorized into two types: natural and forced convection. A fluid moves under natural convection due to density differences (i.e., from temperature, moisture, or other components); thus, heat transfer occurs solely due to a temperature gradient between a solid object and its surrounding fluid (Albright, 1990; ASHRAE, 2013). Conversely, a fluid's motion under forced convection is caused by a fan or pump. Forced convection heat transfer is more rapid and on a unit area basis, often greater than natural convection. Convective heat transfer rate is influenced by properties the of the fluid, such as viscosity, density, thermal expansion and conductivity, specific heat, gravity, and the size and shape of the object (Albright, 1990; ASHRAE, 2013).

For animals, convective heat transfer is affected by animal orientation and surface temperature, surrounding air temperature, and air velocity (DeShazer, Hahn, & Xin, 2009). The housing system type (i.e., mechanically or naturally ventilated), equipment (i.e., presence of fans, heaters, etc.), and local climate, dictate the type of convection, as well as air temperature and velocity. Air velocity can be beneficial in hot climates by helping to cool the animal, but problematic in cold climates by chilling the animal (DeShazer et al., 2009). Convective heat loss increases at approximately the square root of air velocity; hence, a two fold increase in air velocity results in only a 40% increase in convective heat losses. In addition, air temperature must be lower than the body temperature for heat losses to occur (DeShazer et al., 2009).

Radiation

All objects at a given temperature (greater than absolute zero) emit electromagnetic energy, which is absorbed (as heat), transmitted, and reflected by surrounding objects. This exchange process, without the presence of matter (as in conduction and convection), is thermal radiation.

Radiation of thermal energy is a function of the Stefan-Boltzmann constant, emissivity of the object, and the absolute temperature of the object. A perfect emitter is referred to as a “black body”, where the emissivity is equal to unity, that is, all thermal energy is emitted from the surface of the object. For scenarios where thermal radiation persists over a narrow wavelength band (i.e., emittance does not change rapidly as a function of wavelength), the object is termed a “grey body”. Most objects are not a “black body” and have an emissivity less than one. The emissivity of many materials have been quantified by ASHRAE (2013).

The net exchange of diffuse thermal radiation between two objects is determined by the radiation flux of each object and the shape factor between the objects. The angle or shape factor describes the fraction of thermal radiation departing one object and captured by the other object. A non-zero shape factor exists for any object exchanging thermal radiation and has a maximum value of one. Calculation of shape factors can be intensive for complex environments but for various shapes and surfaces, angles factors have been derived in many textbooks. In thermal radiation exchange calculations, it is often assumed that the object in question is a “small” object in “large” surroundings. In this scenario, the “large” surroundings act as a “black body” because all thermal radiation that leaves the “small” object will be absorbed, since none with be reflected back (very small shape factor from “small” object to “large” surroundings).

For animals, their orientation (exposed area to surroundings), skin emissivity, and skin temperature, in conjunction with surrounding surface (e.g., walls, curtains, other animals, ceiling, feeders, etc.) temperatures, shape factors, and emissivities, influence the amount of thermal radiation exchange. Orientation, as discussed previously, is dependent on the animal’s activity. Standing will expose the greatest amount of skin to surrounding surfaces. The emissivity of bare sow skin ranges between 0.96 and 0.98 in the 7.5 to 13.5 μm wavelength range, while hairy regions

were found to have a lower emissivity (Soerensen, Clausen, Mercer, & Pedersen, 2014). Depending on climate, surrounding surface temperatures can be nonhomogeneous. In a hot climate, ceiling surface temperatures can be greater than ambient (due to warm air trapped in the attic). Conversely, in a cold climate, temperature of uninsulated walls and curtains can be near ambient temperature. Regardless of housing style or climate, surface temperatures are often substantially different than skin temperature resulting in an exchange of radiative energy. This portion can be large and at times, be equal or just slightly less than convective heat loss.

Evaporation

The simultaneous transfer of heat and mass between an airstream and a wetted surface adds or removes water vapor (the most abundant greenhouse gas in the atmosphere) from the air. When water changes state from a liquid to a vapor, sensible heat is extracted from the surrounding air or surfaces. The amount of heat needed for this phase change is described by the latent heat of vaporization (decreasing as water temperature increases). The rate of evaporative heat loss is governed by the gradient in the water vapor pressure concentration between the air and the wetted surface. Water vapor pressure is a function of dry-bulb temperature, relative humidity, and atmospheric pressure and typically assumed to be saturated at the wetted surface.

For animals, the same factors that influence convection in addition to the wetted surface area, impact evaporative heat loss. Heat loss via evaporation mainly occurs during respiration and perspiration. During respiration, inhaled air temperature and moisture content are increased as a result of convective and evaporative heat loss in the respiratory tract. Further, expired air is nearly saturated and at a temperature slightly lower than core body temperature, resulting in a relatively large amount of heat loss. This is predominantly why elevated respiration rates are observed in many heat stressed animals. While many animals and humans can perspire to form water droplets

on their skin, swine do not; however, a small amount of passive water diffusion to the skin exists, but only offers a relatively small amount of heat loss.

Energetics

The total energy product of metabolism released as heat includes partitioning of energy from feed and how the animal uses this energy. The main feedback mechanism for thermoregulatory control of physiological (e.g., tissue conductance, respiration rate, etc.) and behavioral (e.g., orientation, feed intake, relation with other animals, etc.) responses is through the central nervous system (DeShazer, 2009).

Thermoregulatory physiology

Homeothermic animals can exist within a large range of TE conditions (survival zone), where death will occur if core body temperature becomes too extreme. The following presents the classic view on thermoregulation for homeotherms as depicted in many sources (Bruce & Clark, 1979; Curtis, 1983; Mount, 1968). Within the survival zone, exists the homeothermy zone under which the animal maintains a normal core body temperature and can regulate heat loss with physiological and behavioral mechanisms. Further, inside the homeothermy zone lies the thermoneutral zone (TNZ). In this zone, the animal uses minimal thermoregulatory effort, such as vaso-modification, pilo-modification, and behavioral changes. The lower end of the TNZ is bounded by the lower critical temperature, where tissue and pelage conductance are minimum and beyond this temperature, metabolic heat production begins to increase (via thermogenesis) to balance the increase in heat loss. The upper end of the TNZ is bounded by the upper critical temperature, while more difficult to clearly define and not universally agreed upon, is regarded as high latent heat loss and the onset of reduced metabolic heat production. In addition, the TNZ is not a fixed range, but rather dynamic. The size and TE conditions corresponding to an animal's TNZ is based on

metabolic heat production (assumed constant in this zone) and the extent of thermoregulatory mechanisms. The zone of least thermoregulatory effort (ZLTE; approximately analogous to the "comfort zone" for humans) is a narrow range contained in the TNZ and defines the range of conditions under which an animal can regulate its heat loss with minimal effort and no subsequent effect on performance (Black, 1986). The ZLTE is bounded by the lower critical temperature and evaporative critical temperature, where tissue conductance is maximum and the partition of latent heat loss begins to increase. Swine performance can be maximized if a TE that allows the animal to exist within its ZLTE is provided.

Metabolic heat production

The thermal balance between an animal and its surroundings is influenced by the amount of metabolically generated heat. Metabolic heat production (HP) is partitioned into maintenance, the heat increment, activity, and thermogenesis (zero within the TNZ; NRC, 2012). Dietary metabolizable energy (ME; i.e., feed gross energy minus gross energy in feces, urine, and fermentation gases) is converted to heat for maintenance (fasting heat production; FHP), heat increment (HI), and net energy (NE) for production (NRC, 2012). Heat increment results from heat of digestion, tissue formation, fermentation, and waste formation for both maintenance and growth processes. An animal's basal metabolic FHP describes the minimum metabolic heat produced by a fasted animal with no thermal stress or strenuous activity. To meet this requirement, dietary ME must at least equal FHP plus HI for maintenance. Typically, dietary ME is much greater than maintenance requirements; thus, allowing a portion of dietary ME to be used for production. This is represented as the production HI and NE for production. Many factors influence metabolic HP, such as genetics, breed, body weight, diet composition, metabolic efficiency, etc. Knowledge

of metabolic HP is essential for ventilation system design (equipment sizing) and for determining the balance point between animal and TE.

Estimates of metabolic HP can be measured empirically by calorimetry or calculated as a function of ME and diet composition. Calorimeters are subdivided into direct and indirect (and several other uncommon types), the latter being more prevalent (McLean & Tobin, 1987). Direct calorimeters quantify total heat dissipation by measuring sensible heat loss to the environment and evaporative losses, while the indirect calorimeter quantifies heat production from quantitative measurements of materials consumed and produced (including respired gases) during metabolism (Nienaber et al., 2009). Metabolic HP is assumed to be accurately determined from O_2 consumption, CO_2 production, CH_4 production, and nitrogen excretion of an animal. Accurate measurement of airflow and gas concentrations are required for confident HP estimates. Numerous indirect calorimeters exist globally (Labussière, Dubois, Van Milgen, & Noblet, 2015; Nienaber & Maddy, 1985; Xin & Harmon, 1996), with different capabilities to partition metabolic HP uses, or heat loss into sensible and latent modes. Among these systems, there is often a lack of statement on measurement uncertainty and quantification of confidence in the final values. Alternative, metabolic HP estimates have been created using the partitioning of GE and the chemical composition of a diet. There have been and will continue to be many different approaches and techniques for estimating metabolic HP of swine (Brown-Brandt, Nienaber, Xin, & Gates, 2004). This has created an abundance of information, with a lack of homogeneity needed for quantitative comparison. Especially, in terms of relating metabolic HP and subsequent animal response to the TE.

Animal response

Below the lower critical temperature (heat loss is greater than metabolic HP), shivering can occur and feed intake (FI) is increased for thermogenesis (Curtis, 1983). In modern swine production systems, this is not a common concern due to affordable and simple heating systems. Conversely, as TE conditions become warmer, the primary consequence is a progressive reduction in voluntary FI (Renaudeau, Gourdine, & St-Pierre, 2011; Thuy, 2005). This loss in FI will reduce performance. Heat stress has generally been regarded to occur once the animal's body temperature begins to rise (beyond the upper critical temperature) outside the TNZ, and FI reduction linked with heat stress. However, as discussed previously, this upper critical temperature is highly debated and – as a consequence, the onset of heat stress. Since the evaporative critical temperature is the upper bound for ZLTE, FI initially begins to decrease outside the upper limit of this zone, and more substantially decreases in heat stress.

The impacts of heat stress on growing pigs has been well explored in literature but with large variability across studies and results (Renaudeau et al., 2011). Voluntary FI was estimated to reduce by 40 to 80 g d^{-1} $°C^{-1}$ between 20°C and 30°C (Le Dividich, Noblet, Herpin, Van Milgen, & Quiniou, 1998). This result was also in agreement with Renaudeau et al. (2011), who added body weight was a major factor in this variability. In addition, Renaudeau et al. (2011) estimated as a result of a large meta-analysis, the reduction in average daily gain for a 50 kg pig was about 18 g d^{-1} $°C^{-1}$ when temperature increases from 20°C to 30°C. While these consequences are quite general, there are many factors affecting FI reduction; such as, animal characteristics (breed, body weight, sex), housing system (surrounding materials, number of pigs per pen, management, sanitary state), thermal environment, duration of exposure, or a combination of these factors. In

order to improve TE control inside swine housing system, improved measurement and understanding of how different factors impact the onset and severity of heat stress is needed.

Characterizing heat exchange and animal response

One TE parameter cannot solely represent the thermal balance between animal and surrounding; hence, several approaches have aimed at reducing the complexity and creating thermal indices or equivalent (effective) temperatures to represent how the total TE impacts animal response. In commercial settings, often only air temperature is used to manage and describe the TE inside swine facilities because it is relatively inexpensive and easy to implement; hence, it is a highly sought parameter compared to the other TE parameters.

Thermal indices

The need to predict and support intelligent TE management decisions related to animal performance, health, and well-being have resulted in the development of thermal indices that represent the effects produced by the heat exchange process. These indices substantially simplify complex physical and biological interactions, and have served as useful tools for guiding management and evaluating risk for one selected performance penalty given different TE treatments. A thorough summary of relevant livestock and poultry thermal indices can be found elsewhere (da Silva & Maia, 2012; DeShazer, 2009; Fournel, Rousseau, & Laberge, 2017). Specifically for swine, the TNZ range changes predominately as a function of body weight. This is attributed to the increasing metabolic HP and the decreasing surface area to mass ratio. Body weight is rarely ever used as an input to a thermal index, and is required to accurately assess the TE of growing pigs.

Modeling

Bioenergetics models have been developed as an alternative approach to assessing the impact of the TE on livestock and poultry. A recent review discusses previous modeling efforts for livestock and poultry in detail (Fournel et al., 2017). These mathematical models can be divided into three categories: empirical, mechanistic, and dynamic data-based models (Aerts, Wathes, & Berckmans, 2003; Black, 1986; Wathes, Kristensen, Aerts, & Berckmans, 2008). Empirical models incorporate data derived from experimental observations from calorimeter or housing studies and not necessarily supported by theory. Mechanistic models focus on mathematically representing physiological and behavioral responses based on thermodynamics or equations derived from empirical studies. These models can be used to simulate HP or performance penalties over a wide range of TE conditions. They are not limited by the physical capabilities of experiments; however, cannot account for the randomness in nature. Advances in computer hardware and software efficiency have greatly reduced computation time and have promoted the increased use of using mechanistic models as a means to incorporate the heat exchange process, metabolism, and thermoregulatory response. As a result, dynamic data-based models have been developed as a means for incorporating measured values into simulating/predicting HP or performance.

In order to meet the growing demand for animal-based protein, modern production systems will need to sustainably improve their production efficiency. A fundamental transition from measuring and assessing the TE with respect to only dry-bulb temperature to a more complete heat balance approach can help achieve this necessary improvement to production performance. There is a need to develop new and innovative tools and techniques capable of describing the thermal balance between group-housed pigs and their surroundings. Further, given the diverse nature of

the housing and ventilation systems, methods to help guide ventilation, heating, and cooling system management and design strategies for engineers and producers are needed.

Objectives

The overall goal of this research was to establish the methodology to measure the TE in swine production facilities to enable the use of a mechanistic model for quantitatively assessing the impact of the TE on swine performance. Specific objectives of this dissertation were to:

1) design, construct, and calibrate an omnidirectional thermal anemometer for accurate airspeed measurement for TESA;
2) create a spatial network of TESAs and deploy them in a commercial wean-finish swine facility to evaluate long-term sensor and data acquisition robustness;
3) evaluate a custom created TE reference system and then use it to test the functional performance of TESA measurements;
4) develop a mechanistic model using inputs from TESA to evaluate the TE and its impact on swine performance; and
5) create the housed swine heat stress index from simulation results generated by the mechanistic model to assess spatiotemporal data collected by TESA in the commercial swine facility.

Organization of dissertation

Chapter 1 provides a general introduction, review of relevant literature, and dissertation objectives – with each following chapter supporting the aforementioned objectives. Chapter 2 is a manuscript presenting the design and calibration of an omnidirectional thermal anemometer. Chapter 3 is a manuscript describing the development and *in situ* performance of a novel Thermal

Environment Sensor Array (TESA). Chapters 4 is a manuscript demonstrating the lab validation of TESA and applicability of using TESA measurements as inputs to model heat exchange. Chapter 5 is a conference proceedings paper detailing a mechanistic, thermal balance model for assessing the TE using TESA measurements. Chapter 6 is a manuscript integrating TESA and the thermal balance model to assess the TE in a commercial swine facility with a newly developed thermal index. My specific contributions to Chapters 2, 3, 4, 5, and 6 are highlighted at the beginning of each chapter. Lastly, Chapter 7 discusses the general conclusions of this dissertation and future work. Appendix A contains other authored bodies of work that supplement this dissertation and other important aspects of animal housing.

References

Aerts, J.-M., Wathes, C. M., & Berckmans, D. (2003). Dynamic data-based modelling of heat production and growth of broiler chickens: development of an integrated management system. *Biosystems Engineering*, *84*(3), 257–266.

Albright, L. D. (1990). *Environment control for animals and plants.* St. Joseph, MI: American Society of Agricultural Engineers.

Alexandratos, N., & Bruinsma, J. (2012). *World agriculture towards 2030/2050: the 2012 revision* (No. ESA Working paper No. 12-03). Rome, Italy: FAO. Retrieved from http://agris.fao.org/agris-search/search.do?recordID=XF2006427483

ASHRAE. (2013). *Handbook of fundamentals*. Atlanta, GA: America Society of Heating, Refrigeration and Air Conditioning Engineers.

Black, J. L. (1986). Simulation of energy and amino acid utilization in the pig. *Research and Development in Agriculture*, *3*(3), 121–145.

Brown-Brandt, T., Nienaber, J., Xin, H., & Gates, R. (2004). A literature review of swine heat production. *Transactions of the ASAE*, 259–270.

Bruce, J. M., & Clark, J. J. (1979). Models of heat production and critical temperature for growing pigs. *Animal Science*, *28*(03), 353–369. https://doi.org/10.1017/S0003356100023266

Curtis, S. E. (1983). *Environmental management in animal agriculture*. Ames, IA: The Iowa State University Press.

da Silva, R. G., & Maia, A. S. C. (2012). *Principles of animal biometeorology* (Vol. 2). Springer Science & Business Media.

DeShazer, J. A. (2009). *Livestock Energetics and Thermal Environmental Management* (1st ed.). St. Joseph, MI: American Society of Agricultural and Biological Engineers.

DeShazer, J. A., Hahn, L., & Xin, H. (2009). Chapter 1: Basic Principles of the Thermal Environment and Livestock Engergetics. In James A. DeShazer, *Livestock Energetics and Thermal Environment Management* (1st ed., pp. 1–22). St. Joseph, MI: American Society of Agricultural and Biological Engineers.

Fournel, S., Rousseau, A. N., & Laberge, B. (2017). Rethinking environment control strategy of confined animal housing systems through precision livestock farming. *Biosystems Engineering*, *155*, 96–123. https://doi.org/10.1016/j.biosystemseng.2016.12.005

Gilbert, M., Conchedda, G., Van Boeckel, T. P., Cinardi, G., Linard, C., Nicolas, G., … Robinson, T. P. (2015). Income disparities and the global distribution of intensively farmed chicken and pigs. *PLoS ONE*, *10*(7). https://doi.org/10.1371/journal.pone.0133381

Hostetler, C. (2015, June 16). Reduce the Impact of Summer Heat. Retrieved November 10, 2016, from http://www.pork.org/checkoff-reports/pork-fires-up-the-fun/reduce-the-impact-of-summer-heat/

IPPA. (2017). *2017 Economic Contributions of the Iowa Pork Industry*. Des Moines, IA: Iowa Pork Producers Association. Retrieved from http://www.iowapork.org/wp-content/uploads/2012/11/state-of-iowa.pdf

Kelley, K. W., Curtis, S. E., Marzan, G. T., Karara, H. M., & Anderson, C. R. (1973). Body surface area of female swine. *Journal of Animal Science*, *36*(5), 927–930.

Kelly, C. F., Bond, T. E., & Garrett, W. (1964). Heat transfer from swine to a cold slab. *Transactions of the ASAE*, *7*(1), 0034–0035. https://doi.org/10.13031/2013.40687

Kittawornrat, A., & Zimmerman, J. J. (2011). Toward a better understanding of pig behavior and pig welfare. *Animal Health Research Reviews*, *12*(1), 25–32.

Labussière, E., Dubois, S., Van Milgen, J., & Noblet, J. (2015). Modelling gas exchanges to partition heat production between fasting, thermic effect of feeding and physical activity in farm animals. *Indirect Calorimetry. Techniques, Computations and Applications. Wageningen Academic Publishers, Wageningen, the Netherlands*, 73–86.

Le Dividich, J., Noblet, J., Herpin, P., Van Milgen, J., & Quiniou, N. (1998). Thermoregulation. *Progress in Pig Science*, 229–263.

McLean, J. A., & Tobin, G. (1987). *Animal and human calorimetry*. Cambridge University Press.

Mench, J. A., James, H., Pajor, E. A., & Thompson, P. B. (2008). The welfare of animals in concentrated animal feeding operations. *Report to the Pew Commission on Industrial Farm Animal Production. Pew Commission on Industrial Farm Animal Production: Washington, DC*.

Mount, L. E. (1968). *The climatic physiology of the pig*. Great Britain: Edward Arnold Publishers Ltd.

Nienaber, J. A., & Maddy, A. L. (1985). Temperature controlled multiple chamber indirect calorimeter-design and operation. *Transactions of the ASAE*, *28*(2), 555–0560.

NRC. (2012). *Nutrient Requirements of Swine* (11th ed.). Washington D.C.: The National Academies Press.

Pork Checkoff, Q. (2009). *Quick Facts: The Pork Industry at a Glance*. Des Moines, IA: National Pork Board.

Renaudeau, D., Gourdine, J.-L., & St-Pierre, N. R. (2011). A meta-analysis of the effects of high ambient temperature on growth performance of growing-finishing pigs. *Journal of Animal Science*, *89*(7), 2220–2230.

Soerensen, D. D., Clausen, S., Mercer, J. B., & Pedersen, L. J. (2014). Determining the emissivity of pig skin for accurate infrared thermography. *Computers and Electronics in Agriculture*, *109*, 52–58. https://doi.org/10.1016/j.compag.2014.09.003

St-Pierre, N. R., Cobanov, B., & Schnitkey, G. (2003). Economic Losses from Heat Stress by US Livestock Industries. *Journal of Dairy Science*, *86*, *Supplement*, E52–E77. https://doi.org/10.3168/jds.S0022-0302(03)74040-5

Thuy, H. T. T. (2005). *Heat stress in growing pigs* (Doctoral). Wageningen University, Wageningen, The Netherlands.

UN. (2017). *World Population Prospects: The 2017 Revision, Key Findings and Advance Tables* (No. Working Paper No. ESA/P/WP/248). New York City, NY: United Nations, Department of Economic and Social Affairs, Population Division.

USDA FAS. (2017). *Livestock and Poultry: World Markets and Trade* (No. April 2017). Washington D.C.: United States Department of Agriculture - Foreign Agricultural Service.

USDA NASS. (2014). *2012 Census of agriculture: United States summary and state data* (No. AC-12-A-51). Washington D.C.: United States Department of Agriculture - National Agricultural Statistics Service.

USDA NASS. (2017). *Quarterly hogs and pigs* (No. June 2017). Washington D.C.: United States Department of Agriculture - National Agricultural Statistics Service.

Wathes, C. M., Kristensen, H. H. er, Aerts, J.-M., & Berckmans, D. (2008). Is precision livestock farming an engineer's daydream or nightmare, an animal's friend or foe, and a farmer's panacea or pitfall? *Computers and Electronics in Agriculture*, *64*(1), 2–10.

Xin, H., & Harmon, J. D. (1996). Responses of group-housed neonatal chicks to posthatch holding environment. *Transactions of the ASAE*, *39*(6), 2249–2254.

CHAPTER 2. OMNIDIRECTIONAL THERMAL ANEMOMETER FOR LOW AIRSPEED AND MULTI-POINT MEASUREMENT APPLICATIONS

Y. Gao, B. C. Ramirez, and S. J. Hoff

A manuscript published in *Computers and Electronics in Agriculture*

This chapter describes the design, construction, and calibration of an Omnidirectional Thermal Anemometer (OTA) for airspeed measurement as a part of the Thermal Environment Sensor Array (TESA; Chapter 3). The OTA is a constant temperature anemometer developed to accurately measure airspeed from approximately still air to ~5.5 m s^{-1}. The calibration and propagation of measurement uncertainty is documented for future applications. The OTA provides reliable and accurate measurement of airspeed for a low cost.

This chapter owes it success to the combined efforts of Brett Ramirez, Yun Gao, and Steven Hoff. I led the calibration reference design and construction, performed the calibration experiments, collected and analyzed calibration data, conducted the uncertainty analysis, and drafted the manuscript. Dr. Gao developed the OTA circuit, selected hardware, and created the final, fully functional OTA. Drs. Gao and Hoff also contributed to the research design and revision of the manuscript.

Abstract

Current control strategies for livestock and poultry facilities need to improve their interpretation of the Thermal Environment (TE) that the animals are experiencing in order to provide an optimum TE that is uniformly distributed throughout the facility; hence, airspeed, a critical parameter influencing evaporative and convective heat exchange must be measured. An

omnidirectional, constant temperature, thermal anemometer (TA) with ambient dry-bulb temperature (t_{db}) compensation was designed and developed for measuring airspeeds between 0 and 6.0 m s^{-1}. An Arduino measured two analog voltages to determine the thermistor temperature and subsequently the power being dissipated from a near-spherical overheated thermistor in a bridge circuit with a transistor and operational amplifier. A custom wind tunnel featuring a 0.1 m diameter pipe with an access for TA insertion was constructed to calibrate the TA at different temperatures and airspeeds, at a constant relative humidity. The heat dissipation factor was calculated for a given airspeed at different ambient temperatures ranging from 18°C to 34°C and used in a unique fourth-order polynomial regression that compensates for temperature using the fluid properties evaluated at the film temperature. A detailed uncertainty analysis was performed on all key measurement inputs, such as the microcontroller analog to digital converter, TA and t_{db} thermistor regression statistics, and the calibration standard, that were propagated through the calibration regression. Absolute combined standard uncertainty associated with temperature corrected airspeed measurements ranged from 0.11 m s^{-1} (at 0.47 m s^{-1}; 30.3% relative) to 0.71 m s^{-1} (at 5.52 m s^{-1}; 12.8% relative). The TA system cost less than $35 USD in components and due to the simple hardware, this thermal anemometer is well-suited for integration into multi-point data acquisition systems analyzing spatial and temporal variability inside livestock and poultry housing.

Introduction

The Animal Occupied Zone (AOZ) Thermal Environment (TE) inside livestock and poultry facilities places the animal at risk for adverse health effects and influences animal well-being, growth performance, and feed conversion efficiency (Curtis, 1983; Hillman, 2009; Mount, 1975; Straw, Zimmerman, D'Allaire, & Taylor, 1999). Further, due to the large variability in spatial and

temporal distribution of TE (Jerez, Wang, & Zhang, 2014; Zhang, Barber, & Ogilvie, 1988), accurate quantification of AOZ TE by a robust data acquisition system is needed, such that the most effective management strategies and facility designs can be implemented.

The TE describes the parameters that influence heat exchange (i.e., convective, conductive, radiative, and evaporative) between an animal and its surroundings (ASHRAE, 2013; Curtis, 1983; DeShazer, Hahn, & Xin, 2009). Convection is an important mode of heat transfer for animals in housed environments that are driven by ambient dry-bulb temperature (t_{db}) and airspeed, with typically only t_{db} used to quantitatively describe and control TE. In a hot ambient t_{db}, airspeed is beneficial (i.e., when t_{db} is lower than skin temperature) to the animal because energy generated internally can be more readily released preserving the animal's body temperature; however, convective heat loss benefit decreases as airspeed increases, limiting the effectiveness of high airspeeds. Desired hot ambient t_{db} AOZ airspeeds in facilities are generally up to 3 m s^{-1} (590 ft min^{-1}). Conversely, animals in a cold ambient t_{db} prefer low airspeeds (i.e., less than 0.5 m s^{-1}) to minimize energy expenditures and avoid drafts that can negatively affect animal performance and health. Therefore, an anemometer is needed to accurately quantify low airspeeds in the AOZ. Heber and Boon (1993) and Luck et al. (2014) have used commercially available anemometers to characterize air velocity distribution and satisfy their research objectives but, lack customization for controller feed-back use and cost effective for widespread use. Measurement of all parameters in the TE would provide control systems and producers with information about the TE that an animal is directly experiencing, such that design and control of TE modification systems can be adjusted to enhance and maintain the optimal TE for enhanced production efficiency and thermal comfort.

Numerous omnidirectional (e.g., ultrasonic, spherical thermal, and laser-based) and unidirectional (e.g., paddlewheel, three-cup, hot-wire, Pitot tube, and vane) anemometer technologies are commercially available and summarized in literature (ASHRAE, 2013). For the anticipated low airspeeds in livestock and poultry facilities, paddlewheel, three-cup, and vane anemometers are ineffective due to shaft friction. While commercially available ultrasonic and laser-based anemometers are accurate at low airspeeds and provide flow field direction, they are cost prohibitive for multi-point measurement applications. Thermal anemometers (i.e., hot-wire or hot-film) are advantageous due to their cost effectiveness, small size (minimal intrusion in the AOZ), omnidirectional capability, and measurement range (ASHRAE, 2013). A hot-wire anemometer, typically a cylindrical wire is unidirectional (non-isotropic heat loss), can be made omnidirectional, if the wire is replaced with a spherical element. In general, Low Velocity Thermal Anemometers (LVTAs) consist of an element (e.g., thermistor, resistance temperature detector, or thermocouple junction) electrically heated above ambient t_{db}. LVTAs maintain either a constant current, constant voltage, or constant temperature at the element (ASHRAE, 2013). Many circuit designs and conditioning methods exist (Bruun, 1996); however, they lack the robustness required for agricultural applications (e.g., durability, customization, etc.) and cost effectiveness for integration into multi-point measurement Data Acquisition (DAQ) systems using inexpensive, open source microcontrollers.

In addition to the transducer, thermal anemometers also require a statement of measurement uncertainty that encompasses the propagation of measurement error through sensor hardware, airspeed calculation, calibration, temperature compensation, frequency response, and direction sensitivity (Popiolek, Jørgensen, Melikov, Silva, & Kierat, 2007). Framework for performing this uncertainty analysis was established by Popiolek et al. (2007), using a commercially available,

omnidirectional LVTA. While this empirical and theoretical analysis exhaustively quantified many key sources of measurement error, analog to digital converter (ADC) error and subsequent transformation to airspeed (by curve-fitting algorithm) were reported by the manufacturer. Variability in thermistor shape and size due to manufacturing is an additional uncertainty source specific to custom developed LVTAs, and is also unknown for commercial LVTAs. Many novel calibration methods for controlling low velocities exist; such as, mounting a LVTA to the end of a swinging arm or pendulum (Al-Garni, 2007; Barfield & Henson, 1971), draining water from a sealed vessel to draw air through a nozzle (Barfield & Henson, 1971; Christman & Podzimek, 1981; Yue & Malmström, 1998), and recording the time required to traverse a measured length (Aydin & Leutheusser, 1980). These diverse and custom approaches to calibration demonstrate that many techniques are plausible, when documented and accompanied with an uncertainty analysis. Likewise, specifically for LVTAs, additional uncertainty is introduced when ambient t_{db} differs from that at calibration; thus, LVTA measurements require compensation for t_{db} (Bruun, 1996). Several theoretical heat transfer based relations and empirical methods through calibration have been developed for t_{db} compensation (Hultmark & Smits, 2010). A simple t_{db} correction method based on calibration data and not theoretical heat transfer law, was applied to airspeeds greater than 3.5 m s^{-1} and t_{db} greater than 33°C for a hot-wire anemometer (Hultmark & Smits, 2010). Little is known about that application of this t_{db} correction method to omnidirectional, constant temperature LVTAs at typical temperatures encountered in livestock housing.

A low-cost, microcontroller-based omnidirectional thermal anemometer, with a well-documented statement of measurement uncertainty was developed to be integrated into a custom TE sensor array (TESA) that measures t_{db}, relative humidity (RH), mean radiant temperature, and airspeed. This novel network of TESAs would provide the capability to study TE spatial and

temporal distribution in livestock and poultry facilities with sufficient measurement density. In addition, incorporation of airspeed measurement into ventilation and heat stress alleviation (e.g., sprinklers) control strategies would allow for intelligent TE management decisions that promote the optimum TE for animal to dissipate internally generated heat required for homeothermic balance. Hence, the objectives of this research were: (1) design an economic, omnidirectional thermal anemometer applicable to low airspeed measurements commonly found in livestock and poultry housing; (2) document the calibration standard, procedure, and ambient t_{db} correction method; and (3) quantify the combined standard uncertainty associated with t_{db} compensated airspeed measurements.

Materials and methods

Theory of operation

The steady-state energy balance for a Thermal Anemometer (TA) thermistor element heated above ambient t_{db} (equation 2.1) has been previously derived in literature.

$$P = \delta\,(t_t - t_{db}) \tag{2.1}$$

where

P = electrical power (W)
δ = heat dissipation factor (W °C^{-1})
t_t = thermal anemometer thermistor temperature (°C)
t_{db} = ambient dry-bulb temperature (°C)

Power required by an electrical source to maintain the element at a constant temperature above ambient t_{db} is a function of the heat dissipation factor (δ) and the temperature difference between the element surface and ambient. Specific to each thermistor, δ depends on surrounding fluid speed, fluid properties (i.e., specific volume, thermal conductively, kinematic viscosity, etc.), and relative thermistor orientation in the flow field. For a spherical thermistor in uncompressed air, under a narrow range of ambient t_{db} such that the air properties do not vary greatly, δ between the

thermistor and surrounding air is assumed solely a function of airspeed. Hence, at the steady-state condition, supplied electrical power equals convective heat losses (equation 2.2).

$$P = h\,A_t\,(t_t - t_{db}) \tag{2.2}$$

where

h = convective heat transfer coefficient (W °C $^{-1}$ m^{-2})
A_t = thermal anemometer thermistor surface area (m^2)

The convective heat transfer coefficient (h) is determined from the thermodynamic properties of the fluid and the relationship between heat transfer and flow around a sphere. The Nusselt number (*Nu*; a function of Reynolds and Prandtl numbers) describes h, thermistor diameter, and fluid thermal conductivity relationship. After simplification, δ can be expressed as function of convective heat losses (equation 2.2).

$$\delta = \frac{Nu\,k}{d_t}\,A_t \tag{2.3}$$

where

Nu = Nusselt number (dimensionless)
k = thermal conductivity at film temperature (W m^{-1} °C $^{-1}$)
d_t = thermal anemometer thermistor diameter (m)

Nusselt numbers for small, spherical thermistor elements have been previously studied and vary greatly in literature (Collis & Williams, 1959; Mori, Imabayashi, Hijikata, & Yoshida, 1968; Rumyantsev & Kharyukov, 2011; Skinner & Lambert, 2009). In addition, accurate measurement of thermistor diameter is difficult; therefore, rather than finding an analytical solution to Nusselt number, a method not based on heat transfer law, but rather the empirical relation between δ and t_{db} using the properties of the free-stream fluid (i.e., kinematic viscosity and thermal conductivity) evaluated at the film temperature was proposed by Hultmark & Smits (2010; equation 2.4).

$$\delta \approx f(Re)\,\frac{k\,A_t}{d_t} \tag{2.4}$$

where

f = functional dependence
Re = Reynold's number (dimensionless)

The Prandtl number is assumed constant over a narrow ambient t_{db} range; thus, Nusselt number is assumed as only a function of Reynolds number (*Re*). Since thermistor area and diameter are constant, equation 2.4 can be further simplified (equation 2.5).

$$\frac{u}{\nu} \approx f\left(\frac{\delta}{k}\right) \tag{2.5}$$

where
u = airspeed (m s^{-1})
ν = kinematic viscosity (m^2 s^{-1})

While the general form of this relationship has been previously derived (Hultmark & Smits, 2010), experimental results were used to determine the functional dependence between $u\ \nu^{-1}$ and $\delta\ k^{-1}$, which is specific to the thermistor size and shape, t_{db} range, and airspeed range. Absolute viscosity is found using the Sutherland correction (Fox, McDonald, & Pritchard, 1985). Also, thermal conductivity can be determined by the correlation presented by Kannuluik & Carman, (1951), and moist air density calculated by the psychrometric equations (ASHRAE, 2013).

Sensor module

Hardware

A spherical, Negative Temperature Coefficient (NTC) thermistor (nominal 470 Ω at 25°C, Model LC471F3K, U.S. Sensor Corp., Orange, CA, USA) was heated above ambient t_{db} by a Constant Temperature Anemometer (CTA) circuit (figure 2.1) based on Schiretz (2012). Convective heat transfer was assumed isotropic; however, full omnidirectional sensing was limited by a small conical region due to the attached lead wires. The CTA circuit consisted of a Wheatstone bridge, four channel differential comparator operational amplifier (TLV2434, Texas Instruments Inc., Dallas, TX, USA), and a NPN transistor (2N2222A, Central Semiconductor Corp.,

Hauppauge, NY, USA). Analog voltages at V_1 and V_2 (figure 2.1) were passed through a voltage follower (not shown) using two of the remaining channels on the operational amplifier prior to measurement with the 10-bit ADC on the microcontroller (Micro, Arduino LLC, Italy).

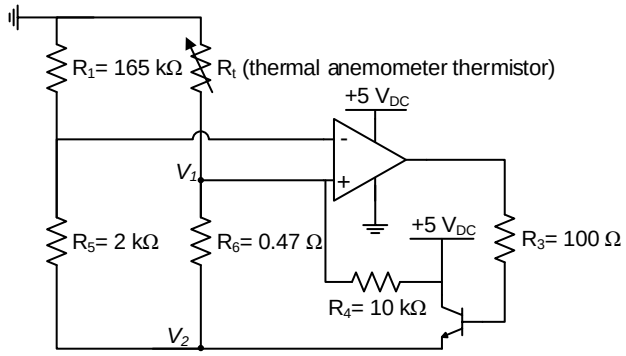

Figure 2.1. Constant temperature thermal anemometer circuit based on Schiretz (2012). Analog voltages measured at V_1 and V_2 were used to determine thermistor temperature and power dissipated.

In the Wheatstone bridge (figure 2.1), the three constant resistors and the one thermistor acted as the four bridge legs. The feedback loop maintains the voltages of non-inverting and inverting inputs of the amplifier approximately equal by adjusting V_2. For example, when airspeed increases, the thermistor temperature decreases corresponding to an increase in thermistor resistance (NTC). This will cause the voltage difference between the non-inverting input and inverting input to increase; therefore, the output voltage from the amplifier increases, which through transistor increases V_2. As V_2 increases, the current passing through R_t increases as well. The temperature of R_t will increase, compensating for the temperature drop caused by increased airspeed; thus, maintaining thermistor temperature constant.

In addition, a NTC thermistor (nominal 10 kΩ at 25°C, NTCLE413-428, Vishay, Malvern, PA, USA) was used to measure ambient t_{db} (not shown in figure 2.1). A divider circuit powered by the microcontroller supply voltage (assumed a constant +5.0 V_{DC}), featured a 10 kΩ resistor (±1% tolerance) in series with the t_{db} thermistor to determine the t_{db} thermistor resistance. The t_{db}

thermistor value was chosen to minimize the dissipated electrical power across the thermistor, as t_{db} thermistor temperature can increase if the power is too high.

Analytical analysis

Kirchhoff's current law was applied to the circuit (figure 2.1) to determine current flowing through the TA thermistor (equation 2.6).

$$I_t = \frac{(V_s - V_1)}{R_4} + \frac{(V_2 - V_1)}{R_6} \tag{2.6}$$

where

I_t = current through the thermal anemometer thermistor (A)
V_s = supply voltage (+5.0 V_{DC})
V_1 = noninverting terminal voltage (V_{DC})
R_4 = resistance (10 kΩ)
V_2 = emitter voltage (V_{DC})
R_6 = resistance (0.47 Ω)

Further, resistance of the thermistor was found using Ohm's law (equation 2.7).

$$R_t = \frac{V_1}{I_t} \tag{2.7}$$

where

R_t = thermistor resistance (Ω)

Thermal anemometer thermistor resistance was used to find temperature, such that the temperature difference between the thermistor and t_{db} could be determined. Likewise, power dissipated by the thermistor to the surrounding air (equation 2.8) was computed and used as an input to determine the heat dissipation factor (equation 2.1).

$$P = I_t V_1 \tag{2.8}$$

where

P = power dissipated by the thermal anemometer (W)

Software

A program developed in the integrated development environment for the microcontroller measured 60 analog voltages sequentially at V_1, V_2, and the ambient t_{db} divider voltage (V_{db}),

approximately every 2 ms when prompted by a custom DAQ software (Matlab R2015b, The MathWorks Inc., Natick, MA, USA). Data were transmitted serially via a Universal Serial Bus (USB) cable to a computer with the DAQ software.

Calibration

Standard

Thermal anemometer calibration was performed with a custom wind tunnel standard constructed of an insulated (thermal resistance = 1.06 m^2 °C W^{-1}), 3.05 m long, 10.16 cm diameter schedule 40 PVC pipe, with a flow-straightener at the entrance of the pipe (figure 2.2). A cable grip to accommodate the airspeed sensor was inserted to a 1.27 cm diameter center bored hole, located 1.524 m from the inlet and 1.016 m from the outlet. This hole was at least ten pipe diameters from the closest upstream obstruction and at least five pipe diameters from the pipe exit to ensure fully-developed flow at the test position (ASHRAE, 2013). Located 90° from the test location, an additional cable grip was added to accommodate the t_{db} thermistor. A 0.15 m diameter reducer also contained a flow-straighter and connected the pipe test section to a 0.61 m by 0.56 m by 0.89 m (H by W by L; interior) well-sealed, wood plenum. Both flow-straightening honeycomb sections were constructed with 5.08 cm long, 0.6 cm diameter plastic drinking straws. The inlet of the plenum contained a 5.08 cm diameter precision nozzle (Helander Metal Spinning Company, Lombard, IL, USA) with four throat static pressure taps. Static pressure was averaged and measured with a pressure transducer (sensitivity = 0.0804 V_{DC} Pa^{-1}, Model 267, Setra Systems Inc., Boxborough, MA, USA). A 10.16 cm diameter schedule 40 PVC pipe connected to a variable speed inline fan mounted 1.3 m upstream of the nozzle inlet was used to control airflow through the test section. A variable speed device (AC-VXP/N:180V800E, Control Resources Inc., Littleton, MA, USA) transformed a 0 to 5 V_{DC} input to control fan speed. Conditioned air supplied

to the test section was drawn via a 4.57 m long, 15.24 cm diameter insulated (thermal resistance = 1.41 m^2 °C W^{-1}) flexible duct from a large insulated plenum. An air handling unit (AA-5474, Parameter Generation and Control, Black Mountain, NC, USA) provided TE control of supply t_{db} and supply RH (HMP-133Y, Vaisala, Helsinki, Finland) during calibration, which was modified from Ramirez, Hoff, Gao, & Harmon (2015).

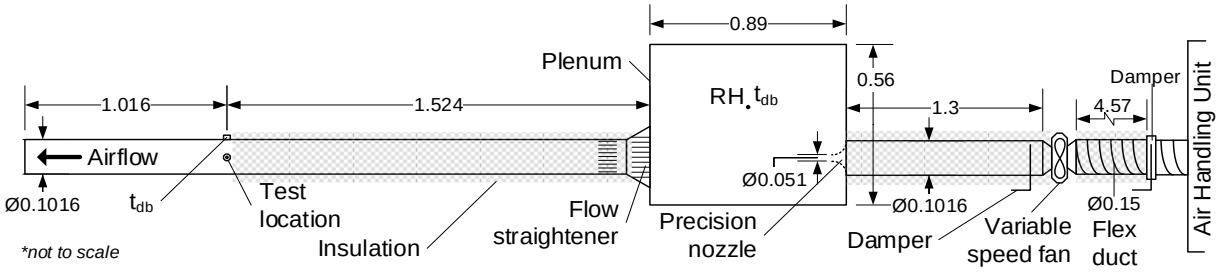

Figure 2.2. Schematic of custom wind tunnel standard used to calibrate the thermal anemometer. Airspeed was controlled via a combination of varying damper positions and modifying fan speed. Dry-bulb temperature and RH was controlled by an air handling unit. All units in meters.

Prior to TA calibration with the standard at the test location (figure 2.2), the reference air velocity at the test location was determined by regressing static pressure through the nozzle against air velocity measured by a reference hot-wire anemometer (sensitivity = 0.5 V_{DC} (m s^{-1})$^{-1}$, Model 8455, TSI Inc., Shoreview, MN, USA). The hot-wire anemometer was secured at the center of the pipe with the cable grip and allowed 1.5 min of stabilization time prior to initiating data collection. Twelve samples of data were recorded for one second, with 60 measurements per sample, from both the hot-wire anemometer and differential pressure transducer with the 14-bit ADC of a multifunction DAQ device (Model USB 1408FS, Measurement Computing Corp., Norton, MA, USA) at a set airflow. Airflows were randomly selected from ~0 to 6 m s^{-1}.

Data acquisition and procedure

The DAQ software controlled inline fan speed via the digital to analog converter (DAC) on the multifunction DAQ device, and recorded analog outputs from the: differential pressure transducer, supply t_{db}, and supply RH via the multifunction DAQ device. In addition, the software transmitted the serial command to the microprocessor to initiate TA data collection.

The thermal anemometer was secured in the center pipe at the test location (figure 2.2) following the same procedure as the reference hot-wire anemometer, and the t_{db} thermistor was secured in the other cable grip (figure 2.2). A total of 12 different airflows, corresponding to airspeeds from ~0 to 6 m s^{-1} were conducted in random order. In addition, supply t_{db} and RH were held constant during calibration and recorded with the multifunction DAQ device. At each airflow, six nominal dry-bulb temperatures (range) were tested: 18.0°C (16.5°C ≤ t_{db} < 20.0°C), 21.5°C (20.0°C ≤ t_{db} < 23.0°C), 24.5°C (23.0°C ≤ t_{db} < 26.0°C), 27.0°C (26.0°C ≤ t_{db} < 28.0°C), 29.5°C (28.0°C ≤ t_{db} < 32.0°C), and 33.0°C (32.0°C ≤ t_{db} < 35.0°C). Actual t_{db} ranged for given a nominal t_{db}, for each airflow, due to heat losses downstream of the air handling unit. Calibration began 2 min after setting the airflow to allow the TA to stabilize in the flow field. The multifunction DAQ device was sampled for 1 s, collecting a total of 60 measurements, followed by TA data collection from the microprocessor. Data from the multifunction DAQ device and the microprocessor were recorded 12 times at each airflow, at randomly selected intervals (as generated by the DAQ software) ranging from 1 to 6 s to decouple any dependence on the prior measurements. Data were analyzed using Matlab (2015).

Time constant

The time constant of the TA was determined by measuring the response to a step change from 0 to ~5.0 m s^{-1} (equation 2.9) and from ~5.0 to 0 m s^{-1} (equation 2.10). At the initial condition,

measurements from the TA were made for 90 s to allow the system to stabilize followed by the step change, and monitored for an additional 45 s. This procedure was repeated six times each for the step-up and step-down experiments. A nonlinear least squares regression (*Matlab*, 2015) of airspeed versus elapsed time was performed to determine the time constant (τ, ~63%) for introducing the TA to high and low flow fields. The time constants served as a metric to determine the time to reach steady-state. The time to reach steady-state was estimated by 3τ (~95% of the steady-state value), assuming first-order system behavior (equations 2.9 and 2.10).

$$u(t) = u_0 + \Delta u\left(1 - e^{\frac{-t+t_0}{\tau}}\right) \tag{2.9}$$

$$u(t) = u_0 + \Delta u\left(e^{\frac{-t+t_0}{\tau}}\right) \tag{2.10}$$

where

$u(t)$	= airspeed as a function of time (m s^{-1})
u_0	= initial u at time t_0 (m s^{-1})
Δu	= difference between u_0 and u at steady-state (m s^{-1})
t	= time (s)
t_0	= initial time (s)
τ	= time constant (s^{-1})

Statistical analysis

The standard uncertainty (denoted by Δ) associated with a measurement is a statistically based approximation of measurement error obtained from propagation of key measurement uncertainty sources (JCGM, 2008; Taylor & Kuyatt, 1994). A zeroth-order uncertainty budget, including Type A (the best available estimate of the expected value of a quantity that varies randomly) and Type B (not obtained from repeated observation, rather based on all available information) evaluations was performed for each sensor and essential hardware to determine the combined standard sensor uncertainty via summation of quadrature. Combined standard sensor uncertainties obtained from the zeroth-order analyses were then inputs that propagated through the analytical solutions (e.g., equations 2.6, 2.7, and 2.8). A truncated first-order Taylor series approximation, assuming

independent measurements, was used to determine combined standard uncertainty associated with propagation of measurement error. Sensitivity coefficients (denoted by partial derivatives) were represented for each input parameter and quantified how the combined standard uncertainty changed with variations of its inputs (JCGM, 2008). A sensitivity analysis was performed to determine the key contributions of input parameters on the combined standard uncertainty associated with t_t, t_{db}, δ, reference air velocity, and ultimately, the predicted airspeed obtained by the TA.

Sensor module

The TA thermistor temperature was found by regressing the Hoge-2 equation (Hoge, 1988) through data (resistance reported at 1°C increments) provided by the TA thermistor manufacturer for the anticipated operation range of 50°C to 150°C (equation 2.11). After calculation of TA thermistor temperature equation 2.11, the TA thermistor temperature was converted from Kelvin to Celsius for subsequent use.

$$T_t{}^{-1} = a_1 + a_2\, ln\, R_t + a_3\, ln\, R_t{}^2 + a_4\, ln\, R_t{}^3 \tag{2.11}$$

where

T_t = thermal anemometer thermistor temperature (K)
R_t = thermistor resistance (Ω)
a_1-a_4 = coefficients

Key parameters required to compute the R_t included two analog voltage measurements (V_1 and V_2) and two bridge resistor values (R_4 and R_6). The standard uncertainty associated with these inputs was evaluated and propagated through the nonlinear regression equation (equation 2.11) to determine the combined standard uncertainty with T_t. A zeroth-order uncertainty budget, including sources from Type A and Type B evaluations was created for analog voltage measurement by the TA microcontroller (table 2.1) for subsequent use to determine T_t and δ.

Table 2.1. Uncertainty budget for analog voltage measurement by microcontroller analog to digital converter.

Source	Value (V_{DC})	Probability distribution	Divisor	Standard uncertainty (V_{DC})
Repeatability[a]	0.0012	Normal	1	0.0012
Quantization error[b]	0.0024	Rectangular	√3	0.0014
Display resolution[c]	5.0E-05	Rectangular	√3	2.89E-05
Combined sensor standard uncertainty, ΔV				0.0019

[a] Largest SE of 30 measurements as found from five constant voltage tests (1.000, 2.501, 3.001, 3.501, and 4.001 V)
[b] ±0.5 ATmega32U4 10-bit ADC resolution = 0.005 V BL^{-1}
[c] ±0.5 smallest display value = 0.0001

Chauvenet's criterion with a maximum allowable deviation of less than 2.618 (n = 60) was applied to the analog voltage measurements in the 60 measurement sample sent from the microcontroller. Data that satisfied the criterion was averaged, such that there was twelve means that represented a given air velocity. Those twelve means were averaged again to represent one value for a given airspeed. The standard error of the mean was calculated from this result (n = 12).

The standard uncertainty associated with a mean analog voltage (equation 2.12) was determined by summing the uncertainty propagated through the computation of the arithmetic mean with the SE of the mean in quadrature.

$$\Delta\bar{V}_j^{\,2} = \frac{\Delta V_j^{\,2}}{n} + SE^2 \tag{2.12}$$

where

j = analog voltage measurement location (V_1, V_2, t_{db} divider, and dP transducer)
$\Delta\bar{V}_j$ = mean analog voltage combined standard uncertainty (V_{DC})
ΔV_j = analog voltage combined standard uncertainty (V_{DC}; table 2.1)
SE = standard error of the mean measured analog voltages (V_{DC})

The standard uncertainty associated with calculating R_t (equation 2.13) was determined from the propagation of mean analog voltage standard uncertainty (equation 2.12) and the standard uncertainty of the resistors in the bridge circuit (figure 2.1). A rectangular probability distribution (JCGM, 2008) was assigned to the manufacturer's non-traceable tolerance for the bridge resistors.

$$\Delta {R_t}^2 = \left(\frac{\partial R_t}{\partial \bar{V}_1}\Delta \bar{V}_1\right)^2 + \left(\frac{\partial R_t}{\partial \bar{V}_2}\Delta \bar{V}_2\right)^2 + \left(\frac{\partial R_t}{\partial R_4}\Delta R_4\right)^2 + \left(\frac{\partial R_t}{\partial R_6}\Delta R_6\right)^2 \quad (2.13)$$

where

ΔR_t = thermal anemometer thermistor resistance combined standard uncertainty (Ω)
ΔR_4 = resistor standard uncertainty (± 1%; Ω; rectangular distribution)
ΔR_6 = resistor standard uncertainty (± 1%; Ω; rectangular distribution)

The standard uncertainty associated with the nonlinear regression (equation 2.11) to predict T_t was determined by computing the Root-Mean-Square Error (*RMSE*; equation 2.14).

$$RMSE = \left(\frac{1}{n}\sum_{i=1}^{n}(y_i - \hat{y}_i)^2\right)^{1/2} \quad (2.14)$$

where

n = number of data
RMSE = root mean square error (dependent variable units)
y_i = dependent variable
$\hat{y}_i$ = predicted value from the regression

The combined standard uncertainty associated with thermistor temperature (equation 2.15) was determined from ΔR_t (equation 2.13), the manufacturer's accuracy, and the nonlinear regression statistics (equation 2.14).

$$\Delta {t_t}^2 = \left(\frac{\partial t_t}{\partial R_t}\Delta R_t\right)^2 + ACC^2 + RMSE^2 \quad (2.15)$$

where

Δt_t = thermal anemometer thermistor temperature combined standard uncertainty (°C)
ACC = manufacturer's accuracy (± 2.0°C; rectangular distribution)
RMSE = root mean square error from nonlinear regression (°C; equation 2.14)

The temperature of the t_{db} thermistor was found by regressing the Hoge-2 equation (Hoge, 1988) through data (resistance reported at 5°C increments) provided by the manufacturer for the anticipated operation range of -25°C to 45°C (equation 2.16). After calculation of t_{db} thermistor temperature by equation 2.16, the t_{db} thermistor temperature was converted from Kelvin to Celsius for subsequent use.

$$T_{db}{}^{-1} = b_1 + b_2\, ln\, R_{db} + b_3\, ln\, R_{db}{}^2 + b_4\, ln\, R_{db}{}^3 \quad (2.16)$$

where

T_{db} = t_{db} thermistor temperature (K)
R_{db} = thermistor resistance (Ω)
b_1-b_4 = coefficients

The uncertainty associated with t_{db} thermistor temperature (equation 2.17) was determined from the propagation of analog voltage uncertainty (table 2.1) and divider resistor uncertainty through the analytical solution to the resistor divider circuit using Ohm's law. A rectangular probability distribution was assigned to the manufacturer's non-traceable tolerance for the divider resistor (10 kΩ). Further, the nonlinear regression (equation 2.16) statistics also contributed. The microcontroller operating voltage (not measured) was assumed to be constant (+5.0 V_{DC}) and have negligible standard uncertainty; thus, excluded from the analysis.

$$\Delta t_{db}{}^2 = \left(\frac{\partial t_{db}}{\partial R_a}\Delta R_a\right)^2 + \left(\frac{\partial t_{db}}{\partial \bar{V}_{db}}\Delta \bar{V}_{db}\right)^2 + ACC^2 + RMSE^2 \quad (2.17)$$

where

Δt_{db} = dry-bulb temperature combined standard uncertainty (°C)
ΔR_a = 10 kΩ resistor in divider circuit (± 1%; Ω; rectangular distribution)
ACC = manufacturer's accuracy (± 0.5°C; rectangular distribution)
RMSE = root mean square error from nonlinear regression (°C)

Standard

A relationship between the precision nozzle differential static pressure and air velocity measured by the reference hot-wire anemometer at the test location (figure 2.2) was developed using a piecewise higher-order polynomial regression (equation 2.18). One discontinuity was selected at the point where the *RMSE* for both functions was minimized; hence, two independent regressions of equation 2.18 were obtained. Both regressions were then used to determine the reference air velocity based on the precision nozzle differential static pressure during TA calibration.

$$u_{ref} = c_1 dP^3 + c_2 dP^2 + c_3 dP + c_4 \quad (2.18)$$

where

u_{ref} = reference airspeed at center of pipe (m s^{-1})
dP = precision nozzle differential static pressure (Pa)
c_1-c_4 = coefficients

A zeroth-order uncertainty budget was created for the differential static pressure transducer (table 2.2) and for the reference hot-wire anemometer (table 2.3). Results of this uncertainty budget, along with the nonlinear regression statistics, were combined and subsequently used as inputs to determine the overall uncertainty associated with the reference air velocity at TA calibration.

Table 2.2. Uncertainty budget for differential static pressure transducer.

Source	Value (Pa)	Probability distribution	Divisor	Standard uncertainty (Pa)
Accuracy RSS[a]	1.244	Rectangular	√3	0.7182
Long term stability	0.1244	Rectangular	√3	0.0718
Quantization error[b]	0.0076	Rectangular	√3	0.0044
Combined standard sensor uncertainty, ΔdP				0.7218

[a] Root Sum Square (at constant t_{db}), ±1.0 % full scale (0 – 124.4 Pa)
[b] ±0.5 sensor resolution = (14-bit ADC resolution, 20 V_{DC} reference range = 3.05E-4 V BL^{-1}) (sensor sensitivity)$^{-1}$

Table 2.3. Uncertainty budget for hot-wire anemometer; where, u_{meas} was evaluated at an arbitrary 0.23 and 5.55 m s^{-1} to show the standard uncertainty range for the sensor.

Source	Value (m s^{-1})	Probability distribution	Divisor	Standard uncertainty (m s^{-1})
Quantization error[a]	6.104E-4	Rectangular	√3	3.5239E-4
Accuracy[b]	$0.02(u_{meas}) + 0.05$	Rectangular	√3	0.0316 – 0.0930
Repeatability[c]	$0.01(u_{meas})$	Normal	1	0.0023 – 0.0556
Resolution[d]	0.007	Rectangular	√3	0.0040
Combined standard sensor uncertainty, Δu_{ref}				0.0319 – 0.1084

[a] ±0.5 sensor resolution = (14-bit ADC resolution, 10 V_{DC} reference range = 0.0012 V BL^{-1}) (sensor sensitivity)$^{-1}$
[b] ±2% of reading plus 0.5% of full scale range (0 – 10 m s^{-1}) = 0.05 m s^{-1}
[c] < ±1.0% of reading (based on one minute average standard deviation)
[d] 0.07% of selected full scale (0 – 10 m s^{-1})

Propagation of uncertainty obtained from the zeroth-order uncertainty budgets (tables 2.2 and 2.3) through the reference nonlinear regression (equation 2.18), combined with the *RMSE*, yielded

the combined standard uncertainty associated with the reference air velocity at TA calibration (equation 2.19).

$$\Delta u'_{ref}{}^{2} = \left(\frac{\partial u'_{ref}}{\partial dP}\Delta dP\right)^{2} + RMSE^{2} + \left(\Delta u_{ref}\right)^{2} \tag{2.19}$$

where

$\Delta u'_{ref}$ = reference airspeed combined standard uncertainty (m s^{-1})

Heat dissipation factor

The standard uncertainty associated with calculation of δ (equation 2.20) was determined from the propagation of uncertainty in the input parameters.

$$\Delta\delta^{2} = \left(\frac{\partial\delta}{\partial\bar{V}_1}\Delta\bar{V}_1\right)^{2} + \left(\frac{\partial\delta}{\partial\bar{V}_2}\Delta\bar{V}_2\right)^{2} + \left(\frac{\partial\delta}{\partial R_4}\Delta R_4\right)^{2} + \left(\frac{\partial\delta}{\partial R_6}\Delta R_6\right)^{2} + \left(\frac{\partial\delta}{\partial t_t}\Delta t_t\right)^{2} + \left(\frac{\partial\delta}{\partial t_{db}}\Delta t_{db}\right)^{2} \tag{2.20}$$

where

$\Delta\delta$ = heat dissipation factor combined standard uncertainty (W °C^{-1})

Calibration

A piecewise higher-order polynomial regression was obtained from the calibration data at airspeeds from ~0.0 to ~5.5 m s^{-1}, over a nominal t_{db} range (18°C to 33°C) to determine the t_{db} compensated airspeed (equation 2.21) using the relationship described in equation 2.5 and proposed by Hultmark & Smits (2010). One discontinuity in the calibration data was selected at the point where the *RMSE* for both functions was minimized; hence, two independent regressions of equation 2.21 were obtained.

$$\frac{u'}{\nu} = d_1\left(\frac{\delta}{k}\right)^{3} + d_2\left(\frac{\delta}{k}\right)^{2} + d_3\frac{\delta}{k} + d_4 \tag{2.21}$$

where

u' = predicted airspeed with t_{db} compensation (m s^{-1})

d_1 - d_4 = coefficients

Predicted airspeed combined standard uncertainty (equation 2.22) was determined by propagation of parameter uncertainty in equation 2.5 and the addition of the nonlinear regression

statistics. Air properties (i.e., thermal conductivity, absolute viscosity, and density) were assumed to have negligible uncertainty.

$$\Delta u'^2 = \left(\frac{\partial u'}{\partial \delta}\Delta\delta\right)^2 + \Delta u'_{ref}{}^2 + RMSE^2 \quad (2.22)$$

where

$\Delta u'$ = predicted airspeed combined standard uncertainty (m s^{-1})

Results and discussion

Sensor module

The final cost of the Thermal Anemometer (TA) system was approximately $35 USD (including circuit components and microcontroller, but excluding labor). Cost of commercially available low velocity anemometers can be substantially more and do not include stated standard uncertainty. At 22°C, ~0.103 A (325 mW) of current at 5 V_{DC} was supplied to the TA system in still air and ~0.139 A (695 mW) in a ~5.5m s^{-1} flow field.

Coefficients for the nonlinear regression of the Hoge-2 equation (equation 2.11) to determine TA thermistor temperature (t_t) were a_1 = 1.638E-3, a_2 = 2.77E-4, a_3 = -1.718E-6, and a_4 = 3.3536E-7. The coefficient of determination (R^2) = 1 and RMSE = 0.0064°C.

Average (±standard deviation) t_t during calibration was 103.7°C (±0.29°C) with an associated combined standard uncertainty (Δt_t) ranging from 0.8°C to 1.9°C (figure 2.3). It is important during TA operation that t_t is constant and consistent at different airspeeds and t_{db} to ensure repeatable results. This critical low distribution t_t is also observed in figure 2.3. There is no apparent trend between t_{db} and Δt_t (figure 2.3), but it is important Δt_t is minimized to avoid propagating the uncertainty through the subsequent equations. The sensitivity analysis showed on average that analog voltage (ΔV_1 and ΔV_2) measurement uncertainty combined for a ~95.9% (±1.5% each) contribution to Δt_t, while the bridge resistor (R_4 and R_6) uncertainties contributed on average <<1%

and 4.1% (±1.5%), respectively. The *RMSE* from the Hoge-2 regression contributed much less 1%.

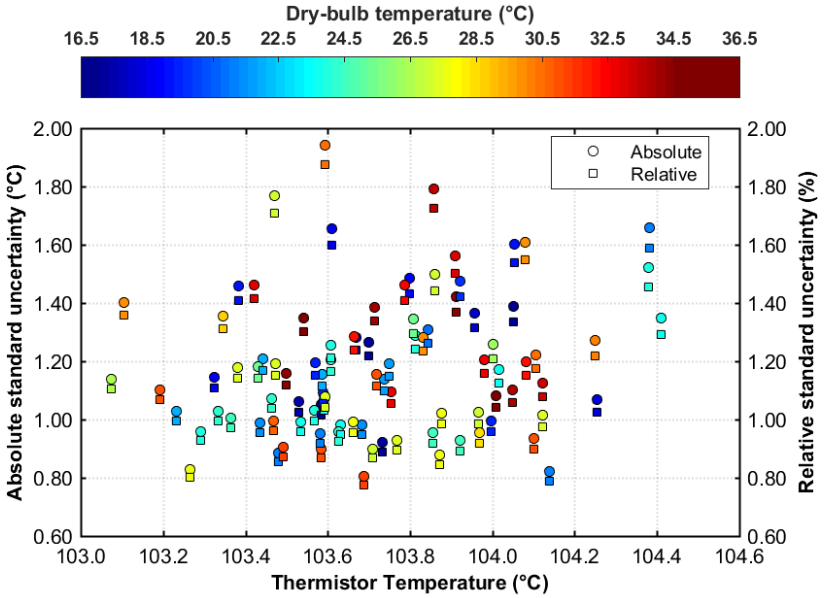

Figure 2.3. Absolute and relative combined standard uncertainty associated with thermistor temperature measurement during thermal anemometer calibration.

Coefficients for the nonlinear regression of the Hoge-2 equation (equation 2.16) to determine dry-bulb thermistor temperature (t_{db}) were b_1 = 7864E-4, b_2 = 2821E-4, b_3 = -3.01E-6, and b_4 = 2.877E-7. The R^2 = 1 and RMSE = 6.971E-4°C.

Combined standard uncertainty associated with t_{db} (Δt_{db}) measurement during calibration (16.5°C ≤ t_{db} ≤ 35.5°C) ranged from 0.32°C (at 16.8°C) to 0.33°C (at 33.3°C; figure 2.4), corresponding to 1.93% to 0.95%, respectively, of the actual measurement. The sensitivity analysis showed the manufacturer's accuracy to contribute the greatest to Δt_{db} (~79%), followed by the voltage divider resistor tolerance (~21%) and lastly, the analog voltage measurement (<<1%). Since, manufacturer's accuracy dominates the relative contribution to Δt_{db}, the steady absolute Δt_{db} is reasonable (figure 2.4).

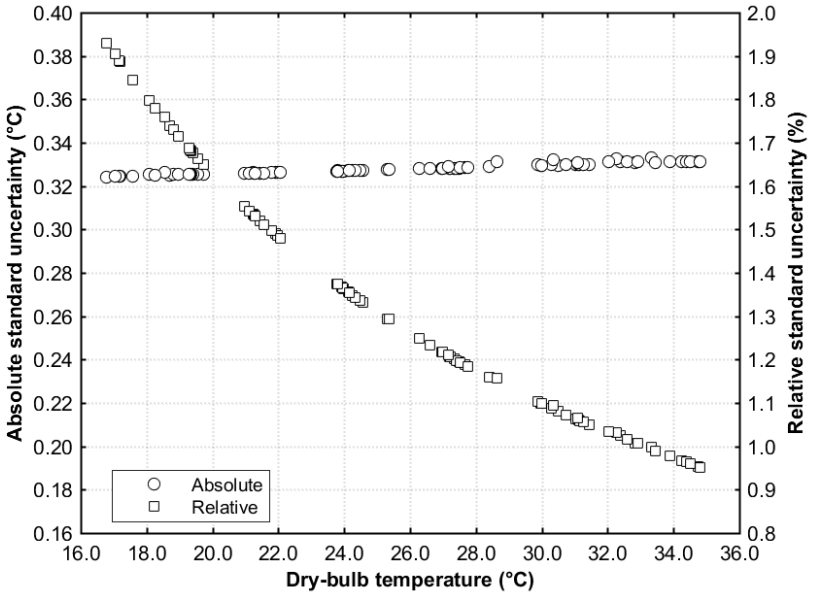

Figure 2.4. Absolute and relative combined standard uncertainty associated with dry-bulb temperature measurement during thermal anemometer calibration.

Standard

The piecewise nonlinear regression for the reference velocity measured at the test location and the differential static pressure across the precision nozzle (figure 2.5; equation 2.18) yielded two sets of coefficients: (1) c_1 = 0.0004627, c_2 = -0.01428, c_3 = 0.2579, and c_4 = -0.5563 for airspeeds less than 1.4 m s^{-1} (R^2 = 0.9965; RMSE = 0.0282 m s^{-1}), and (2) c_1 = 2.97e-06, c_2 = -0.0009404, c_3 = 0.139, and c_4 = -0.3354 (R^2 = 0.9944; RMSE = 0.1095 m s^{-1}) for airspeeds greater than 1.4 m s^{-1}. The discontinuity at 1.4 m s^{-1} (figure 2.5) was chosen to have the smallest *RMSE* for both high and low velocities. If a continuous nonlinear regression was fit through that data, the *RMSE* would be 0.0937 m s^{-1}, compared to a *RMSE* of 0.0282 m s^{-1}, obtained from the regression through data less than 1.4 m s^{-1}. At a nominal 0.5 m s^{-1}, the continuous regression *RMSE*, on a relative basis, would be 18.7% of the nominal airspeed, while the piecewise regression was only 5.6%. Turbulence intensity at the pipe core (location of airspeed sensors) ranged from 4.3% to 5.9% for

all flows. The maximum differential static pressure standard deviation was 2.27 Pa at 0.09 m s^{-1}, suggesting the reference was stable within the margin of quantified doubt at a constant air velocity.

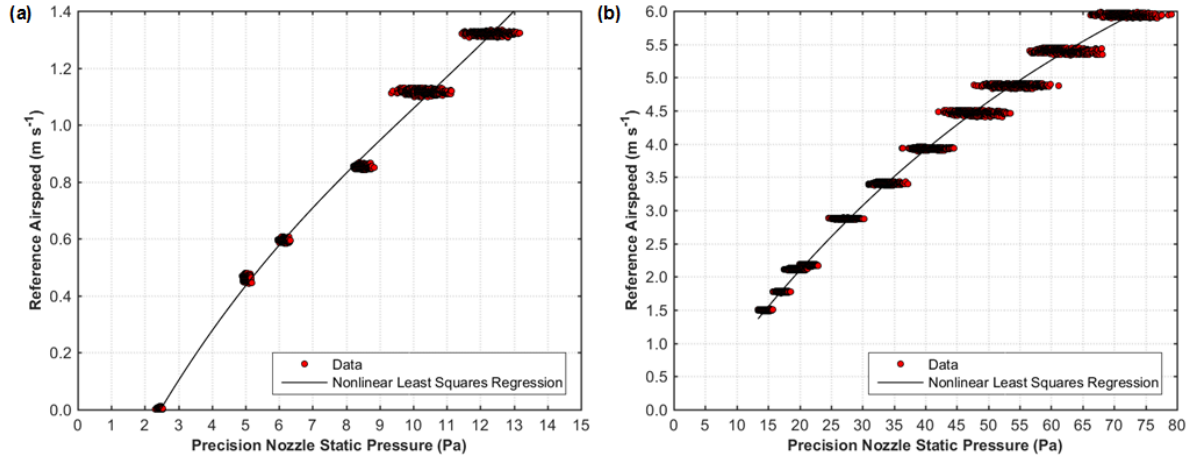

Figure 2.5. Piecewise nonlinear regressions for low airspeed (a) and high airspeeds (b) used to determine the reference airspeed at the test location based on precision nozzle differential static pressure obtained from the standard.

The combined standard uncertainty of the reference velocity ($\Delta u'_{ref}$) used to calibrate the TA ranged from 0.05 to 0.16 m s^{-1} over a ~0.0 to 5.9 m s^{-1} range (figure 2.6). Relative $\Delta u'_{ref}$ was greater at low velocities due to the reference's reading scale plus 0.05 percent full scale accuracy (table 2.3; figure 2.7). At less than 1.4 m s^{-1}, relative $\Delta u'_{ref}$ (figure 2.6) ranged from 4.4% (0.05 m s^{-1} at 1.3 m s^{-1}) to 13.0% (0.06 m s^{-1} at 0.4 m s^{-1}). When greater than 1.4 m s^{-1} relative $\Delta u'_{ref}$ ranged from 2.7% (0.16 m s^{-1} at 5.9 m s^{-1}) to 8.3% (0.12 m s^{-1} at 1.5 m s^{-1}). Separation of the regressions was critical to reducing uncertainty at low velocities. Since, the *RMSE* is constant over the entire regression, this causes large relative uncertainties at low velocities. This can be improved by using two separate nonlinear regressions to reduce the overall standard uncertainty at low velocities. While it is uncommon to possess uncertainty in the calibration standard or reference, this experimental setup does have measurement error for its standard values (i.e., velocity and differential pressure) and must be accounted in the overall uncertainty associated TA airspeed measurement and prediction.

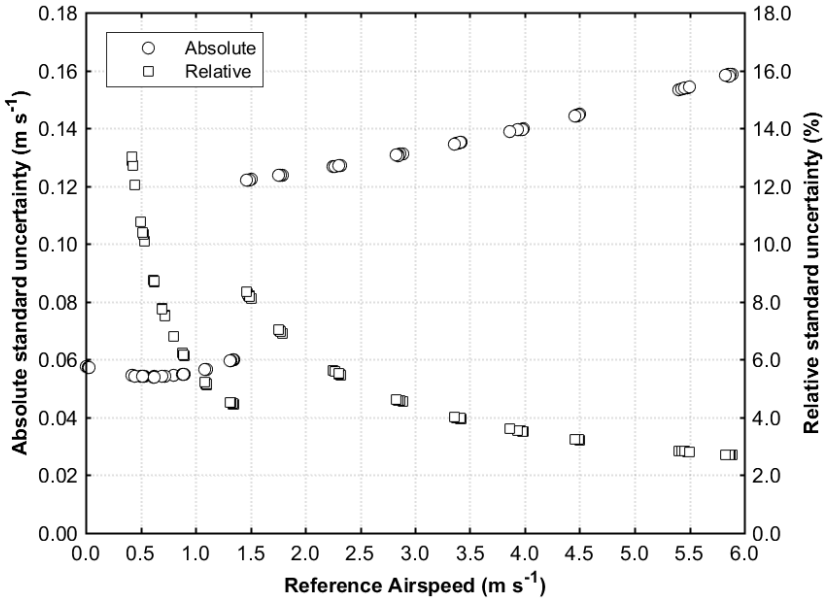

Figure 2.6. Absolute and relative combined standard uncertainties for the reference airspeed at the center of the pipe used to determine the overall combined standard uncertainty associated with measured airspeed. The discontinuity at 1.4 m s^{-1} is due to the fact that two individual regressions were applied; thus, separating influence of the *RMSE* on the reference combined standard uncertainty.

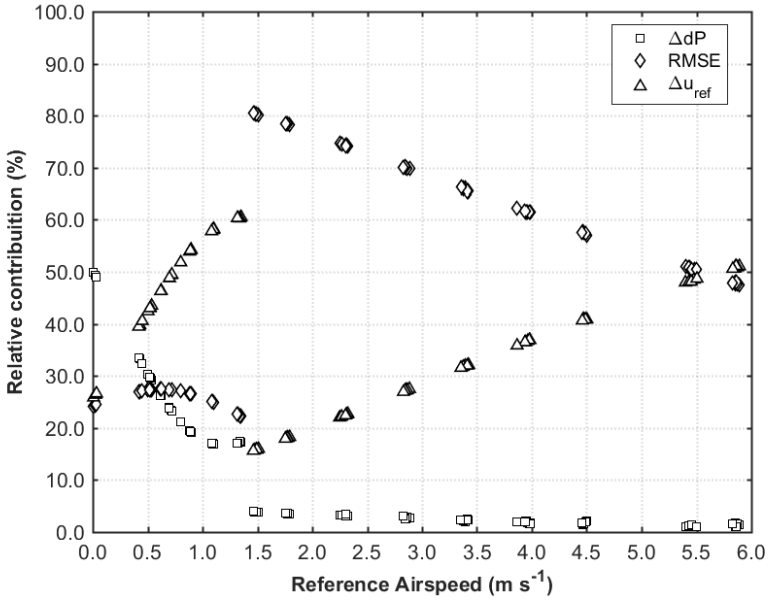

Figure 2.7. Sensitivity analysis for reference velocity combined standard uncertainty. The discontinuity at 1.4 m s^{-1} is due to the fact that two individual regressions were applied; thus, separating influence of the *RMSE* on the reference combined standard uncertainty

Calibration

At six nominal t_{db} (range), 18.0°C (16.5°C ≤ t_{db} < 20.0°C), 21.5°C (20.0°C ≤ t_{db} < 23.0°C), 24.5°C (23.0°C ≤ t_{db} < 26.0°C), 27.0°C (26.0°C ≤ t_{db} < 28.0°C), 29.5°C (28.0°C ≤ t_{db} < 32.0°C), and 33.0°C (32.0°C ≤ t_{db} < 35.0°C), results showed a physical relationship between the heat dissipation factor (δ) and t_{db} (figure 2.8), which is indicative of previous findings and heat transfer theory (Abdel-Rahman, Tropea, Slawson, & Strong, 1987; Bowers, Willits, & Bowen, 1988; Hultmark & Smits, 2010). Relative humidity was maintained at an average 49.9% ±3.3% through calibration. Heat dissipation factors ranged from approximately 1.5 (0 m s^{-1}; all nominal t_{db}) to 4.3 mW $°C^{-1}$ (5.9 m s^{-1}; 18°C nominal t_{db}). As air velocity decreased, convective losses also decreased; thus, a smaller relative difference between δ across t_{db}. At a given velocity, δ was expected to be lower for warmer t_{db} based on heat transfer theory, increasing in magnitude to the coldest t_{db}. This trend appears to be evident in the collected data, for example, clearly shown at a nominal 4 and 3.5 m s^{-1} (figure 2.8). In general, at a given airspeed δ was lower for warmer t_{db} compared with colder t_{db}. Uncertainties in the measurement system and calibration reference most likely contributed to inconsistencies among δ at a given velocity, resulting in some measured δ not exactly adhering to heat transfer theory.

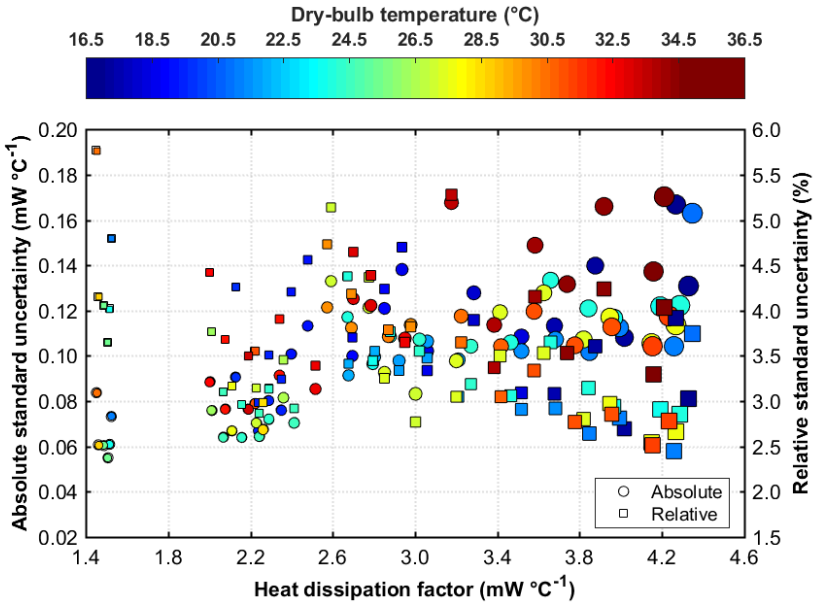

Figure 2.8. Thermal anemometer calibration data colored by actual dry-bulb temperature.

Heat dissipation factor combined standard uncertainty ($\Delta\delta$; figure 2.9) ranged from about 0.06 to 0.08 at 0 m s^{-1} (any nominal t_{db} tested) to 0.17 mW $°C^{-1}$ at 5.8 m s^{-1} (nominal 33°C). No apparent pattern between airspeed and t_{db} with $\Delta\delta$ was evident. Relative $\Delta\delta$ ranged from 2.4% at 5.5 m s^{-1} (nominal 21°C) to 5.8% at 0 m s^{-1} (nominal 31°C; figure 2.9). For a given reference velocity, the maximum absolute difference between δ at the warmest and colder t_{db} was approximately 0.1 mW $°C^{-1}$. Since it can be assumed that the possible estimated values of the parameters contributing to the calculation of δ are approximately normally distributed with approximate standard deviation represented by $\Delta\delta$, the unknown value of δ is believed to lie in the interval defined by combined standard uncertainty with a level of confidence of approximately 63% (Taylor & Kuyatt, 1994). While δ for any nominal t_{db} range is not statistically different, a physical relation still exists; hence, t_{db} compensation is still required.

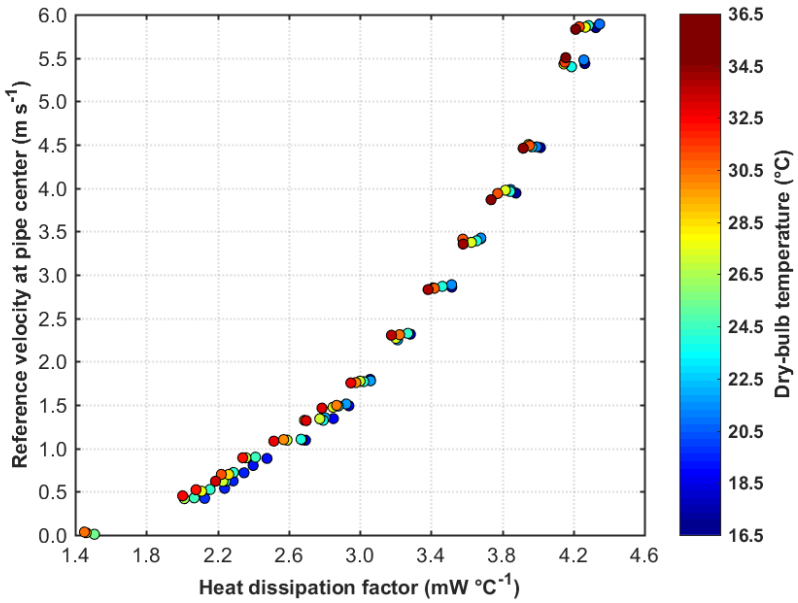

Figure 2.9. Absolute and relative combined standard uncertainty associated with heat dissipation factor calculation during thermal anemometer calibration. Marker area size correlates to reference velocity during calibration.

The sensitivity analysis showed analog voltage measurement were the greatest contributors (figure 2.10) to $\Delta\delta$, with a combined average of 74.9% (2.5%). This result was most likely attributed to the 10-bit ADC resolution of the microcontroller. Given the number of measurements and the importance of V_1, V_2, and V_{db}, in determining δ, the ADC resolution was the limiting factor in the TA system. However, the low cost, ease of use, and wide functionality of the microcontroller makes it suitable for multi-point measurement applications. An increase in the ADC resolution could decrease $\Delta\delta$ and ultimately improve the TA. Other parameters on average, such as, bridge resistors (R_4 and R_6) uncertainty (2.9%), Δt_t (20.6%), and Δt_{db} (1.6%) contributed to $\Delta\delta$.

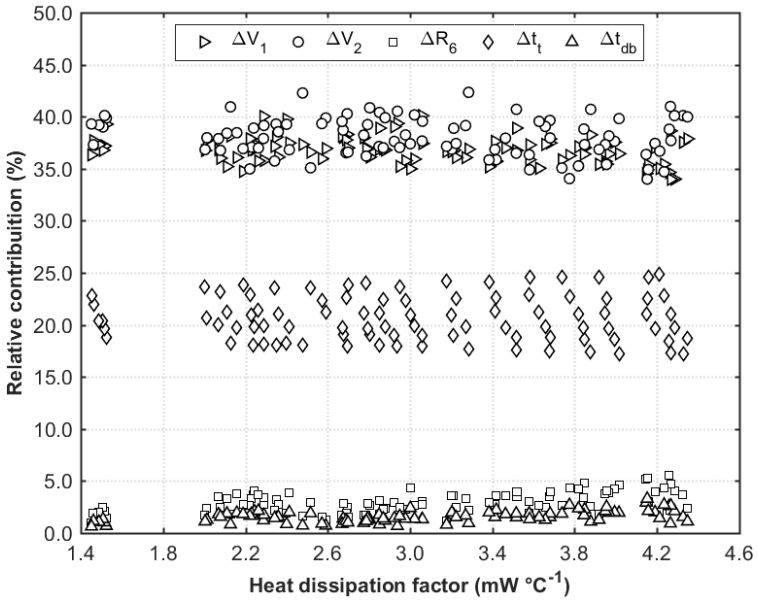

Figure 2.10. Sensitivity analysis for combined standard uncertainty associated with heat dissipation factor calculation during thermal anemometer calibration. Bridge resistor R_4 was omitted for clarity and its low contribution to heat dissipation factor uncertainty.

Coefficients for the fourth-order polynomial dry-bulb temperature compensation regression (equation 2.21; figure 2.11) at velocities <2 m s^{-1} were d_1 = 1.282E07, d_2 = 1.081E07, d_3 = -4.099E05, d_4 = -9.219E03 (R^2 = 0.9842; RMSE = 0.0675 m s^{-1}), and at velocities ≥2 m s^{-1} were d_1 = -1. 049E09, d_2 = 4.495E08, d_3 = -5.897E07, d_4 = 2.549E06 (R^2 = 0.9857; RMSE = 0.1462 m s^{-1}). The discontinuity at 2.0 m s^{-1} (figure 2.5) was chosen to have the smallest *RMSE* for both high and low velocities. If a continuous nonlinear regression was fit through that data, the *RMSE* would be 0.1176 m s^{-1}, compared to the 0.0675 m s^{-1} obtained for the regression through data less than 2 m s^{-1}. At a nominal 0.5 m s^{-1}, the continuous regression *RMSE*, on a relative basis, would be 23.5% of the nominal airspeed, while the piecewise regression was only 13.5%. The regression statistics for each curve demonstrates that the proposed correction technique by Hultmark and Smits (2010) accurately describes the influences of different t_{db} on the calibration.

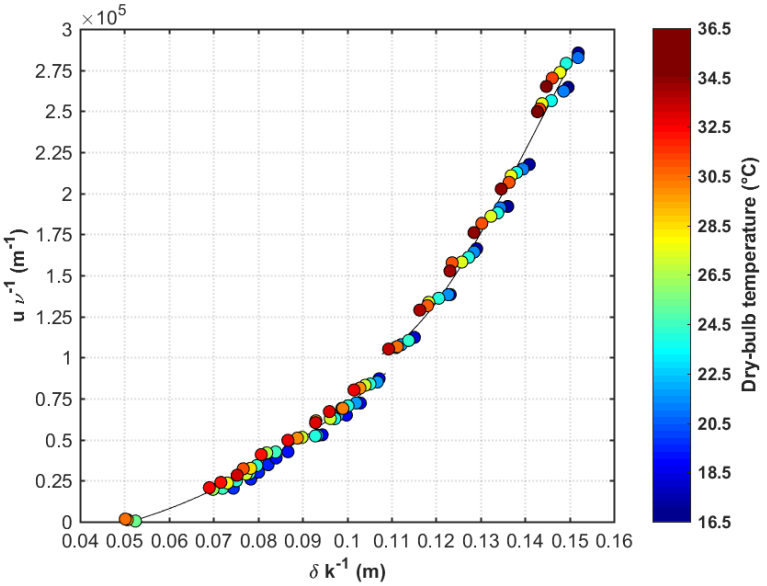

Figure 2.11. Thermal anemometer calibration with t_{db} compensation. Two unique fourth-order polynomial regressions were used to separate velocities <2 m s^{-1} and ≥2 m s^{-1} to reduce uncertainty at low velocities.

The combined standard uncertainty associated with predicted airspeed ($\Delta u'$) ranged from 0.11 (at 0.46 m s^{-1}) to 0.71 m s^{-1} (at 5.52 m s^{-1}; figure 2.12). At low velocities, there were small differences among $\Delta u'$, while at higher velocities, $\Delta u'$ varied much more as shown by the dispersion of circular markers in figure 2.12. This was most likely due to the turbulent velocities at the higher airspeeds. For this reason, two separate regression were used such that the larger *RMSE* at the higher velocities does not impact the $\Delta u'$ at the lower velocities. Relative $\Delta u'$ decreased as velocity increased, with a range from 7.85% (5.67 m s^{-1}) to 30.3% (0.40 m s^{-1}). Due to the propagation of measurement error through the uncertainty analysis, measured airspeeds are believed to lie in the interval defined by $\Delta u'$ with a level of confidence of approximately 63%. The sensitivity analysis (figure 2.13) showed for velocities <2 m s^{-1}, the relative contribution of $\Delta\delta$ to initially increase as velocity increased and then decrease as the discontinuity was approached. While *RMSE* and Δu_{ref} were similar in magnitude and decreasing as velocity increased, the relative contribution of Δu_{ref} began to increase as the discontinuity was approached. For velocities increasing beyond 2 m s^{-1}, the *RMSE* and Δu_{ref} had similar magnitude and trend (figure 2.13), while

the relative contribution of $\Delta\delta$ increased. A decrease in the overall uncertainty associated with the reference and the microcontroller ADC, to reduce the uncertainty in δ, may ultimately lead to a decrease in $\Delta u'$.

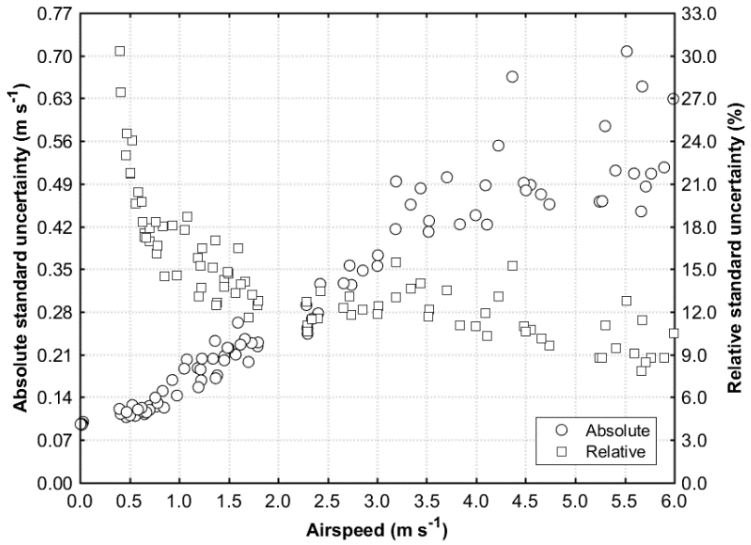

Figure 2.12. Absolute and relative combined standard uncertainty associated with thermal anemometer predicted airspeed with t_{db} compensation during calibration.

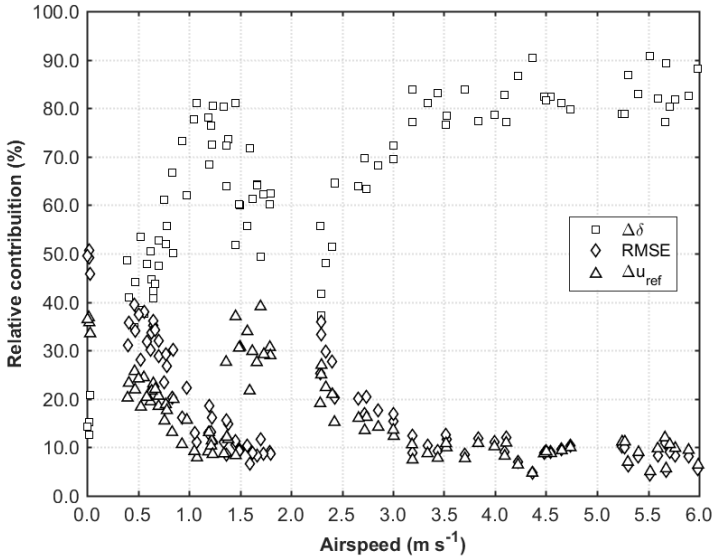

Figure 2.13. Sensitivity analysis for combined standard uncertainty associated with thermal anemometer predicted airspeed during calibration.

Time constant

Average (±standard deviation) time to reach steady-state (3τ) was 3.14 ±0.31 s (step-up) and 2.15 ±0.20 s (step-down; table 2.4; figure 2.14). The R^2 were ~0.94 (step-up) and greater than 0.99

(step-down) for each regression. The *RMSE* provided an estimate of the overall uncertainty over the regression. The step-up caused the system to reach steady-state slower compared with the step-down, due to the behavior of the bridge circuit generating more power to maintain a constant temperature at the thermistor (figure 2.14). Time to reach steady-state was used to improve experimental and operational protocols. That is, the TA has limited applications in turbulent flows where airspeed may be changing faster than 3τ.

Table 2.4. Nonlinear regression coefficients and statistics summary for time constant and time to reach steady-state for a step-up and step-down.

Step change (m s^{-1})	τ (s^{-1})	R^2	RMSE (m s^{-1})	Time to reach steady-state (s)
0 to ~5	1.05 ±0.10	~0.94	0.19 ±0.01	3.14 ±0.31
~5 to 0	0.72 ±0.07	>0.99	0.04 ±0.01	2.15 ±0.20

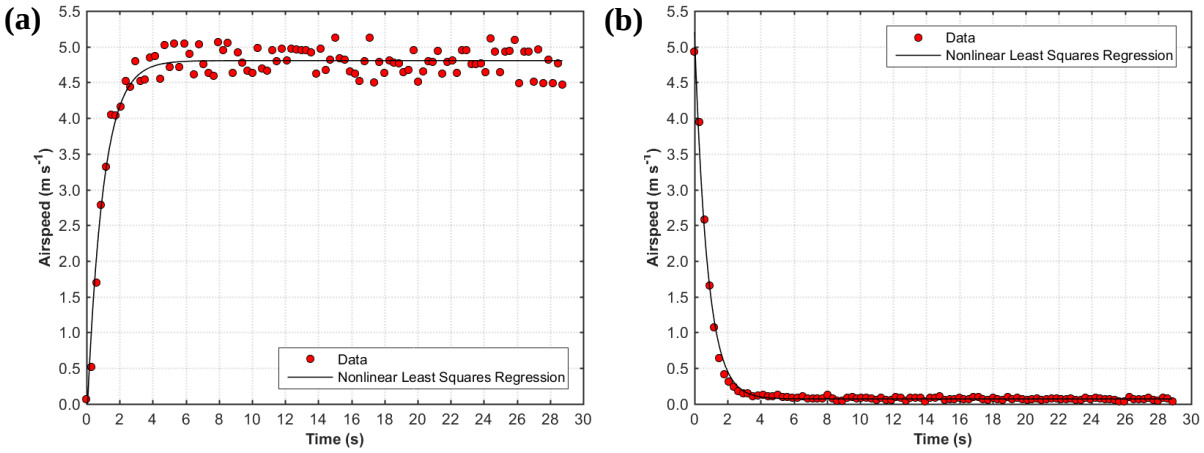

Figure 2.14. Nonlinear regression and data to determine the time constant for step-up (a) and step-down (b).

Conclusions

A constant temperature thermal anemometer with a measurement range between 0 and 6 m s^{-1} with dry-bulb temperature compensation was designed, constructed, and calibrated with an absolute standard uncertainty ranging from approximately 0.11 to 0.71 m s^{-1} and a relative standard uncertainty ranging from approximately 7.85% to 30.3%. The low-cost (less than $35 USD excluding labor) and simple hardware, make this thermal anemometer well-suited for

integration into multi-point data acquisition systems analyzing spatiotemporal variability inside livestock and poultry housing. The uncertainty analysis presented here establishes the framework for performing and determining the uncertainty associated with similar measurement systems.

Acknowledgments

This research was supported with funding provided by the Iowa Pork Producers Association under NPB Project 14-242. The authors would like to acknowledge the contributions of undergraduate student Grant Hoppes during the preparation and completion of this work.

The research work of Yun Gao was partly supported by the Fundamental Research Funds for the Central Universities of China (2013PY052).

References

Abdel-Rahman, A., Tropea, C., Slawson, P., & Strong, A. (1987). On temperature compensation in hot-wire anemometry. Journal of Physics E: Scientific Instruments, 20(3), 315.

Al-Garni, A. M. (2007). Low speed calibration of hot-wire anemometers. Flow Measurement and Instrumentation, 18(2), 95–98.

ASHRAE. (2013). Handbook of fundamentals. Atlanta, GA: America Society of Heating, Refrigeration and Air Conditioning Engineers.

Aydin, M., & Leutheusser, H. J. (1980). Very low velocity calibration and application of hot-wire probes. DISA Information, 1, 17.

Barfield, B. J., & Henson, W. H. (1971). Calibration of hot-wire and hot-film probes. Transactions of the ASAE, 14(6), 1100–1102. http://doi.org/10.13031/2013.38462

Bowers, C. G., Willits, D. H., & Bowen, H. D. (1988). Comparison of temperature correction methods for hot wire anemometers. Transactions of the ASAE, 31(5), 1552–1555. http://doi.org/10.13031/2013.30899

Bruun, H. H. (1996). Hot-wire anemometry: principles and signal analysis. Measurement Science and Technology, 7(10). Retrieved from http://iopscience.iop.org/0957-0233/7/10/024

Christman, P. J., & Podzimek, J. (1981). Hot-wire anemometer behaviour in low velocity air flow. Journal of Physics E: Scientific Instruments, 14(1), 46.

Collis, D. C., & Williams, M. J. (1959). Two-dimensional convection from heated wires at low Reynolds numbers. Journal of Fluid Mechanics, 6(03), 357–384.

Curtis, S. E. (1983). Environmental Management in Animal Agriculture. Ames, IA: The Iowa State University Press.

DeShazer, J. A., Hahn, L., & Xin, H. (2009). Chapter 1: Basic Principles of the Thermal Environment and Livestock Engergetics. In James A. DeShazer, Livestock Energetics and Thermal Environment Management (1st ed., pp. 1–22). St. Joseph, MI: American Society of Agricultural and Biological Engineers.

Fox, R. W., McDonald, A. T., & Pritchard, P. J. (1985). Introduction to fluid mechanics (Vol. 7). John Wiley & Sons New York.

Heber, A. J., & Boon, C. R. (1993). Air velocity characteristics in an experimental livestock building with nonisothermal jet ventilation. ASHRAE, Atlanta, GA. (139-1151).

Hillman, P. E. (2009). Chapter 2: Thermoregulatory Physiology. In J. A., DeShazer, Livestock Energetics and Thermal Environment Management (1st ed., pp. 23–48). St. Joseph, MI: American Society of Agricultural and Biological Engineers.

Hoge, H. J. (1988). Useful procedure in least squares, and tests of some equations for thermistors. Review of Scientific Instruments, 59(6), 975–979. http://doi.org/10.1063/1.1139762

Hultmark, M., & Smits, A. J. (2010). Temperature corrections for constant temperature and constant current hot-wire anemometers. Measurement Science and Technology, 21(10), 105404.

JCGM. (2008). Evaluation of measurement data - Guide to the expression of uncertainty in measurement (First). Geneva, Switzerland: Working Group 1 of the Joint Committee for Guides in Metrology (JCGM/WG 1).

Jerez, S. B., Wang, X., & Zhang, Y. (2014). Quantification of ventilation effectiveness for air quality control in animal buildings. ASHRAE Transactions, 120(1), 460–468.

Kannuluik, W. G., & Carman, E. H. (1951). The temperature dependence of the thermal conductivity of air. Australian Journal of Chemistry, 4(3), 305–314.

Luck, B. D., Davis, J. D., Purswell, J. L., Kiess, A. S., Hoff, S. J., & Olsen, J. W. (2014). Effect of Measurement Density on Characterizing Air Velocity Distribution in Commercial Broiler Houses. Transactions of the ASABE, 57(5), 1443–1454.

Mori, Y., Imabayashi, M., Hijikata, K., & Yoshida, Y. (1968). Unsteady Heat and Mass Transfer from Small Bodies. The Japan Society of Mechanical Engineers, 11(43), 193.

Mount, L. E. (1975). The assessment of thermal environment in relation to pig production. Livestock Production Science, 2(4), 381–392. http://doi.org/10.1016/0301-6226(75)90121-9

Popiolek, Z., Jørgensen, F. E., Melikov, A. K., Silva, M. C. G., & Kierat, W. (2007). Assessment of uncertainty in measurements with low velocity thermal anemometers. International Journal of Ventilation, 6(2), 113–128.

Ramirez, B. C., Hoff, S. J., Gao, Y., & Harmon, J. D. (2015). Commissioning of a novel animal thermal environment replication and measurement system. In 2015 ASABE Annual International Meeting (p. 1). American Society of Agricultural and Biological Engineers.

Rumyantsev, A. V., & Kharyukov, V. G. (2011). The characteristic size of a sphere in convective heat transfer. Measurement Techniques, 54(5), 524–528.

Schiretz, H. (2012). The Modern Devices wind speed sensor. Greelong, Victoria , Austraila: Deakin University.

Skinner, A. J., & Lambert, M. F. (2009). Evaluation of a warm-thermistor flow sensor for use in automatic seepage meters. Sensors Journal, IEEE, 9(9), 1058–1067.

Straw, B. E., Zimmerman, J. J., D'Allaire, S., & Taylor, D. J. (1999). Disease of swine. Ames, Iowa: Iowa State Press.

Taylor, B. N., & Kuyatt, C. E. (1994). Guidelines for evaluating and expressing the uncertainty of NIST measurement results. Gaithersburg, MD: US Department of Commerce, Technology Administration, National Institute of Standards and Technology.

Yue, Z., & Malmström, T. G. (1998). A simple method for low-speed hot-wire anemometer calibration. Measurement Science and Technology, 9(9), 1506.

Zhang, Y., Barber, E. M., & Ogilvie, J. R. (1988). Simulation of the dynamic thermal environment in a swine barn. American Society of Agricultural Engineers.

CHAPTER 3. THERMAL ENVIRONMENT SENSOR ARRAY: PART I. DEVELOPMENT AND FIELD PERFORMANCE ASSESSMENT

B. C. Ramirez, Y. Gao, S. J. Hoff, and J. D. Harmon

A manuscript to be submitted to *Biosystems Engineering*

This chapter describes the design, construction, and field performance of a novel thermal environment sensor array (TESA) capable of describing parameters that impact an animal's ability to exchange heat with its environment. A TESA consists of dry-bulb temperature, relative humidity, airspeed (Chapter 2), and black globe temperature measurements. Custom signal processing and microcontroller control for each TESA were developed. A network of 44 TESAs was constructed and deployed in a commercial wean-finish swine facility to evaluate its robustness over time. TESA has established a new standard of spatial and temporal thermal environment monitoring with reasonable accuracy, simplicity, and cost.

This chapter owes its success to the teamwork of Brett Ramirez, Yun Gao, Steven Hoff, and Jay Harmon. I led the design and construction of TESA, research design and deployment in the facility, collected and analyzed data, and drafted the manuscript. Dr. Gao developed the circuity for all the TESA sensors, selected hardware, and created the first prototype of TESA. Drs. Gao, Harmon, and Hoff also contributed to the research design and revision of the manuscript.

Abstract

Current Thermal Environment (TE) monitoring and control strategies for livestock and poultry facilities need to have enhanced measurement capabilities in order to provide an optimum TE based on the thermal demands of the animal. Hence, a spatial network of Thermal Environment Sensor Arrays (TESAs), each with a custom Data Acquisition (DAQ) system, was developed to

describe the TE (except conduction) and deployed in a commercial swine facility to perform a preliminary assessment on robustness and capabilities under production settings. A TESA featured a dry-bulb temperature (t_{db}), black globe temperature, airspeed, and relative humidity (RH) sensor. For each TESA, a custom circuit board featured an Arduino, signal conditioning, and communication hardware. Data were exchanged over a RS-485 bus on command from a computer with custom software. A total of 44 TESAs were suspended about 1 m above the slats in a wean-finish swine facility (22 TESAs per room) located in central Iowa, USA. After closeout, all TESA were validated with a reference system to determine individual time constants and assess if a significant bias correction was needed (except for airspeed). Total number of usable measurements for subsequent analysis for all sensors per TESA averaged (95% CI) 202,310 (199,187, 205,437). In summary, 7% t_{db} thermistor, 9% digital t_{db}, and 27%RH sensors required correction after 170.5 d inside the facility. The utilization of low-cost sensors, open-source software, and microcontrollers allowed this novel network to provide sufficient measurement density to promote future queries on the uses of TE data in livestock and poultry facilities.

Introduction

The growing global population is projected to increase by 2.4 billion people from 2015 to 2050 (UN, 2015) and will require a secure animal-based protein supply raised in energy, water, and feed efficient housing systems that do not adversely impact the environment. A housing system operating within the animal's optimum Thermal Environment (TE) is one approach to enhance animal well-being and growth performance (Curtis, 1983; Renaudeau, Gourdine, & St-Pierre, 2011), while simultaneously reducing facility resource usage, as well as total feed consumed and days on feed. The TE describes the parameters that influence heat exchange (i.e., convective, conductive, radiative, and evaporative) between an animal and its surroundings (ASHRAE, 2013;

Curtis, 1983; DeShazer, Hahn, & Xin, 2009); however, all required parameters that describe the TE a housed animal experiences are rarely quantified, resulting in a lack of accurate TE control that is optimal for the animal. Hence, there is a requisite need for advanced techniques to accurately assess and ultimately, control the TE based on how the animal exchanges heat with its surroundings (Fournel, Rousseau, & Laberge, 2017).

The parameters used to describe the TE include dry-bulb temperature (t_{db}), relative humidity (RH), airspeed, and mean radiant temperature (t_{mr}). Dry-bulb temperature is frequently the main parameter used to describe and control TE in commercial animal production systems; however, it exclusively impacts only the convective and evaporative modes of heat loss and also requires airspeed and RH. The RH must be known with t_{db} to estimate latent heat loss (i.e., by respiration or wetted skin evaporation) by determining the water vapor pressure gradient between surrounding air and the saturated surface or fluid of interest. Airspeed influences convective and evaporative heat transfer rates, and can substantially increase heat loss (beneficial in a hot t_{db}; unfavorable in a cold t_{db}). Lastly, t_{mr} is the uniform temperature of the surroundings in which radiant heat transfer from the animal's surface equals that in the actual surroundings. Due to the difficulty to instrument, t_{mr} and airspeed are often neglected in livestock facilities; despite, Bond et al. (1952), Mount (1967), Mount (1964), and Beckett (1965) having showed radiative heat losses to be a substantial source of heat loss from swine.

The incorporation of the these four parameters into a single Thermal Environment Sensor Array (TESA) that is robust and practical for application in livestock and poultry facilities, would allow for the integration and application of advanced techniques. For human occupied buildings, many commercially available TE measurement systems exist to quantify indoor thermal comfort statistical values (e.g., draught rate, predicted mean vote, and predicted percentage dissatisfied;

ASHRAE, 2013). These systems are cost-prohibited for use in multi-point Data Acquisition (DAQ) systems, feature proprietary hardware and software that limit flexibility, and are designed for relatively clean, low airspeed environments. In animal production systems, various combinations of t_{db}, RH, airspeed, and/or t_{mr} have been monitored (Brown-Brandl et al., 2014; Hayes et al., 2013; Vilela et al., 2015), but rarely all together. There is a unique opportunity, specific to animal production systems, for a sensor network that focuses on the TE demands of the animal.

A TESA and DAQ were developed and validated with a well-documented statement of measurement uncertainty for capturing the TE spatial and temporal distribution in swine facilities. This system was developed to simultaneously quantify the TE the animals experience in order to enable an animal-centric approached to swine production. The utilization of low-cost sensors, open-source software, and microcontroller based control allows this novel network of TESAs and accompanying DAQ to provide sufficient measurement density, such that design and control of TE modification systems can be adjusted to enhance and maintain the optimal TE for improved animal production efficiency and thermal comfort. Hence, the objectives of this research were: (1) develop TESA and accompanying DAQ; (2) deploy 44 TESAs in a deep-pit, wean-finish swine barn for six months to assess system robustness and accuracy over time; and (3) preliminarily assess the TE under normal production operating conditions.

Materials and methods

Thermal environment sensor array

An individual Thermal Environment Sensor Array (TESA; figure 3.1) was developed to measure dry-bulb temperature (t_{db}), relative humidity (RH), airspeed, and estimate mean radiant temperature (t_{mr}) from the globe temperature (t_g) of a Black Globe Thermometer (BGT). Sensor

signals from a TESA were connected via a 3.05 m long, nine-conductor wire to screw terminals mounted on the TESA Data Acquisition (TESA DAQ) custom Printed Circuit Board (PCB).

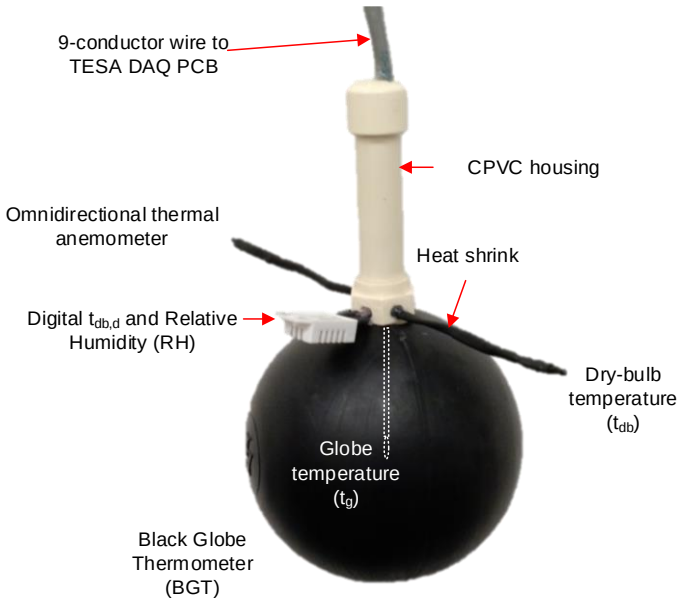

Figure 3.1. A Thermal Environment Sensor Array (TESA) featuring dry-bulb temperature, relative humidity, airspeed, and black globe thermometer sensors. Globe temperature is obtained from a dry-bulb temperature sensor secured at the center of the black globe thermometer.

Sensors

Ambient t_{db} and t_g were measured with a Negative Temperature Coefficient (NTC) thermistor (nominal 10 kΩ at 25°C, NTCLE413-428, Vishay, Malvern, PA, USA; figure 3.1). Gao, Ramirez, & Hoff (2016) provide further details regarding the signal conditioning and nonlinear regression coefficients for these two thermistors. Additionally, a single wire, digital interface $t_{db,d}$ and RH sensor (RHT03, MaxDetect Technology Co. Ltd., Shenzhen, China; figure 3.1) was used. Valid sensor operation ranged from -40°C to 80°C ($t_{db,d}$) and 0% to 100% (RH; non-condensing).

A custom Omnidirectional Thermal Anemometer (OTA; figure 3.1) was developed to measure airspeeds between 0 and 5.5 m s^{-1}. A near-spherical, NTC thermistor (nominal 470 Ω at 25°C, Model LC471F3K, U.S. Sensor Corp., Orange, CA, USA) was heated above ambient t_{db} by

a Constant Temperature Anemometer (CTA) circuit in order to estimate the electrical power dissipated by the OTA as a function of airspeed and the fluid properties of the air for a given t_{db}. Gao et al. (2016) provides further detail regarding the sensor design, calibration, and t_{db} compensation approach.

The net exchange of radiant energy between objects is the algebraic sum of all the radiant fluxes in which the object is exposed. Dimensions, locations, and thermal characteristics (i.e., surface temperature and emissivity) of the surrounding exposed objects must be known to calculate the flux of each object; however, this method becomes increasingly difficult and time consuming to implement, when the number of sources is large and geometries complex (ASHRAE, 2013; ISO 7726, 2001, p. 77). The BGT is a cost effective and simple approach to estimate t_{mr} when coupled with ambient t_{db} and airspeed measurements at the level of the BGT (Bond & Kelly, 1955; Pereira, Bond, & Morrison, 1967; Purswell & Davis, 2008). A BGT (figure 3.1) was constructed from a 0.1016 m diameter, flat black, hollow plastic sphere (3FXE7, W.W. Grainger Inc.) with a nominal 1.27 cm CPVC male adapter threaded into a 0.635 cm diameter hole in the top of the plastic sphere. Outer emissivity was assumed to be 0.95 (ASHRAE, 2013) and the plastic sphere wall thickness was 0.81 mm. A rubber stopper with a small axial hole was inserted into the CPVC male adapter to secure the t_{db} thermistor at the center of the BGT.

Zeroth-order uncertainty analysis

A zeroth-order uncertainty budget, including Type A (the best available estimate of the expected value of a quantity that varies randomly) and Type B (not obtained from repeated observation, rather based on all available information) evaluations was created for each TESA sensor. Results from the zeroth-order uncertainty budget were then propagated through any

analytical solutions that use measurements as inputs, to ultimately determine the combined standard uncertainty (denoted by Δ) associated with the calculated value.

The procedure to compute the combined standard uncertainty associated with the TESA DAQ microcontroller analog to digital conversion, t_{db} and t_g measurement (via NTC thermistor), and airspeed measurement are reported in Gao et al. (2016). Contributors to the zeroth-order uncertainty for the digital t_{db} and RH sensor (provided by the manufacturer) were, the stated accuracy (±0.5°C; ±2%), reading resolution (±0.1°C; ±0.1%), repeatability (±0.2°C; ±1%), RH hysteresis (±0.3%), and RH long-term stability (±0.5%), and also assumed to have a rectangular probability distribution. The results of the zeroth-order uncertainty budget for all the sensors and computed value are summarized in table 3.1.

Table 3.1. Zeroth-order uncertainty budget summary for TESA sensors.

Parameter	Description	Sensor	Interface	Zeroth-order standard uncertainty (Δ^0_x)		Unit
t_{db}	Dry-bulb temperature	NTC thermistor	Analog	$\Delta^0 t_{db}$	= 0.33	°C
$t_{db,d}$	Dry-bulb temperature	AMig	Digital	$\Delta^0 t_{db,d}$	= 0.31	°C
RH	Relative humidity	Polymer humidity capacitor	Digital	$\Delta^0 RH$	= 1.33	%
u	Airspeed	OTA	Analog	$\Delta^0 u$	= 0.11 (at 0.47 m s^{-1}) to 0.71 (at 5.52 m s^{-1})	m s^{-1}
t_g	Globe temperature	NTC thermistor	Analog	$\Delta^0 t_g$	= 0.33	°C

Data acquisition and serial communication

The TESA DAQ featured a custom designed (Eagle v7.4, CadSoft Computer GmbH, Pleiskirchen, Germany) and manufactured PCB (OSH Park) for containing the signal conditioning circuits (figure 3.2).

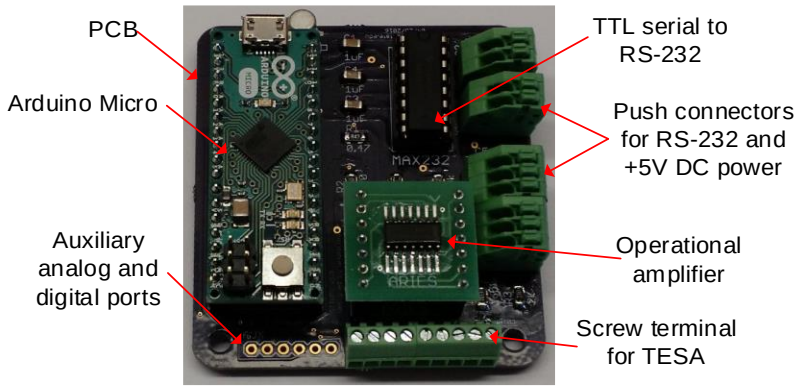

Figure 3.2. Thermal Environment Sensor Array Data Acquisition (TESA DAQ) on the custom Printed Circuit Board (PCB) with microcontroller, signal conditioning, and serial communication for a single TESA.

Printed circuit board and housing

The PCB (figure 3.2) included the CTA circuit, t_{db} divider circuits, a microcontroller (Arduino Micro, Arduino LLC, Italy), and a serial TTL to RS-232 converter (MAX232IN, Texas Instruments Inc., Dallas, TX, USA). The operational amplifier in the CTA circuit was replaceable if the device failed or needed replacement. Similarly, the microcontroller could be readily removed for programming or replacement. Eight capacitors (each 1 µF) were required for the serial TTL to RS-232 converter, in addition to one 10 kΩ resistor for the digital t_{db} and RH sensor.

Two TESA DAQs (i.e., one per TESA) were housed in a 0.136 × 0.136 × 0.09 m (L × W × D) weatherproof housing (NBF-32010, Bud Industries Inc., Willoughby, OH, USA) for protection from the environment (figure 3.3). Four cable grips were installed to provide watertight connections for the two TESA signal wires, serial communication, and +5 V_{DC} power transformer (WSU050-1500, Triad Magnetics, Perris, CA, USA).

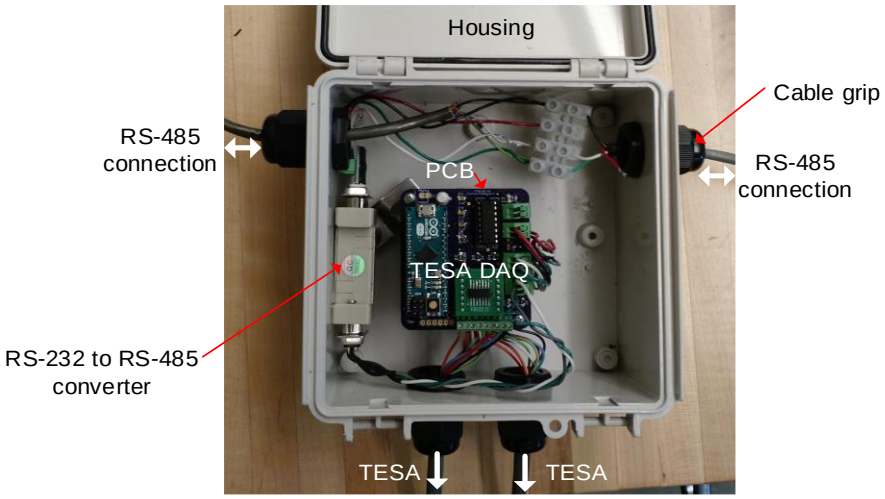

Figure 3.3. Weatherproof housing containing two TESA DAQ on PCBs (stacked) for deployment of two TESAs and serial communication hardware.

Serial communication network

The serial data communication network featured bidirectional data transfer between a notebook computer and every deployed TESA DAQ (figure 3.4). A unique address identification number was programmed onto each TESA DAQ microcontroller such that a handshake protocol (bidirectional data transfer) could be implemented in a multipoint RS-485 network. On command, the terminal data communication device (i.e., TESA DAQ microcontroller) sent collected sensor data through a TTL serial to RS-232 converter (figure 3.2) then a RS-232 to RS-485 converter (ATC-106, ATC Technology Co., Ltd, Wilmington, MA, USA; figure 3.3). RS-485 was used due to its robustness and stability over long-distances in electrically noisy environments. A RS-485 bus to universal serial bus converter (USB-RS485-PCBA, FTDI Ltd, Glasgow, United Kingdom) was interfaced with the computer and a Custom Data Management Software (CDMS). TESA DAQs were arranged in series, that is, one three-conductor cable (+485, -485, ground) between each housing (one RS-232 to RS-485 converter per housing). This approach also minimized

communication cable length and was relatively easier to implement, but with more labor than other communication protocols, such as wireless.

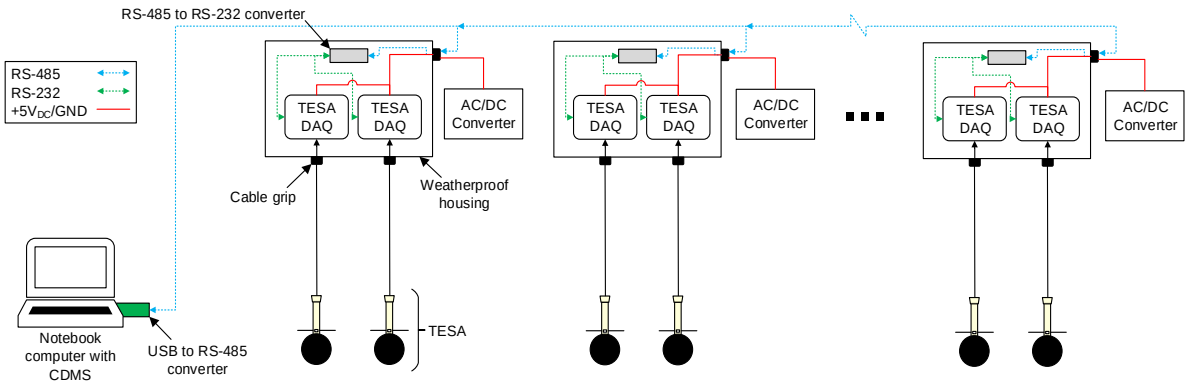

Figure 3.4. Schematic of serial communication network connecting two TESA DAQs per weatherproof housing together with the notebook.

Software

One TESA DAQ program (figure 3.5a) was developed in the integrated development environment for the microcontroller and when prompted by the CDMS (Python 2.7, Python Software Foundation, Beaverton, Oregon, USA; figure 3.5b) on the computer returned the mean of 20 sequentially measured (approximately every 2 ms) analog voltages (two for airspeed, two for t_{db}), digital t_{db}/RH measurements, and time between analog voltage measurements. The CDMS controlled sampling interval between data transmission requests to each TESA DAQ and timestamped incoming data.

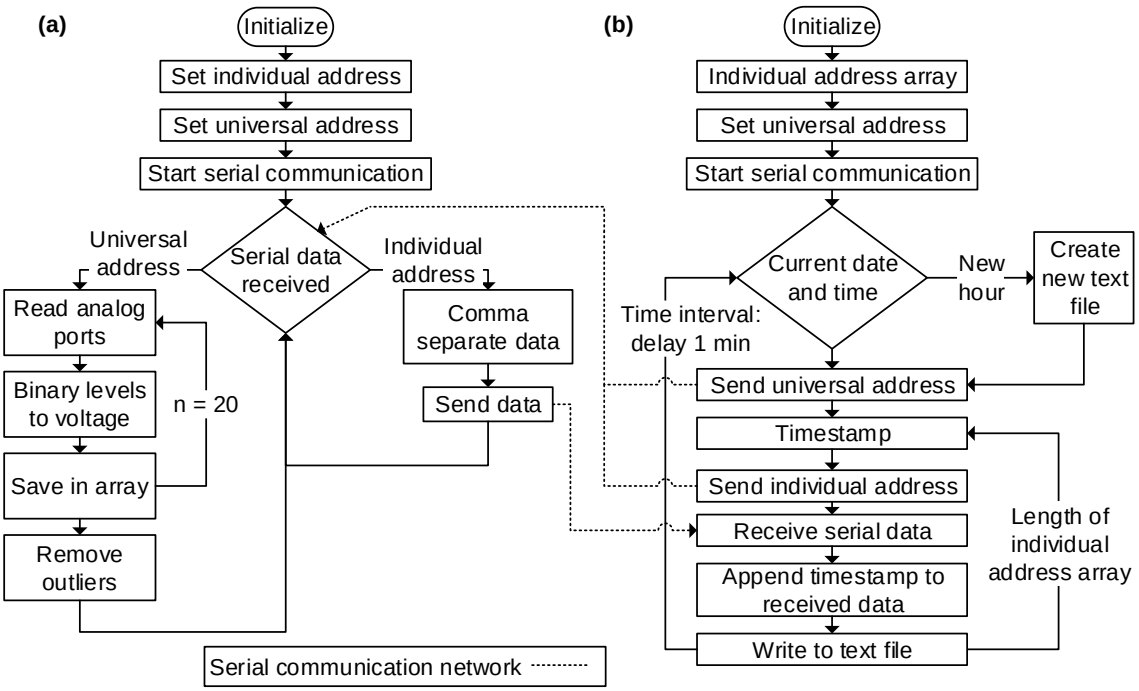

Figure 3.5. Pseudo algorithm for custom (a) TESA DAQ program (executed on microcontroller) and (b) CDMS software (executed on notebook computer). The universal address is a command for all TESAs to begin to measure values; while the individual address is to announce one TESA to send back data. The time interval between each loop in CDMS is adjustable to determine the sampling interval.

Field deployment

As part of a larger study, a total of 44 TESAs were deployed in a deep-pit, wean-finish swine facility located within 8.9 km of Pocahontas, IA, USA (42°44'04.2"N, 94°40'18.4"W) from August 8th, 2016 to January 25th, 2017 (figure 3.6). The goal was to collect preliminary data on the ability of TESA to describe the TE inside each room under normal production operating conditions and then assess the robustness of TESA after a flow of pigs. The facility featured two side-by-side rooms, with room dimensions (L × W × H) of 61 m × 15.2 m × 2.54 m and each housing ~1200 hd in 12 pens. The length of the building was orientated along the East-West axis. The negative pressure ventilation system was fully mechanical with power (i.e., fresh air distributed through ceiling inlets in cold to mild conditions) to tunnel (i.e., fresh air pulled the length of the building

from the tunnel curtain at the one end wall to fans at the other end wall in hot conditions) operation. Ambient t_{db} and RH were recorded at the facility by the ventilation controller every 15 min. A total of 22 TESAs were suspended about 1 m above the fully-slated concrete floor in each room corresponding to figure 3.6. A text file containing the comma-separated data from all 44 TESAs at a 1 min sampling interval was created and saved every hour on removable flash memory.

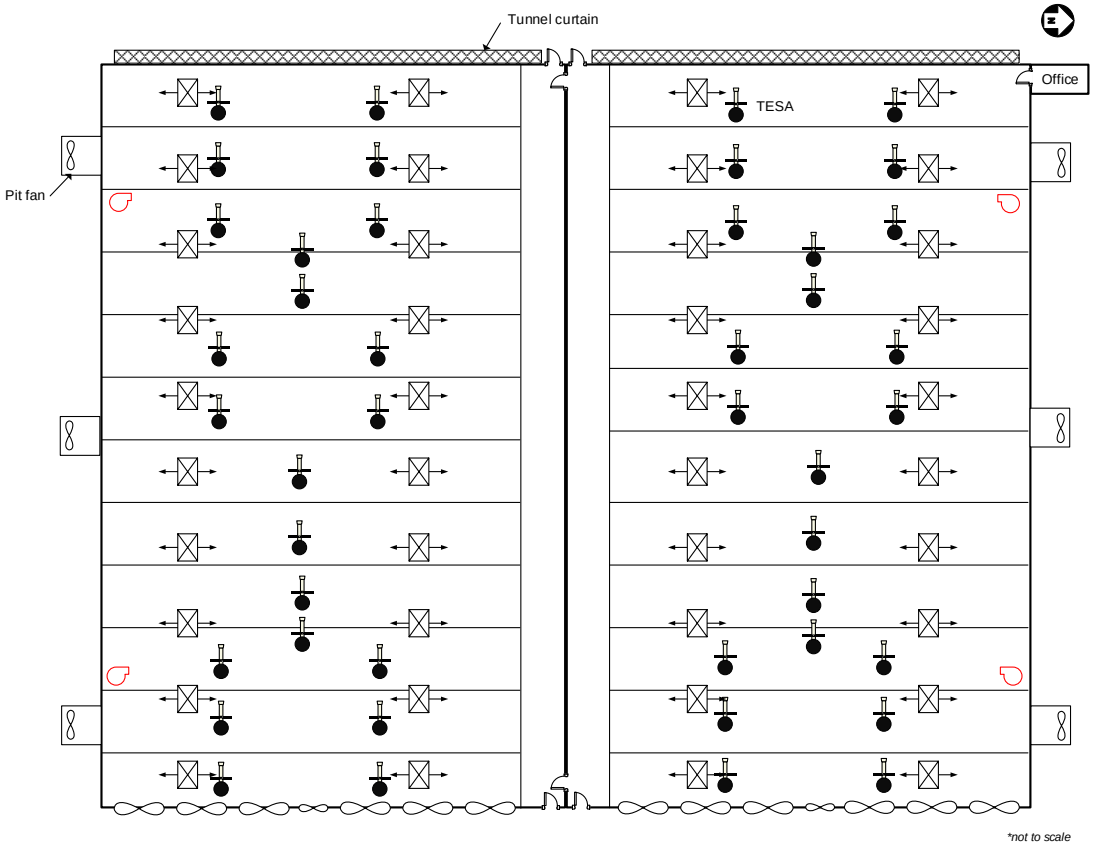

Figure 3.6. Schematic of TESA installation as a part of a larger study. A total of 44 TESAs were deployed in deep-pit, wean-finish swine facility located within five miles of Pocahontas, IA, USA from August 8th, 2016 to January 25th, 2017.

Data post-processing

Text files were first imported into Matlab (R2017a, The Mathworks, Inc., Natick, Massachusetts, USA) with any rows of data containing unimportable cells excluded (i.e., garbled text, etc.). Each row of data (corresponding to a TESA) was first checked to make sure at least 15

measurements were included in the mean value that was returned by the TESA DAQ. Next, analog voltages for the thermistors were inspected to be between a rational range of 1 to 4 V_{DC}. Any values outside this range were discarded. Similarly, for the digital t_{db} and RH, values outside of 10°C and 40°C and 5% and 100%, respectively were discarded. Data were then saved to .mat files to decrease future processing time. Analog voltages were then transformed to physical values following the equations in Gao et al. (2016). Data were filtered again to confirm values were within the measurement limit of the sensors and no erroneous data types were present. All faulty, missing, or discarded data were stored as Not-a-Number.

Mean radiant temperature

For calculation of t_{mr}, the thermal balance (ISO) equating radiative exchanges of surrounding surfaces to the losses due to convection was solved using the t_g, BGT diameter, assumed emissivity, t_{db}, and airspeed. The standard equation presented in ISO, assumes the BGT is at steady-state conditions, which is valid when the TE in the room changes slower than the response time of the BGT. In a typical swine production facility, forced air furnaces in the winter cause rapid increases in t_{db}, faster than the response time of the BGT, which consequently falsely decreases the estimation of t_{mr}.

Field performance evaluation

Once the barn was no longer stocked and prior to washing, the system was powered down and each TESA was enclosed in a yellow plastic bag, and then secured to the ceiling to avoid possible moisture damage from power washing. After the rooms were cleaned, each TESA was removed from the bag and approximately one week of empty facility data was collected. The Mobile Temperature and Relative Humidity Reference (MTRHR) system was then used to validate the t_{db} and RH sensors of all 44 TESAs.

Experimental setup

The MTRHR featured a 1500 W electric resistance heater with a transition to a 0.1524 m diameter flex duct that contained an inline fan to constantly supply tempered air to a vertical 0.2032 m diameter galvanized round duct (figure 3.7). Each TESA was placed inside the vertical duct, near a reference t_{db} and RH sensor (HMP110 with HMT120, Vaisala, Helsinki, Finland). The reference sensor analog signals were conditioned with a divider circuit and processed with a 16-bit analog to digital converter (ADS-1115, Adafruit Industries LLC, New York City, New York, USA) interfaced with a microcontroller (Arduino Micro, Arduino LLC, Italy).

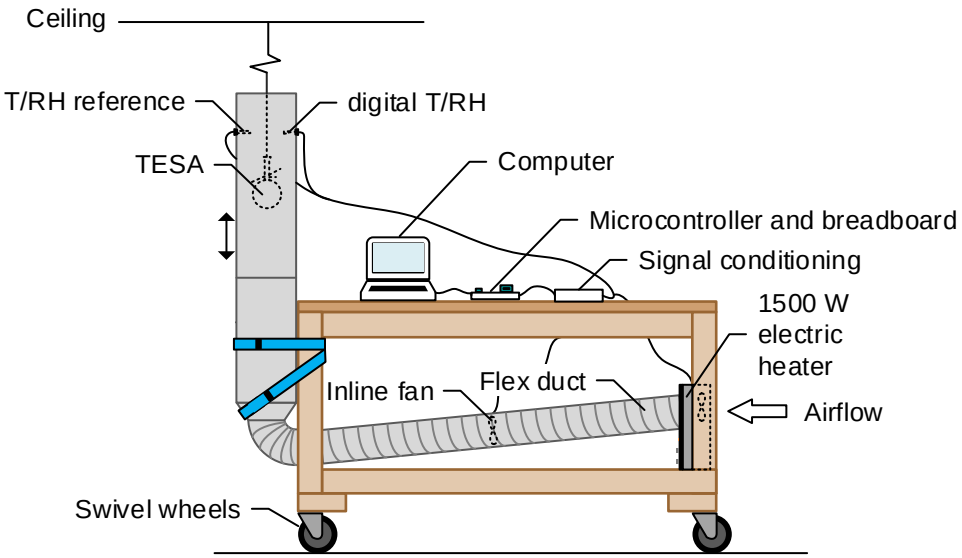

Figure 3.7. Schematic of Mobile Temperature and Relative Humidity Reference (MTRHR) system used to evaluate each TESA in the facility after about six months of recording.

Procedure

For each sensor, initial conditions and the difference between the initial conditions and the steady-state conditions were uniquely determined due to fluctuating conditions in the room. The initial condition was determined as the mean of 12 measurements (~36 s) prior to the step change. Once in the duct, the sensors were monitored for about 4 to 5 min.

Once the sensor was at steady-state conditions (as determined by the time constant of a first-order model), 12 measurements were randomly selected from the data to decoupled the time dependence between measurements. These randomly selected measurements were then averaged to form the mean steady-state value. The same approach was applied to the reference sensor measurements.

Time constant

The time constant of the thermistor t_{db}, digital t_{db}, and RH sensors for each TESA was determined by measuring the response to a step change from the ambient conditions inside the room to the tempered, steady conditions inside MTRHR. A nonlinear, least squares regression (R2017a, The Mathworks, Inc., Natick, Massachusetts, USA) of temperature (equation 3.1a; step-up) and RH (equation 3.1b; step-down) versus elapsed time was performed to determine the time constant (τ), assuming first-order system behavior. The time constant served as a metric to determine the time to reach steady-state conditions, estimated by 4τ (~99% of the steady-state value), to enable subsequent calculation of the mean steady-state value (i.e., single-point calibration value).

$$t_{db}(t) = t_{db_0} + \delta t_{db}\left(1 - e^{\frac{-t+t_0}{\tau}}\right) \tag{3.1a}$$

$$RH(t) = RH_0 + \delta RH\left(e^{\frac{-t+t_0}{\tau}}\right) \tag{3.1b}$$

where

$x(t)$	= TESA sensor response as a function of time (°C or %)
x_0	= initial mean sensor value at time t_0 (°C or %)
δx	= difference between x_0 and x at steady-state (°C or %)
t	= time (s)
t_0	= initial time (s)
τ	= time constant (s^{-1})

Statistical analysis

A Welch's t-test was performed to determine if the mean reference value was statistically different from the mean TESA sensor value during steady-state conditions with the variances of the sensor and reference assumed to be unequal and estimated from independent assessments of standard uncertainty. Contributors to the zeroth-order uncertainty (table 3.2) for the reference t_{db} and RH sensor (provided by the manufacturer) were stated accuracy (±0.2°C; ±1.5%), factory calibration uncertainty (±1.1%), stability over 2 years (±2%), and analog output accuracy (HMT120; ±0.1% full scale output signal; ±0.05°C; ±0.125%).

Table 3.2. Zeroth-order uncertainty budget for the sources needed to determine the standard uncertainty associated with reference t_{db} and RH measurements.

Parameter	Value	Probability distribution	Divisor	Standard uncertainty
$\Delta^0 t_{ref}$ [a]	0.12°C	Normal	1	0.12°C
$\Delta^0 RH_{ref}$ [b]	1.16%	Normal	1	1.16%
ΔR_{ref} [c]	2.49 Ω	Rectangular	√3	1.44 Ω
ΔV_{ref} [d]	3.81E-5 V BL^{-1}[e]	Rectangular	√3	2.20E-5 V BL^{-1}

[a] t_{db} zeroth-order standard uncertainty from manufacturer specifications
[b] RH zeroth-order standard uncertainty from manufacturer specifications
[c] divider resistor (249 Ω) tolerance (±1.0%)
[d] ±0.5 ADS-1115 16-bit ADC resolution = 7.63E-5 V BL^{-1}
[e] Binary Level (BL)

For a single measurement sample, the standard uncertainty associated with the reference t_{db} and RH measurement (equation 3.2) was determined by propagating the sources (ΔR_{ref} and ΔV_{ref}; table 3.2) through the analytical solution derived from the divider circuit (Appendix A).

$$\Delta x_{ref}{}^2 = \left(\frac{\partial x_{ref}}{\partial V_{ref}}\Delta V_{ref}\right)^2 + \left(\frac{\partial x_{ref}}{\partial R_{ref}}\Delta R_{ref}\right)^2 \quad (3.2)$$

where

Δx_{ref} = single sample reference standard uncertainty (°C or %)
ΔV_{ref} = analog voltage standard uncertainty (V_{DC})
ΔR_{ref} = divider resistor standard uncertainty (Ω)

The combined standard uncertainty associated with the mean steady-state t_{db} and RH reference (equation 3.3) was determined as the root-sum square of the standard uncertainty associated with

each sample (equation 3.2) comprised in the mean, the zeroth-order standard uncertainty (table 3.2), and the standard error of the mean steady-state value.

$$\Delta\bar{x}_{ref}{}^2 = \frac{\sum \Delta x_{ref}{}^2}{n} + \left(\Delta^0 x_{ref}\right)^2 + \left(\frac{s_{ref}}{\sqrt{n}}\right)^2 \tag{3.3}$$

where

$\Delta\bar{x}_{ref}$ = mean steady-state reference combined standard uncertainty (°C or %)
$\Delta^0 x_{ref}$ = zeroth-order standard uncertainty for reference sensor (°C or %; table 3.2)
s_{ref} = steady-state standard deviation for reference sensor (°C or %)
n = number of steady-state measurements

Similarly, for a given TESA sensor, the combined standard uncertainty associated with the mean steady-state value (equation 3.4) was determined as the root-sum square of the zeroth-order standard uncertainty (table 3.1), and the standard error of the mean steady-state value.

$$\Delta\bar{x}_{TESA}{}^2 = (\Delta^0 x_{TESA})^2 + \left(\frac{s_{TESA}}{\sqrt{n}}\right)^2 \tag{3.4}$$

where

$\Delta\bar{x}_{TESA}$ = mean steady-state TESA combined standard uncertainty (°C or %)
$\Delta^0 x_{TESA}$ = zeroth-order standard uncertainty for TESA sensor (°C or %; table 3.1)
s_{TESA} = steady-state standard deviation for TESA sensor (°C or %)

Equation 3.5 provides the basis for a hypothesis test whether a TESA sensor was unacceptable (i.e., significant bias exists). Assuming $\bar{x}_{TESA}$and $\bar{x}_{ref}$ are distributed according to a normal distribution with the standard error estimated by equation 3.3. Then, z_{calc} is distributed according to a normal distribution with mean zero and unity variance, with infinite degrees of freedom. The test for significance was two-sided.

$$z_{calc} = \frac{\bar{x}_{TESA} - \bar{x}_{ref}}{\sqrt{\Delta\bar{x}_{TESA}{}^2 + \Delta\bar{x}_{ref}{}^2}} \tag{3.5}$$

where

z_{calc} = z-statistic
$\bar{x}_{TESA}$ = mean TESA sensor steady-state value (°C or %)
$\bar{x}_{ref}$ = mean reference steady-state value (°C or %)

For $\bar{x}_{ref}$ found to be significant ($p < 0.05$), a bias correction was applied to the TESA sensor measurement (equation 3.6).

$$x'^{*}_{TESA} = x'_{TESA} + \left(\bar{x}_{TESA} - \bar{x}_{ref}\right) \quad (3.6)$$

where
x'^{*}_{TESA} = bias corrected future measured value (°C or %)
x'_{TESA} = future measured value (°C or %)

Since it was infeasible to have a calibration reference wind tunnel present for the OTA, airspeed was assessed on a relative basis, that is, Chauvenet's criterion with a maximum allowable deviation of less 2.52 was used to eliminate outliers, and then a box-and-whisker diagram was utilized to visualize the data.

Results and discussion

Thermal environment sensor array

A TESA was estimated to cost approximately 120 USD (excluding the cost of labor) for custom PCB, sensors, housing, and accompanying hardware. Additionally, three-conductor wire, the RS-485 bus to USB converter, and a computer and needed. The concept of TESA is similar to networks created for commercial buildings calculate and/or control predicted mean vote (Tse & Chan, 2008; Ye, Yang, Chen, & Li, 2003), except, TESA has been sealed and weatherproofed to be suitable in animal production environments.

Field deployment

The TESA DAQ system was deployed inside the facility for 170.51 d and on average (95% CI), collected 154.54 d (152.16, 156.93) of data at a sampling interval of approximately 1.1 min. This sampling interval was longer than originally targeted (1 min) due to the increase in wire between TESA DAQs that was not previously tested. Total number of usable measurements (after

post-processing) for all sensors per TESA averaged 202,310 (199,187, 205,437). The minimum and maximum total number of measurements for all TESAs were 164,124 and 207,280, respectively.

The most common cause for data loss during deployment was attributed to automatic updates restarting the operating system of the notebook computer running the CDMS (accounted for ~10 days). Other issues were due to the CDMS consuming too much memory, which required a restart of the notebook computer. Other problems encountered included several sensors malfunctioning for unknown reasons and were replaced as soon as it was possible. Scrambled data was encountered from several TESA DAQs and was often attributed to loose wires at the screw terminals and an occasionally failed RS-485 to RS-232 converter.

Both wireless and wired sensors networks (i.e., signal transducers plus DAQ and transmission) have been developed using a variety of communication protocols and hardware interfaces to monitor indoor TE, each with a diverse range of successes and challenges (Ali, Zanzinger, Debose, & Stephens, 2016; Darr & Zhao, 2008; Darr, Zhao, Ehsani, Ward, & Stombaugh, 2005; Tse & Chan, 2008). Wireless sensor networks offer reduced installation labor and time as sensors and nodes can easily be placed throughout a building and lack long connecting wires; however, this can adversely affect costs, and require optimization of the location of network nodes and base stations to ensure data transmission is reliable. Also, if the terminal nodes are powered by a portable power source (e.g., batteries), labor is required to ensure the network has power.

Dust accumulation on all the sensors, except the OTA, was observed within the first several weeks. The OTA was maintained at approximately 100°C, which was able to burn the dust particles before they were able to accumulate on the heated thermistor. The digital t_{db} and RH

sensor was intentionally mounted with sensing elements pointing down (figure 3.1) and the back of the sensor housing facing upward. This approach lessened the effect of dust; however, the results of the field performance evaluation do show some variability among sensors. The top half of the BGT accumulated a thicker film of dust, which will have a subsequent effect on the emissivity and response time of the BGT. Dust in livestock and poultry facilities is still a major barrier for implementing advanced measurement systems.

In total, for all 44 TESAs each with five sensors, approximately 40.5 million data were collected. The magnitude of data and spatial discretization achieved by the TESA DAQ system will allow future data mining techniques to explore how the controllers and facility itself respond to changing climate conditions.

Field performance evaluation

Once the time to reach steady-state (4τ) was determined for each thermistor t_{db} and digital tdb and RH sensors, for all 44 TESAs, the mean TESA sensor value was statistically compared to the mean reference value during steady-state conditions.

Time constant

The time to reach steady-state and nonlinear regression statistics are summarized in table 3.3 for all 44 TESA thermistor t_{db}, digital t_{db}, and digital RH sensors. Examples of the data and first-order regression model fit are shown in figure 3.7. While the results of the analysis is unique to each TESA sensor, the summary in table 3.3 provides insight to the overall performance of the group of sensors. Since the TE inside the facility during the field performance evaluation was dynamic, x_0 were uniquely determined for each sensor; hence, variation in this mean of this value were anticipated. The difference between x_0 and x at steady-state (i.e., δx) was expected to have low variation as the heat source (1500 W) and inline fan flowrate were constant. Due to small

tolerances achieved in today's sensor manufacturing, τ should also have low variation; however, differences in τ between sensors was most likely attributed to the conditions the sensors experienced inside the barn. Time to reach steady-state was greatest for RH and smallest for the t_{db} thermistor (table 3.3). The RH sensing mechanism (capacitance) is susceptible to particulate matter accumulation and can easily result in longer response time and inaccurate measurements. The RMSE provides an estimate of the overall uncertainty over the regression and the validity of the first-order behavior assumption. In addition, inspection of coefficient of determination (R^2) for all sensors showed the nonlinear regression model accounted for greater than 90% of the variance.

Table 3.3. Summary of average (95% CI) of time to reach steady-state (4τ) and nonlinear regression statistics for the thermistor t_{db}, digital t_{db}, and digital RH sensors for all TESA (n = 44).

Parameter	x_0 (°C or %)	δx (°C or %)	τ (s^{-1})	4τ (s)	RMSE (°C or %)	R^2
t_{db}	13.84 (13.14, 14.53)	6.71 (5.96, 7.46)	21.79 (13.38, 30.21)	87.17 (53.5, 120.84)	0.4 (0.19, 0.61)	0.89 (0.83, 0.96)
$t_{db,d}$	11.87 (11.37, 12.38)	8.69 (8.03, 9.34)	45.84 (33.74, 57.94)	173.8 (124.15, 223.46)	0.33 (0.17, 0.5)	0.96 (0.92, 1)
RH	27.4 (25.08, 29.72)	23.69 (20.95, 26.43)	52.2 (40.76, 63.64)	208.8 (163.04, 254.55)	0.81 (0.48, 1.14)	0.96 (0.92, 1)

The time to reach steady-state was used to determine when steady-state conditions in the MTRHR system was achieved and the sensors could be calibrated. Also, this analysis provides insight to the response time of the sensors and the subsequent information that can be discerned from the data (i.e., ventilation response and the rate at which the TE changes inside the room).

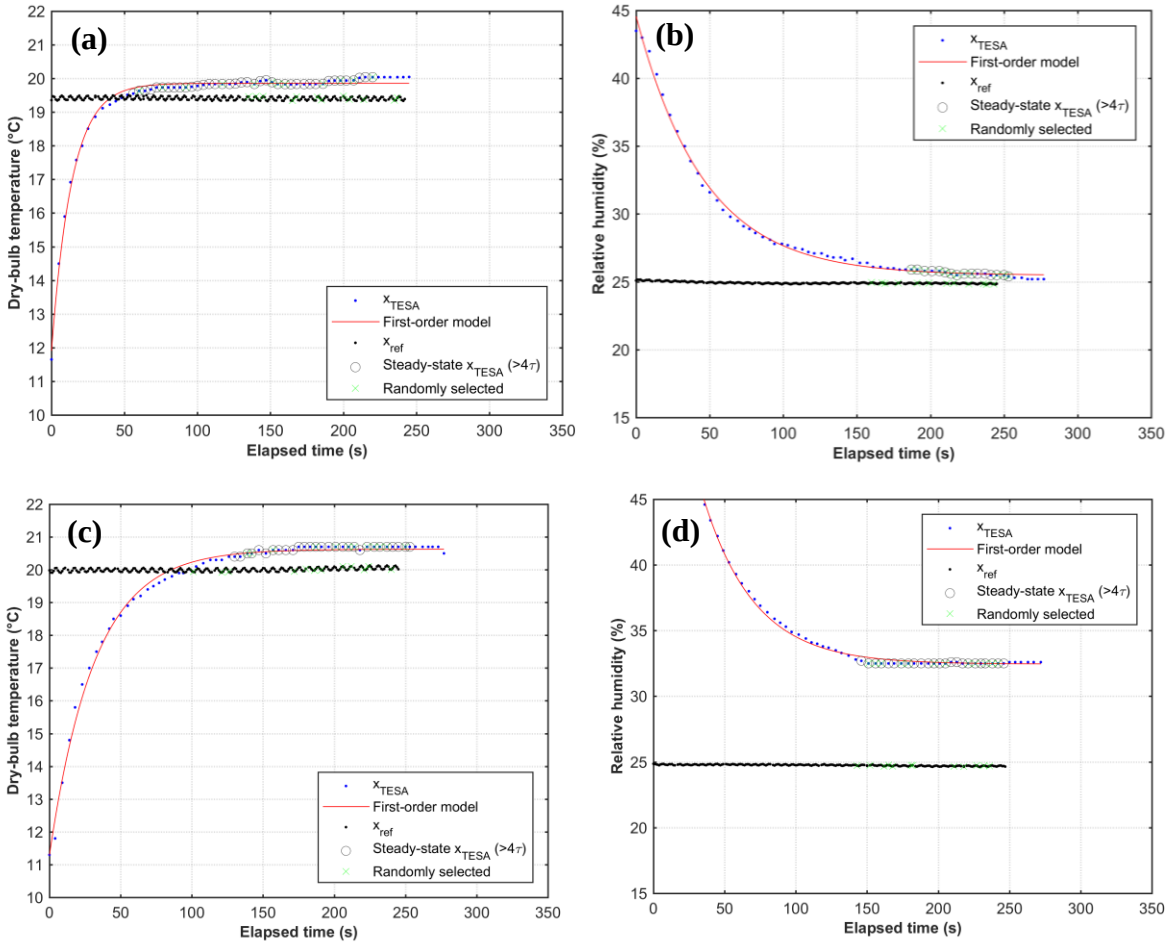

Figure 3.8. Example of first-order model fit to TESA tdb thermistor (a), RH (b and d), and digital tdb (c) data and measurements that were randomly selected from the estimated time to reach steady-state for both TESA and the reference. TESA sensors in (a), (b), and (c) did not require a bias correction, while (d) was found to be significantly different from the reference.

Calibration

A summary of the input parameters for equation 3.5 to calculate the t-statistic for assessing if a significant bias existed between the steady-state TESA and reference sensor values is presented in table 3.5. Figure 3.7 shows examples of data during the steady-state and which data were randomly selected to estimate the mean used for the significance test (equation 3.6). While the decision to correct measurements of a single TESA sensor was uniquely determined for each sensor, the summary in table 3.4 provides insight to the overall performance of the group of sensors. The standard deviation of the steady-state for both TESA and reference sensors was small,

as anticipated. In summary, 3 t_{db} thermistor, 4 digital t_{db}, and 12 RH sensors required correction after the 170.53 d inside the facility. Typically, RH sensors do not perform well in dusty and high ammonia environments. Overall, given the cost and accuracy of the selected digital T/RH sensor in this study, the performance was quite well.

Table 3.4. Summary of parameters for in-field calibration of all TESA thermistor t_{db}, digital t_{db}, and digital RH TESA sensors.

	Range (min, max) [a]						n with
Parameter	$\bar{x}_{TESA}$ (°C or %)	s_{TESA} (°C or %)	$\Delta\bar{x}_{TESA}$ (°C or %)	$\bar{x}_{ref}$ (°C or %)	s_{ref} (°C or %)	$\Delta\bar{x}_{ref}$ (°C or %)	p < 0.05[b]
t_{db}	15.32 - 23.42	0.03 - 4.32	0.31 - 1.29	14.84 - 21.4	0.01 - 18.38	0.37 - 5.33	3
$t_{db,d}$	17.19 - 25.54	0.04 - 3.06	0.31 - 0.94	14.84 - 21.4	0.01 - 18.38	0.37 - 5.33	4
RH	3.79 - 44.15	0.03 - 6.24	1.42 - 1.67	16.78 - 33.55	0.03 - 16.38	1.17 - 4.88	12

[a] n = 44
[b] that is, number of sensors that require bias correction

The standard uncertainty associated with the mean steady-state TESA and reference sensors was an estimate of the variance from the random sampling error (independent steady-state measurements) and the manufacturer's specifications. For a single measurement, Δx_{ref} was larger than anticipated, and after further inspection by a sensitivity analysis of the input parameters, the divider resistor tolerance (±1%) accounted for more than 98% of the total uncertainty. The other two sources of uncertainty ($\Delta^0 x_{ref}$ and SE), combined to only account for less than 6% of the total uncertainty associated with $\Delta\bar{x}_{ref}$. Even though the reference sensor was produced with high accuracy (low uncertainty), the required signal conditioning circuit (i.e., divider resistor) to obtain an analog voltage ultimately increased $\Delta\bar{x}_{ref}$. Signal conditioning circuits should utilize low tolerance (< ±1%) resistors. The lack of necessary signal conditioning circuitry for digital sensors is a major benefit.

Figure 3.8 graphically depicts the mean OTA airspeeds for each TESA obtained during calibration. Four OTAs were determined to require replacement. While there is some variability

in data (~1.5 to ~3.5 m s^{-1}), it is difficult to discern the source. It may be attributed to OTA changing over time or the experimental method. Slight differences in the manufacturing of each TESA may have results in the OTA being at different positions in the MTRHR duct; hence, different airspeeds.

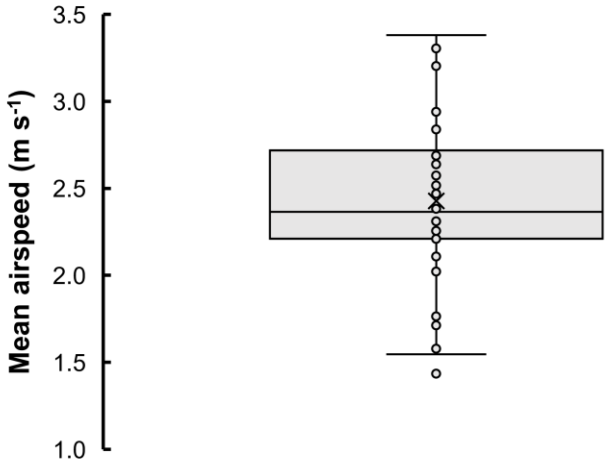

Figure 3.9. Box-and-whisker diagram for OTA during calibration.

Conclusions

A TESA and accompanying DAQ were developed and validated with a well-documented statement of measurement uncertainty for capturing the TE spatial distribution and temporal distribution in swine facilities. The utilization of low-cost sensors, open-source software, and microcontroller based control allowed this novel network to provide sufficient measurement density to promote future queries on the uses of TE data in livestock and poultry facilities.

A TESA can provide a complete description of parameters that influence the rate of heat exchange via the different modes (except conduction) that an animal experiences in its surroundings. Further, a network of TESAs allows for a high level of spatial discretization such that different regions of a facility can be evaluated in terms of uniformity, ventilation system performance, and ventilation controller performance. The capabilities of a TESA DAQ system

supports an enhanced ability to create and validate computational models that often lack all the TE parameters and discretization.

Livestock and poultry facility environments are difficult to instrument and maintaining quality measurements over time is even more challenging. The TESA DAQ system offers a robust approach to instrumenting these environments, while understanding sensors must be periodically cleaned and verified in order to maintain high sensor performance. Further, a modified t-test accounting for random error (from sampling) and sensor performance (manufacturer specifications) was created for conducting the single-point calibration and to determine statistically significant bias existed. While t_{db} affects convective and evaporative heat loss, it must be combined with other TE measurements to create a complete description of how an animal exchanges heat with its surrounding. The development of TESA is a necessary advancement in PLF.

Acknowledgments

This research was supported with funding provided by the Iowa Pork Producers Association under NPB Project 14-242. The authors would like to acknowledge the contributions of undergraduate students Grant Hoppes, Heather Tenboer, and Oluwadurotimi Koya during the preparation and completion of this work.

The research work of Yun Gao was partly supported by the National Key Research and Development Program of China (2016YFD0500506).

References

Ali, A. S., Zanzinger, Z., Debose, D., & Stephens, B. (2016). Open Source Building Science Sensors (OSBSS): A low-cost Arduino-based platform for long-term indoor environmental data collection. *Building and Environment*, *100*, 114–126. https://doi.org/10.1016/j.buildenv.2016.02.010

ASHRAE. (2013). *Handbook of fundamentals*. Atlanta, GA: America Society of Heating, Refrigeration and Air Conditioning Engineers.

Beckett, F. E. (1965). Effective Temperature for Evaluating or Designing Hog Environments. *Transactions of the ASAE*, *8*(2), 0163–0166. https://doi.org/10.13031/2013.40457

Bond, T. E., & Kelly, C. F. (1955). The globe thermometer in agricultural research. *Agricultural Engineering*, *36*(4), 251–255.

Bond, T. E., Kelly, C. F., & Heitman Jr, H. (1952). Heat and moisture loss from swine. *Agric. Eng*, *33*(3), 1948–154.

Brown-Brandl, T., Hayes, M., Xin, H., Nienaber, J., Li, H., Eigenberg, R. A., … Shepard, T. (2014). Heat and Moisture Production of Modern Swine. *ASHRAE Transactions*, *120*.

Curtis, S. E. (1983). *Environmental Management in Animal Agriculture*. Ames, IA: The Iowa State University Press.

Darr, M. J., & Zhao, L. (2008). A wireless data acquisition system for monitoring temperature variations in swine barns. American Society of Agricultural and Biological Engineers. https://doi.org/10.13031/2013.25614

Darr, M. J., Zhao, L., Ehsani, M. R., Ward, J. K., & Stombaugh, T. S. (2005). Evaluation of controller area network data collection system in confined animal feeding operations. American Society of Agricultural and Biological Engineers. https://doi.org/10.13031/2013.18363

DeShazer, J. A., Hahn, L., & Xin, H. (2009). Chapter 1: Basic Principles of the Thermal Environment and Livestock Engergetics. In James A. DeShazer, *Livestock Energetics and Thermal Environment Management* (1st ed., pp. 1–22). St. Joseph, MI: American Society of Agricultural and Biological Engineers.

Fournel, S., Rousseau, A. N., & Laberge, B. (2017). Rethinking environment control strategy of confined animal housing systems through precision livestock farming. *Biosystems Engineering*, *155*, 96–123. https://doi.org/10.1016/j.biosystemseng.2016.12.005

Gao, Y., Ramirez, B. C., & Hoff, S. J. (2016). Omnidirectional thermal anemometer for low airspeed and multi-point measurement applications. *Computers and Electronics in Agriculture*.

Hayes, M. D., Xin, H., Li, H., Shepherd, T. A., Zhao, Y., & Stinn, J. P. (2013). Heat and moisture production of Hy-Line brown hens in aviary houses in the Midwestern US. *Transactions of the ASABE*, *56*(2), 753–761.

ISO 7726. (2001). *Ergonomics of the thermal environment — instruments for measuring physical quantities*. Geneva: International Standardization Organization.

Mount, L. E. (1964). Radiant and convective heat loss from the new-born pig. *The Journal of Physiology*, *173*(1), 96–113.

Mount, L. E. (1967). The heat loss from new-born pigs to the floor. *Research in Veterinary Science*, *8*(2), 175–186.

Pereira, N., Bond, T. E., & Morrison, S. R. (1967). Ping-pong ball into black-globe thermometer. *Agricultural Engineering*, *48*(6), 341.

Purswell, J. L., & Davis, J. D. (2008). Construction of a low cost black globe thermometer. *Applied Engineering in Agriculture. ASABE*, *24*(3), 379–381.

Renaudeau, D., Gourdine, J.-L., & St-Pierre, N. R. (2011). A meta-analysis of the effects of high ambient temperature on growth performance of growing-finishing pigs. *Journal of Animal Science*, *89*(7), 2220–2230.

Tse, W. L., & Chan, W. L. (2008). A distributed sensor network for measurement of human thermal comfort feelings. *Sensors and Actuators A: Physical*, *144*(2), 394–402. https://doi.org/10.1016/j.sna.2008.02.004

UN. (2015). *World Population Prospects: The 2015 Revision, Key Findings and Advance Tables* (No. Working Paper No. ESA/P/WP.241). New York City, NY: United Nations, Department of Economic and Social Affairs, Population Division.

Vilela, M. O., Oliveira, J. L., Teles Junior, C. G., Tinôco, I. F., Baptista, F. J., Barbari, M., … Souza, C. F. (2015). Spatial variation of enthalpy in a commercial broiler house in a hot climate region. Retrieved from https://dspace.uevora.pt/rdpc/handle/10174/17506

Ye, G., Yang, C., Chen, Y., & Li, Y. (2003). A new approach for measuring predicted mean vote (PMV) and standard effective temperature (SET∗). *Building and Environment*, *38*(1), 33–44. https://doi.org/10.1016/S0360-1323(02)00027-6

Appendix 3. Equations

The following equations are the transfer functions for converting reference t_{db} and RH from analog voltage to a physical value for a single measurement sample. The standard uncertainty of the inputs to equations 1 and 2 (ΔR_{ref} and ΔV_{ref}) are propagated through equations 1 and2 to determine the standard uncertainty associated with reference t_{db} and RH measurements (equation 2).

$$t_{ref} = -40°\text{C} + (V_{t\_ref} - V_{out,low}) \times \left(\frac{(60°\text{C} - (-40°\text{C}))}{(V_{out,high} - V_{out,low})} \right) \quad (1)$$

$$RH_{ref} = 0\% + (V_{rh\_ref} - V_{out,low}) \times \left(\frac{(100\% - 0\%)}{(V_{out,high} - V_{out,low})} \right) \quad (2)$$

where

t_{ref} = reference dry-bulb temperature (°C)
V_{t_ref} = measured reference analog voltage (V_{DC})
$V_{out,low}$ = reference sensor minimum output voltage (V_{DC}; = 4 mA × R)
$V_{out,up}$ = reference sensor maximum output voltage (V_{DC}; = 20 mA × R)
R = divider resistor value (249 Ω)
RH_{ref} = reference relative humidity (%)
V_{rh_ref} = measured reference analog voltage (V_{DC})

CHAPTER 4. FUNCTIONAL PERFORMANCE EVALUATION OF A NOVEL THERMAL ENVIRONMENT SENSOR ARRAY

B. C. Ramirez, Y. Gao, S. J. Hoff, and J. D. Harmon

A manuscript submitted to *Transactions of ASABE*

This chapter describes the commissioning of a validation system created for the performance testing of the thermal environment sensor array (TESA; Chapter 3). A chamber was constructed to provide different combinations of dry-bulb temperature, relative humidity, airspeed, and surrounding surface temperatures to test a TESA at different combinations of thermal environment conditions. The goal of the validation was to compare estimated total heat loss from a theoretical heat transfer model with TESA measurements as inputs with the measured total heat loss from an ideal temperature source. Total heat loss estimated by TESA showed reasonable comparison with the ideal temperature source, indicating TESA may be a practical device to estimate total heat loss for swine (Chapter 5).

This chapter owes its success to the collaboration of Brett Ramirez, Yun Gao, Steven Hoff, and Jay Harmon. I led the design and construction of the validation system, commissioning of the validation system, research design and testing of TESA, collected and analyzed data, and drafted the manuscript. Drs. Gao, Harmon, and Hoff also contributed to the research design and revision of the manuscript.

Abstract

The Thermal Environment (TE) inside livestock and poultry facilities has a substantial impact on animal growth performance and facility energy usage; therefore, the TE must be quantified correctly to maintain the optimal TE that maximizes feed efficiency and consumes minimal

resources. To achieve this goal, the Thermal Environment Sensor Array (TESA) and accompanying data acquisition system were previously developed by Ramirez et al. (2017) to measure dry-bulb temperature (t_{db}), black globe temperature, airspeed, and relative humidity (RH). While measurement of each parameter is useful individually, it is more informative when they are combined to estimate and assess the total impact the TE is having on an animal. Hence, the objectives were to (1) design, construct, and commission a TE simulation system named Animal Thermal Environment Replication and Measurement System (AThERMS); and (2) compare total sensible heat loss estimated by TESA to a reference Ideal Temperature Source (ITS) when subjected to different TE conditions inside AThERMS. AThERMS is a 1.04 x 1.17 x 1.04 m chamber inside a large insulated enclosure, where air supplied by an air handling unit provides unique combinations of t_{db}, RH, and airspeeds, while independently controlling chamber surface temperature (t_s). Commissioning of AThERMS included a qualitative (smoke visualization) and quantitative (three-dimensional traverse) velocity characterization in the central region of the chamber and verification of similar and stable t_s for all six surfaces. Analysis of velocity contours at three nominal flowrates indicated steady patterns and at three nominal t_s (13°C, 23°C, and 33°C), during a 2 h steady state operation, that maximum average difference between any two of the six t_s was 0.26°C. Then, a TESA was suspended in AThERMS adjacent to the ITS (15.24 cm diameter black copper sphere with a heater immersed in water). Both ITS and TESA were subjected to two nominal airspeeds (~0.5 and 2.0 m s^{-1}), each at three nominal t_{db} (17°C, 25°C, and 33°C) with mean radiant temperature approximately equal to the nominal t_{db}. Total heat loss was estimated from heat transfer theory with TESA measurements as inputs and compared to measured root-mean square power required to maintain a constant water temperature in the ITS. Overall, predicted total heat loss underestimated measured power for all six tests. Future work

needs to improve the accuracy measuring power at low total heat losses. AThERMS can be used to simulate different TEs a housed animal may experience and provide steady reference conditions to verify TE measurements. TESA is a novel and effective tool for understanding the TE distribution and estimating total heat loss.

Introduction

Accurate quantification of the Thermal Environment (TE) inside livestock and poultry houses is essential for improving the production efficiency needed to address future global food security demands without neglect of environmental impact. The TE influences animal well-being, growth performance, and can place the animal at risk for adverse health effects (Ames, 1980; Close, 1987; Curtis, 1983; Renaudeau, Gourdine, & St-Pierre, 2011; Thuy, 2005). Often in both commercial and research settings, only dry-bulb temperature (t_{db}) and occasionally relative humidity (RH) are used to describe the TE. These two parameters alone can only be used to indirectly quantify sensible and latent heat loss. Further, when only t_{db} and RH are used to develop empirical indices (e.g., temperature-humidity index) relating the TE to an animal's behavioral and/or physiological response(s), these indices become invalid when other aspects of the TE change, that is, elevated airspeeds or extreme surrounding surface temperatures. Airspeed influences forced convective and evaporative heat loss, while surrounding surface temperatures describe the impact of thermal radiation. The addition of airspeed and mean radiant temperature are required to correctly model total heat loss and require monitoring to improve our understanding of the impact the TE has on animals. Hence, accurate quantification of the overall TE and estimations of total heat loss from easily measured TE parameters are needed to improve current measurement and ventilation systems.

A Thermal Environment Sensor Array (TESA) and accompanying Data Acquisition (DAQ) for measurement of t_{db}, black globe temperature, airspeed, and RH were previously developed by (Ramirez, Gao, Hoff, & Harmon, 2017). This robust measurement system has the capability to provide discretized, spatiotemporal TE data inside livestock and poultry facilities. A performance assessment of TESA is needed to ensure accurate individual measurements, as well as the combination of the four TE parameters, such that total heat loss can be accurately estimated. A reference measurement system that can provide a stable t_{db}, RH, airspeed, and mean radiant temperature to assess a TESA does not exist. Hence, the objectives were to (1) design, construct, and commission a TE simulation system termed the Animal Thermal Environment Replication and Measurement System (AThERMS); and (2) compare total sensible heat loss estimated by TESA to a reference Ideal Temperature Source (ITS) when subjected to different TE conditions inside AThERMS.

Materials and methods

The Animal Thermal Environment Replication and Measurement System (AThERMS) was first constructed and commissioned (Ramirez, Hoff, Gao, & Harmon, 2015), then used to conduct the functional performance evaluation of a Thermal Environment Sensors Array (TESA)(Ramirez, Gao, & Hoff, 2016). A TESA consisted of dry-bulb temperature (t_{db}) via thermistor, t_{db} and relative humidity (RH) via a digital sensor, airspeed, and black globe temperature (t_g) measurements. Airspeed was measured with a custom Omnidirectional Thermal Anemometer (OTA) and further details regarding the sensor design, calibration, and t_{db} compensation approach are described in (Gao, Ramirez, & Hoff, 2016). The t_g was used in the convective and radiative balance (ISO 7726, 2001) on the black globe to calculate mean radiant temperature (t_{mr}). A detailed description of the sensors and communication network can be found in (Ramirez et al., 2017).

AThERMS design and construction

The Animal Thermal Environment Replication and Measurement System (AThERMS; figure 4.1; figure 4.2; figure 4.3) was designed to simulate different radiative, convective, and evaporative TEs a housed animal may experience. Different t_{db}, RH, and airspeeds were simulated at the center of a large chamber constructed of 0.7 mm (0.0276 in.) thick sheet metal painted gloss white (assumed emissivity of 0.98) to replicate a "grey" body. Interior dimensions (L × W × H; figure 4.3) were 1.04 × 1.17 × 1.04 m (41 × 46 × 41 in.). All six sides of the chamber (>90% of area in thermal radiation exchange with a black globe) were maintained at the same surface temperature (t_s). The inlet to the chamber featured a 0.15 m (6 in.) diameter opening with a 4.77 mm (0.188 in.) perforated hole diameter diffuser, to straighten the flow and increase the surface area of the wall (as opposed to leaving the inlet open). The outlet consisted of a 0.20 m (8 in.) diameter opening, with 6.35 mm (0.25 in.) hole perforated hole diameter diffuser mounted in the center of the wall opposite the inlet (figure 4.1). The inlet and outlet were sealed with weather stripping and the interior of the chamber was sealed with silicone. A sealed door (figure 4.2) was positioned on the inlet side to allow access to the interior of the chamber. AThERMS was housed inside a larger Insulated Enclosure (IE; figure 4.1) constructed of 0.051 m (2 in.) thick rigid foam board insulation (R-10) with exterior dimensions (L × W × H) of 2.44 × 2.44 × 1.83 m (8 × 8 × 6 ft). Concentric ring diffusers placed on opposite sides of the IE distributed air around AThERMS, inside the IE to control t_s (figure 4.1). A 0.15 m (6 in.) diameter outlet (top of the IE) returned air back (figure 4.1) to the Air Handling Unit (AHU; figure 4.1) with make-up air from the room available when required. A t_{db} and RH sensor (HMP-133Y, Vaisala, Helsinki, Finland) was located near the return in the IE.

The AHU (figure 4.1; AA-5474, Parameter Generation and Control, Black Mountain, NC, USA) conditioned air (at a set t_{db} and RH) supplied to both AThERMS (figure 4.2) and IE (figure 4.1) through a 0.15 m (6 in.) diameter duct split via a wye with flow controlled to AThERMS by an actuated damper (figure 4.1; figure 4.2; remaining flow went to the IE diffusers). Maximum flow provided by the AHU was 0.33 m^3 s^{-1} (700 cfm) with 3000 W (10236 BTU h^{-1}) sensible heating and 5275 W (1.5 ton) cooling capacity.

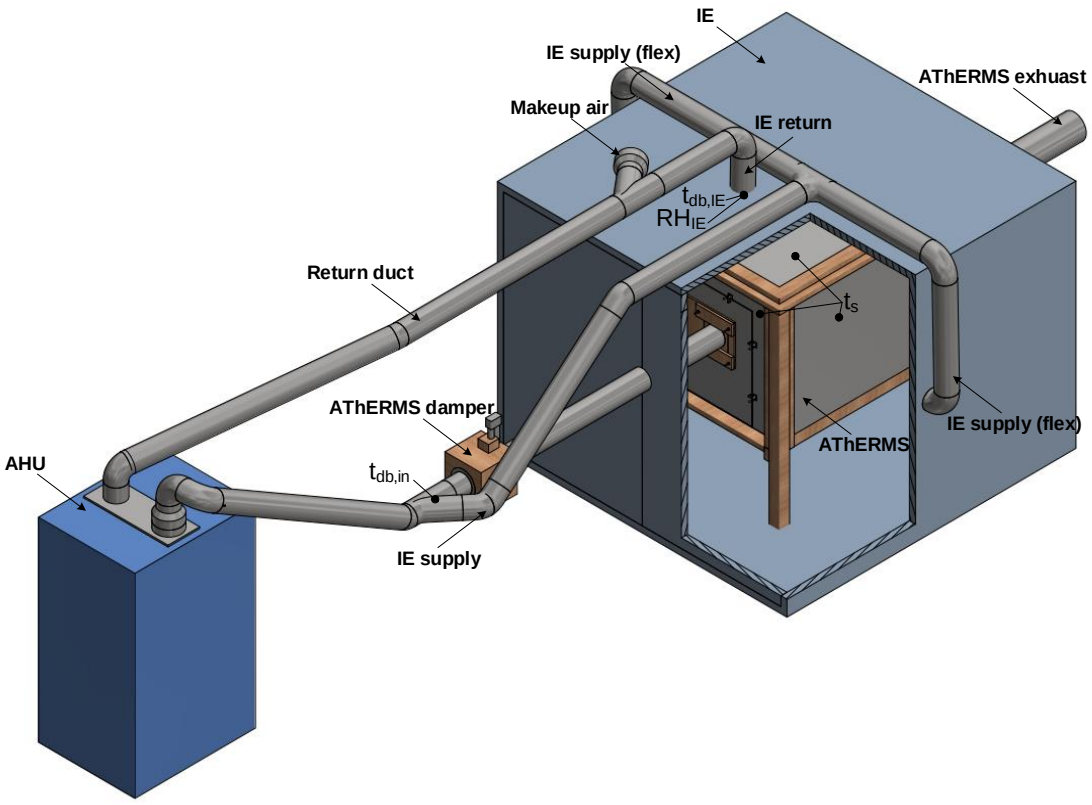

Figure 4.1. Schematic of AHU, IE, and AThERMS. Conditioned air from AHU to AThERMS was controlled by an actuated damper with excess flow supplied to each side of IE via flex duct (modeled as rigid for simplicity). AThERMS exhausted air to the room and air circulating around AThERMS and inside IE was returned back to AHU.

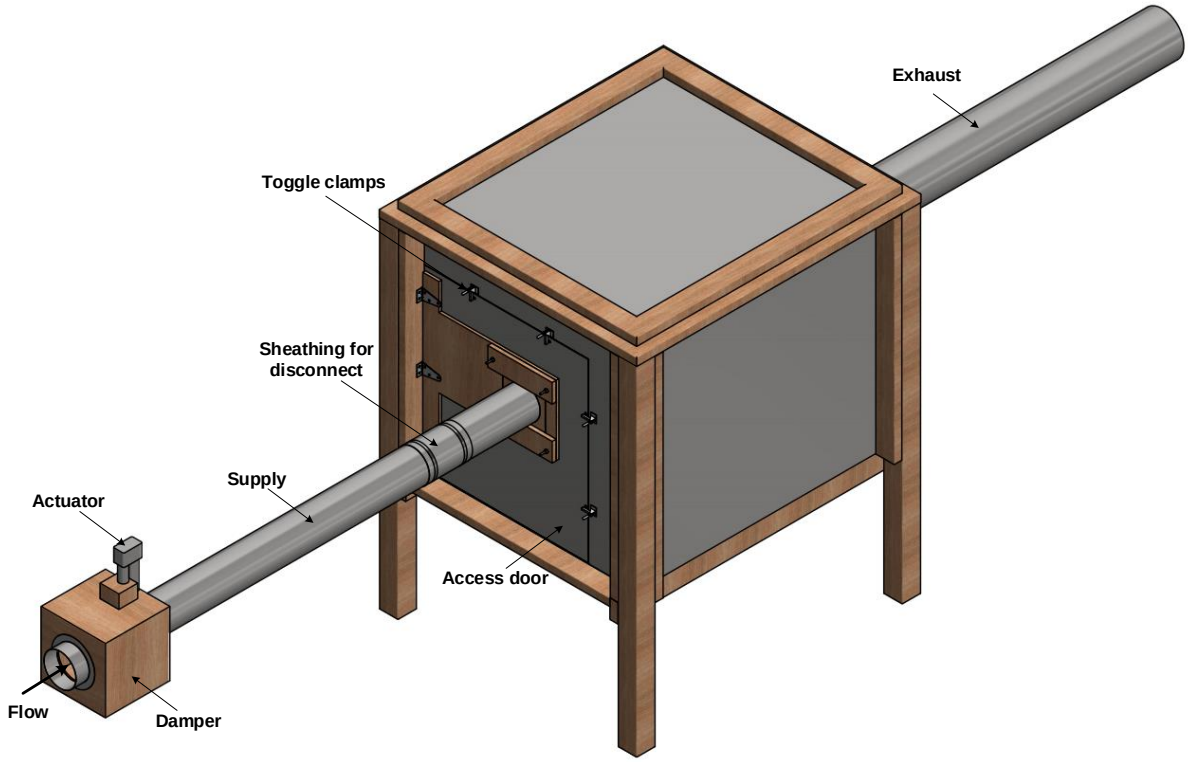

Figure 4.2. Detailed schematic of AThERMS from figure 4.1. An actuated damper controlled flow from AHU, supplied via rigid duct. A sheathing secured by hose clamps connected the access door duct to the supply duct. Toggle clamps secured the weather-stripped access door in place.

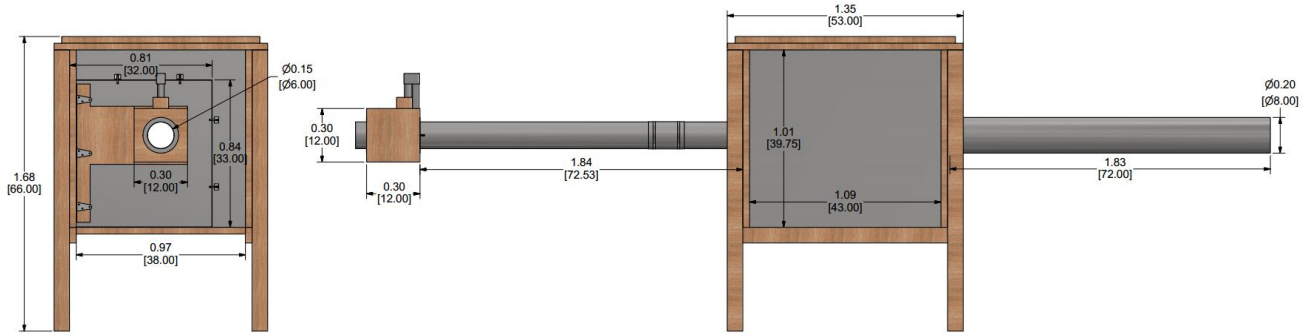

Figure 4.3. Dimensioned drawing of AThERMS. All units in meters [in.].

AThERMS performance evaluation

AThERMS performance was verified to provide a consistent and stable TE after completion and prior to TESA functional performance testing.

Airspeed

Flow through AThERMS was visualized using smoke (S102, Regin HVAC Products, Inc., Oxford, CT, USA) injected into the supply duct and recorded with a small video camera. Light sources were placed on the bottom of the chamber and black background was added opposite of the camera to aid in visualization of the flow patterns.

Three nominal supply flowrates: (i) low, (ii) medium, and (iii) high, controlled by the actuated damper (figure 4.1; figure 4.2), were used to evaluate airspeeds (commonly found in swine facilities) in the central region (figure 4.4a) of AThERMS. A three-dimensional traverse (figure 4.4) was conducted using a hot-wire anemometer (Model 8455, TSI Inc., Shoreview, MN, USA) across an 0.25 × 0.25 × 0.20 m (10 ×10 × 8 in.) volume. Three 12 V_{DC} linear actuators (HDA10-2 and HDA8-2, Robotzone LLC., Winfield, KS, USA) moved the anemometer in the x, y, and z directions (figure 4.4b), and about 243 measurement locations were randomly tested. Velocity was assumed only in the y-direction (figure 4.4a) and confirmed by smoke visualization. Position of anemometer relative to center of the chamber was determined by calibrating actuator displacement against the analog response (from an internal 10kΩ potentiometer) and measuring the offset for the side and bottom surfaces. Six airspeeds per measurement location were sampled every second from the anemometer, which internally calculates the average every 50 ms. Average velocity at each measurement location was used to determine TI and construct a three-dimensional velocity profile using three-dimensional linear interpolation of a 5 mm (0.2 in.) mesh grid. All uniformity tests were conducted at a constant $t_{db,in}$ (20°C) and RH_{in} (50%).

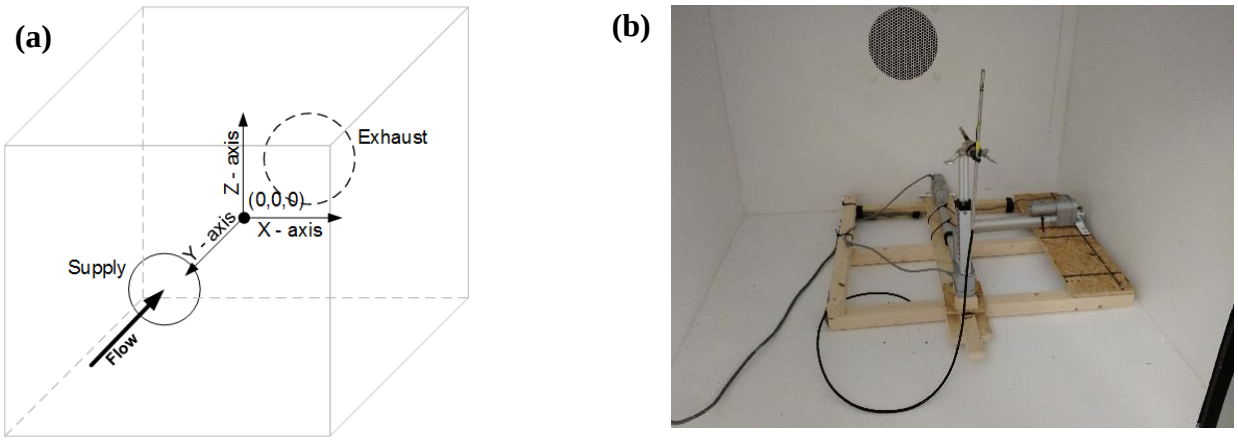

Figure 4.4. (a) Coordinate system for airspeed measurements with the origin at the center of the chamber. (b) Three linear actuators used to complete three-dimensional airspeed traverse in the center (location of BGT) using a hot-wire anemometer.

Dry-bulb and surface temperature

Ambient temperature stability was confirmed by using a t_{db} sensor (NTCLE413E2 thermistor, Vishay Intertechnology Inc., Malvern, PA, USA) located near the center of AThERMS. A datalogger (Micro, Arduino LLC, Italy) sampled t_{db} every 2 s and was recorded with custom developed software (Python 2.7, Python Software Foundation, Beaverton, Oregon, USA).

A stable and evenly distributed t_s on each of the six sides of AThERMS was verified using six digital infrared (IR) temperature sensors (MLX90614, Melexis NV, Leper, Belgium) each mounted to a surface of a small cube (figure 4.5a) which was suspended in the center of AThERMS (figure 4.5b) and a t_s was recorded every 6 s (Uno R3, Arduino Inc., Italy). The IR cube placement was verified to not impact t_s prior to testing by placing the IR cube in the center of AThERMS. The IR sensors were calibrated by the manufacturer with an emissivity of 1.0; hence, t_s was corrected using the Stefan-Boltzmann law and the interior surface emissivity of AThERMS.

Mean IR t_s was analyzed during the steady-state phase for nominal AHU supply set points ($t_{db,in}$): (i) 13°C (55.4°F), (ii) 23°C (73.4°F), (iii), 33°C (91.4°F). An uncertainty analysis (table 4.1) was performed for the IR sensor to establish the confidence in t_s. Standard uncertainties obtained from the Type B evaluation were much greater than the Type A evaluation (i.e., standard error); thus, standard error was neglected but still identified to emphasize its importance (table 4.1).

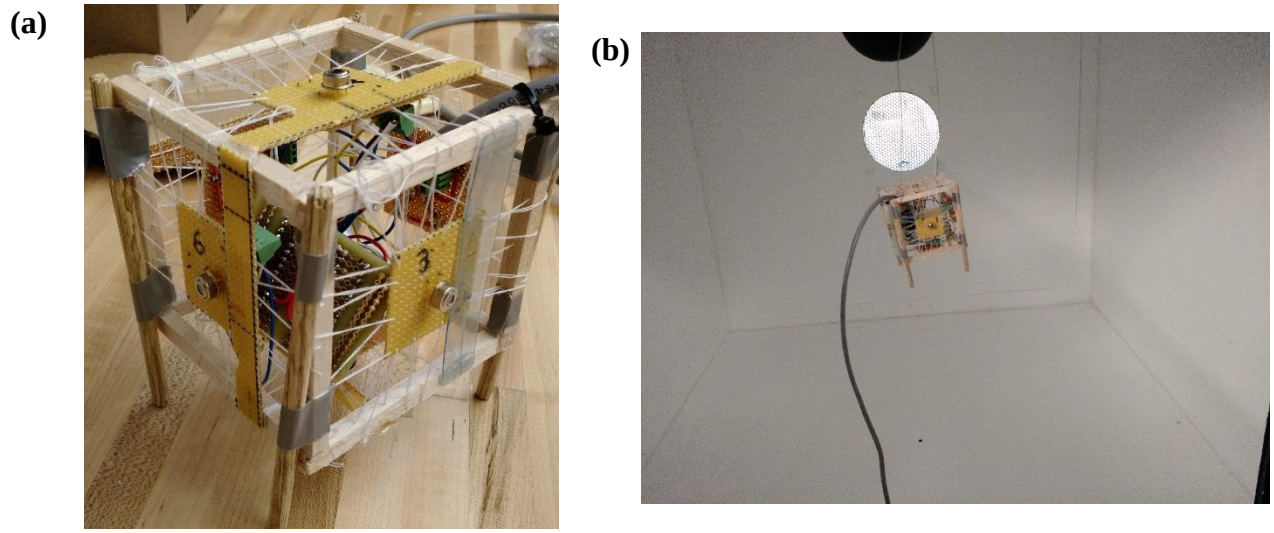

Figure 4.5. (a) Close up of six digital IR sensors mounted on each surface of a cube and (b) suspended in the center of AThERMS.

Table 4.1. Uncertainty analysis for digital IR sensor. Standard error was very small relative to other standard uncertainties; thus, neglected.

Source	Value (°C)	Probability distribution	Divisor	Standard uncertainty (°C)
Standard Error	-	Normal	1	-
Reading Resolution[1]	0.01	Rectangular	√3	8.33E-6
Accuracy[2]	0.5	Rectangular	√3	0.083
Measurement Resolution[3]	0.02	Rectangular	√3	0.003
Combined standard uncertainty				0.29
Coverage factor, k[4]				2
Expanded uncertainty				0.58

[1] indicated t_s can lie with equal probability anywhere in the interval t_s – 0.005 to t_s + 0.005
[2] range: 0°C to 50°C
[3] SMBus protocol resolution, indicated t_s can lie with equal probability anywhere in the interval t_s – 0.01 to t_s + 0.01
[4] approximately 95% confidence interval and infinite degrees of freedom

A nonlinear, least squares regression was performed in Matlab (R2016a, The Mathworks, Inc., Natick, Massachusetts, USA) on the mean t_s (i.e., all six sides averaged) versus elapsed time to

determine the time constant (τ, ~63%) for heating and cooling the system (equation 4.1). The time constants served as a metric to determine the time to reach steady-state. The time to reach steady-state was estimated by 3τ (~95% of the steady-state value), assuming first-order system behavior (equation 4.1).

$$t_s(t) = t_{s,0} + \Delta t_s \left(1 - e^{\frac{-t+t_0}{\tau}}\right) \quad (4.1)$$

where

$t_s(t)$ = surface temperature as a function of time (°C)
$t_{s,0}$ = initial t_s at time t_0 (°C)
Δt_s = difference between $t_{s,0}$ and t_s at steady-state (°C)
t = time (min)
t_0 = initial time (min)
τ = time constant (min)

TESA performance evaluation

The performance of a TESA was assessed by subjecting the TESA to various TE conditions inside AThERMS. Individual TESA measurements were compared with respect to reference conditions and then, the combination of individual measurements was used to estimate total heat loss compared to the power required to maintain an Ideal Temperature Source (ITS).

Analytical analysis

An ITS (i.e., a source of thermal energy that can maintain a specified temperature regardless of thermal energy exchange by the system) will ultimately balance the power required to maintain a specified temperature with the combined convective and radiative losses of the TE (equation 4.2). For any object, the transient sensible thermal balance is:

$$mc\frac{dT}{dt} = q''_{gen} - q''_{conv} - q''_{rad} \quad (4.2)$$

where

m = mass (kg)
c = specific heat of mass (J kg^{-1} K^{-1})
T = absolute temperature of an object's mass (K)
t = time (s)
q''_{gen} = generated heat flux inside an object (W m^{-2})
q''_{conv} = convective heat flux (W m^{-2})
q''_{rad} = radiative heat flux (W m^{-2})

Assuming steady-state and substituting in the appropriate rate equations yields (equation 4.3):

$$q_{gen} = h_{cv}A(T_s - T_{db}) + \epsilon\sigma A(T_s^4 - T_{mr}^4) \quad (4.3)$$

where

q_{gen} = total generated heat (W)
h_{cv} = convective heat transfer coefficient for an object's geometry (W K^{-1} m^{-2})
A = object surface area (m^2)
T_s = surface absolute temperature (K)
ϵ = emissivity (0.95)
σ = Stefan-Boltzmann constant (5.6697E-8 W m^{-2} K^{-4})
T_{mr} = mean radiant temperature (K)

The sensible TE can be quantified by TESA and then used to estimate the sum of the convective and radiative losses (q_{total}), with knowledge of the object's geometry. The sensible heat balance states q_{total} must equal the rate of thermal energy being generated inside ITS (equation 4.4); thus, measurement of electrical power to maintain the ITS at a constant temperature (equation 4.4) was the reference value to compare with q_{total} (equation 4.3) estimated by TESA.

$$q_{gen} = P_{gen} = V_{AC}I_{RMS} = q_{total} \quad (4.4)$$

where

P_{gen} = measured electrical power to maintain ITS at constant temperature (W)
I_{RMS} = root-mean-square AC current (A)
V_{AC} = AC voltage (120 $V_{AC\ RMS}$)
q_{total} = predicted combined radiative and convective heat loss by TESA (W; equation 4.3)

Experimental setup

The ITS was a 0.15 m (6 in.) diameter copper sphere with 1.09 mm (0.04 in.) thick walls painted flat black and filled with water (1.85 L; 113 in^3; figure4. 6). The sphere replicated a

geometry with well-known empirical heat transfer relations for forced and natural convection. A 6.03 cm (2.4 in.) long, 100 W electrical cartridge resistance heater (HDL00001, TEMPCO Electric Heater Corp., Wood Dale, Illinois, USA) was secured in a 1.27 cm (0.5 in.) diameter hole bored at the top of the sphere. A TRIAC (AC-VXP/N:180V800E, Control Resources, Inc., Littleton, MA, USA) transformed a 0 to +5 V_{DC} input to control AC output to the heater. A metal wire shaped in a zigzag pattern was inserted inside the sphere and rotated with constant speed to enhance mixing and heat distribution from the cartridge heater; therefore, it was assumed the ITS had an isotropic surface temperature. A waterproof temperature sensor was placed in the water and acted as the feedback sensor for proportional–integral–derivative (PID) control of the water temperature ($t_{water;}$ figure 4.6). A 4-channel, 16-bit analog to digital converter (ADS1115, Adafruit, New York City, New York, USA) was interfaced with a microcontroller (Micro, Arduino LLC, Italy) that contained a custom DAQ and PID (v1.0.1, PID Library, Beauregard, 2015) control software created in the integrated development environment of the microcontroller.

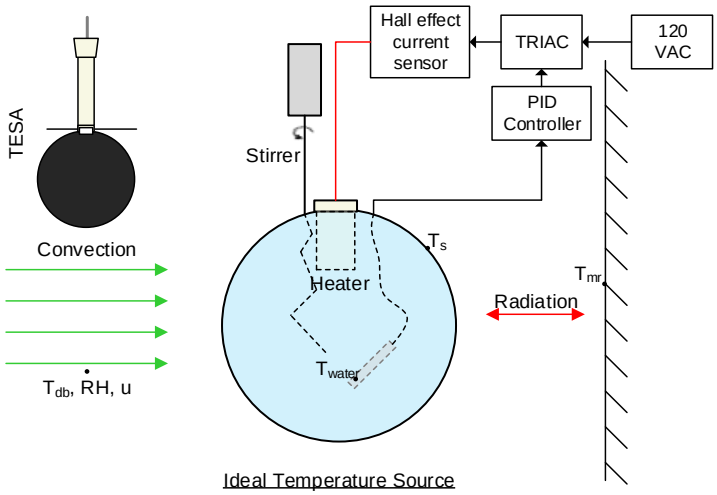

Figure 4.6. Experimental setup with thermal environment sensor array and ideal heat source (black sphere with a heater).

Data acquisition and procedure

Two nominal airspeeds (~0.5 and 2.0 m s^{-1}) were tested at three nominal t_{db} (17°C, 25°C, and 33°C) where t_{mr} was equal to the nominal t_{db}. Water temperature setpoint was 39°C to approximate the core body temperature of a pig. Data were recorded in a comma delimited text file and processed using Matlab (R2016a, The Mathworks, Inc., Natick, Massachusetts, USA). The t_{db}, t_{mr}, and t_{water} of ITS were allowed to reach steady-state prior to estimating q_{total} and for calculating the RMS power required by the ITS. Once at the steady-state condition, the analysis was conducted over at least a 30 min interval. Raw voltage measurements were transformed to their corresponding physical value, and then the physical quantity was averaged over the steady-state period.

A Simulink model was developed and used to solve for the theoretical q_{total} using TESA measurements and compared to measured power required to maintain the ITS at a constant t_{water}.

Results and discussion

AThERMS performance evaluation

Airspeed

Flow visualization with smoke confirmed the magnitude of velocity to be predominately in the y-direction (figure 4.7a). Although some smoke swirls in the center of AThERMS, a steady jet forms as air enters the chamber and exits through the outlet (figure 4.7b). Some air collides with the surface surrounding the outlet and recirculates back to form the jet (figure 4.7c).

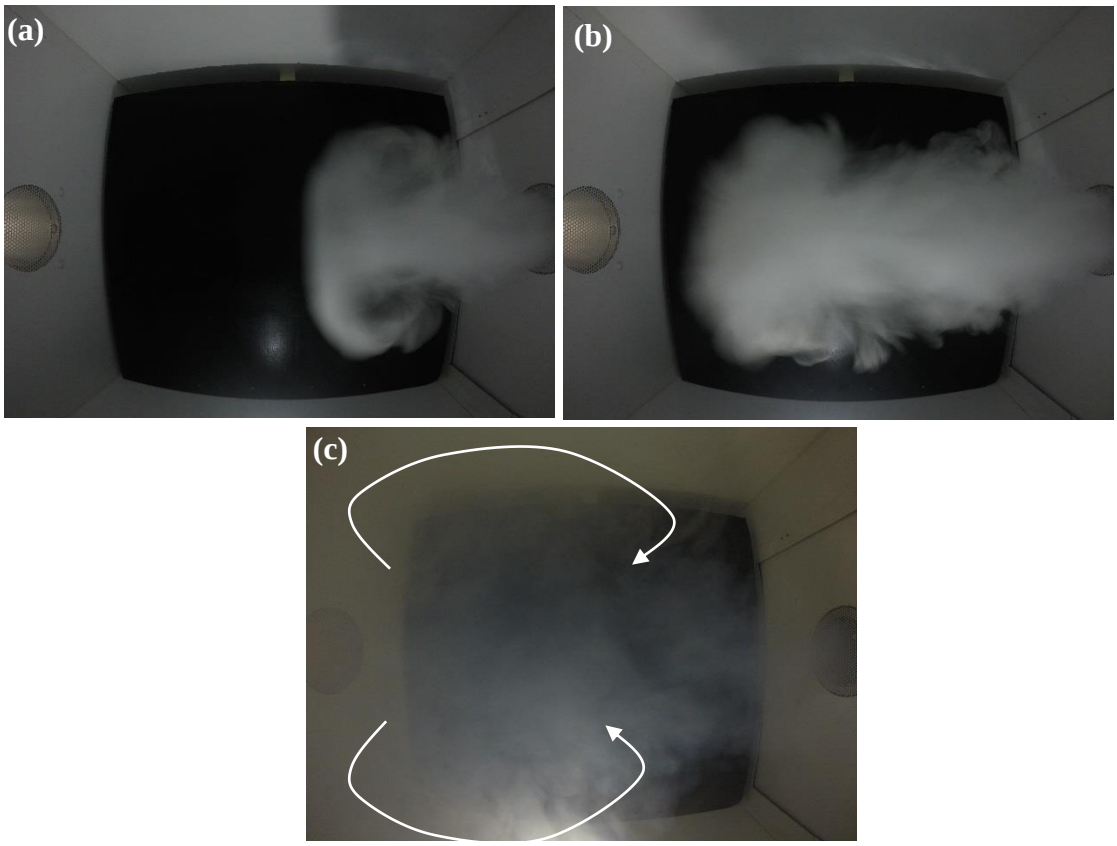

Figure 4.7. At a nominal low flow, (a) smoke initially entering AThERMS, (b) formation of the jet, and (c) some smoke circulates back to the jet.

Each of the three nominal supply flowrates tested (low, medium, high), showed consistent velocity profiles in the central region of AThERMS (figure 4.8). These results aided in determining possible locations of the OTA that accurately reflects the typical convective environment experienced by TESA. The OTA must not impact t_{mr} measurement or measure airspeed in the boundary region around the sphere. The optimum location is the best estimate of the "free stream" airspeed passing the ball. Control of and uniform flow patterns are not always possible in commercial swine facilities.

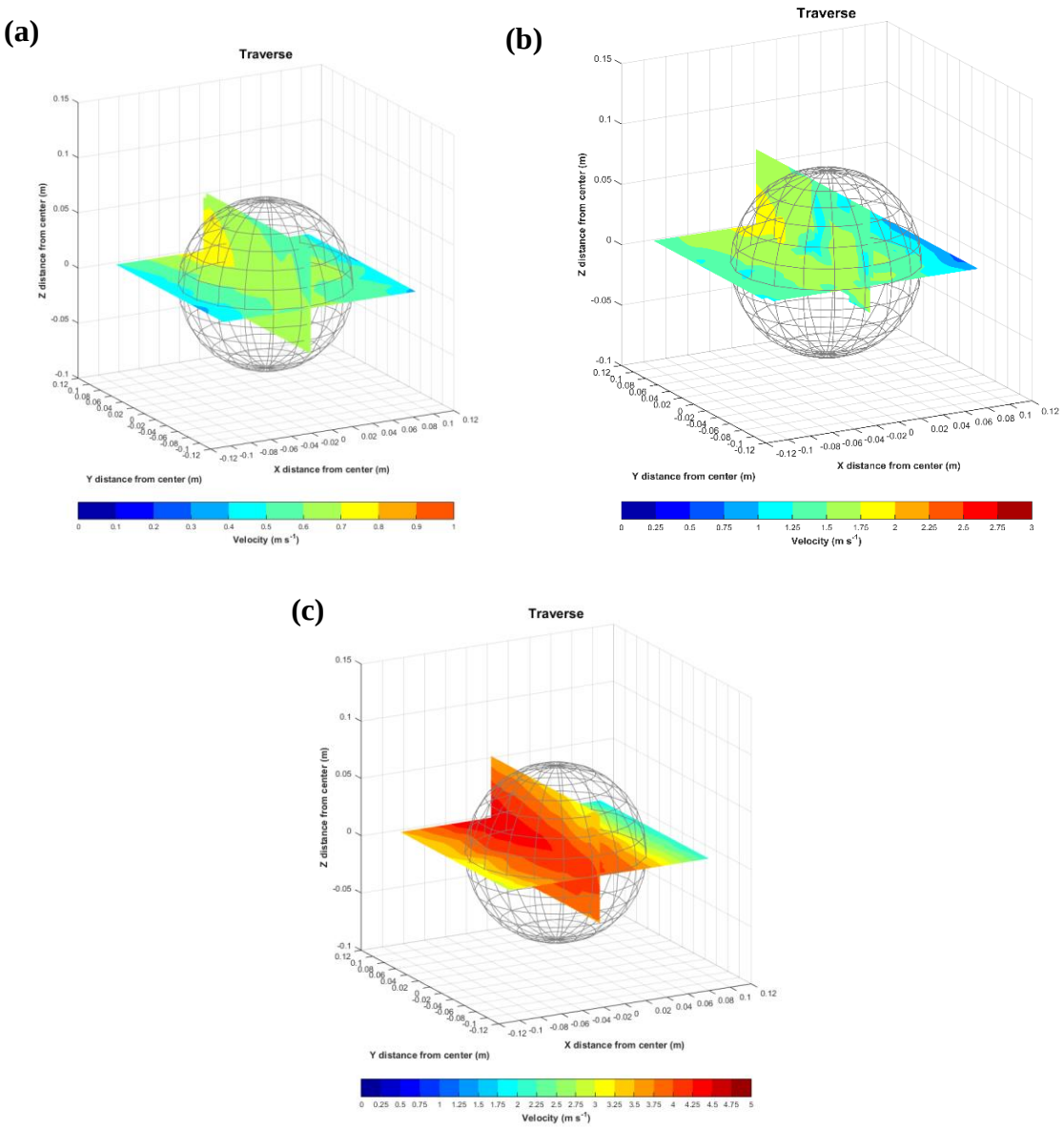

Figure 4.8. Velocity visualization for (a) low, (b) medium, and (c) high nominal supply flowrates where TESA was located in AThERMS.

Dry-bulb and surface temperature

A stable temperature inside AThERMS ($t_{db,bgt}$) was observed for each of the three nominal AHU set points (table 4.2). This indicates a reliable t_{db} for determining convective heat transfer

coefficients for the TESA and ITS. Low fluctuations in $t_{db,in}$ from the AHU considerably aided in maintaining stable t_s and $t_{db,bgt}$.

Table 4.2. Mean (± standard deviation) of steady-state temperatures at three nominal supply set point temperatures.

	Nominal AHU supply temperature (°C)		
Surface ID[1]	13	23	33
$t_{s,left}$	14.66 ± 0.05	23.03 ± 0.03	31.66 ± 0.11
$t_{s,top}$	14.54 ± 0.05	23.01 ± 0.04	31.81 ± 0.10
$t_{s,back}$	14.60 ± 0.05	22.96 ± 0.04	31.55 ± 0.11
$t_{s,bottom}$	14.65 ± 0.05	23.01 ± 0.04	31.63 ± 0.10
$t_{s,front}$	14.61 ± 0.05	22.97 ± 0.04	31.58 ± 0.11
$t_{s,right}$	14.49 ± 0.07	23.07 ± 0.05	31.83 ± 0.10
Dry-bulb temperature ID			
$t_{db,in}$[2]	13.03 ± 0.06	23.03 ± 0.06	33.00 ± 0.07
$t_{db,IE}$[3]	14.67 ± 0.11	22.82 ± 0.02	30.97 ± 0.13
$t_{db,bgt}$[4]	14.95 ± 0.07	23.06 ± 0.03	31.17 ± 0.13

[1] n = 2898
[2] n = 480
[3] n = 481
[4] n = 7610

All six interior surfaces of AThERMS were found to provide uniform and stable surface temperatures at the three nominal supply air temperatures ($t_{db,in}$) tested (figure 4.9; table 4.2). At 23°C $t_{db,in}$ (figure 4.9b), mean t_s was very similar to mean $t_{db,in}$ (supplied to both AThERMS and IE), while for the 13°C (figure 4.9a) and 33°C (figure 4.9c) $t_{db,in}$, mean t_s was higher and lower than the $t_{db,in}$, respectively. This difference was most likely attributed to heat loss through the uninsulated supply ducts and the IE. Ambient dry-bulb temperature of the room housing the IE and AThERMS was approximately 22°C and flow to AThERMS was about 0.0064 $m^3\ s^{-1}$ (13.5 CFM) while the remaining flow went to the IE (increases heat losses through the supply ducts). This explanation also rationalizes the difference between $t_{db,in}$ and $t_{db,IE}$. At 23°C, mean t_s was very similar to mean temperature inside AThERMS ($t_{db,bgt}$), while at 13°C and 33°C, mean t_s was lower and higher than the $t_{db,bgt}$, respectively. This difference is not statistically significant based on the standard uncertainties of the two measurement sensors and DAQs. A possible explanation may be

due to a slight difference in assumed emissivity of the digital IR sensor and the actual emissivity of the white surface or the influence of temperature on the digital IR sensor measurement. Further, these results simplify the thermal radiation network from seven nodes (six surfaces plus the BGT) to a trivial two-node problem, since all six t_s are equal there is no thermal radiation exchange between them. This corroborates the theoretical assumption of the "large enclosure" scenario, where the surroundings are a uniform temperature.

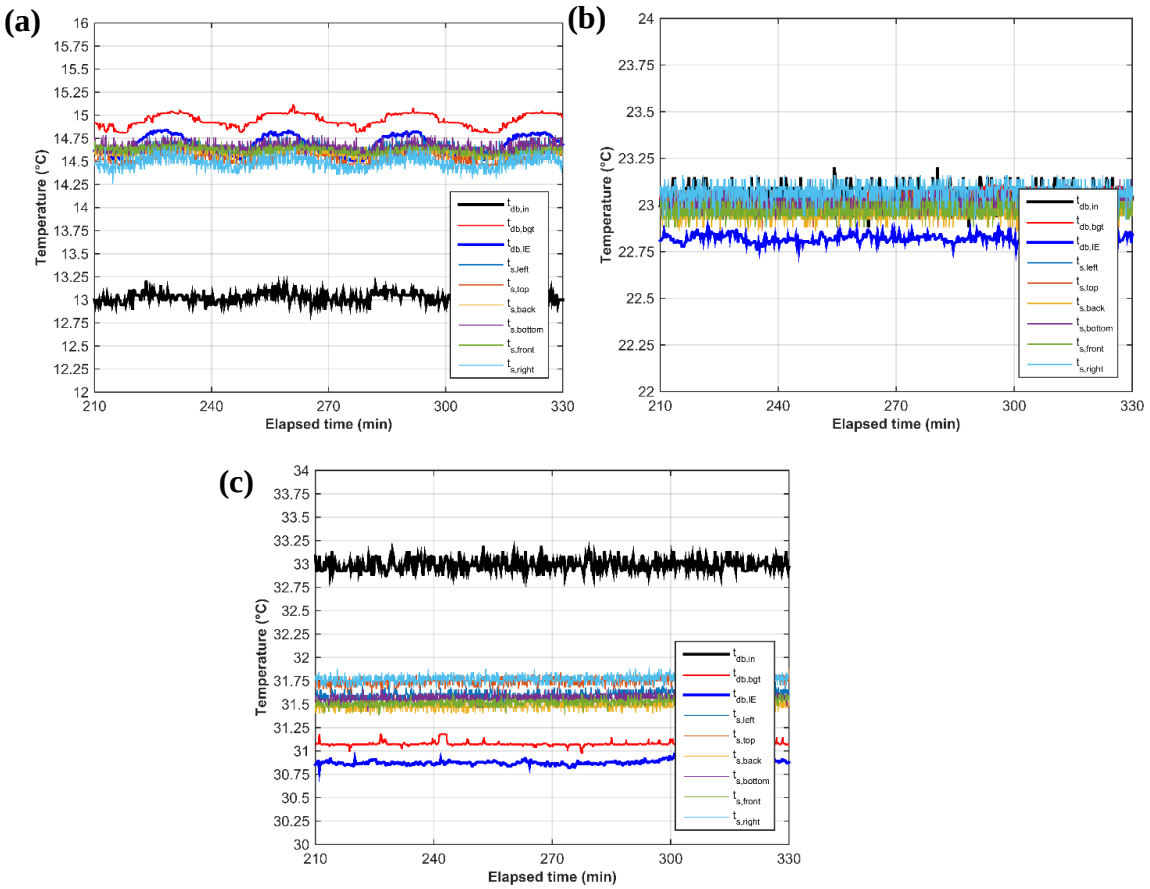

Figure 4.9. For three nominal AHU supply set point temperatures ($t_{db,in}$), (a) 13°C, (b) 23°C, and (c) 33°C, results showed uniform and stable surface temperature and AThERMS dry-bulb temperature.

Time to reach steady-state (3τ) was 85.2 min (cooling) and 42.0 min (heating; table 4.3). Coefficients of determination (R^2) were greater than 0.97 for each regression (figure 4.10). The Root Mean Square Error (RMSE) provided an estimate of the overall uncertainty over the regression. Heating caused the system to reach steady-state faster compared with cooling, due to

the equipment in the AHU. Sensible heat was directly transferred to the air by five looped coils, whereas for cooling, air passes through an evaporative cooling spray chamber. Time to reach steady-state was used to improve experimental and operational protocols when a TESA or any other sensor are placed inside the AThERMS.

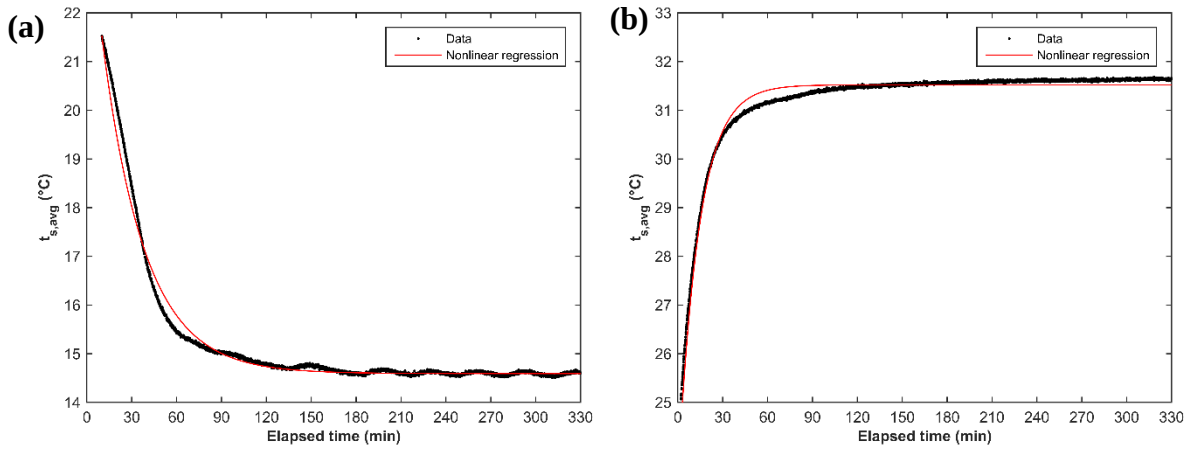

Figure 4.10. Nonlinear regression to determine the time constant for (a) cooling and (b) heating AThERMS.

Table 4.3. Nonlinear regression coefficients and statistics summary to estimate the time to reach steady state (3τ) for cooling and heating AThERMS.

Nominal AHU supply temperature (°C)	$t_{s,0}$ (°C)	Δt (°C)	t_0 (min)	R^2	RMSE (°C)	Time to reach steady-state (min)
13	21.5	-6.98	10.05	0.986	0.1602	85.2
33	24.5	7.02	2.08	0.979	0.1364	42.0

TESA performance evaluation

Six experiments were conducted at two airspeeds for three nominal t_{db}. A summary of the steady-state average from measurements obtained at ITS and TESA is provided in table 4.4. Overall, during the steady-state condition, both the power output of the heater (figure 4.11) and the TE inside AThERMS (figure 4.12) were stable; however, airspeed had a range of about 0.1 m s^{-1}, most likely attributed to turbulence. The resultant impact on calculation of q_{total} was negligible. The unique design of AThERMS allows for this fine control and stable supply of different TE.

Table 4.4. Summary of average (± standard deviation) TE conditions and ITS water temperature during each of the six experiments. The last row, t_{mr_IR}, was obtained from the IR sensor cube to verify the t_{mr} calculation.

Parameter	Test 1	Test 2	Test 3	Test 4	Test 5	Test 6
$t_{db\_digital}$ (°C)	17.2 ± 0.01	25.50 ± 0.04	33.53 ± 0.03	33.15 ± 0.05	25.50 ± 0.01	18.77 ± 0.05
$t_{db\_thermistor}$ (°C)	17.39 ± 0.01	25.51 ± 0.01	33.56 ± 0.05	32.91 ± 0.01	25.42 ± 0.04	18.82 ± 0.03
Airspeed (m s^{-1})	2.19 ± 0.03	2.22 ± 0.03	2.22 ± 0.03	0.42 ± 0.04	0.43 ± 0.03	0.38 ± 0.04
t_{water} (°C)	39.02 ± 1.07	39.01 ± 0.08	39.26 ± 0.13	39.13 ± 0.12	38.97 ± 0.11	39.31 ± 0.35
t_{mr} (°C)	17.39 ± 0.01	25.51 ± 0.01	33.67 ± 0.26	33.2 ± 0.04	25.37 ± 0.09	18.53 ± 0.07
t_{mr_IR} (°C)	17.27 ± 0.16	25.24 ± 0.09	33.21 ± 0.06	33.03 ± 0.07	25.13 ± 0.06	17.85 ± 0.12

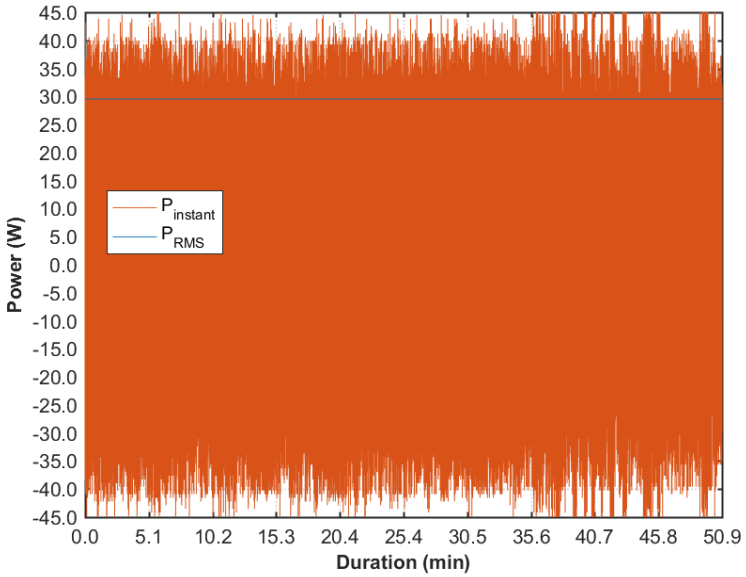

Figure 4.11. Example of instantaneous power measurement and calculated Root-Mean Square (RMS) power for test 2 during the steady-state period. The RMS power was compared with the theoretical heat loss predicted from TESA measurements and a Simulink model.

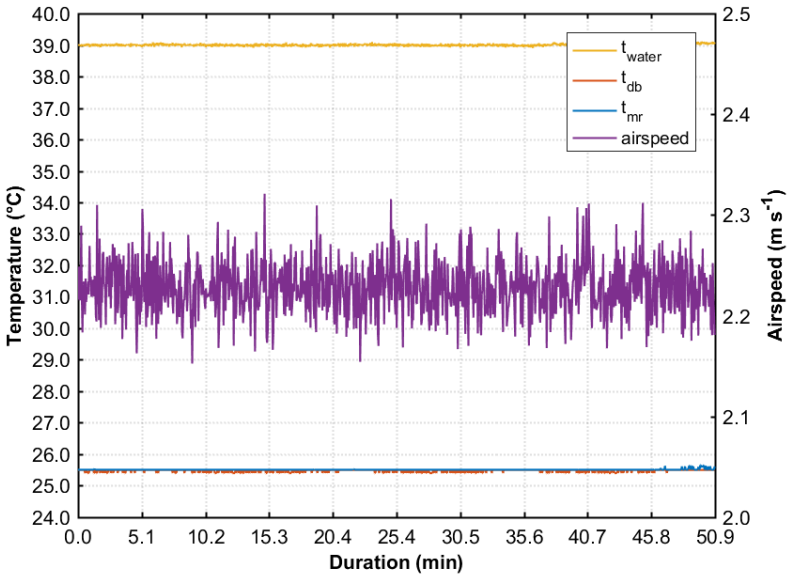

Figure 4.12. Example of the TE conditions measured by TESA and t_{water} inside the ITS for test 2 over the steady-state period.

In order for the ITS to function with ideal behavior, t_{water} inside the sphere must be approximately constant. Figure 4.12 demonstrates that the t_{water} is nearly constant (± 0.XX ^{o}C) over the steady-state period, without observation of major fluctuations. This narrow control band is most likely attributed to the tuning of the PI controller implemented on the microcontroller.

The sensible modes of q_{total} were partitioned for each of the six experiments (figure 4.13). Convection was the greatest fraction of q_{total} in each experiment. The relative proportion of convection losses to radiative losses increased as airspeed increased except for the 25°C, 0.43 m s^{-1} test, where heat loss due to convection was about three times as much as radiation (figure 4.5).

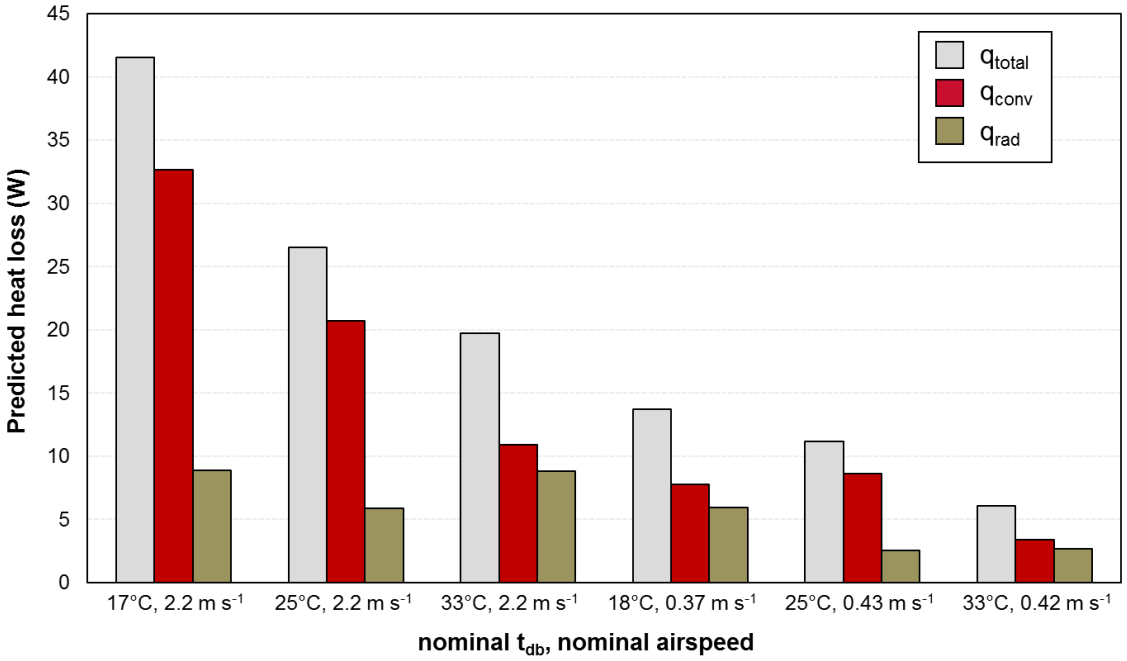

Figure 4.13. Partitions of convective and radiative heat loss, and total heat loss from the ITS as predicted by TESA measurements of the TE.

When the measured power generated by the ITS to maintain a constant t_{water} in the sphere was compared with the predicted total heat loss (q_{total}) by TESA from TE measurements in AThERMS, the predicted q_{total} tended to underestimate measured ITS P_{gen} (figure 4.14). A potential cause for this consistent underestimation may be due the empirically derived relations used to estimate the convective heat transfer coefficient. Note, at the lowest nominal t_{db} and highest airspeed, predicted

q_{total} had the lowest relative difference compared to measured ITS P_{gen}. This is most likely attributed to being able to measure larger values (highest q_{total} among six experiments) with greater accuracy due the full-scale nature of most instruments. Conversely, the lower observed q_{total} had the greatest relative difference between predicted and measured.

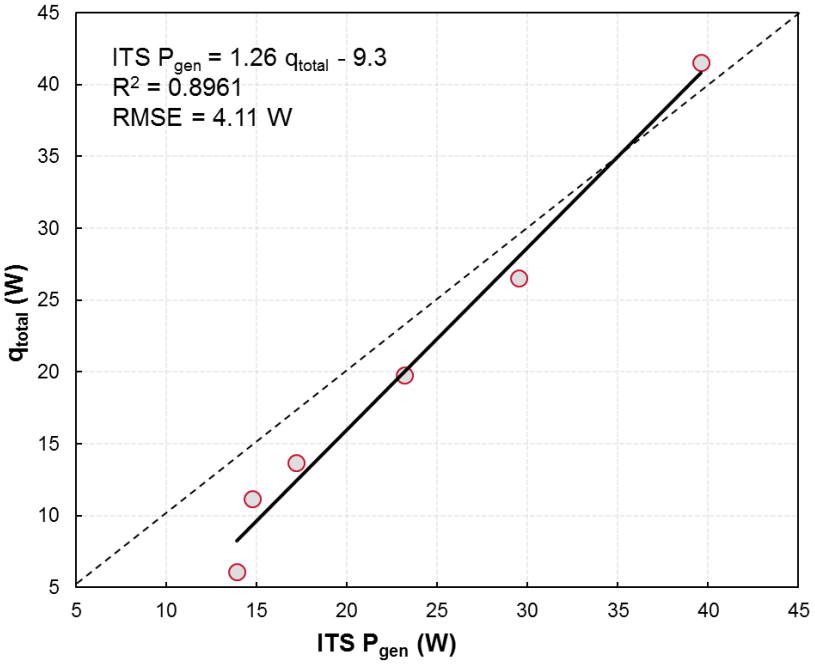

Figure 4.14. Comparison of the power generated by the ITS to maintain a constant water temperature in the sphere with the predicted total heat loss by TESA from TE measurements in AThERMS.

Conclusion

A novel Thermal Environment Sensor Array (TESA) was evaluated in different Thermal Environments (TEs) provided and controlled by the Animal Thermal Environment Replication and Measurement System (AThERMS). AThERMS can be successfully used to simulate different TEs experienced in the animal occupied zone of livestock and poultry facilities as well as function as a reference to calibrate or verify TE measurements. AThERMS was the initial step to creating a system capable of testing the performance of a TESA. At two nominal airspeeds and t_{db} equal to t_{mr}, the feasibility of TESA to estimate the convective and radiative heat losses seems promising; however, improvements in measurement system are needed to better estimate low scale q_{total}.

Future work includes the collection and analysis of data for t_{mr} not equal to t_{db}. The ultimate goal for TESA is to be implemented in a commercial swine production facility to characterize and compare the TE performance of different ventilation controllers and building designs.

Acknowledgements

This research was supported with funding provided by the Iowa Pork Producers Association under NPB Project 14-242. The authors would like to acknowledge the contributions of undergraduate students Grant Hoppes, Heather Tenboer, and Oluwadurotimi Koya during the preparation and completion of this work.

The research work of Yun Gao was partly supported by the National Key Research and Development Program of China (2016YFD0500506).

References

Ames, D. (1980). Thermal Environment Affects Production Efficiency of Livestock. *BioScience*, *30*(7), 457–460. https://doi.org/10.2307/1307947

Close, W. H. (1987). The influence of the thermal environment on the productivity of pigs. *BSAP Occasional Publication*, *11*, 9–24. https://doi.org/10.1017/S0263967X00001713

Curtis, S. E. (1983). *Environmental Management in Animal Agriculture*. Ames, IA: The Iowa State University Press.

Gao, Y., Ramirez, B. C., & Hoff, S. J. (2016). Omnidirectional thermal anemometer for low airspeed and multi-point measurement applications. *Computers and Electronics in Agriculture*.

ISO 7726. (2001). *Ergonomics of the thermal environment — instruments for measuring physical quantities*. Geneva: International Standardization Organization.

JCGM. (2008). *Evaluation of measurement data - Guide to the expression of uncertainty in measurement* (First). Geneva, Switzerland: Working Group 1 of the Joint Committee for Guides in Metrology (JCGM/WG 1).

Ramirez, B. C., Gao, Y., & Hoff, S. J. (2016). Development and validation of a spatial and temporal thermal environment sensor array and data acquisition system. In *2016 ASABE Annual International Meeting*. American Society of Agricultural and Biological Engineers.

Ramirez, B. C., Gao, Y., Hoff, S. J., & Harmon, J. D. (2017). Development and field performance assessment of a novel thermal environment sensor array for animal housing systems. *Biosystems Engineering*.

Ramirez, B. C., Hoff, S. J., Gao, Y., & Harmon, J. D. (2015). Commissioning of a novel animal thermal environment replication and measurement system. In *2015 ASABE Annual International Meeting* (p. 1). American Society of Agricultural and Biological Engineers.

Renaudeau, D., Gourdine, J.-L., & St-Pierre, N. R. (2011). A meta-analysis of the effects of high ambient temperature on growth performance of growing-finishing pigs. *Journal of Animal Science*, *89*(7), 2220–2230.

Taylor, B. N., & Kuyatt, C. E. (1994). *Guidelines for evaluating and expressing the uncertainty of NIST measurement results*. Gaithersburg, MD: US Department of Commerce, Technology Administration, National Institute of Standards and Technology.

CHAPTER 5. AN IMPROVED ASSESSMENT OF THE EFFECTIVE ENVIRONMENT FOR ANALYSIS OF HEAT STRESS MITIGATION TECHNIQUES

B. C. Ramirez, S. J. Hoff, and J. D. Harmon

A paper to be published in the proceedings of the 2017 *International Symposium on Animal Environment and Welfare*

This chapter describes a mechanistic thermal balance model for estimating feed intake of non-disease challenged, *ad libitum* fed pigs. The model accepts the four thermal environment parameters measured by the thermal environment sensor array (Chapter 3), elevation, body weight, and group size. Then, initially estimates total heat loss assuming initial conditions, and proceeds to determine if metabolic heat production and heat loss can be balanced. As mean body temperature increases or decreases based on the animal's thermal demand, different behavioral and physiological response are induced in the thermal zones (i.e., thermoneutral, heat stress, etc.). The model was used to explore different cooling strategies commonly used in the swine industry to provide housing management recommendations.

This chapter owes its success to the cooperation of Brett Ramirez, Steven Hoff, and Jay Harmon. I led the design and implementation of the model, research design, analyzed results, and drafted the manuscript. Drs. Hoff and Harmon contributed to the research design and revision of the manuscript.

Abstract

Heat stressed (HS) pigs typically reduce metabolic heat production (MHP) by decreasing voluntary feed intake (FI) to compensate for their relatively low ability to dissipate excess body

heat. Consequently, growth performance decreases and costs for the producer increase. In commercial and research settings, often only dry-bulb temperature (t_{db}) and occasionally relative humidity are used to describe and control the thermal environment (TE) under HS conditions. Therefore, the objective is to describe, validate, and implement a mechanistic model for grow-finish pigs to accurately assess the effective environment and predict fractional FI resulting from different HS mitigation strategies. The capacity to dissipate heat was developed to assess the onset of HS by relating total heat loss to MHP within the zone of least thermoregulatory effect (ZLTE). Three HS mitigation strategies (elevated airspeed, indirect cooling, and direct cooling) were tested at different TE conditions to show the impact on fractional FI. All three strategies helped pigs remain within their ZLTE under hotter TE conditions. While indirect cooling (evaporative pad) reduced t_{db}, the increase in moisture resulted in earlier onset of HS, if airspeed was less than 1 m s^{-1}. In addition, direct cooling (sprinklers) was found to require airspeeds greater than 1 m s^{-1} for sufficient water evaporation; thus, ensuring pigs can lose heat. This newly developed model serves as an engineering tool to explore the impact of changing one or a combination of TE parameters on swine FI.

Introduction

An accurate understanding of how the thermal environment (TE) housed pigs experience impacts their ability to dissipate metabolically generated heat is essential for improving the production efficiency needed to address future global food security demands without neglect of environmental impact. Further, if the projections on climate change materialize (IPCC, 2014), the intensity and duration of heat stress (HS) on housed pigs will continue to increase (Renaudeau et al., 2011). Pigs experiencing HS typically decrease voluntary feed intake (FI) to reduce metabolic heat production (MHP) and compensate for their poor ability to dissipate heat; thus, pigs require

housing in a TE where heat exchange can be balanced with minimal thermoregulatory effort. An improved understanding of the TE conditions that cause HS and the subsequent impact on performance are required to develop the best solutions for reducing the negative impacts of HS.

The TE describes the sensible (convection, conduction, and radiation) and latent (evaporation) heat exchange between an animal and its surroundings (ASHRAE, 2013; DeShazer, 2009) – and can be expressed by the following parameters: dry-bulb temperature (t_{db}), relative humidity (RH), airspeed, and mean radiant temperature (t_{mr}). Numerous thermal indices have been developed for swine, connecting TE parameters to physiological responses (DeShazer, 2009). These indices are often incomplete (i.e., only expressed as t_{db} and RH) and cannot fully describe the total impact of the heat exchange process. Conversely, empirical and mechanistic bioenergetic models have been successfully developed to provide insight to animal performance and response to the complete TE (Black, 1986). There is a unique opportunity to connect a mechanistic model with performance outputs to evaluate an existing TE and explore HS mitigation technologies.

A mechanistic, thermal balance model was developed based on the work of Fialho et al. (2004) to study effects of the TE on swine FI. This new model was then used to explore HS abatement strategies and improve our understanding of the heat exchange process. Thus, the objectives of this research were: (1) to describe a thermal balance model that uses common TE measurements to predict the environment's capacity to dissipate heat (CDH) from grow-finish pigs and (2) explore different HS alleviation strategies.

Materials and methods

In conjunction with nutrition, management, genetics, etc. swine performance can also be maximized if TE allows the animal to exist in its zone of least thermoregulatory effort (ZLTE; approximately analogous to the "comfort zone" for humans; DeShazer, 2009). A pig's ZLTE is

bounded by the lower critical temperature (t_l; Mount, 1974), where tissue and pelage conductance are minimum and MHP begins to increase (via thermogenesis) to balance the increase in heat loss, and by the evaporative critical temperature (t_e; Black, 1986), where tissue conductance is maximum and the partition of latent heat loss begins to increase. Within the ZLTE, a pig can effortlessly maintain thermoregulation by physiological and behavioral modifications with no impact on FI or growth performance (Mount, 1974).

Capacity to dissipate heat

Pigs housed within their ZLTE will have a constant MHP for maintenance and growth energy requirements; therefore, the TE must have the capacity to dissipate all metabolically produced heat (equation 5.1), or once outside ZLTE, they are thermally unbalanced with their surroundings and must re-balance through changing FI or by facilitating arduous thermoregulation efforts.

$$CDH = q_{total} MHP_{ZLTE}^{-1} \quad (5.1)$$

where
CDH = capacity to dissipate heat, dimensionless
q_{total} = total sensible and latent heat loss (W)
MHP_{ZLTE} = metabolic heat production for best growth performance within the ZLTE (W)

Mechanistic model

The thermal balance model used to evaluate q_{total} was adapted from Fialho et al. (2004) and simulates the thermal exchange for non-disease challenged, *ad libitum*, group or individually housed pig(s), assuming the effects of TE on the animal(s) can be completely expressed by the animals' mean body temperature (t_b), integrated over the volume of the animal. The t_b is marginally different from core body temperature (t_c), which is more difficult to measure and relatively static over a wide range of conditions. Therefore, t_b is expected to vary more than t_c and is used as the

central thermoregulation mechanism to model the animal's behavioral and physiological responses to different TEs.

Four zones of thermoregulation were defined: cold stress zone, ZLTE, evaporative zone, and HS zone. Cold stress zone occurs for $t_b < t_l$, that is, $q_{total} > MHP_{ZLTE}$ (i.e., CDH > 1) and in order to avoid decreasing t_b, the pig must increase FI to increase MHP; hence, a loss in feed efficiency and production. The ZLTE is defined between t_l and t_e, with $q_{total} = MHP_{ZLTE}$ (i.e., CDH = 1) for maximum growth performance. Further, within the ZLTE, the animal can change tissue resistance, behavior (i.e., huddling, wallowing, posture), and contact area with the floor. Mathematical descriptions of these mechanisms are described in detail in Fialho et al. (2004). The evaporative zone (i.e., CDH < 1) is defined between t_e and the upper critical temperature (t_u), where the animal initially decreases FI (negative performance), and can increase respiration rate and passive water diffusion through its skin. Beyond t_u, the animal can only decrease FI and t_b increases as a result.

Fialho et al. (2004) outlined the heat and mass transfer procedures adopted in this work with minor modifications made to some equations. Namely, the water (on skin) evaporation model was enhanced to include the latent heat of vaporization and Lewis relation for mass transfer as a function of skin temperature and the TE, rather than constant. A detailed flow chart outlining the relationship between TE and the animal's response, as well as the execution of the model is outlined in figure 5.1. The model accepts the four TE parameters, elevation (Z), BW, and group size – then, initially estimates q_{total} assuming initial conditions, and proceeds to determine the t_b at which MHP_{ZLTE} and q_{total} balance. As t_b increases or decreases based on the animal's thermal demand, different behavioral and physiological responses are induced in the aforementioned zones. Once the model has converged within a specified tolerance (T = ±0.2 W), CDH, t_b, and FI are returned.

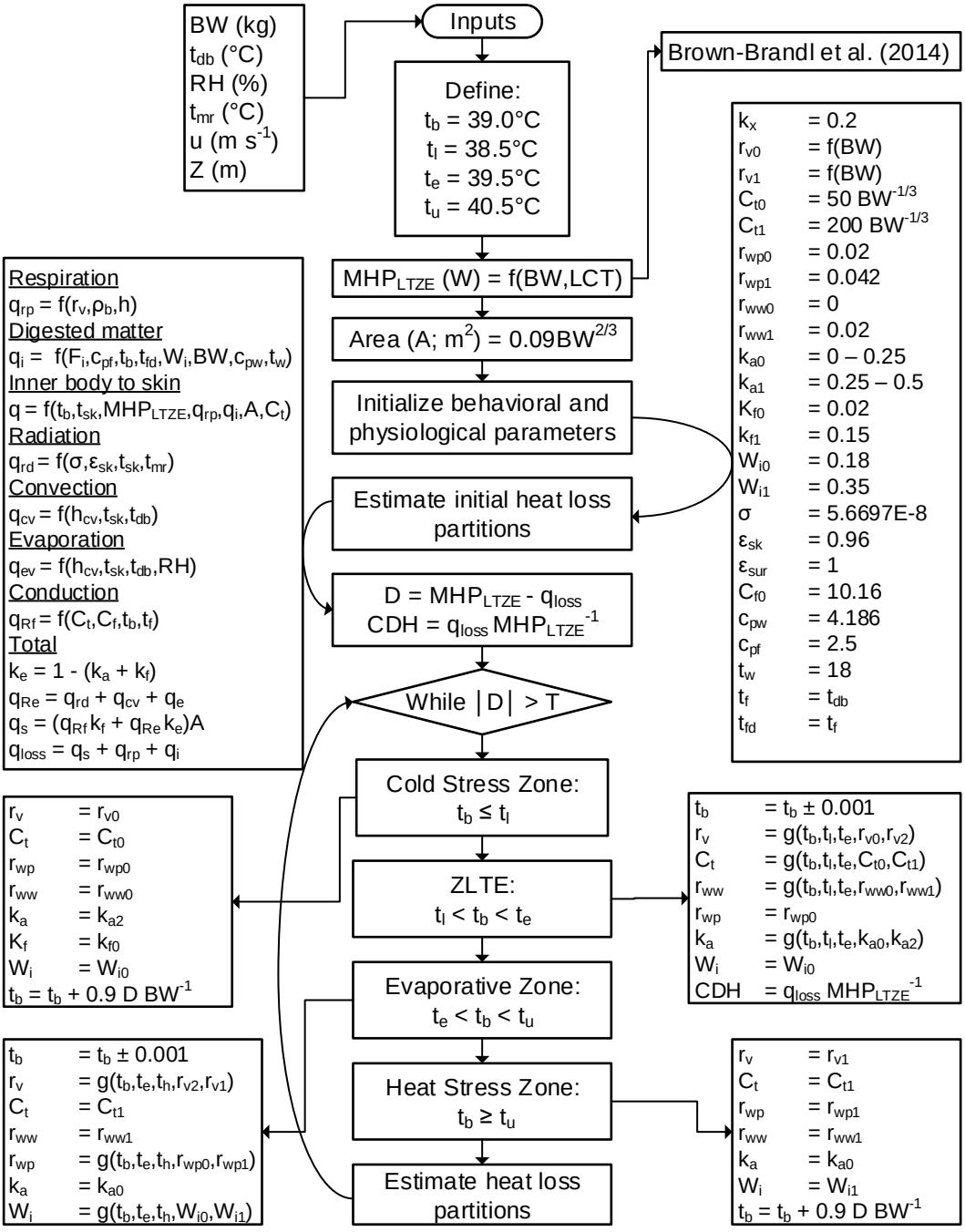

Figure 5.1. Flow chart of the mechanistic swine thermal balance model. Parameter definitions can be found in Fialho et al. (2004). General functional dependence is denoted by f, and g denotes a linear transition function between the minimum (e.g., C_{t0}) and maximum (e.g., C_{t1}) values with the specified zone t_b limits.

Validation

The mechanistic model was compared to empirical FI data and semi-empirical fractional FI (FFI) models. Where, FFI is the FI under different TE conditions expressed as a fraction of FI at ZLTE (e.g., FFI = 1 represents ZLTE FI; FFI = 0.5 represents a 50% reduction in FI from FI at ZLTE). The impact of only RH on FI was isolated through comparison with the semi-empirical, broken line model described by Thuy (2005). The experiment used to create the broken line model reported a constant BW (60 kg), airspeed (0.3 m s^{-1}) and group size (n = 10) at three RH (50%, 65%, and 80%) for t_{db} between 16°C to 32°C. The t_{mr} was assumed equal to t_{db}.

The mechanistic model was also compared to the NRC (2012) model, R2011 model by Renaudeau et al. (2011), NRCmod model by White et al. (2015), and temperature-duration (TD) model also by White et al. (2015). These models are a function of t_{db}, BW, and duration (assumed 1 h for TD model only). The FFI are direct outputs for NRC, NRCmod, and TD, but for R2011, the FI values were predicted at each TE condition and divided by the corresponding predicted ZLTE (LCT + 3°C) FI value. For comparison with these four semi-empirical models, a range of simulated BW (35 to 110 kg) and t_{db} (15°C to 32°C) were used with airspeed assumed constant (0.3 m s^{-1}), t_{mr} equal to t_{db}, and constant group size (n = 30). Since, MHP is a function of BW, larger pigs have more heat to dissipate and a lower surface area to BW ratio, both characteristics have major implications on q_{total}. The large group size more accurately reflected commercial housing practices. A linear model was fit to simulated FFI against each of these prediction models and evaluated by the root-mean-square error (RMSE). Residuals were plotted against t_{db} to visually evaluate goodness of fit.

Heat stress mitigation strategy comparison

Three HS mitigation strategies were each modeled over an ambient t_{db} range (16°C to 32°C) to explore the impact on FFI for a constant BW pig (90 kg). They were (1) airspeed, (2) indirect evaporative cooling via pad, and (3) direct cooling via sprinkling (assumed large droplet, low pressure). Airspeed: five airspeeds (0.5, 1.0, 1.5, 2.0, and 2.5 m s^{-1}) were simulated with RH held constant at 50%. Indirect cooling: for each ambient t_{db}, three ambient RH (40%, 60%, and 80%) were assumed to pass through a 0.72 efficient evaporative pad. Then, three airspeeds (1.0, 2.0, and 3.0 m s^{-1}) were simulated at the t_{db} and RH conditions downstream of the pad. Direct cooling: the increase in wetted skin area was modeled by changing the fraction wet by wallowing ($r_{ww}1$) from 0.03 to 0.30. Three airspeeds (1.0, 2.0, and 3.0 m s^{-1}) and three RH (40%, 60%, and 80%) were tested. For all three HS mitigation strategies, group size (n = 30) was constant and t_{mr} equal to t_{db}. The impact of each strategy was assessed by comparing FFI against t_{db}.

Results and discussion

The goal of the model was to simulate the effect of different TE conditions that cause pigs to no longer exist within their ZLTE, thereby resulting in a reduction of FI. While holding other TE parameters constant over a range of t_{db}, the model reasonably simulated the critical effective temperature (t_{ceff}), that is, the point where pigs were no longer within their ZLTE. This is evident by analysis of when CDH is less than unity (figure 5.2). It is important to note the shift from ZLTE to HS is brought on by the thermal imbalance between the pig and its TE. This thermal imbalance is caused by the inability of the TE to dissipate MHP by sensible and latent modes, which are described by t_{db}, RH, airspeed, and t_{mr}, not solely t_{db}. As BW increased, the effective conditions (i.e., total impact on the pig's heat balance) at which CDH was less than unity also increased. This agrees with previously proposed models (Renaudeau et al., 2011).

Analysis of the partitions of q_{total} (figure 5.3) show sensible modes (mainly convection and radiation) are the largest contributors within the ZLTE. Once $t_b > t_e$, the contribution of latent modes (respiration and diffusion) began to increase. This progression from predominately sensible to latent modes and the inflection point at which they begin to change agrees with previous models and empirical calorimetry data (Brown-Brandl et al., 2014). Since pigs rely mainly on latent modes during HS, the addition of moisture to the air by evaporative cooling incoming air can potentially increase the impact of HS, if the convective heat loss in the animal occupied zone is not simultaneously increased.

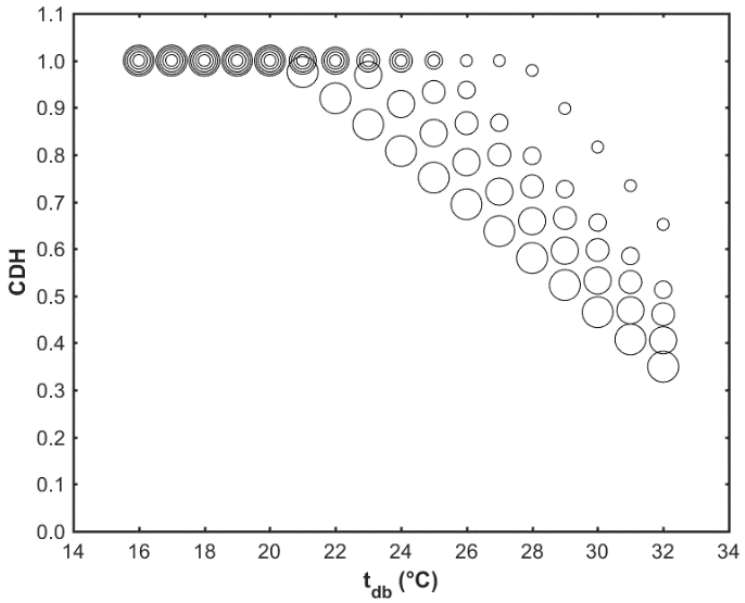

Figure 5.2. The inflection point where CDH is less than unity indicates the pig is no longer within its ZLTE. Symbol size is proportional to BW (35 to 110 kg).

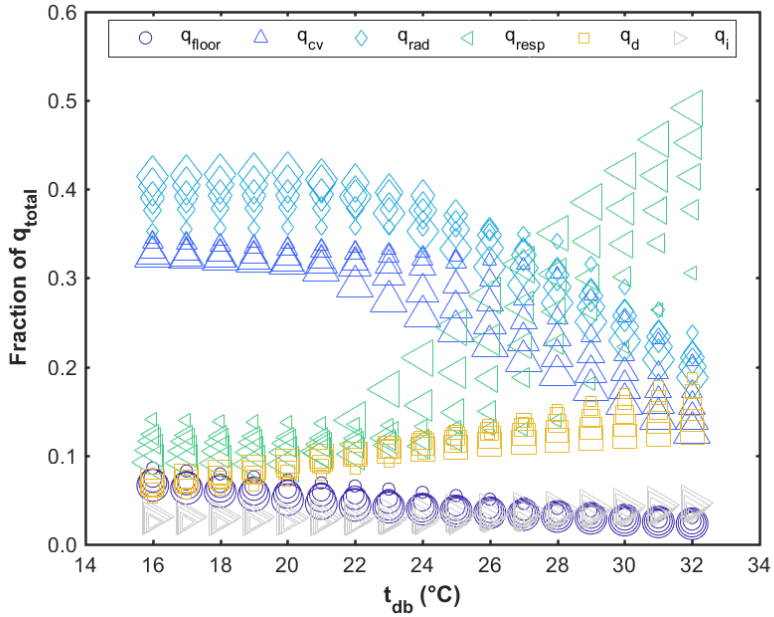

Figure 5.3. Partition of different sensible and latent modes of heat loss. Subscript definitions: cv (convection), rad (radiation), resp (respiration), d (diffusion), and i (ingestion). Symbol size is proportional to BW (35 to 110 kg).

Validation

The mechanistic model showed reasonable comparison with the broken line model empirically derived by Thuy (2005). The inflection point caused by the effect of RH on predicted FI was similar. The simulated FI at the hottest effective conditions (>30°C and >60%) was much lower than estimated by the broken line model. This is most likely attributed to a lack of metabolic information included in the broken line model. In addition, further calibration of this mechanistic model is needed to reduce this observed difference.

Simulated FFI against FFI predicted by the four models showed evident trends in residuals based on visual examination (figure 5.4), with error increasing in hotter TE conditions. The RMSE were 0.036 (NRC), 0.024 (NRCmod), 0.018 (R2011), and 0.020 (TD). The FFI agreement was best for the R2011 and TD models. These models are only a function of BW and t_{db}; hence, to assess the effectiveness of different cooling strategies and minimize the FI penalty of HS, they must include the other TE parameters. This also extends to addressing the need for improved TE

monitoring during HS or calorimeter studies. A robust and accurate measurement system, such as the TE sensor array (Ramirez, Gao, & Hoff, 2016), is one step toward improving monitoring in order to understand the thermal balance between pigs and their TE.

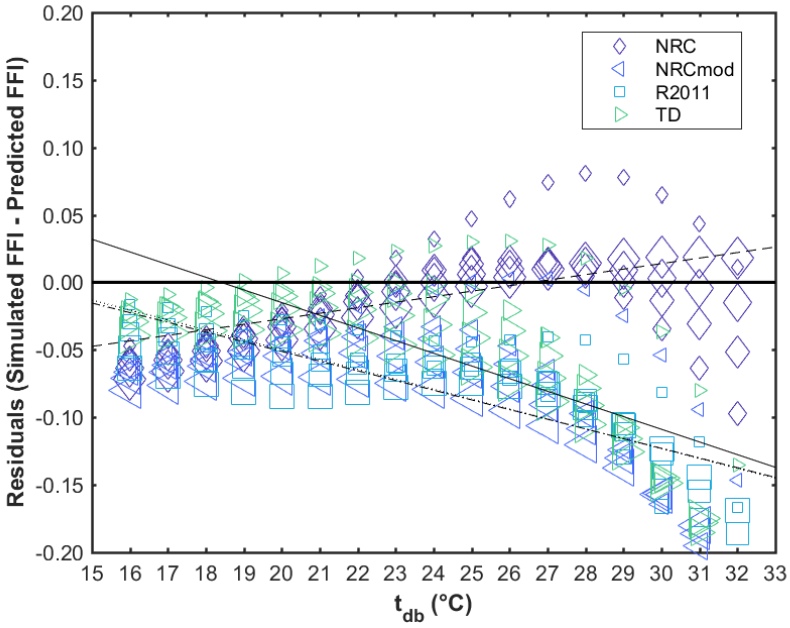

Figure 5.4. Residuals comparison for simulated FFI and predicted FFI from four published models. A linear model was fit to each set of residuals to show agreement. Symbol size is proportional to BW (35 to 110 kg).

Heat stress mitigation strategy comparison

Three HS mitigation strategies (airspeed, indirect, and direct cooling) were compared to evaluate the combinations of TE parameters that yield the lowest FFI penalty during HS. The R2011 model results were included in figures 5.5, 5.6, and 5.7 to show how the model's accuracy could be improved for different climates. For airspeed (figure 5.5), the t_{db} where simulated FFI decreased from unity increased as airspeed increased. That is, pigs could remain within their ZLTE under hotter TE conditions with the addition of airspeed. While the FFI tended to increase as airspeed increased at a given t_{db}, the increase from 2 to 3 m s^{-1} only yielded marginally higher FFI.

While indirect cooling (evaporative pad) reduced t_{db}, the humidity ratio of the exiting air consequently increased due to the evaporation of water (figure 5.6). The cooler, but higher

moisture air can still cause HS (since the pig cannot lose as much latent heat) if not properly combined with airspeed (or manipulation of a different TE parameter).

Regardless of RH, the application of water (via sprinklers) to the pig and concurrent airspeed of at least 1 m s^{-1} prevented the pigs from incurring a FFI less than 0.9 over the range of t_{db} tested (figure 5.7). Airspeed control is key with the application of sprinkling because the pig can only dissipate heat if the water is evaporating. Essentially, at airspeeds less than 1 m s^{-1}, water evaporation is limited, and heat dissipation minimal.

The latent heat of vaporization absorbed by either the evaporative pad or the pig when water evaporates can be greater than the amount of heat the pig needs to dissipate and can cause cold stress. Most indirect and direct cooling systems are controlled with on/off decisions that do not take into account the amount of heat they can remove. Incorporation of a mechanistic model in control system design is important to prevent HS and optimize the TE based the amount of heat the pig can dissipate.

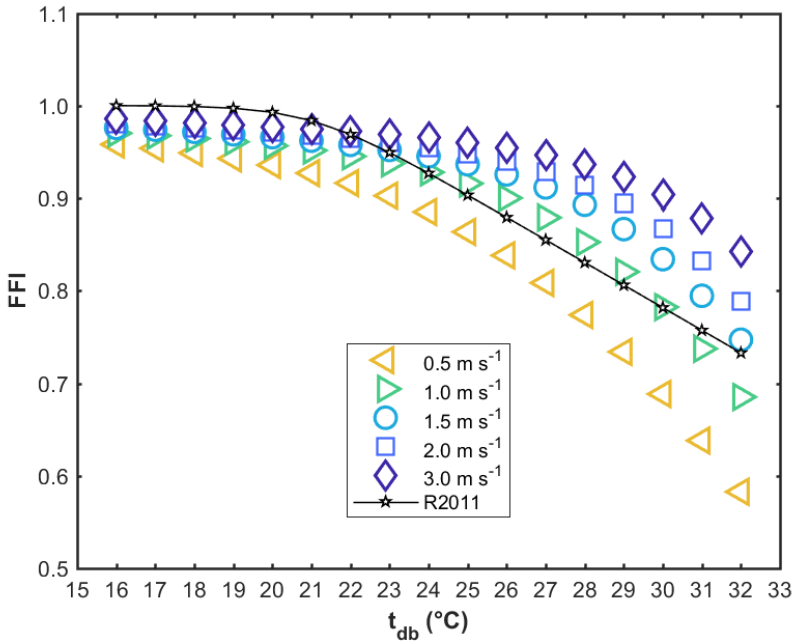

Figure 5.5. Airspeed: impact of elevated airspeed on FFI at constant BW (90 kg) and RH (50%).

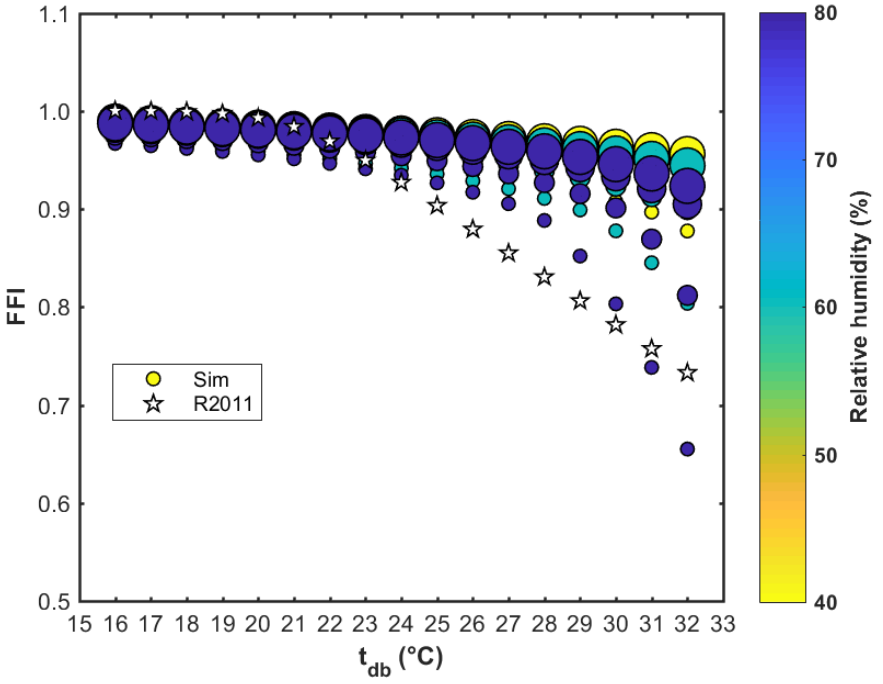

Figure 5.6. Indirect cooling: TE conditions are downstream of an evaporative cool pad at upstream ambient RH of 40%, 60%, and 80%. Circle size is proportional to airspeed (0.5 to 3.0 m s^{-1}).

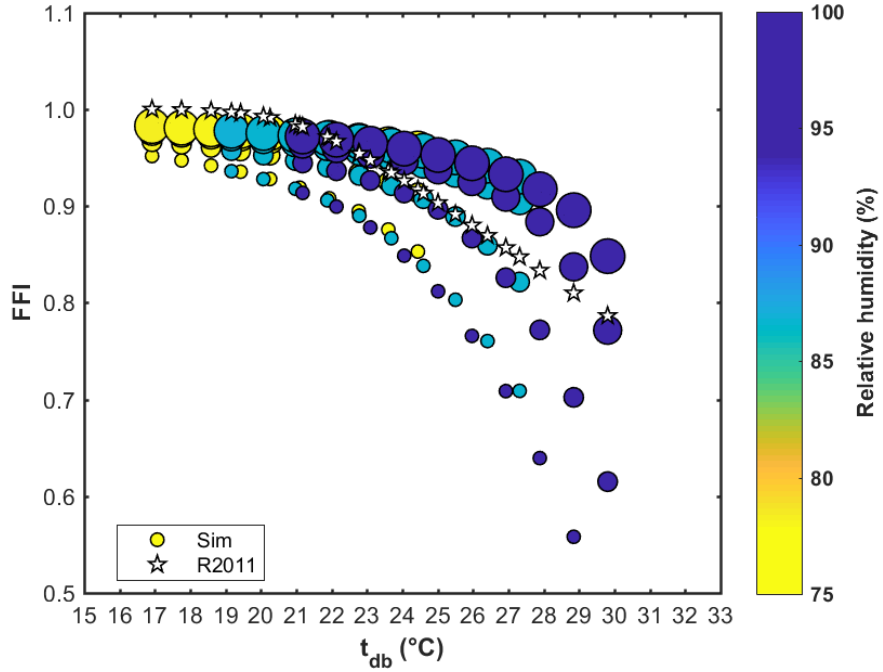

Figure 5.7. Direct Cooling: impact of wetting simulated pigs 30% via sprinklers on FFI at different RH and airspeeds. Circle size is proportional to airspeed (0.5 to 3.0 m s^{-1}).

Conclusions

The mechanistic model presented in this study was effective at estimating FFI as a function of group size, BW, t_{db}, RH, t_{mr}, and airspeed. Current FFI prediction models are only based on BW and t_{db}, and need to incorporate additional parameters to show how the combination of TE

conditions can reduce FI. This model serves as an engineering tool to explore the impact of changing one or a combination of TE parameters on swine FI. In addition, coupling mechanistic models with facility design can help improve the implementation and method of assessing cooling technologies. This model does not include the effect of body composition (protein to fat ratio), diet, thermal effect of feeding, or activity.

Acknowledgements

This research was supported with funding provided by the Iowa Pork Producers Association under NPB Project 14-242.

References

ASHRAE. (2013). Handbook of fundamentals. Atlanta, GA: America Society of Heating, Refrigeration and Air Conditioning Engineers.

Black, J. L. (1986). Simulation of energy and amino acid utilization in the pig. Research and Development in Agriculture, 3(3), 121–145.

Brown-Brandl, T., Hayes, M., Xin, H., Nienaber, J., Li, H., Eigenberg, R. A., … Shepherd, T. (2014). Heat and Moisture Production of Modern Swine. ASHRAE Transactions, 120.

DeShazer, J. A. (2009). Livestock Energetics and Thermal Environmental Management (1st ed.). St. Joseph, MI: American Society of Agricultural and Biological Engineers.

Fialho, F. B., Bucklin, R. A., Zazueta, F. S., & Myer, R. O. (2004). Theoretical model of heat balance in pigs. Animal Science, 79(1).

IPCC. (2014). Climate Change 2014: Mitigation of Climate Change (Working Group III - Mitigation of Climate Change No. Assessment Report 5). Intergovernmental Panel on Climate Change.

Mount, L. E. (1974). The concept of thermal neutrality. In Heat loss from animals and man: Assessment and control (pp. 425–439). London, UK: Butterworths.

NRC. (2012). Nutrient Requirements of Swine (11th ed.). Washington D.C.: National Academies Press.

Ramirez, B. C., Gao, Y., & Hoff, S. J. (2016). Development and validation of a spatial and temporal thermal environment sensor array and data acquisition system. In 2016 ASABE Annual International Meeting.

Renaudeau, D., Gourdine, J.-L., & St-Pierre, N. R. (2011). A meta-analysis of the effects of high ambient temperature on growth performance of growing-finishing pigs. Journal of Animal Science, 89(7), 2220–2230.

Thuy, H. T. T. (2005). Heat stress in growing pigs (Doctoral). Wageningen University, Netherlands.

White, R. R., Miller, P. S., & Hanigan, M. D. (2015). Evaluating equations estimating change in swine feed intake during heat and cold stress. Journal of Animal Science, 93(11), 5395–5410.

CHAPTER 6. THERMAL ENVIRONMENT SENSOR ARRAY: PART II. APPLYING THE DATA TO ASSESS GROW-FINISH SWINE HOUSING

B. C. Ramirez, S. J. Hoff, and J. D. Harmon

A manuscript to be submitted to *Biosystems Engineering*

This chapter describes the development of the housed swine heat stress index (HS2I) to analyze the impact of the thermal environment on swine performance and the practical application to empirically collected data. Simulated animal responses from the mechanistic model (Chapter 5) were generated for a wide range of thermal environment conditions to an index capable of translating thermal environment sensor array measurements (Chapter 3) to a relative dimensionless value. The HS2I was then applied to the spatiotemporal TESA data collected at a commercial grow-finish facility (Chapter 3) to determine the adequacy of the ventilation system.

This chapter owes it success to the teamwork of Brett Ramirez, Steven Hoff, and Jay Harmon. I led the research design, index development, analyzed the data, and drafted the manuscript. Drs. Hoff and Harmon also contributed to the research design and revision of the manuscript.

Abstract

Current Thermal Environment (TE) assessment techniques for controlling livestock and poultry facilities often solely use dry-bulb temperature (t_{db}) and occasionally relative humidity (RH), as assessment parameters. In addition, the recently developed TE sensor array (TESA; Part I) quantifies t_{db}, RH, airspeed and black globe temperature, but there is no existing method or index value able to incorporate these additional TE parameters needed to accurately assess the TE based on the thermal demands of the animal. Hence, the goal of this study was to develop a

technique for evaluating the TE as a function of mean body temperature difference from thermally comfortable (Δt_b) using body weight, t_{db}, RH, and airspeed inputs. Multiple regression analysis of the simulated data from the mechanistic thermal balance model for group-housed growing pigs was used to develop the housed swine heat stress index (HS2I), which scales impact of the TE from 0 (thermally comfortable) to 10 (severe heat stress). Further, a wetted skin adjustment parameter was included to enable analyzing TE with sprinklers. Agreement between simulated and predicted Δt_b without wetted skin (R^2 = 0.98; RMSE =0.061°C) and wetted skin (R^2 = 0.97; RMSE =0.054°C) showed good agreement. The HS2I was applied to assess the spatiotemporal TE data collected by TESA in the commercial wean-finish facility presented in Part I of this series. Advanced methods to measure and evaluate the thermal environment (TE) in swine facilities are needed to sustainably provide animal-based protein for the increasing global population. The HS2I can be used to evaluate the potential impact of the TE in existing facilities and as design tool to explore different ventilation and cooling strategies

Introduction

Livestock and poultry are homoeothermic animals that utilize a cascade of thermoregulatory mechanisms (physiological and behavioral) to maintain a thermal balance with their surroundings. Further, homeotherms must satisfy the following: heat loss (q_{loss}) to the environment must equal the total energy product of metabolism (DeShazer, 2009). An animal can become thermally unbalanced (i.e., body temperature outside the normal narrow range) if q_{loss} exceeds or falls below metabolic heat production (HP) – resulting in heat or cold stress. If the projections on climate change materialize (IPCC, 2014), the intensity and duration of heat stress on housed swine will continue to increase (Renaudeau et al., 2011). The negative consequences of heat stress are well-documented and include decreased growth performance (Collin, van Milgen, Dubois, & Noblet,

2001; Renaudeau et al., 2011; Thuy, 2005) and substantial economic losses (Stalder, 2015; St-Pierre, Cobanov, & Schnitkey, 2003). Hence, techniques to assess the potential impact of the thermal environment (TE) on swine performance are needed to improve heat stress prediction and alleviation through development of management strategies and cooling technologies.

The TE describes the parameters (i.e., dry-bulb, floor, and mean radiant temperature, relative humidity, and airspeed) that influence the partitions (i.e., convective, conductive, radiative, and evaporative) of q_{loss} between an animal and its surroundings. One TE parameter cannot solely represent or estimate q_{loss}; however, in many animal production systems, often only dry-bulb temperature (t_{db}) is used to control and assess the associated impact of the TE on animal performance. The recently developed TESA (Part I) provides a nearly complete TE monitoring solution (neglecting conduction), but due to the limited availability of existing metrics to comprehensively quantify the total TE impact, there is a requisite need for novel approaches to incorporate the TE parameters available from TESA to assess the TE.

Thermal indices (TIs) for livestock and poultry have been well-summarized in literature (da Silva & Maia, 2012; DeShazer, 2009; Fournel, Rousseau, & Laberge, 2017). These TIs substantially simplify complex physical and biological interactions for typically one selected physiological (e.g., body temperature or respiration rate) or performance production response (e.g., feed intake, milk production, weight gain, etc.) given only select combinations of the TE (e.g., t_{db} and relative humidity), while either neglecting or assuming the other TE parameters are constant. Grow-finish pigs currently lack a suitable TI. Previous efforts have resulted in the wet-bulb (t_{wb})/t_{db} temperature index (WDTI) by Ingram (1965) for pigs weighing between 20 to 30 kg. Roller & Goldman (1969) associated the WDTI to four physiological parameters for pigs weighing from 30 to 90 kg exposed to t_{db} (34°C to 43°C) and t_{wb} (23°C to 31°C) conditions for 200 min. Both these

studies fail to capture early onset of heat stress that results in a performance decline over the large body weight (BW) range of grow-finish pigs. The enthalpy concept, proposed by Beckett (1965) and later refined by Moura, Naas, Silva, Sevegnani, & Corria (1997), has been useful to evaluate swine housing but fails to incorporate long-wave radiation and airspeed. With many TIs, BW is often neglected; however, for growing pigs, inclusion of BW is critical because fasting HP increases as an allometric function of BW ($a \times BW^{0.6}$; NRC, 2012) and the surface area to BW ratio decreases with increasing BW. Both these characteristics have major implications on q_{loss}. However, to accurately design or evaluate the TE for housed pigs, an index that relates q_{loss}, rather than just a fraction of q_{loss} (i.e., mainly convective via t_{db}), and as a function of BW to a performance or physiological response is needed.

This study describes the development and application of an approach to evaluate the TE in grow-finish pig housing using TE measurements from TESA and estimated BW as inputs. Hence, the objectives of this paper were to: (1) describe a mechanistic thermal balance model to estimate q_{loss} for grow-finish pigs, (2) use the mechanistic model results to derive the housed swine heat stress index (HS2I), and (3) apply HS2I to analyze spatiotemporal TESA data from a case study to demonstrate feasibility.

Materials and methods

Mechanistic model

The thermal balance model, developed in Matlab (R2017a, The Mathworks, Inc., Natick, Massachusetts, USA), was adapted from Fialho et al. (2004) and simulated the thermal exchange for non-disease challenged, *ad libitum*, group or individually housed pig(s). The effects of TE on the animal(s) were assumed to be completely expressed by the animals' mean body temperature (t_b), integrated over the volume of the animal. A detailed description and operation of the model

can be found in (Ramirez, Hoff, & Harmon, 2017a). Essentially, the model sets initial conditions and proceeds to iterate t_b through physiological and behavioral thermoregulation responses. The resulting t_b can then be used to estimate feed intake from a complex transfer function.

Housed swine heat stress index

The HS2I was developed to convert the simulated t_b (physiological response) difference from 39°C (Δt_b; the assumed t_b of a pig existing within its thermal comfort zone) into a dimensionless indexed value ranging from 0 (thermally comfortable) to 10 (severely heat stressed), with intermediate values 3 to 6 as moderately heat stressed.

Simulated Δt_b (n = 15,517) was generated for combinations of BW (50 to 120 kg in 10 kg increments), t_{db} (16°C to 33°C in 1°C increments), relative humidity (10% to 90% in 5% increments), airspeed (0.2 m s^{-1} and 0.5 to 3.0 m s^{-1} in 0.5 m s^{-1} increments). Mean radiant temperature was assumed equal to t_{db} – a reasonable assumption in housed environments with high ventilation rates and modern levels of building insulation. Elevation (300 m) and group size (n = 30) were constant. Prior to initial fitting, Δt_b outliers were removed such that the simulated data contained -0.25°C < Δt_b < 1.5°C.

For a fixed BW (100 kg) and airspeed (0.2 m s^{-1}), cross-sectional plots were created to show the relationship between Δt_b and t_{db} for each RH (n = 17). Each cross-section plot then was individually fit with a quadratic model (equation 6.1) using least squares regression in Matlab (R2017a, The Mathworks, Inc., Natick, Massachusetts, USA).

$$\Delta t_b = p_1 {t_{db}}^2 + p_2 t_{db} + p_3 \quad (6.1)$$

where

Δt_b = simulated mean body temperature difference from 39°C (°C)
t_{db} = dry-bulb temperature (°C)
p_n = coefficients

The resulting estimated values (i.e., model coefficients; p) approximately showed how RH could be incorporated in the model at a fixed airspeed and BW. Cross-section plots of the estimated values of each of the three coefficients versus t_{db} were examined to determine the relationship of the estimated values over the t_{db} range. This led to an additional quadratic model for each coefficient as a function of RH (example for one coefficient shown in equation 6.2).

$$p_1 = f(RH) = \beta_1 RH^2 + \beta_2 RH + \beta_3 \quad (6.2)$$

where

f = function dependence
RH = relative humidity (%)
β_n = coefficients

The effects of t_{db} and RH (for a fixed BW and airspeed) were combined to form equation 6.3.

$$\Delta t_b' = f(RH) {t_{db}}^2 + f(RH) t_{db} + f(RH) \quad (6.3)$$

where

$\Delta t_b'$ = predicted mean body temperature difference at fixed BW and airspeed (°C)

Next, airspeed was incorporated into the model by creating cross-sectional plots to show the relationship between $\Delta t_b'$ (predicted as a function of t_{db} and RH at 0.2 m s^{-1}) and simulated Δt_b for each airspeed (n = 7). Each cross-section plot then was individually fit with a 2-term power model. The resulting estimated values approximately showed how airspeed could be incorporated in the model by adjusting $\Delta t_b'$. Cross-section plots of the estimated values of each of the three coefficient versus simulated Δt_b were examined to determine the relationship of the estimated values over the simulated Δt_b range. This led to an additional 2-term power model for each coefficient as a function of airspeed (equation 6.4).

$$\Delta t_b'' = f(u) {\Delta t_b'}^2 + f(u) \Delta t_b' + f(u) \quad (6.4)$$

where

$\Delta t_b''$ = predicted mean body temperature difference at fixed BW (°C)
$f(u)$ = coefficients as a quadratic function of airspeed (u)

Lastly, the effect of BW was added to $\Delta t_b''$ by the same aforementioned procedure. A quadratic model was fit to each of the cross-sectional plots (n = 8) of $\Delta t_b''$ and simulated Δt_b. A cubic model for each coefficient as a function of BW was used (equation 6.5).

$$\Delta t_b''' = f(BW)\Delta t_b''^2 + f(BW)\Delta t_b'' + f(BW) \quad (6.5)$$

where

$\Delta t_b'''$ = predicted mean body temperature difference (°C)

The effects of directly wetting the animal's skin (commonly achieved by low-pressure sprinkling used in many grow-finish facilities) was incorporated into HS2I (equation 6.6) by subtracting the predicted difference ($\Delta t_{b,w}'$) between $\Delta t_{b,w}$ (wet) and Δt_b (normal) from $\Delta t_b'''$.

$$\Delta t_b'''' = \Delta t_b''' - S_{on}\Delta t_{b,w}' \quad (6.6)$$

where

$\Delta t_b''''$ = predicted mean body temperature difference with wet skin effect (°C)

S_{on} = binary wetting coefficient (wet: $S_{on} = 1$; normal; $S_{on} = 0$)

$\Delta t_{b,w}'$ = predicted mean body temperature difference between wet and normal skin (°C)

The predicted $\Delta t_{b,w}'$ was developed following the same procedure used to find $\Delta t_b'''$. A linear model was used to express the effects of t_{db} with coefficients described by a 2-term power model as a function of RH. Then, predicted $\Delta t_{b,w}'$ was adjusted by a quadratic model with coefficients described by a quadratic model as a function of airspeed. Lastly, $\Delta t_{b,w}'$ was adjusted by a linear model with coefficients described by a quadratic model as a function of BW. The final $\Delta t_b''''$ was linearly scaled from 0 to 10 using max and min values of Δt_b (equation 6.7).

$$HS2I = y_1\Delta t_b'''' - y_0 \quad (6.7)$$

where

HS2I = housed swine heat stress index (0 to 10 dimensionless)

y_n = linear scaling coefficients

Validation

The accuracy of estimating $\Delta t_b''''$ for $S_{on} = 0$ and 1 was assessed by analyzing the linear agreement between Δt_b and $\Delta t_b''''$. Regression goodness-of-fit statistics and visual inspection of the residuals were used for assessment. Further, a sensitivity analysis was performed to evaluate the

absolute and relative impact of $\Delta t_b''''$ prediction error on HS2I that was possibly incurred due to the numerous fitting of the coefficients of the parameters. For -0.25°C < $\Delta t_b''''$ < 1.25°C, two levels of $\Delta t_b''''$ prediction error (based on analysis of the residuals) were used: ±0.1°C and ±0.3°C.

Since no direct comparison with other TIs is available (although, see the comprehensive climate index for cattle by Mader, Johnson, & Gaughan, 2010), HS2I was compared with the feed intake (FI) and critical temperature (CT) models developed by Renaudeau et al. (2011) from a meta-analysis of modern research studies. In addition, HS2I was compared with the previously established WDTI proposed by Roller & Goldman (1969). Renaudeau et al. (2011) established a semi-logarithmic function for FI as a function of CT (a function of BW) – essentially, the t_{db} where FI decreases linearly. For comparison, the FI model was expressed in terms of fractional FI (FFI). Where, FFI is the FI under different TE conditions expressed as a fraction of FI at zone of least thermoregulatory effort (ZLTE; defined at t_{db} = lower critical temperature + 3°C). For example, FFI = 1 represents ZLTE FI; FFI = 0.5 represents a 50% reduction in FI from FI at ZLTE. HS2I was superimposed over FFI and CT for a range of t_{db} (16°C to 33°C) and BW (60 to 120 kg). The other TE conditions were assumed to be associated with controlled research settings (i.e., indirect calorimeters or small group-housed facilities) with airspeed (0.2 m s^{-1}) and RH (60%) constant.

HS2I was calculated for WDTI (= $0.75 \times t_{db} + 0.25 \times t_{wb}$) ranging from 58 to 93 (since WDTI was originally developed in units of °F for t_{db} and t_{wb}) for three BWs (60, 90, 120 kg) and four airspeeds (0.5, 1.0, 2.0, 3.0 m s^{-1}). In addition, the intersection of HS2I = 3 (early onset of heat stress impact) with the CT (for a given BW) and WDTI model alert threshold (74) were examined.

Case study

A total of 44 TESAs (22 in each room) simultaneously collected t_{db}, RH, airspeed, and black globe temperature approximately every minute inside a deep-pit, wean-finish swine facility located

in central Iowa. Part I of this study outlines the specific details of the facility, ventilation system, deployment of the TESA network, and data collection procedures. Data were collected from two flows of pigs: flow 1: August 12, 2017 to January 26, 2017 and flow 2: February 12, 2017 to July 16, 2017. Weather data, including ambient t_{db} (t_a) and dew point temperature were downloaded at 1 min intervals from an Automated Surface Observing System (ASOS) station located 59 km from the facility (https://mesonet.agron.iastate.edu/).

Data analysis

Data were preprocessed in Matlab (R2017a, The Mathworks, Inc., Natick, Massachusetts, USA) to remove any garbled text, extraneous values, duplicate values, etc. The unique timestamps from all 44 TESAs were used to assemble a reference timestamp array, such that timestamps missing from a particular TESA were replaced with not-a-time (NaT) and all 44 TESA datasets had the same length (every row had an identical timestamp or NaT).

Initial and final BW was provided by the producer (BW was unable to be measured throughout the study) and intermediate value were found using a cubic regression of a growth curve for average pigs from weaning to 28 weeks of age (PIC, 2013). Then, HS2I was calculated for every timestamp using TESA measured t_{db}, RH, and airspeed data and the estimated BW. The sprinklers were not activated during this study ($S_{on} = 0$).

The $t_{mr} = t_{db}$ assumption was validated by initially applying a moving average (20 element window, approximately equal to 20 min) to the t_{db}, airspeed, and t_g data for each TESA. The ISO 7726 (2001) procedure for forced convection over a 0.1016 m diameter sphere with an assumed 0.98 emissivity was used to estimate t_{mr}. The $t_{mr} = t_{db}$ assumption was analyzed for each room by the linear regression coefficients and regression statistics between t_{db} and t_{mr}, for the total study period, for $t_a \leq 20°C$, and $t_a > 20°C$.

Since t_a has a substantial impact on TE inside the facility, HS2I data was separated into eight bins based on t_a ($t_a \leq 0°C$; $0°C < t_a \leq 5°C$; $5°C < t_a \leq 10°C$; $10°C < t_a \leq 15°C$; $15°C < t_a \leq 20°C$; $20°C < t_a \leq 25°C$; $25°C < t_a \leq 30°C$; $t_a > 30°C$). Descriptive statistics for a random subsample of HS2I (n = 600) in each room were calculated for each t_a bin. Further, each room was divided into four zones (n = 6, 5, 5, and 6 TESAs) spanning the length of the room (zone 1 to 4). For each zone, descriptive statistics for a random subsample of HS2I (n = 600) were calculated for each t_a bin.

The non-weighted uniformity of HS2I within a room was assessed by a uniformity coefficient, which relates the average deviation of each location from the room average (equation 6.8).

$$\gamma = 1 - \frac{1}{\sqrt{n}} \sum_{i=1}^{n} \frac{\sqrt{(HS2I_i - \overline{HS2I})^2}}{\overline{HS2I}} \tag{6.8}$$

where

γ	= uniformity coefficient (dimensionless)
n	= sample size ($16 \leq n \leq 22$)
$\overline{HS2I}$	= average HS2I
i	= TESA location ($1 \leq i \leq 22$)

A uniformity coefficient equal to unity indicates completely uniform and was calculated for the total study period and separated into the aforementioned eight t_a bins.

Results and discussion

Housed swine heat stress index

The final coefficient values for equations 6.1 to 6.7 (and the numerous cross-section equations not shown) to calculate HS2I are summarized in table 6.1. In addition, table 6.1 reiterates the valid input physical ranges and their associated units. While implementation of the set of equations to compute HS2I in table 6.1 is nontrivial, it is possible given the advances in computing power and programming. While the mechanistic model could be executed with desired TE inputs to achieve the estimated impact of the TE, the time required for convergence can be upwards of 2 s. The

mechanistic model also cannot accept inputs as arrays (n by 1 data); hence, it must be executed once for every unique set of TE conditions. The major benefit of this set of equations to calculate HS2I is that it can handle large arrays quickly, with substantially reduced computation time. Furthermore, the intricately modeled behavioral and physiological interactions in the mechanistic model were not intended to be utilized or understood by all users. This set of equations; however, can be widely adopted by a vastly larger group of users.

Table 6.1. Summary of regression coefficients for calculating HS2I for group housed, grow-finish pigs. Each equation is read horizontally with coefficients for each $f(x)$[a] or $g(x)$[b] listed underneath. Inputs and valid ranges are t_{db} (16°C to 33°C), RH (10% to 90%), airspeed (u; 0.2 to 3.0 m s^{-1}), and BW (50 to 120 kg). The effect of skin wetting is optional, S_{on} = 1 (wetted skin) or 0 (normal).

$\Delta t_b' =$	$f(RH)$	$t_{db}^2 +$	$f(RH)$	$t_{db} +$	$f(RH)$
β_1	2.492E-07		-8.072E-06		6.561E-05
β_2	9.543E-06		-3.002E-04		3.228E-03
β_3	-1.224E-04		5.477E-02		-5.928E-01

$\Delta t_b'' =$	$f(u)$	$\Delta t_b'$	$^{f(u)} +$	$f(u)$	
β_1	5.507E-02		-6.907E-02	2.091E-02	
β_2	-2.948E-01		3.028E-01	-1.953E-01	
β_3	1.133E+00		1.014E+00	-1.029E-01	

$\Delta t_b''' =$	$f(BW)$	$\Delta t_b'' +$	$f(BW)$		
β_1	-3.154E-06		1.006E-05		
β_2	-2.490E-03		4.579E-03		
β_3	1.250E+00		-4.944E-01		

$\Delta t_{b,w}' =$	$g(RH)$	t_{db}	$^{g(RH)} +$	$g(RH)$	
α_1	1.478E-05		-1.980E-03	-9.510E-04	
α_2	3.713E-04		2.045E+00	-2.433E-02	

$\Delta t_{b,w}'' =$	$f(u)$	$\Delta t_{b,w}'^{\,2} +$	$f(u)$	$\Delta t_{b,w}' +$	$f(u)$
β_1	-1.659E-01		4.420E-02		1.398E-02
β_2	9.741E-01		-4.858E-01		-3.879E-02
β_3	-1.137E+00		1.377E+00		4.843E-04

$\Delta t_{b,w}''' =$	$f(BW)$	$\Delta t_{b,w}'' +$	$f(BW)$		
β_1	-2.166E-05		2.310E-06		
β_2	-2.418E-03		2.242E-03		
β_3	1.526E+00		-2.741E-01		

$\Delta t_{b,w}'''' =$ $\Delta t_b''' - S_{on}\,\Delta t_{b,w}'''$ (equation 6.6) $\rightarrow$ $HS2I =$ $4.0148\,\Delta t_{b,w}'''' - 0.2961$ (equation 6.7)

[a] $f(x) = \beta_1 x^2 + \beta_2 x + \beta_3$

[b] $g(x) = \alpha_1 x + \alpha_2$

Validation

Model agreement between estimated Δt_b from the mechanistic model and $\Delta t_b''''$ predicted (S_{on} = 0) is shown in figure 6.1. The coefficient of determination (R^2) was 0.98 and root-mean-square error (RMSE) was 0.061°C. The slope (0.978) and intercept (0.0085) showed good linear agreement between the estimated and predicted values. Visual inspection of the residuals (figure 6.1) showed no apparent trend as a function of Δt_b as well as airspeed or BW. Lowest residuals were for Δt_b < 0.25°C. While the highest residuals were between 0.3°C < Δt_b < 0.9°C – and tended to be for larger BW (denoted by shape size) at intermediate to high airspeeds. This may be attributed to the large number of combinations of TE and BW that yield 0.3°C < Δt_b < 0.9°C, while the extreme Δt_b are only effected by a small number combinations. Typically, lower BW and higher airspeed will cause Δt_b to be lower, as opposed to high BW and low airspeed, where Δt_b will be higher compared to the normal range.

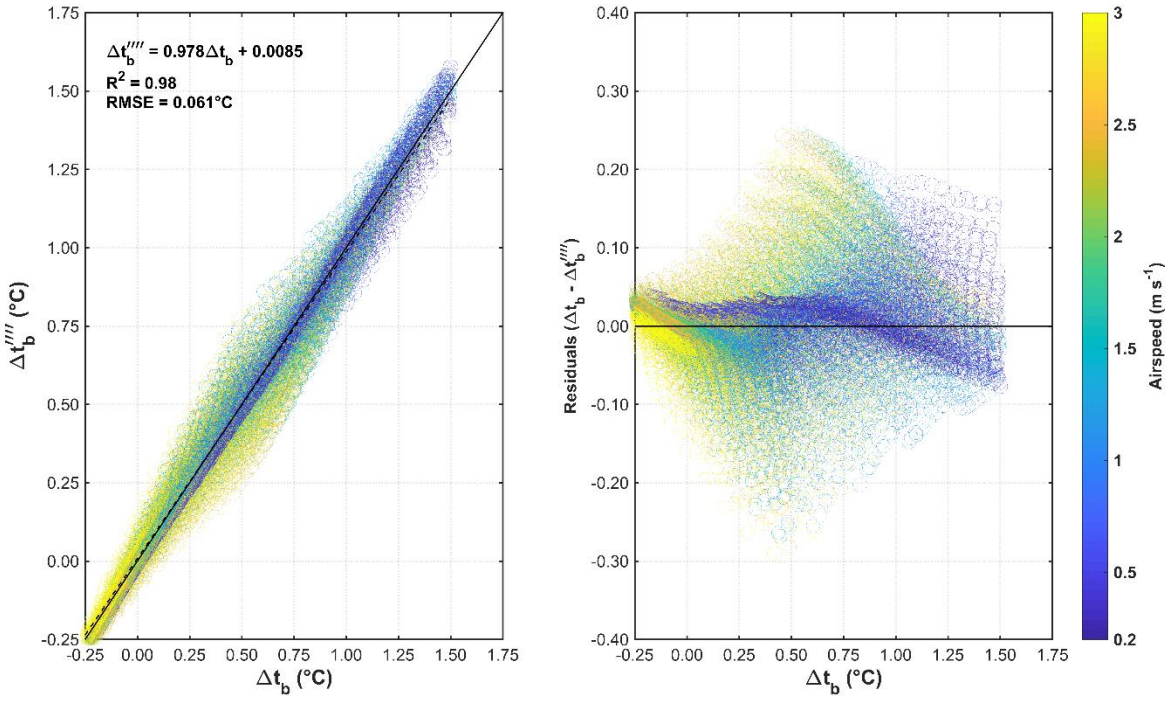

Figure 6.1. Agreement between Δt_b estimated from the mechanistic model at different combinations of TE and BW (n=15,517) and $\Delta t_b''''$ predicted (S_{on} = 0) using the set of equations in table 6.1. Shape size is proportional to BW.

With effect of wet skin included (S_{on} = 1), model agreement between Δt_b and $\Delta t_b''''$ predicted is shown in figure 6.2. The R^2 were 0.97 and RMSE was 0.054°C. The slope (1.07) and intercept (-0.0058) showed good linear agreement between the estimated and predicted values. Visual inspection of the residuals (figure 6.2) showed no apparent trend as a function of Δt_b, but some trends for airspeed are visible (denoted by color).

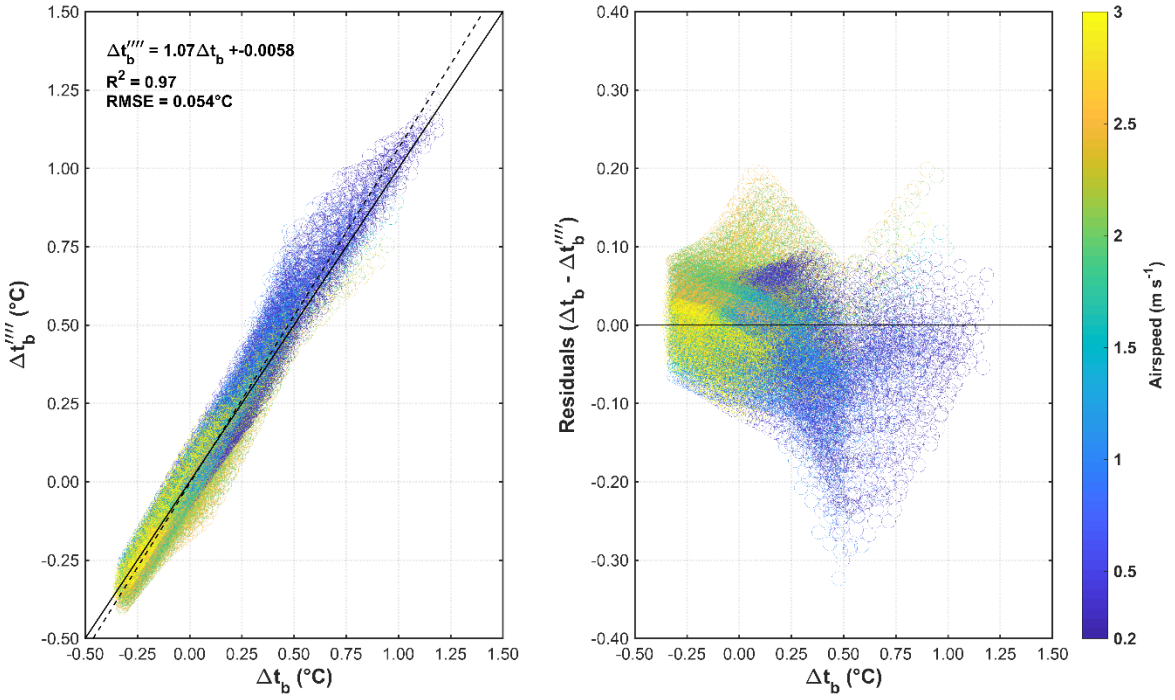

Figure 6.2. Agreement between Δt_b estimated from the mechanistic model at different combinations of TE and BW (n=15,517) and $\Delta t_b''''$ predicted (S_{on} = 1) using the set of equations in table 6.1. Shape size is proportional to BW.

While the error over the majority of TE conditions and BW was small (denoted by the low RMSE), there were some residual values that were much larger (e.g., -0.3°C at Δt_b = 0.5°C; figure 2); thus, indicating, some TE and BW combinations that could yield potentially high error in HS2I. A sensitivity analysis (figure 6.3) shows the absolute and relative impact of $\Delta t_b''''$ estimation error present due to the inadequate fitting some of the parameters. For a ±0.1°C error, HS2I varied ±0.8 and for a ±0.3°C error, HS2I varied ±1.6 between -0.25°C < $\Delta t_b''''$ < 1.25°C. Within the three defined regions of HS2I (0 to 3; 4 to 7; 8 to 10) a less than HS2I±1 error is manageable because

HS2I remains within or near the threshold for a region. The larger error has more substantial implications as it could indicate the difference between thermally comfortable and moderately heat stressed.

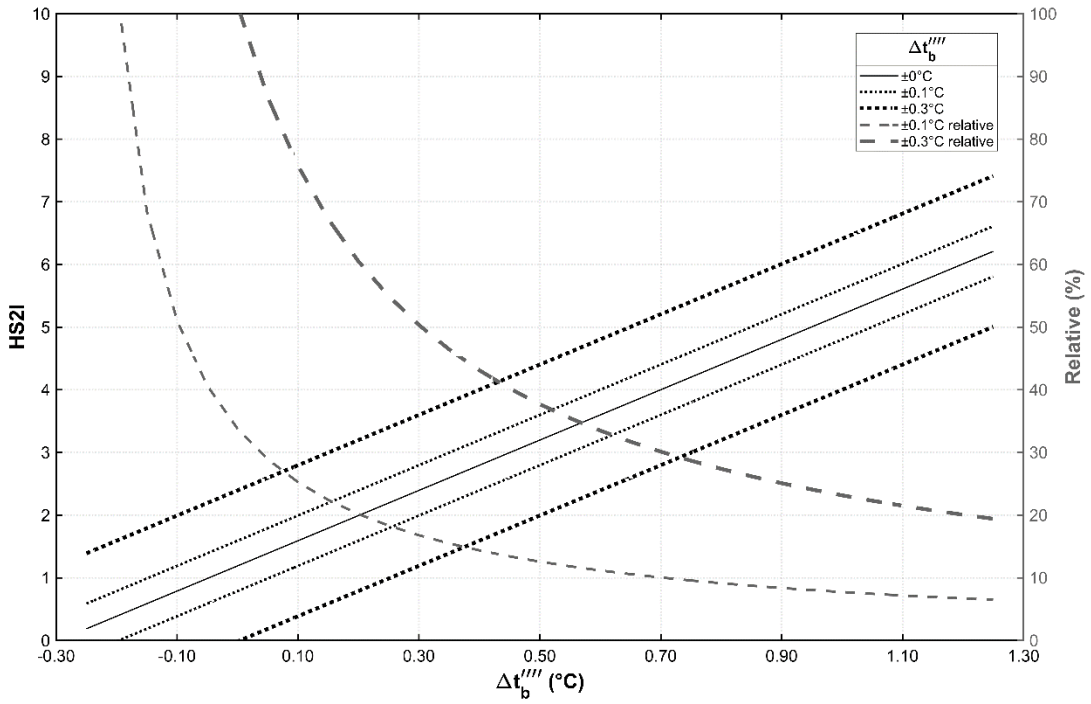

Figure 6.3. Sensitivity analysis demonstrates the potential impact of $\Delta t_b''''$ estimation error attributed to fitting multiple regression during the development of HS2I. Based on the visual inspection of the residuals (figure 6.1 and 6.2), error < ±0.1°C are expected for $\Delta t_b''''$ < 0.3°C.

The FFI and CT models developed by Renaudeau et al. (2011) showed reasonable agreement for predicting the onset of heat stress for a range of BW (figure 6.4). The CT is used to predict the t_{db} where FFI begins to decrease at an increased rate – this would correspond to HS2I = 3. The actual and ideal agreement where CT and HS2I = 3 intersect for different BWs is shown in figure 6.4. Also apparent is the dependence of BW on the onset and extent of heat stress. As observed in both the FFI model and HS2I, heat stress occur at less warm TE conditions and has a greater impact as TE conditions get warmer. The FFI and CT models do not include the effects of RH or airspeed. If so, an increase in airspeed would increase CT (increased airspeed results in increased heat loss) or conversely, an increased RH (once sensible heat loss has decreased) would decrease CT, as pigs

would not be able to utilize latent heat loss modes. Nevertheless, CT is a practical and useful tool but there are opportunities to develop a comprehensive CT that includes the effects of airspeed and RH.

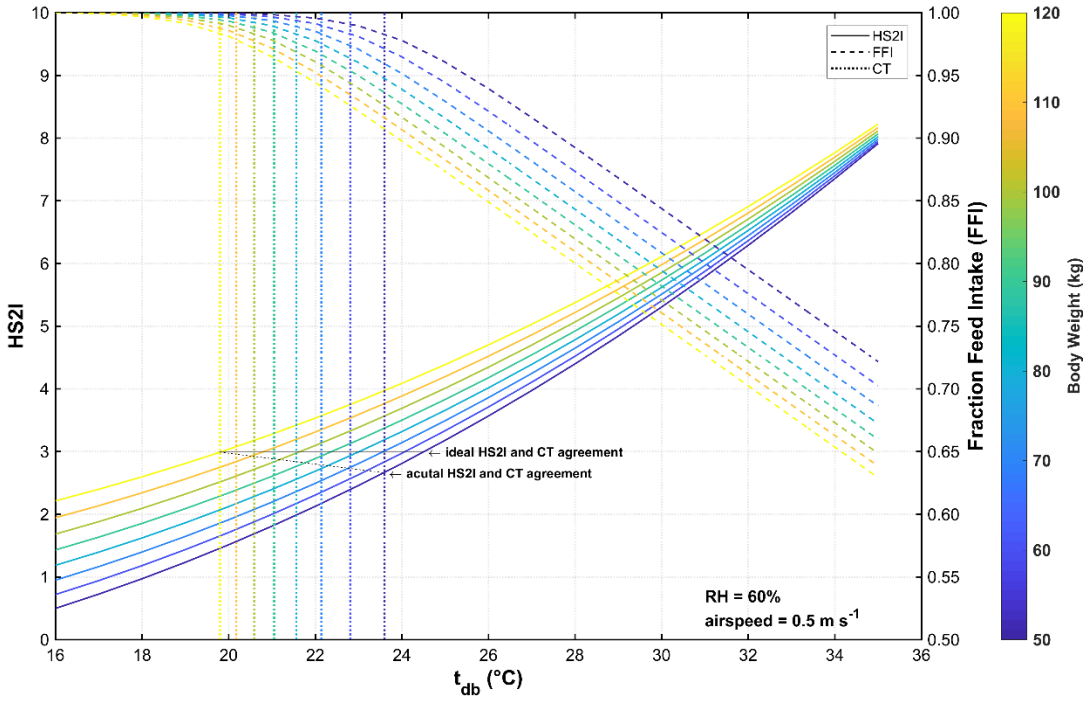

Figure 6.4. Agreement between HS2I with FFI and critical temperature (CT) models developed by Renaudeau et al. (2011). The onset of performance penalties due to heat stress is defined by CT and a HS2I = 3.

HS2I was compared to WDTI (Roller & Goldman, 1969) over a BW and airspeed range to demonstrate the physiological relevance to WDTI (figure 6.5). Commonly associated threshold values for the temperature humidity index (THI; analogous to WDTI) are normal: ≤74; alert: 75 to 78; danger: 79 to 83; and emergency: ≥84 (figure 6.5; DeShazer, 2009). The nearest HS2I curves to the intersection of alert threshold (WDTI = 74) and HS2I = 3 for 60, 90, and 120 kg pig are WDTI = 73 (2 m s^{-1}), 74 (1 m s $^{-1}$), and 75.5 (0.5 m s^{-1}), respectively. WDTI was developed with 60 to 90 kg pigs presumably housed in low airspeed conditions (i.e., less than 1 m s^{-1}). There appears to be reasonable agreement between HS2I = 3 and the alert threshold when airspeed is accounted for. However, WDTI was developed at conditions of WDTI > 87. At these conditions,

pigs will rely heavily on latent modes of heat loss (i.e., elevated respiration, wallowing, maximized passive diffusion), where t_{wb} has a substantial impact of the rate of heat loss. The relative proportions of the t_{db} and t_{wb} weights are dependent on the conditions from which the data was collected.

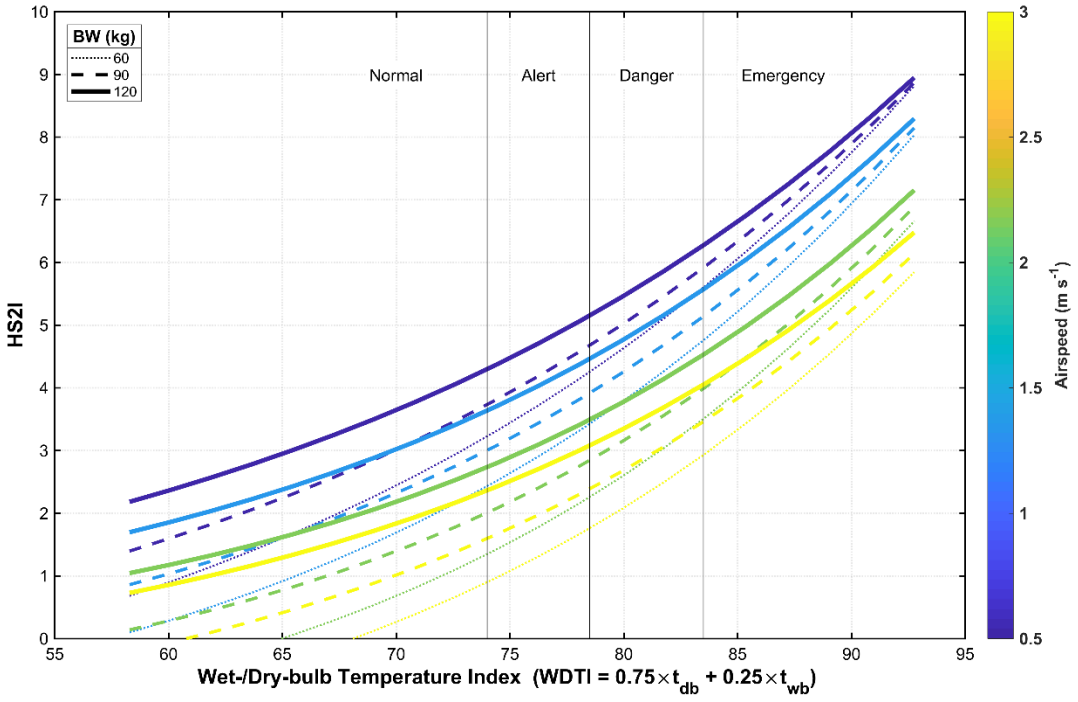

Figure 6.5. Comparison of HS2I and the wet-/dry-bulb temperature index (WDTI; Roller & Goldman, 1969) for three BW and airspeeds. Commonly associated threshold values for WDTI are normal: ≤74; alert: 75 to 78; danger: 79 to 83; and emergency: ≥84 (DeShazer, 2009).

Elevated airspeeds are commonly used in commercial grow-finish facilities to alleviate the effects of heat stress (Albright, 1990). For increasing airspeeds, HS2I decreased as well, but only marginally for airspeeds greater than 2 m s^{-1}, as illustrated in figure 6.5. Further, the difference in HS2I between 0.5 and 3 m s^{-1} for the 60 kg pigs is greater than the 120 kg pigs. These results agree with previous literature, where the convective benefit has shown to decrease with increasing airspeeds (Hoff, 2013). Forced-convection heat loss was estimated in the mechanistic model from the results of empirical correlations for convective heat transfer coefficients in cross flow over a circular cylinder (Holman, 2002). Li, Rong, & Zhang (2016) showed these correlations to be a

reasonable assumption for pigs and the relative impact of the turbulence intensity – animal body orientation interaction at different airspeeds on the average convective heat transfer coefficient. The heat transfer process is influenced by the flow processes. The rapidly increasing convective heat loss is explained by the developing turbulent eddy motion in the separated flow on the rear side of the cylinder and the transition of the boundary layer to turbulent. This eddy motion at separation continues to increase, resulting in an increase in heat transfer but with decreasing effect.

Lastly, the effect of wetted skin (S_{on} = 1) on HS2I (figure 6.6) was examined for a constant BW (110 kg) and a range of RH (50% and 70%) and airspeed (0.5 to 3 m s^{-1}). Both RH and airspeed had an effect of HS2I – this agrees with mass and heat transfer theory. For example, at 34°C, low airspeed (0.5 m s^{-1}), and high RH (70%; t_{wb} = 29°C), HS2I decreases from 9.0 to 7.4, when wetted (~1.6 HS2I difference). In comparison, at 34°C, high airspeed (> 2 m s^{-1}), and regardless of RH, HS2I decreases from 9.0 to less than 4 once wetted (> 5 HS2I difference). An approximately 3.1 times difference in HS2I. The effect of RH on HS2I with non-wetted skin is evident as shown by the ~1.7 HS2I difference from 70% to 50% regardless of airspeed. A similar effect was observed by Thuy (2005) and is reasonable because, t_{db} is approaching skin temperature (sensible heat loss is minimized) and latent heat loss modes are utilized by the pig, but the high t_{wb} inhibits the efficiency of these modes. Interestingly, the effect of RH on HS2I with wetted skin was more prevalent at low airspeeds compared to high airspeeds. There is a ~1.3 HS2I difference between RHs of 50% and 70% at 0.5 m s^{-1} – as opposed to a ~0.9 HS2I difference at the same RH at >2 m s^{-1}. Similarly, HS2I decreases marginally with increasing airspeed with wetted skin and for a given t_{db}, decreasing RH has a more substantial effect.

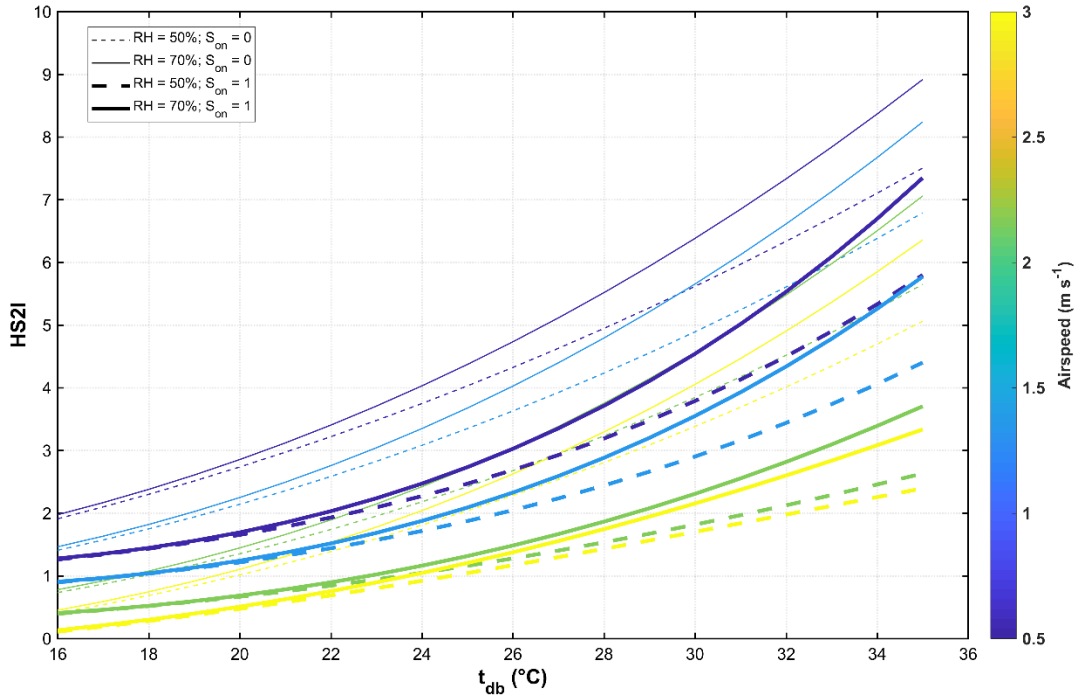

Figure 6.6. Demonstration of the effect of wetted skin (S_{on} = 1) on HS2I for a constant BW (110 kg) pig. At 34°C (0.5 m s^{-1}; RH = 70%; HS2I = 9), the combination of wetted skin and elevated airspeed (> 2 m s^{-1}; regardless of RH) reduced HS2I to less than 4.

The considerably greater heat loss rate associated with wetted skin and concurrently elevated airspeeds requires careful interpretation for practical considerations. As depicted in figure 6.6, for 110 kg pigs (near market weight), HS2I remains below 4 for t_{db} < 35°C. While this is positive for this sized pig, lighter BW may be negatively affected by wetted skin, if t_{db} is not sufficiently high enough. For example, 60 kg pigs remain at HS2I < 3 at t_{db} < 29°C and ≥ 0.5 m s^{-1}, regardless of RH. This has major implications for sprinkler control systems in grow-finish facilities. Airspeed, BW, and t_{db} (also RH, but is rarely accommodated for in modern control systems) need to be accounted for in the management decisions for the sprinkler 'on' conditions. Furthermore, control of sprinkler systems could be optimized to maximize heat loss with minimize water usage by adjusting the evaporation time ('off' interval) to include the TE inside the facility (Ramirez, Hoff, & Harmon, 2017b).

Case study

For all ambient temperatures (t_a) encountered for flow 2, the $t_{db} = t_{mr}$ assumption was reasonable based on inspection of the descriptive statistics of a linear model agreement between t_{db} and t_{mr} for 22 TESAs in each room (table 6.2). The mean slope for each room was nearly unity good linear agreement; however, the intercept was greater than zero for both rooms. This suggests that t_{mr} tended to be slightly higher than t_{db}. For $t_a \leq 20°C$, the t_{mr} was anticipated to be greater than t_{db} in the S room due to the length of building (curtain sided) being exposed to the sun. With pigs present, it may be difficult to detect the increased curtain surface temperature. When the rooms were empty (early February when ambient temperatures are less than 0 °C), the increased curtain surface temperature was measureable by the TESAs located nearest the curtain (data not shown). Most likely, the heat production from the pigs and the forced air furnaces reduced the ability to discern any environmental factors. Interestingly, an increased intercept and decreased slope associated with $t_a > 20°C$ was found, implying surrounding surfaces tended to be warmer than t_a but this difference decreased as t_a increased. The moving average was imperative to improving the estimation of t_{mr} because the forced air furnaces rapidly increased t_{db} and airspeed, resulting in swift and unrealistic decreases in t_{mr}.

Table 6.2. Average (95% confidence interval) linear regression statistics resulting from t_{db} versus t_{mr} for the north (N) and south (S) room (n = 22 each) for the whole study and two ambient temperature (t_a) ranges.

	Slope	Intercept	R^2	RMSE (°C)
All t_a				
N room	0.966 (0.999, 0.933)	2.824 (3.563, 2.084)	0.831 (0.884, 0.777)	1.598 (1.958, 1.237)
S room	0.994 (1.121, 0.867)	1.547 (3.291, -0.196)	0.850 (0.934, 0.767)	1.779 (2.740, 0.819)
$t_a \leq 20°C$				
N room	0.998 (1.045, 0.951)	2.002 (2.968, 1.037)	0.807 (0.868, 0.745)	1.605 (2.005, 1.204)
S room	1.053 (1.135, 0.971)	0.193 (1.248, -0.863)	0.852 (0.935, 0.768)	1.628 (2.430, 0.826)
$t_a > 20°C$				
N room	0.794 (0.820, 0.767)	7.511 (8.285, 6.737)	0.894 (0.927, 0.862)	1.035 (1.215, 0.854)
S room	0.722 (0.842, 0.602)	8.684 (9.863, 7.504)	0.845 (0.928, 0.763)	1.498 (2.755, 0.241)

Mean HS2I (95% CI) binned by t_a for the South (S) and North (N) rooms for flow 1 (Aug-12, 2016 to Jan-26, 2017) and 2 (Feb-2, 2017 to July-16, 2017) are presented in table 6.3. Due to a configuration error during flow 1 during the first six weeks of the study, the t_{db} in N room was higher than S room. While this is not apparent in table 6.3, this may suggest that both rooms were maintained warmer than needed. For flow 2, both rooms maintained reasonable TEs (i.e., HS2I < 4) for a large portion of the study. Since t_a influences the TE inside the rooms, warmer t_a results in a higher HS2I, but since this facility was tunnel ventilated, it is assumed that the elevated airspeed maintained a low HS2I even with increased t_a.

Table 6.3. Mean HS2I (95% CI) binned by ambient temperature (t_a) for the South (S) and North (N) rooms for flow 1 (Aug-12, 2016 to Jan-26, 2017) and 2 (Feb-2, 2017 to July-16, 2017).

	N room		S Room	
Flow:	1	2	1	2
$t_a \leq 0°C$	2.76 (2.80, 2.72)	1.86 (1.89, 1.84)	2.79 (2.83, 2.76)	1.92 (1.95, 1.89)
$0°C < t_a \leq 5°C$	2.35 (2.38, 2.31)	2.18 (2.21, 2.15)	2.56 (2.60, 2.52)	2.27 (2.30, 2.25)
$5°C < t_a \leq 10°C$	2.69 (2.73, 2.64)	2.31 (2.34, 2.27)	2.70 (2.74, 2.65)	2.56 (2.59, 2.53)
$10°C < t_a \leq 15°C$	3.79 (3.83, 3.74)	2.30 (2.33, 2.27)	3.57 (3.61, 3.53)	2.91 (2.94, 2.88)
$15°C < t_a \leq 20°C$	4.57 (4.61, 4.52)	2.27 (2.31, 2.24)	4.27 (4.31, 4.24)	3.10 (3.14, 3.06)
$20°C < t_a \leq 25°C$	5.17 (5.21, 5.13)	2.54 (2.58, 2.50)	4.53 (4.57, 4.50)	3.28 (3.32, 3.24)
$25°C < t_a \leq 30°C$	5.64 (5.68, 5.60)	2.90 (2.94, 2.86)	5.39 (5.42, 5.36)	3.38 (3.42, 3.34)
$t_a > 30°C$	5.14 (5.19, 5.10)	3.34 (3.39, 3.29)	5.01 (5.05, 4.97)	3.73 (3.77, 3.69)

Mean (95% CI) HS2I for four zones (1 to 4) distributed down the length of the building binned by t_a for N and S rooms for flows 1 and 2 are shown in table 6.4. During tunnel ventilation (i.e., fresh air pulled the length of the building from the tunnel curtain at the one end wall to fans at the other end wall in hot conditions), if there is not adequate fan capacity, heat and moisture can accumulate down the length of the building. Based on the average values obtained in each zone, it appears the facility had sufficient fan capacity as no increasing trend of HS2I is observed. Further, the N room for flow 2 shows HS2I to be greater than 3 for as low as $10°C < t_a \leq 15°C$. The lowest t_{db} setpoint in the facility was ~19.4°C and this occurred during the summer with the heaviest BW

pigs. This was most likely more attributed to the combination of low airspeeds and inadequate ventilation when the ventilation is transitioning between ceiling inlets and tunnel mode.

Table 6.4. Mean (95% CI) HS2I for four zones (1 to 4) down the length of the building binned by ambient temperature (t_a) for the South (S) and North (N) rooms for flow 1 (Aug-12, 2016 to Jan-26, 2017) and 2 (Feb-2, 2017 to July-16, 2017).

		N room		S Room	
Zone	Flow:	1	2	1	2
1	$t_a \leq 0°C$	2.54 (2.60, 2.49)	1.63 (1.73, 1.54)	2.61 (2.65, 2.57)	1.59 (1.68, 1.50)
	$0°C < t_a \leq 5°C$	2.14 (2.19, 2.08)	1.79 (1.87, 1.70)	2.18 (2.23, 2.14)	1.93 (2.02, 1.84)
	$5°C < t_a \leq 10°C$	2.27 (2.36, 2.17)	2.00 (2.06, 1.95)	2.18 (2.23, 2.13)	2.29 (2.34, 2.25)
	$10°C < t_a \leq 15°C$	3.39 (3.53, 3.25)	1.85 (1.92, 1.77)	3.09 (3.20, 2.98)	2.48 (2.53, 2.43)
	$15°C < t_a \leq 20°C$	4.17 (4.30, 4.04)	1.96 (2.06, 1.87)	3.92 (4.04, 3.80)	2.63 (2.71, 2.55)
	$20°C < t_a \leq 25°C$	4.76 (4.88, 4.64)	2.35 (2.45, 2.26)	4.21 (4.34, 4.08)	2.81 (2.90, 2.72)
	$25°C < t_a \leq 30°C$	5.23 (5.33, 5.13)	2.55 (2.63, 2.48)	5.20 (5.32, 5.08)	2.87 (2.94, 2.81)
	$t_a > 30°C$	4.87 (4.96, 4.79)	2.91 (2.99, 2.83)	4.69 (4.80, 4.57)	3.23 (3.29, 3.17)
2	$t_a \leq 0°C$	2.85 (2.90, 2.79)	1.88 (1.97, 1.78)	3.06 (3.11, 3.02)	1.92 (2.02, 1.83)
	$0°C < t_a \leq 5°C$	2.36 (2.42, 2.31)	2.10 (2.19, 2.01)	2.67 (2.72, 2.63)	2.23 (2.32, 2.14)
	$5°C < t_a \leq 10°C$	2.50 (2.59, 2.41)	2.31 (2.37, 2.25)	2.70 (2.75, 2.64)	2.61 (2.66, 2.56)
	$10°C < t_a \leq 15°C$	3.82 (3.96, 3.68)	2.15 (2.22, 2.08)	3.61 (3.71, 3.51)	2.79 (2.84, 2.74)
	$15°C < t_a \leq 20°C$	4.66 (4.79, 4.53)	2.15 (2.24, 2.06)	4.33 (4.43, 4.23)	2.90 (2.96, 2.85)
	$20°C < t_a \leq 25°C$	5.17 (5.29, 5.05)	2.38 (2.48, 2.29)	4.48 (4.59, 4.37)	3.14 (3.21, 3.07)
	$25°C < t_a \leq 30°C$	5.64 (5.74, 5.54)	2.59 (2.65, 2.53)	5.33 (5.44, 5.22)	3.17 (3.22, 3.12)
	$t_a > 30°C$	5.10 (5.21, 5.00)	2.97 (3.03, 2.92)	4.93 (5.02, 4.84)	3.54 (3.58, 3.49)
3	$t_a \leq 0°C$	2.90 (2.96, 2.85)	1.98 (2.07, 1.88)	3.16 (3.20, 3.12)	2.14 (2.23, 2.04)
	$0°C < t_a \leq 5°C$	2.53 (2.58, 2.48)	2.30 (2.39, 2.20)	2.95 (3.00, 2.91)	2.48 (2.58, 2.39)
	$5°C < t_a \leq 10°C$	2.85 (2.94, 2.75)	2.59 (2.65, 2.53)	3.05 (3.10, 2.99)	2.96 (3.01, 2.91)
	$10°C < t_a \leq 15°C$	4.16 (4.31, 4.01)	2.47 (2.54, 2.41)	3.90 (4.00, 3.81)	3.29 (3.34, 3.24)
	$15°C < t_a \leq 20°C$	5.05 (5.18, 4.92)	2.48 (2.57, 2.39)	4.50 (4.61, 4.39)	3.56 (3.62, 3.50)
	$20°C < t_a \leq 25°C$	5.55 (5.68, 5.43)	2.73 (2.83, 2.64)	4.60 (4.74, 4.47)	3.71 (3.78, 3.64)
	$25°C < t_a \leq 30°C$	6.13 (6.23, 6.03)	2.95 (3.01, 2.90)	5.54 (5.65, 5.43)	3.68 (3.74, 3.62)
	$t_a > 30°C$	5.66 (5.76, 5.56)	3.37 (3.43, 3.31)	5.19 (5.28, 5.10)	4.06 (4.10, 4.02)
4	$t_a \leq 0°C$	2.53 (2.58, 2.48)	2.02 (2.12, 1.93)	2.43 (2.47, 2.39)	2.14 (2.24, 2.03)
	$0°C < t_a \leq 5°C$	2.25 (2.30, 2.20)	2.07 (2.16, 1.97)	2.41 (2.47, 2.36)	2.09 (2.18, 1.99)
	$5°C < t_a \leq 10°C$	2.50 (2.58, 2.41)	2.34 (2.39, 2.29)	2.60 (2.68, 2.52)	2.43 (2.49, 2.37)
	$10°C < t_a \leq 15°C$	3.64 (3.77, 3.51)	2.50 (2.56, 2.44)	3.46 (3.56, 3.36)	2.98 (3.05, 2.91)
	$15°C < t_a \leq 20°C$	4.42 (4.54, 4.30)	2.68 (2.76, 2.60)	4.23 (4.34, 4.13)	3.40 (3.46, 3.34)
	$20°C < t_a \leq 25°C$	4.87 (4.98, 4.75)	3.05 (3.14, 2.96)	4.39 (4.52, 4.27)	3.61 (3.68, 3.53)
	$25°C < t_a \leq 30°C$	5.51 (5.60, 5.43)	3.43 (3.49, 3.37)	5.43 (5.55, 5.31)	3.69 (3.75, 3.62)
	$t_a > 30°C$	5.01 (5.10, 4.93)	3.90 (3.95, 3.85)	5.15 (5.25, 5.06)	4.07 (4.12, 4.03)

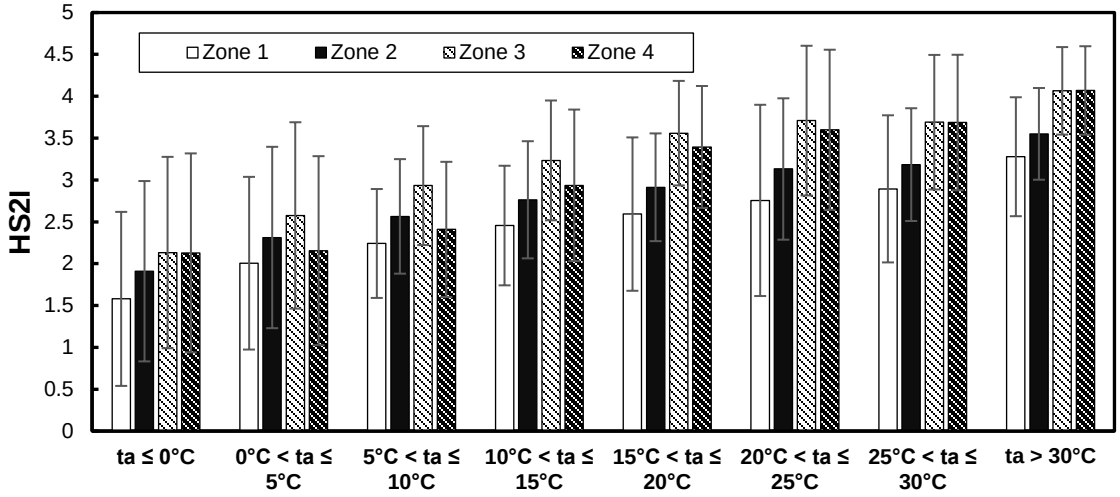

Figure 6.7. Example of mean (95% CI) HS2I for four zones (1 to 4) down the length of the building binned by ambient temperature (t_a) for the North room for flow 2 (Feb-2, 2017 to July-16, 2017).

Mean (95% CI) uniformity coefficient (maximum = 1) binned by t_a is presented in figure 6.7. For both rooms and flows, uniformity coefficient tended to decrease from the coldest bin to the $10°C < t_a \leq 15°C$ and then increase to the warmest bin – with highest values found near the extreme bins. This result seems reasonable as the controller can adjust inlet opening and heater run time to maintain t_{db} setpoint during colder conditions. Conversely, at warmer conditions, which usually exceed the t_{db} setpoint, the transitions between power to tunnel can lead to a more severe lack of uniformity. This result also suggests that mild weather ventilation (t_a range 5°C to 20°C) is one of the major challenges prohibiting the delivery and control of a thermally optimal and uniform environment in modern swine facilities.

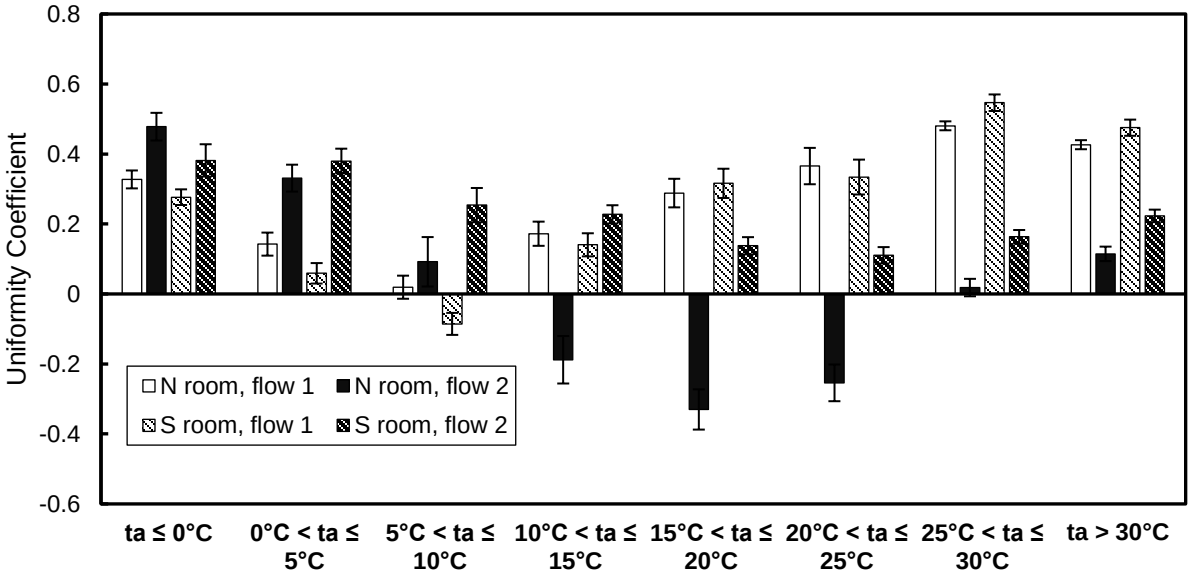

Figure 6.8. Mean (95% CI) uniformity coefficient (maximum = 1) binned by ambient temperature (t_a) for the South (S) and North (N) rooms for flow 1 (Aug-12, 2016 to Jan-26, 2017) and 2 (Feb-2, 2017 to July-16, 2017).

Conclusions

Advanced methods to measure and evaluate the thermal environment (TE) in swine facilities are needed to sustainably provide animal-based protein for the increasing global population. The lack of a thermal index specific to growing pigs (~55 million in production) capable of capturing the individual and combined effects of t_{db}, RH, airspeed, and body weight has driven the need for the housed swine heat stress index (HS2I). The HS2I can be used to evaluate the potential impact of the TE in existing facilities and as a design tool to explore different ventilation and cooling strategies. More specifically, for the comparison of commercially available elevated airspeeds, evaporative pads, and sprinklers. Other potential technologies or management strategies can now be readily be compared. The application of HS2I to spatiotemporal data collected in a commercial facility provides preliminary insight for using HS2I to assess the TE. The HS2I is a major innovation necessary to improve the TE design, assessment, and control.

Acknowledgements

This research was supported with funding provided by the Iowa Pork Producers Association under NPB Project 14-242. The authors would like to acknowledge the contributions of undergraduate students Grant Hoppes, Heather Tenboer, Oluwadurotimi Koya, Sara Weyer, and Jesse Klaes during the preparation and completion of this work.

References

Albright, L. D. (1990). *Environment control for animals and plants.* St. Joseph, MI: American Society of Agricultural Engineers.

Beckett, F. E. (1965). Effective Temperature for Evaluating or Designing Hog Environments. *Transactions of the ASAE*, *8*(2), 0163–0166. https://doi.org/10.13031/2013.40457

Collin, A., van Milgen, J., Dubois, S., & Noblet, J. (2001). Effect of high temperature on feeding behaviour and heat production in group-housed young pigs. *British Journal of Nutrition*, *86*(01), 63–70. https://doi.org/10.1079/BJN2001356

da Silva, R. G., & Maia, A. S. C. (2012). *Principles of animal biometeorology* (Vol. 2). Springer Science & Business Media.

DeShazer, J. A. (2009). *Livestock Energetics and Thermal Environmental Management* (1st ed.). St. Joseph, MI: American Society of Agricultural and Biological Engineers.

Fournel, S., Rousseau, A. N., & Laberge, B. (2017). Rethinking environment control strategy of confined animal housing systems through precision livestock farming. *Biosystems Engineering*, *155*, 96–123. https://doi.org/10.1016/j.biosystemseng.2016.12.005

Hoff, S. J. (2013). The impact of ventilation and thermal environment on animal health, welfare and performance. In *Livestock Housing: Modern Management to Ensure Optimal Health and Welfare of Farm Animals* (pp. 209–236). Wageningen Academic Publishers. https://doi.org/10.3920/978-90-8686-771-4_11

Holman, J. P. (2002). *Heat Transfer* (9th ed.). New York City, NY: McGraw-Hill.

Ingram, D. L. (1965). The effect of humidity on temperature regulation and cutaneous water loss in the young pig. *Research in Veterinary Science*, *6*, 9–17.

IPCC. (2014). *Climate Change 2014: Mitigation of Climate Change* (Working Group III - Mitigation of Climate Change No. Assessment Report 5). Intergovernmental Panel on Climate Change.

ISO 7726. (2001). *Ergonomics of the thermal environment — instruments for measuring physical quantities*. Geneva: International Standardization Organization.

Li, H., Rong, L., & Zhang, G. (2016). Study on convective heat transfer from pig models by CFD in a virtual wind tunnel. *Computers and Electronics in Agriculture*, *123*(Supplement C), 203–210. https://doi.org/10.1016/j.compag.2016.02.027

Mader, T. L., Johnson, L. J., & Gaughan, J. B. (2010). A comprehensive index for assessing environmental stress in animals. *Journal of Animal Science*, *88*(6), 2153–2165.

Moura, D. J., Naas, I. A., Silva, I. J. O., Sevegnani, K. B., & Corria, M. E. (1997). The use of enthalpy as a thermal comfort index. In *Proceedings of the 5th Livestock Environment Symposium* (Vol. 1, pp. 577–583). Bloomington, MN.

NRC. (2012). *Nutrient Requirements of Swine* (11th ed.). Washington D.C.: The National Academies Press.

PIC. (2013). *Wean to finish manual*.

Ramirez, B. C., Hoff, S. J., & Harmon, J. D. (2017a). An improved assessment of the effective environment for analysis of heat stress mitigation techniques. In *Int. Symp. on Animal Environ. & Welfare*. Chongqing, China.

Ramirez, B. C., Hoff, S. J., & Harmon, J. D. (2017b). Design and feasibility of a novel sprinkler control algorithm for swine heat stress alleviation. *Journal of Animal Science*, *95*(supplement2), 5–6. https://doi.org/10.2527/asasmw.2017.012

Renaudeau, D., Gourdine, J.-L., & St-Pierre, N. R. (2011). A meta-analysis of the effects of high ambient temperature on growth performance of growing-finishing pigs. *Journal of Animal Science*, *89*(7), 2220–2230.

Roller, W. L., & Goldman, R. F. (1969). Response of swine to acute heat exposure. *Transactions of the ASAE*, *12*(2), 164–0169.

Stalder, K. J. (2015). *Pork industry productivity analysis*. Des Moines, IA: National Pork Board.

St-Pierre, N. R., Cobanov, B., & Schnitkey, G. (2003). Economic Losses from Heat Stress by US Livestock Industries. *Journal of Dairy Science*, *86*, *Supplement*, E52–E77. https://doi.org/10.3168/jds.S0022-0302(03)74040-5

Thuy, H. T. T. (2005). *Heat stress in growing pigs* (Doctoral). Wageningen University, Wageningen, The Netherlands.

CHAPTER 7. GENERAL CONCLUSIONS

Five technical manuscripts were developed as individual components of this dissertation – and when combined, create a unique corpus of knowledge containing the methodology required to measure, understand, and assess the thermal environment (TE) in swine housing. Modern and future intensified swine production systems are necessary for meeting the increasing global animal-based protein demand. They are still in their infancy, in terms of providing an optimized design and control of the TE. This dissertation provides the necessary framework and initial steps required to improve production efficiency through advancing TE measurement and evaluation. The TE sensor array (TESA) is forward progress in transitioning beyond only measuring dry-bulb temperature and has created a novel opportunity to evaluate the TE from a heat balance approach. Our understanding of the TE and how it affects pig performance were advanced by the development and refinement of a mechanistic thermal balance model for grow-finish pigs. This model and TESA together, created and demonstrated an opportunity to develop several novel techniques for assessing the quality of the TE in a commercial grow-finish facility. As a result, the newly created housed swine heat stress index (HS2I) will produce numerous prospective approaches to quantify the total impact of TE for guiding ventilation design and risk management decisions. This dissertation is unique and complete since it provides all the key mechanisms for measuring, understanding, and assessing the TE.

This dissertation highlights pioneering advances in TE instrumentation, specifically for quantifying the requisite parameters for describing the sensible and latent modes of heat loss from swine. A heat balance approach is needed to further progress the ventilation system design, feedback sensors, and control of the TE. Since, total heat loss must equal the total heat produced as a product of metabolism, a housing system should provide and control a TE such that can it can

remove the amount of heat needed for the animal to remain in thermal balance. Classically, the goal of the ventilation system was to provide the conditions that maintain the animals within their thermoneutral zone, but in order to meet the simultaneous economic and food security demands, housing systems will need to operate within the animal's zone of least thermoregulatory effort (comfort zone). To accomplish this, a much more narrow range of TE conditions needs to be maintained; hence, both instrumentation and control systems need to be advanced. Ideally, ventilation systems will target removing the amount of heat produced at maximum production performance. However, this thermal balance point will ultimately be a function of time and is unique for every animal in a room, so this small comfort region will need to be expanded such that it could incorporate the majority of the animals in a given TE. Additionally, an improvement is needed to create more specialized TE zones within a room to deliver the thermal demand required for particular animals. This thermal balance point is also a function of body weight, dietary energy content, genetics, management, health status, etc. and must be continuously kept up to date as conditions in the facility change, if this methodology is to be implemented in a commercial setting.

While this dissertation focuses primarily on the narrow facet of grow-finish swine, a large economic and meat-producing sector of animal production, the fundamentals presented here could be extended to other stages of swine production as well as other livestock and poultry. Grow-finish swine serve as a good foundation due to their, while outdated, well-described metabolic heat production, thermoregulatory responses, and housing systems. In the breeding, gestation, and farrowing stages of swine production, the extreme variation in animal weights (heavy body weights for sows and gilts versus farrowed piglets) and additional energy demands due to reproduction, would require manipulation of the mechanistic model and additionally, the physical location of where to measure the TE. Other livestock, such as beef and dairy cattle, as well as

poultry, such as broilers, layers, turkey breeder stock, and grow-out turkeys, all have unique physiological, metabolic, and reproductive demands that would have to be accounted for in a mechanistic model. Regardless of species, reproductive status, and growth stage – an ideal heat production associated with maximum production or growth performance exists. A heat balance approach to TE control and design is required if improvements in production efficiency are desired; however, optimal TE control must be continually adjusted based on health status, genetic line, etc. autonomously with advanced electronic feedback.

While TESA was originally intended for standalone research applications, it could be readily incorporated into commercial ventilation controllers by removing the microprocessor, digital sensors, and serial communication, and replacing them with analog sensors. Most controllers feature multiple analog to digital converters that could accommodate these additional sensors. The next step would be to develop new control logic for operating fans, heaters, etc. Another potential application is to adopt TESA into a standalone datalogger configuration for short or long-term deployment. A TESA in this configuration could serve as a useful tool for identifying and troubleshooting inadequate ventilation, heating, and cooling. The sensors accompanying TESA and its housing were shown to be robust, but more effort is needed to ensure these sensors can remain accurate and precise in the dynamic and extreme environments inside swine (or poultry) facilities. This initial design and execution of TESA have created numerous potential opportunity to expand TESA for other indoor and outdoor environments.

The newly developed HS2I is the first of its kind (specific to pigs) capable of incorporating multiple parameters in a single dimensionless value. It further demonstrates the ingenuity needed to integrate of all the TE parameters, such that the heat balance approach is not neglected. Since the data to derive this index were created from a mechanistic model, rather than empirically

collected, no random variation exists. A unique opportunity exists to validate the mechanistic model with empirically collected animal responses and further refine this index. Nevertheless, HS2I has substantial importance for the swine industry. The method outlined here could also be used to develop more indices that are specific to certain stages of production. For example, farrowing, boar studs, gilt development, where the uniqueness of both the animal and housing style require individually validated measurement systems and models. This index could also be integrated into a ventilation control system to replace traditional air temperature decisions. In the event electronics or the internet are unavailable, but assessing the potential impact of heat stress is desired, the index could be translated graphically, in the form of a nomogram, and coupled with the handheld meters commonly available to most producers.

Overall, these studies individually and collectively will help the swine industry by providing new technology and methods for measuring, understanding, and assessing the thermal environment. While much of the work presented in this dissertation is still in the research phase, effort is needed to evolve the instrumentation and concepts into commercially available products – but, the critical foundational methodology and ideas for development are documented here. This dissertation advances the corpus of information required to provide food security for the growing global population through economically and sustainably housed livestock and poultry.

Future work

There are many potential avenues for further developing and applying the methods and ideas documented in this dissertation. The following list includes, but is not limited to prospective opportunities.

- A more robust and analog version of TESA is needed for unified integration into modern ventilation control systems. These controllers could also incorporate control logic based on HS2I or other advanced control algorithms.
- Combine TESA with machine vision to link real-time behavioral responses and growth with the TE to improve model parameters and control.
- Extensive updating of model parameter limits (i.e., maximum and minimum values) and the response shape (i.e., linear, exponential, allometric, etc.) between those limits is needed. Parameters needing updated include, tissue and pelage thermal conductance, respiratory rate and heat loss, passive skin diffusion rate and evaporative heat loss. The goal is to update these parameters for modern genetics, heavier finishing weights, body composition, nutrition, etc.
- The same method and procedures used to develop HS2I could be utilized to modify and apply HS2I to meet the thermal demands of other stages of pig production. For example, pre-weaned pigs, farrowing sows, gilt development, gestation, boars, etc. would be primary targets to apply HS2I.
- Develop and apply a heat balance approach based on the specific thermal demands of the animals to design, assess, and control other livestock and poultry facilities.

APPENDIX. AUTHORED REFEREED PAPERS, CONFERENCE PAPERS, AND ABSTRACTS

Design and feasibility of an impact based odor control system

Ramirez, B. C., Hoff, S. J., & Tong, L. (2016). Design and feasibility of an impact based odor control system. *Applied Engineering in Agriculture*, 32(4). doi:10.13031/aea.32.11522.

Abstract

Legislation and rural communities are increasingly requesting reductions in odor emitted from swine production facilities. If odor is regarded solely as a nuisance, and not an environmental hazard (as in this research), such that the objective of treating ventilation exhaust air is to prevent odor from impacting nearby receptors, it is unnecessary to treat exhaust air when dispersed odor is not identifiable. This approach maximizes odor reduction potential when most needed, with economic benefit through decreased energy and resource usage by simply operating the mitigation device for less time. The objectives of this paper were to: develop an on-off, real-time control system for on-farm odor mitigation devices and provide insight on the potential reduction in operation time of any odor mitigation strategy for climatic variability. The Impact Based Odor Control System (IBOCS) monitors wind speed, wind direction, and insolation to determine atmospheric stability, and utilizes location of nearby receptors relative to a facility to conclude if exhaust air requires treatment. A prototype of IBOCS was developed and consisted of an Arduino to execute the control algorithm and manage sensor measurements, receptor directional locations, and device activation or deactivation. The user interface included an eight-direction toggle switch indicator (receptor directional location), power switch, automatic/manual switch to override IBOCS, and additional tactile inputs for manual control. The feasibility of implementing IBOCS was evaluated at five simulated locations (MN, IA, MO, IN, and NC) in the United States by computing the reduction in annual mitigation device operation based on IBOCS logic from Typical Meteorological Year 3 data sets. Regardless of receptor location relative to a simulated facility site, IBOCS logic estimated annual mitigation technology operation to range from 64.4% (NC) to 71.4% (IN). Further, the minimum estimated annual operation ranged from 14.2% (IA) to 27.9% (MO) with only one receptor present. The overall goal of IBOCS is to reduce the impact of dispersed odor while concurrently decreasing operational expenses for expensive mitigation technologies.

Introduction

Odor dispersion from swine facilities has experienced scrutiny from rural communities and regulators. Swine odors produced from the breakdown of manure by microorganisms are dispersed during land application of slurry, manure storage facilities, and building ventilation exhaust air (Janni, 2010; Liu, Powers, & Mukhtar, 2014). Typically, exhaust air from swine facilities is untreated, resulting in odors containing hundreds of chemicals, including volatile organic compounds, ammonia, hydrogen sulfide, and many other substances found at low concentrations (Millner, 2009; Zhang et al., 2002; Zhu, 2000), to be potentially detected by the human olfactory response. Odors can become a nuisance to nearby receptors (e.g., neighbors, communities, people outside, etc.) and with more potential regulation on odor and gaseous emissions levels (Ferguson, Tebbutt, & Woodruff, 2010; Henry et al., 2007; Honeyman, 1996; Jacobson et al., 1999; Liu et al., 2014; Stowell, Henry, Koelsch, & Schulte, 2007; Vukina, Roka, & Palmquist, 1996), there is a requisite need for developing and implementing odor mitigation technologies that reduce the impact on surrounding receptors and are cost effective for swine producers to implement.

If odor is regarded solely as a nuisance, and not an environmental hazard, such that the objective of treating exhaust air is to reduce the odor impact for nearby receptors, it is often unnecessary to treat all exhaust air, all of the time. Many factors such as atmospheric stability, which is a function of wind direction, wind speed, and insolation (i.e., solar radiation), in conjunction with receptor relative location and distance from a facility influence if dispersed odor is identifiable. These factors have been incorporated into several odor dispersion simulation models for siting new facilities (Cimorelli et al., 2005; Hoff, Bundy, & Harmon, 2008; Hoff, Bundy, Harmon, & Johnson, 2008; L. D. Jacobson et al., 2005). If dispersed odor is not identifiable; hence, not a potential nuisance to nearby receptors, operation of a mitigation technology could be substantially reduced by either bypassing or powering off the device. This on-off control approach maximizes odor reduction potential when most needed, with economic benefit through decreased energy and resource usage by simply operating the mitigation device for less time. A control system is needed to assess atmospheric stability, determine potential impact region(s) downwind of a facility, and automatically deactivate or activate a mitigation device when needed.

Several methods have been developed to mitigate odors from swine facility exhaust air such as biofilters, wet scrubbers, oil spraying, ultraviolet light, electrostatic precipitation, which are thoroughly discussed in literature ("Air Management Practices Assessment Tool (AMPAT)," 2015; Liu et al., 2014). Operation of these devices is typically continuous and lack any control mechanism. Operating costs and energy usage varies greatly among technologies, ranging from \$0.05~\$0.5 per head produced (biofilters) to ~\$2 per head produced (wet scrubbers). There are considerable opportunities to decrease operating costs though intermittent operation; however, this technique may affect device longevity. For example, frequent power cycling to an actuator, fan, or light bulb may cause devices to wear or need replacement more often. Biofilters in particular may require a minimum flow and moisture to sustain the microbial communities and remain effective (Li et al., 1996). Similarly, for devices utilizing pumps, check valves must be installed in appropriate locations to avoid running a pump dry or repeatedly priming a pump.

This research views odor as a nuisance; therefore, reducing identification by nearby receptors is most critical. The Impact Based Odor Control System (IBOCS) was developed to cost effectively operate mitigation devices used in swine production systems where odor control is limited to events that would most likely impact surrounding receptors. IBOCS monitors

atmospheric stability and utilizes the input of nearby receptor(s) direction relative to a facility to determine if odorous exhaust air needs to be attenuated. To achieve these goals, the objectives were to: (1) instrument and develop a control system for controlling on-farm mitigation devices, and (2) provide insight on the potential reduction in operation time of any odor mitigation strategy for climatic variability.

Materials and methods

Atmospheric stability

The rise of gas plumes and subsequent dispersion of gas plumes are substantially influenced by the amount of turbulence in the ambient air (Beychok, 1994). The Pasquill Stability Classes (PSCs) categorize the amount of turbulence in the atmosphere into finite levels based on wind speed and insolation. Stability classes (table A.1) are composed of classes: A (most unstable or most turbulent), B (unstable), C (slightly unstable), D (neutral), E (slightly stable), and F (most stable or least turbulent). Odor plumes have a higher likelihood to remain near the ground in a stable atmosphere (defined as class D through F) and subsequently, are detected by nearby downwind receptors; thus, odor mitigation may be required. Alternatively, an unstable atmosphere (defined as class A through C) implies odor plumes rise and mix vertically close to the odor emission source (low lateral dispersion). Odor exhausted from swine facilities into an unstable atmosphere disperses before reaching nearby receptors and odor mitigation is deactivated, bypassed, or powered off.

Table A. 1. Meteorological conditions that define the Pasquill Stability Classes (Beychok, 1994). The shaded region indicates when a mitigation device is operational and corresponds to equations A.1, A. 2, and A.3.

	Day-time insolation			Night-time cloud cover[d]	
Surface wind speed, m s^{-1} (mph)	Strong[a]	Moderate[b]	Slight[c]	> 4/8 cloud	< 3/8 cloud
< 2 (4.5)	A	A-B	B	-	-
2-3 (4.5-6.7)	A-B	B	C	E	F
3-5 (6.7-11.2)	B	B-C	C	D	E
5-6 (11.2-13.4)	C	C-D	D	D	D
> 6 (13.4)	C	C	D	D	D

[a] > 598.3 W m^{-2}

[b] 301.3 - 598.3 W m^{-2}

[c] < 301.3 W m^{-2}

[d] neutral class D applies to heavy overcast skies, day or night

Equipment and sensors

A prototype of IBOCS was developed to establish hardware requirements and demonstrate control system functionality. The control system algorithm was programmed using the integrated development environment for the microprocessor (Mega 2560, Arduino LLC, Italy). Data were stored on a removable flash memory via a datalogger (SD card shield V4.0, Seeed Development Limited, Shenzhen, China). Due to potential lack of computers or internet access at swine production facilities, a real time clock (RTC Module, Freetronics Pty Ltd., Crodon South, Australia) was used to timestamp recorded data.

IBOCS required sensors to measure wind direction, wind speed, and insolation. Minimum sensor criteria was established to be a wind vane with at least 5° of measurement resolution and threshold wind speed of less than 2 m s^{-1}. The anemometer should have a threshold that is the same

as the wind vane. A horizontally mounted pyranometer measured total (global) direct and diffuse solar radiation to determine insolation. The choice of sensors is determined by the end user.

Input of receptors relative to a facility was indicated by an eight-position switchboard (figure A.1) corresponding to eight compass locations (every 45°). The presence of a receptor was indicated by depressing the receptor directional location switch (figure A.1). Two switches may be used to indicate a receptor located between two directional positions (e.g., a receptor located at 112.5°, from North, switches located at 90° and 135° may be depressed). Other features included hand (manual) or automatic (auto) operation mode in the event a device required maintenance. Once in hand operation mode, momentary switches could be used for manual control over the device, such as raising or lowering an actuator.

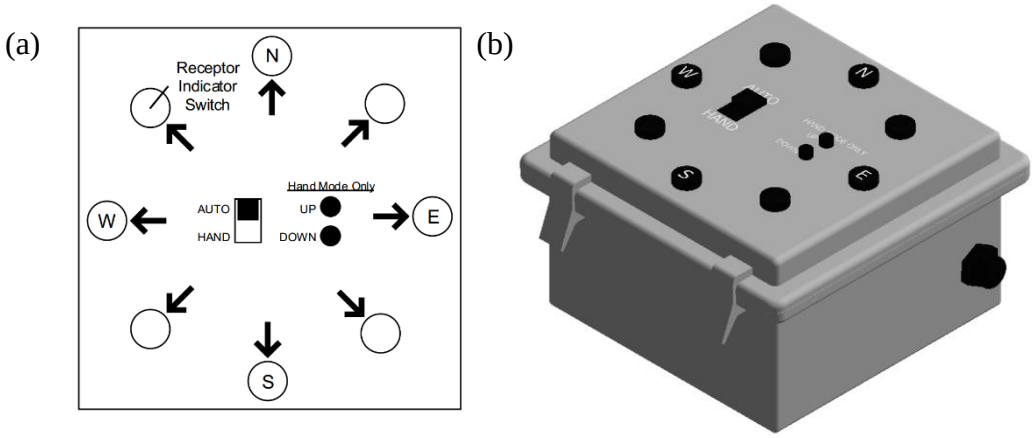

Figure A.1. (a) User interface for receptor directional indicator for IBOCS. Eight receptors are possible and located every 45° around a facility. (b) Three-dimensional drawing of IBOCS prototype.

Control logic

The algorithm determined the mean insolation, wind speed, and wind direction every 15 min from measurements made once a minute (n = 15), and stored identified receptors (figure A.2). The software selectable control decision frequency was chosen to satisfy the following: the objective of reducing the likelihood of identifiable odors from impacting surrounding receptors, to quickly respond to changing atmospheric conditions, and to not prematurely degrade equipment.

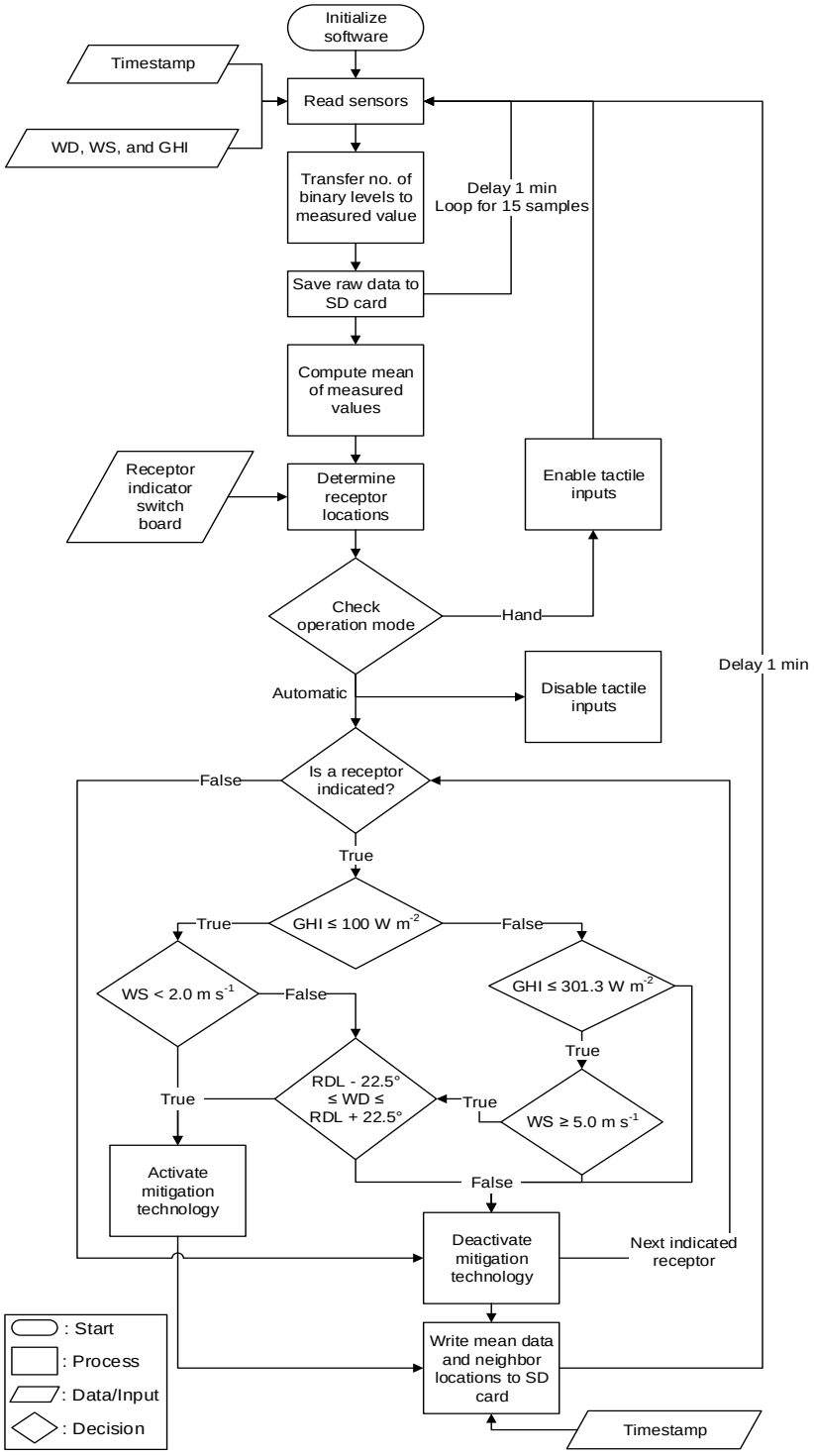

Figure A.2. Pseudo control logic algorithm for IBOCS.

A mitigation technology was determined to be activated for classes D through F (encompassed by equations A.1, A.2, and A.3) and deactivated, for classes A through C (table A.1), based on work completed by Hoff et al. (2008), Hoff et al. (2008) and Jacobson et al. (2005).

$$WS \geq 5.0 \;\&\; GHI \leq 301.3 \;\&\; RDL - 22.5° \leq WD \leq RDL + 22.5° \quad \text{(A.1)}$$

$$GHI \leq 100.0 \;\&\; WS \geq 2.0 \;\&\; RDL - 22.5° \leq WD \leq RDL + 22.5° \quad \text{(A.2)}$$

$$GHI \leq 100.0 \;\&\; WS < 2.0 \quad \text{(A.3)}$$

where

WS = mean wind speed (m s^{-1})
GHI = mean global horizontal insolation (W m^{-2})
RDL = receptor directional location (°)
WD = mean wind direction (°)

Equation A.1 is valid only during the daytime (i.e., 100 ≤ GHI ≤ 301.3 W m^{-2}) and when average wind direction is within the ±22.5° region of the RDL. This region is larger than the ±10° utilized in other odor siting models (Hoff, Bundy, & Harmon, 2008), in order to ensure all potential receptor locations are covered by the control logic. Albeit, if the standard deviation of wind direction is greater than 22.5° and receptor directional locations are identified adjacent to the mean wind direction, the mitigation device is activated. If equation A.1 is satisfied and wind direction is such that a receptor would not be impacted, the mitigation device is deactivated (figure A.2). Equations A.2 and A.3 include classes D through F during nighttime (i.e., GHI ≤ 100.0 W m^{-2}) and are achievable regardless of wind speed (table A.1). However, the lowest wind speed category for a defined PSC is: < 2 m s^{-1} (table A.1); therefore, 2 m s^{-1} was used as the minimum wind speed that would disperse odor in the direction of a downwind recipient. Hence, input of RDL is used for wind speeds greater than 2 m s^{-1} (equations A.1 and A.2). For wind speeds less than 2 m s^{-1}, reliable measurement of wind direction may not be possible (sensor threshold will vary based on technology) and odor is assumed to disperse omnidirectionally from the facility. When below the wind vane or anemometer sensor threshold, assumed to be 2 m s^{-1}, wind speed is recorded as 0 m s^{-1}, and wind direction recorded as 0° (North is 360°). Equation A.2 is valid at night when the wind is strong enough to disperse odor, such that a downwind receptor would be impacted (similar to equation A.1); hence, the RDL must be within the ±22.5° region. Conversely, equation A.3 corresponds to nighttime only, during light breeze conditions; hence, WD and subsequently, RDL are ignored, and the mitigation technology is activated, as long as a receptor is indicated to be present anywhere on the receptor indicator switchboard.

Input of receptor distance from the facility was not included in the control logic. While this is an important factor in odor identification, the user's discretion must be used to determine if the receptors distance from the facility is such that the receptor will be impacted. Siting tools and odor dispersion models could be used to assist with this decision.

Feasibility evaluation

The dynamic and diverse nature of atmospheric conditions, coupled with the geographical and temporal dependence, led to the evaluation of IBOCS using Typical Meteorological Year 3 (TMY3; Wilcox & Marion, 2008) data sets at five different locations (Mankato, MN; Boone, IA; Jefferson City, MO; Grissom, IN; and Fayetteville, NC) in the United States (figure A.3). Rather than use experimentally obtained data, TMY3 data sets are intended for design evaluations (such

as this one) and solely collecting data at 1 min intervals in one location would not provide adequate insight to the potential reduction in mitigation technology operation in regions where odor is often a nuisance. TMY3 data sets are derived from historical data in hourly intervals for one year; hence, this method will be overestimating mitigation technology operation time compared to the recommended aforementioned control decision frequency of every 15 min. Frequency of mitigation device operation was evaluated hourly for one year based on the criteria in equations A.1, A.2, and A.3, with global horizontal insolation, wind speed, and wind direction obtained from the TMY3 data sets. In addition, percent annual operation was analyzed by PSC (table A.1), receptor directional location (i.e., wind direction ±22.5° of the eight compass positions and calm), and meteorological season. In addition, a sensitivity analysis was performed to simulate the potential reduction in annual cost to operate a mitigation device for different mitigation device operating costs (cost per head produced) if IBOCS were implemented. TMY3 data were imported and processed using Matlab (R2015b, The MathWorks Inc., Natick, MA, USA).

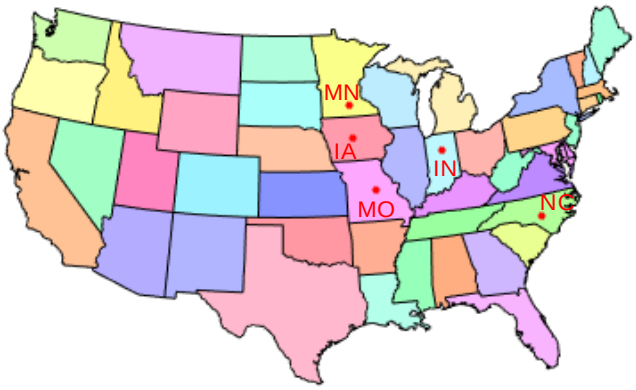

Figure A.3. Simulated facility locations at Mankato, MN; Boone, IA; Jefferson City, MO; Grissom, IN; and Fayetteville, NC identified by their state abbreviation.

Results and discussion

Regardless of receptor location relative to a simulated facility site, IBOCS criteria estimated annual mitigation device operation (figure A.4) to range from 64.4% (NC) to 71.4% (IN); thus, an approximate 29% to 36% reduction compared to continuous operation. This was attributed to unstable atmospheric conditions as indicated by PSCs that cause rapid vertical mixing of odor plumes near the source (class A through class C); hence, no mitigation required. Lower overall wind speed regions (MO and NC) showed less annual operation (figure A.4) due to the smaller contribution of equations A.1 and A.2 to the total annual operation; however, in those regions where wind speed decreases at night, a mitigation device will be activated a greater percentage of the year. The higher wind speed regions have greater opportunity to reduce mitigation device operation because if a receptor is not positioned downwind, there is no need to mitigate. Addition of receptor location relative to the simulated facility, plus wind direction would further decrease mitigation device operation time.

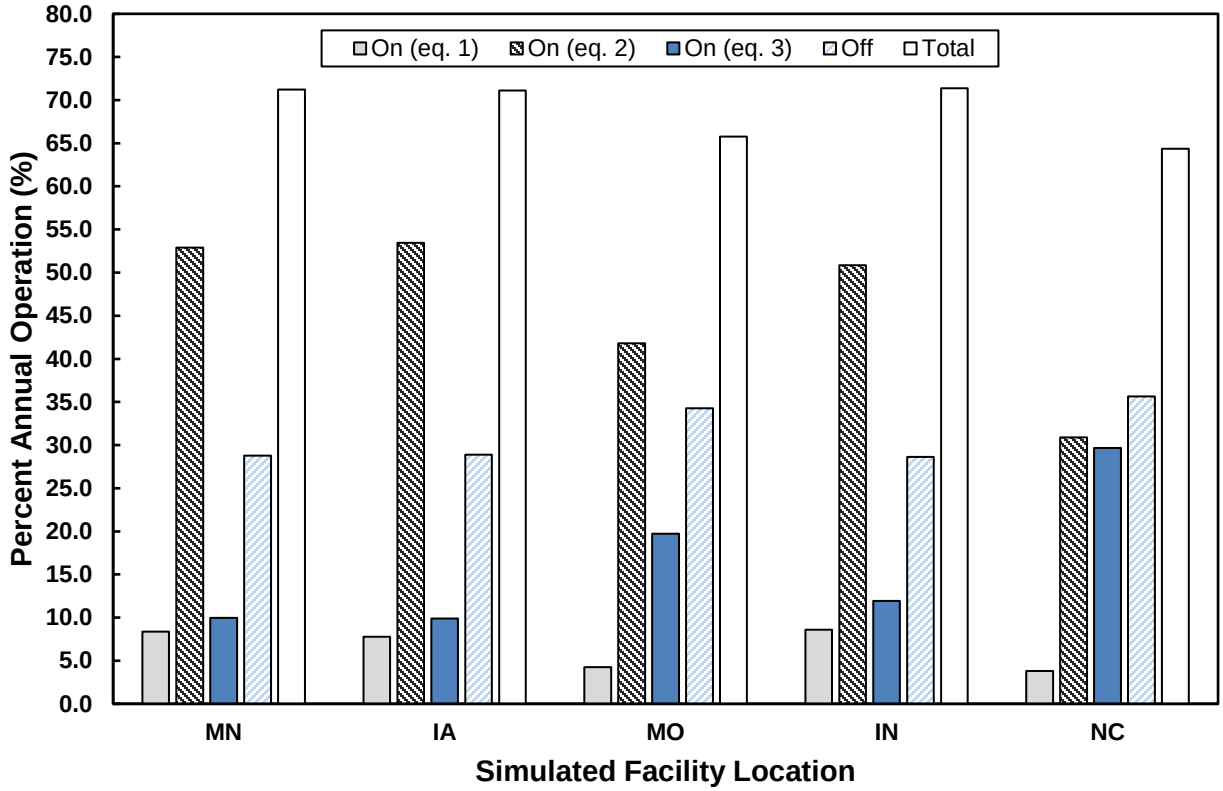

Figure A.4. At five simulated facilities located in the United States, IBOCS logic decreased annual mitigation operation regardless of receptor location relative to the facility. Mitigation was operational for a larger percentage of the year during night (eq. A.2 and eq. A.3) compared to daytime (eq. A.1).

Analysis of PSC frequency, regardless of relative receptor location to the simulated facility site, showed nighttime (classes D-F) to require mitigation operation the most frequent among simulated facilities (figure A.5). This result suggests control decisions with illuminance, rather than insolation may be incorporated. For example, insolation could be directly replaced with illuminance in equations A.1, A.2, and A.3, using a correlation found between the two. Further, since commercially available pyranometers are more expensive than visible light sensors (e.g., cadmium sulfide), this could decrease the capital cost of IBOCS. Another alternative could be to utlize equations of time and solar time equations (ASHRAE, 2013) to replace the pyranometer or visible light sensor, and further reduce the capital cost of IBOCS. Additional programming and input of the facility's geographical location (i.e., latitude and longitude) would be required.

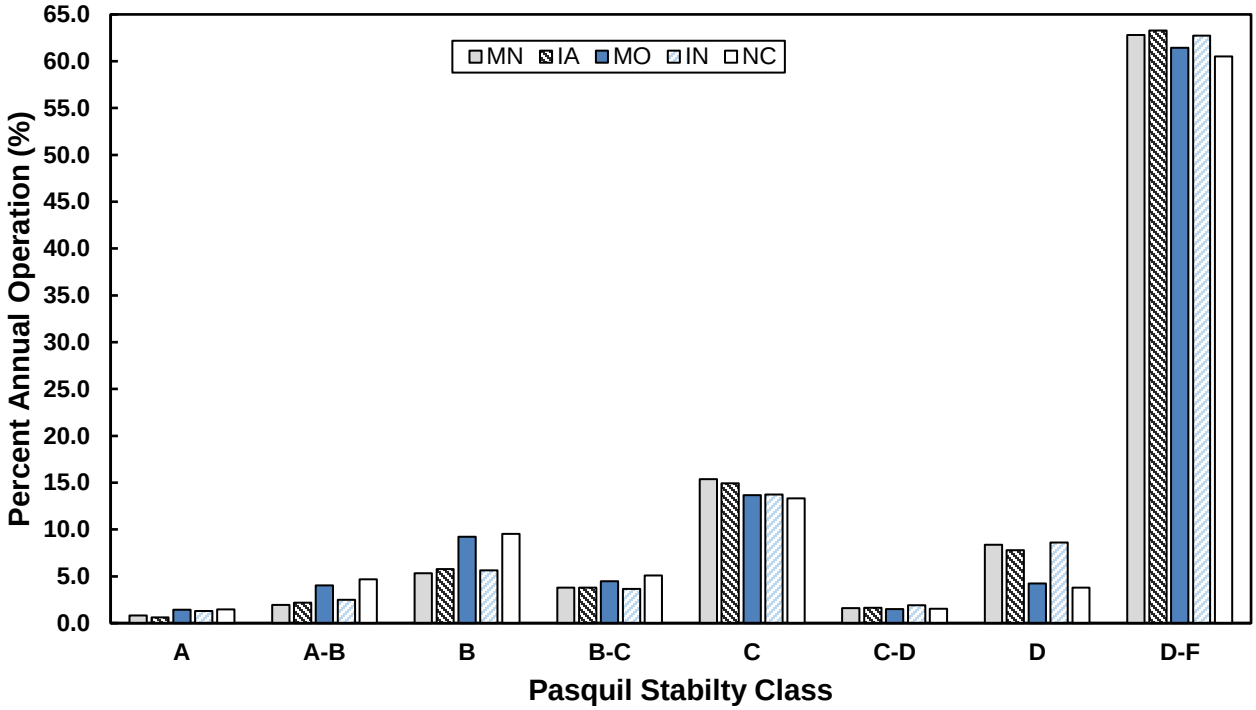

Figure A.5. Regardless of receptor location relative to the simulated facility site, the most frequently estimated Pasquil Stability Class was during nighttime.

Although the decision to operate a mitigation device for Class C was excluded, a more conservative approach could be to integrate mitigation device operation for Class C into the control logic (equation A.4). In the event Class C is included, annual mitigation operation is estimated to range from 79.2% (NC) to 88.2% (NC). This is an additional 14.9% (NC) to 16.9% (MN) increase in operation, compared to when Class C was excluded from the control logic (figure A.4).

$$(WS \geq 5.0 \;\&\; GHI \geq 301.3 \mid WS \geq 2.0 \;\&\; GHI \leq 301.3) \;\&\; RDL - 22.5° \leq WD \leq RDL + 22.5° \quad \text{(A.4)}$$

where

WS = mean wind speed (m s^{-1})
GHI = mean global horizontal insolation (W m^{-2})
RDL = receptor directional location (°)
WD = mean wind direction (°)

Estimated mitigation device operation analyzed by meteorological season (figure A.6) showed operation during winter to be more prevalent, with an average (±standard deviation) annual operation of 38.3% ±2.2% across the five simulated facility locations. Mean annual operation during spring (11.7% ±0.75%) and fall (13.7% ±0.5%) were similar across simulated facilities. Operation during the summer was the lowest at 5.2% ±0.3%. Receptor identification will most likely be more common during the spring, summer, and fall seasons as people tend to be traveling and outdoors; however, these three seasons combine for just 44% of the mean percent annual operation across simulated facilities. If winter was excluded, annual mitigation device operation could range from 28.9% (MO) to 32.1% (IA).

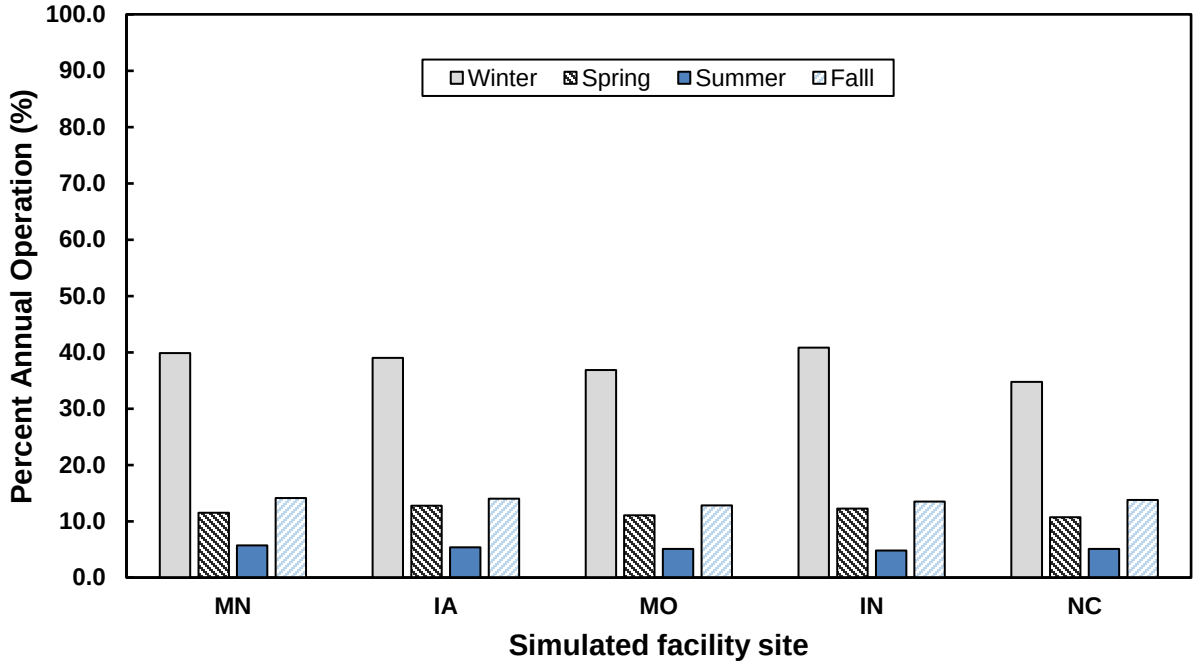

Figure A.6. Regardless of receptor location relative to the simulated facility site, winter was estimated to require to the most mitigation device operation.

Annual estimated mitigation device operation could be further reduced if at least one receptor was indicated to be present (figure A.7). For example, if only one receptor was present, the minimum annual (including winter) operation ranged from 14.2% (located SE of simulated facility; IA) to 27.9% (located E of simulated facility; MO). This difference was attributed to the greater frequency of low wind speeds in MO compared to IA, in which the mitigation device is active regardless of receptor location and with one receptor present. Maximum annual (including winter) operation ranged from 37.9% (located E of simulated facility; MO) to 56.9% (located N of simulated facility; IA). If winter was excluded, the minimum annual operation ranged from 1.5% (located SW of simulated facility; IA) to 6.8% (located SW of simulated facility; MO). Maximum annual operation with winter excluded for one receptor directional location present ranged from 4.5% (located SW of simulated facility; IN) to 7.4% (located E of simulated facility; MO). There are many possible combinations of facility geographical location, number of receptors, and their location relative to a facility; hence, this analysis can provide insight to some potential annual operation times (direct cost saving to producer) for different configurations. If a siting model was not utilized or if legislation requires, this analysis could be used to estimate conceivable costs and operation frequency for potential mitigation technologies with and without IBOCS. More accurate wind direction sensors, such as sonic anemometers, could be utilized and feature low thresholds (i.e., typically <0.1 m s^{-1}) and high wind direction resolution at low wind speeds. This technology could be used to reduce the nominal threshold value of 2 m s^{-1} in equations A.2 and A.3; however, this technology is considerably more expensive than mechanical wind vanes and 3-cup anemometers. By reducing the threshold in equations A.2 and A.3, mitigation device operation could be further reduced by including the receptor directional location in the criteria.

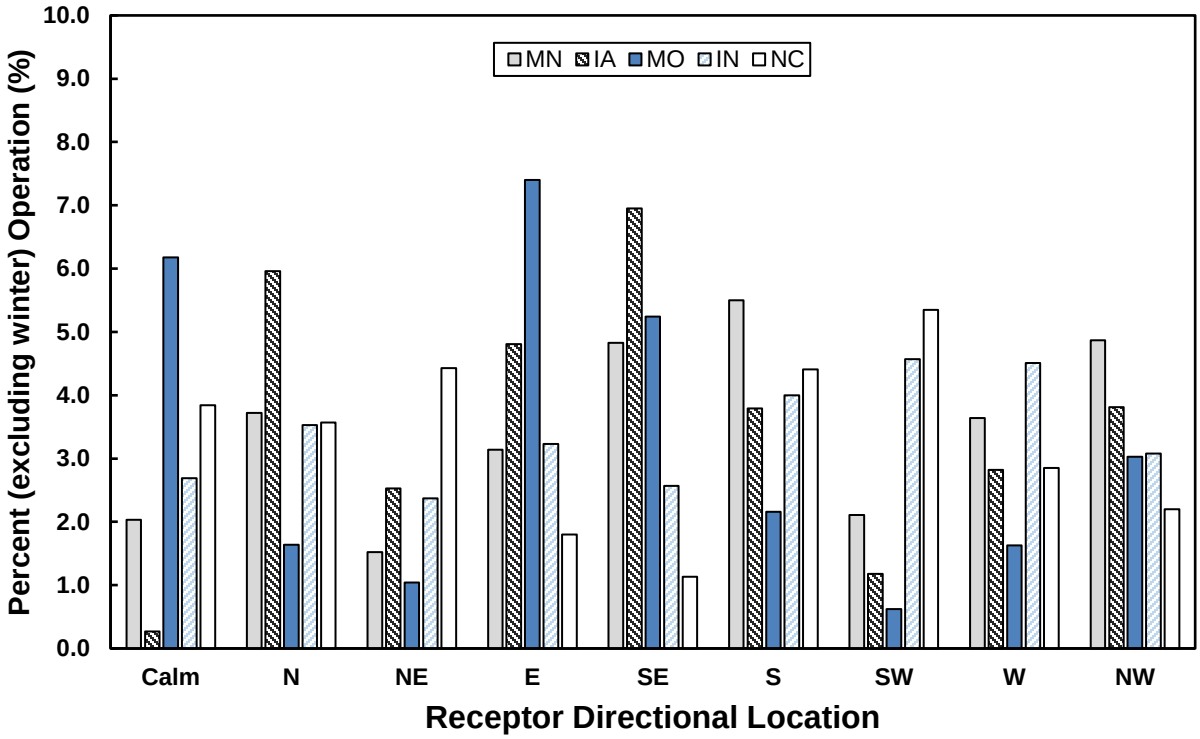

Figure A.7. Addition of wind direction further reduced annual (excluding winter) mitigation technology operation and could be used to determine conceivable costs and operation frequency for potential mitigation technologies with or without IBOCS. Calm is specified from the TMY3 datasets and has an undefined wind speed threshold (Wilcox & Marion, 2008).

The sensitivity analysis results showed that for higher mitigation device operating costs, a reduction in annual mitigation device operation with IBOCS logic implemented, substantially reduced annual operating costs (figure A.8). For mitigation devices with lower operating costs, a reduction in operation time had a reduced impact on annual operating costs. For example, a 30% reduction in annual mitigation device operation for a technology that cost $1 per head produced to operate, could reduce annual operating costs by approximately $2600 (figure A.8). Whereas, compared to a technology that cost $0.01 per head produced to operate, only about $26 yr^{-1} could be saved (figure A.8). Further, a 60% reduction in annual mitigation device operation for a technology that cost $1 per head produced to operate, could reduce annual operating costs by approximately $5200. IBOCS may not offer a considerable reduction in annual operating costs for mitigation devices that are inexpensive to operate, but technologies that cost more to operate, IBOCS could provide large annual economic savings.

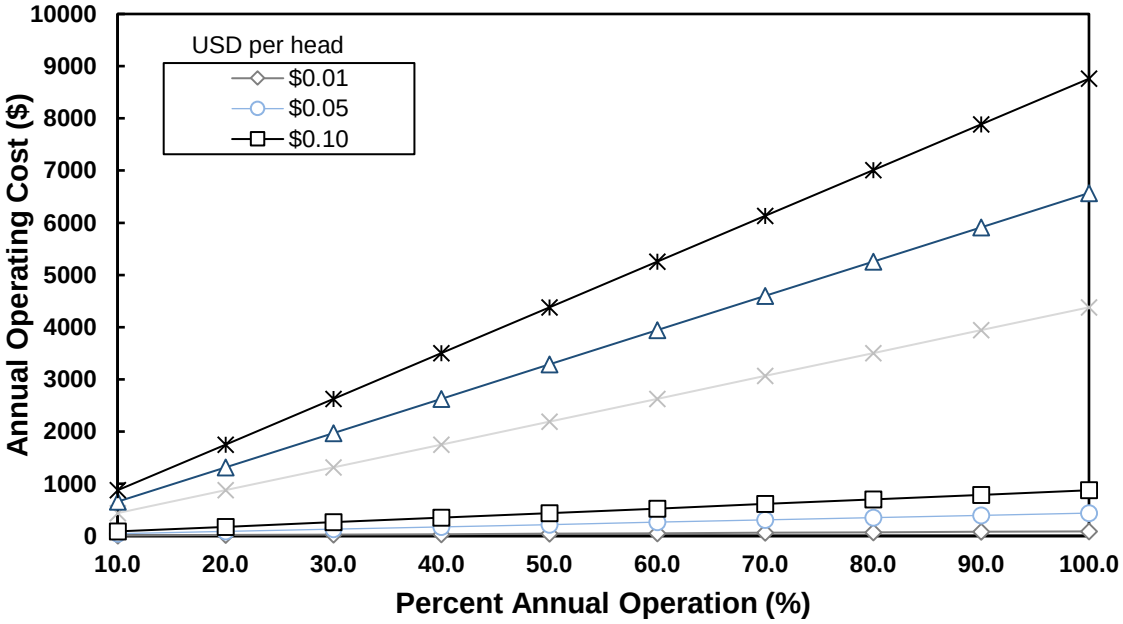

Figure A.8. Sensitivity analysis results showed a reduction in annual mitigation device operation substantially reduced annual operating costs for more expensive mitigation technologies.

Conclusions

Odor is a growing issue in the swine industry and, when considered a nuisance, requires mitigation to decrease identification by surrounding receptors. An Impact Based Odor Control System (IBOCS) was developed to cost effectively operate odor mitigation devices where, odor control is limited to events that would most likely impact surrounding receptors. An IBOCS prototype was created to monitor key parameters of atmospheric stability and utilize the input of nearby receptors directional location relative to a facility to determine if exhaust air required odor attenuation. The feasibility of this design and control logic were evaluated using hourly Typical Meteorological Year 3 (TMY3) data sets for five different locations (Mankato, MN; Boone, IA; Jefferson City, MO; Grissom, IN; and Fayetteville, NC) in the United States. Regardless of receptor location relative to a simulated facility site, IBOCS criteria decreased annual mitigation device operation by an estimated range from 64.4% (NC) to 71.4% (IN). Further, the minimum estimated annual operation ranged from 14.2% (IA) to 27.9% (MO) with only one receptor present.

Methods commonly used by siting models for new facility construction were adapted and implemented in a real-time monitoring and control system. IBOCS logic and hardware can be easily and readily implemented on a variety of on-off odor mitigation devices. Further work on the effect of on-off controlled equipment longevity is needed. IBOCS provides a real time and cost effective method to control odor mitigation devices while positively benefiting surrounding receptors. This analysis shows the feasibility and potential cost saving that will lead to informed decisions on implementing mitigation technologies.

Acknowledgments

The authors would like to thank our cooperating producer, Mr. Greg Carlson, for allowing access to facilities used during the early development of IBOCS.

References

Air Management Practices Assessment Tool (AMPAT). (2015). Retrieved June 28, 2015, from http://www.agronext.iastate.edu/ampat/.

ASHRAE. (2013). *Handbook of Fundamentals*. Atlanta, GA: America Society of Heating, Refrigeration and Air Conditioning Engineers.

Beychok, M. R. (1994). *Fundamentals of gas Stack dispersion* (3rd ed.). Irvine, CA: Milton Beychok, Pub.

Cimorelli, A. J., Perry, S. G., Venkatram, A., Weil, J. C., Paine, R. J., Wilson, R. B., … Brode, R. W. (2005). AERMOD: A Dispersion Model for Industrial Source Applications. Part I: General Model Formulation and Boundary Layer Characterization. *Journal of Applied Meteorology*, *44*(5), 682–693. http://doi.org/10.1175/JAM2227.1.

Ferguson, J. E., Tebbutt, S. M., & Woodruff, S. L. (2010). What's The Big Stink? An Introduction To Managing Odor in Agriculture. American Society of Agricultural and Biological Engineers. http://doi.org/10.13031/2013.32642.

Henry, C. G., Hoff, S. J., Jacobsen, L. D., Schulte, D. D., D'Abreton, P. C., Ormerod, R. J., … Billesbach, D. P. (2007). Downwind Odor Predictions from Four Swine Finishing Barns Using CALPUFF. American Society of Agricultural and Biological Engineers. http://doi.org/10.13031/2013.23857.

Hoff, S. J., Bundy, D., & Harmon, J. D. (2008). Modeling receptor odor exposure from swine production sources using CAM. *Applied Engineering in Agriculture*, *24*(6), 821.

Hoff, S. J., Bundy, D., Harmon, J., & Johnson, C. D. (2008). A receptor-based siting strategy for swine production systems. *Proceedings: Mitigating Air Emissions from Animal Feeding Operations. May*, 19–21.

Honeyman, M. S. (1996). Sustainability issues of US swine production. *Journal of Animal Science*, *74(6)*, 1410–1417.

Jacobson, L. D., Guo, H., Schmidt, D. R., Nicolai, R. E., Zhu, J., & Janni, K. A. (2005). Development of the OFFSET model for determination of odor-annoyance-free setback distances from animal production sites: Part I. Review and experiment. *Transactions of the ASAE*, *48*(6), 2259–2268.

Jacobson, L. D., Moon, R., Bicudo, J., Janni, K., Zhu, J., Schmidt, D., … others. (1999). Generic Environmental impact statement on animal agriculture. *A Summary of the Literature Related to Air Quality and Odor (H). Prepared for the Environmental Quality Board*. Retrieved from http://www.mnplan.state.mn.us/pdf/1999/eqb/scoping/aircha.pdf.

Janni, K. (2010). Agricultural Odors What is the stink about? *Resource Magazine*, *17*(5), 8–9.

Liu, Z., Powers, W., & Mukhtar, S. (2014). A review of practices and technologies for odor control in swine production facilities. *Applied Engineering in Agriculture*, *30*(3), 477–492.

Li, X. W., Hoff, S. J., Bundy, D. S., Harmon, J., Xin, H., & Zhu, J. (1996). Biofilter-a malodor control technology for livestock industry. *Journal of Environmental Science and Health . Part A: Environmental Science and Engineering and Toxicology*, *31*(9), 2275–2285. http://doi.org/10.1080/10934529609376490.

Millner, P. D. (2009). Bioaerosols associated with animal production operations. *Bioresource Technology*, *100*(22), 5379–5385. http://doi.org/10.1016/j.biortech.2009.03.026.

Stowell, R. R., Henry, C. G., Koelsch, R. K., & Schulte, D. D. (2007). Association of Odor Measures with Annoyance: An Odor-Monitoring Field Study. American Society of Agricultural and Biological Engineers. http://doi.org/10.13031/2013.23893.

Vukina, T., Roka, F., & Palmquist, R. B. (1996). Swine odor nuisance. *Voluntary Negotiation, Litigation, and Regulation: North Carolina= S Experience, CHOICES, First Quarter*, 26–29.

Wilcox, S., & Marion, W. (2008). *Users manual for TMY3 data sets*. National Renewable Energy Laboratory Golden, CO. Retrieved from http://www.nrel.gov/docs/fy08osti/43156.pdf.

Zhang, Q., Feddes, J., Edeogu, I., Nyachoti, M., House, J., Small, D., … Clark, G. (2002). Odour production, evaluation and control. *Report Prepared for Manitoba Livestock Manure Management Initiative Inc., Winnipeg, Manitoba*. Retrieved from http://www.ontariopork.on.ca/portals/0/Docs/Research/Environment/10_1_2002_comprehensive_odour_mgt_solutions_manitoba.pdf.

Zhu, J. (2000). A review of microbiology in swine manure odor control. *Agriculture, Ecosystems & Environment*, *78*(2), 93–106. http://doi.org/10.1016/S0167-8809(99)00116-4.

Design and feasibility of a novel sprinkler control algorithm for swine heat stress alleviation

Ramirez, B. C., Hoff, S. J., & Harmon, J. D. (2017). Design and feasibility of a novel sprinkler control algorithm for swine heat stress alleviation. Presented at American Society of Animal Science Midwest Section/American Dairy Science Association Midwest Brach Joint Meeting 2017, Omaha, NE. Abstract No. 12.

Abstract

Pigs have a relatively low capacity to dissipate excess body heat and depend more on reducing metabolic heat production through a reduction in voluntary feed intake in hot conditions, resulting in a growth performance decrease. Effectiveness of typical cooling devices (e.g., evaporative coolers or sprinklers) in facilities is governed by the Water Vapor Pressure (WVP) concentration gradient between the air (a function of dry-bulb temperature; t_{db}, Relative Humidity; RH, and atmospheric pressure) and saturated WVP at a wet surface. Traditional Sprinkler Control Systems (TSCS) often operate solely on t_{db} feedback and at fixed 'off' intervals to allow dispersed water to evaporate. This control strategy does not account for the WVP concentration gradient; hence, water is wasted and only a limited amount of latent heat can be released from the animal. Therefore, the objectives were to develop and simulate a novel Variable Interval Sprinkler Control System (VISCoS) that dynamically changes the 'off' interval based on t_{db}, RH, and airspeed feedback. A theoretical convective mass transfer model (i.e., evaporation) estimated water evaporation rate as a function of the thermal environment, surface area, skin temperature, and volume of water applied. A pig's geometry was assumed a cylinder approximately 30% wet with a 1 mm film of water. The feasibility of implementing VISCoS was evaluated at six locations (AZ, IA, MN, MO, IN, and NC) by simulating water usage for a 1000 hd, mechanically ventilated, grow-finish building with an assumed water delivery (75.71 L/min), sprinkler 'on' time (30 s), and constant BW (100 kg). Typical Meteorological Year 3 weather data (365 d) was used to determine outdoor t_{db} and RH at each location, where indoor t_{db} was assumed 2°C greater than outdoor t_{db} with a 2 m/s air velocity across the animal's back. The VISCoS performance was compared with two TSCSs with fixed 'off' intervals (15 and 30 min; 'on' $t_{db} \geq 29.44$°C). Simulation results for each region showed water usage for 15 min (154, 72, 60, 50, 80, 164 m^3) and 30 min (79, 37, 31, 26, 41, 83 m^3) 'off' interval TSCS to be greater than VISCoS (49, 15, 8, 10, 17, 44 m^3). Duration (±SD) for complete water evaporation estimated by VISCoS (19.6±1.4, 28.0±3.6, 27.8±2.5, 31.8±6.5, 32.2±3.3, 26.9±3.3 min) varied by region and provides insight on incorporating more thermal environment measurements to reduce water usage and maximize latent heat loss capabilities for pigs.

Development and evaluation of an evaporation model for predicting sprinkler interval time

Ramirez, B. C., Hoff, S. J., Harmon, J. D., & Patience, J. F. (2017). *Development and evaluation of an evaporation model for predicting sprinkler interval time*. Presented at American Society of Agricultural and Biological Engineers Annual International Meeting 2017, Spokane, WA. Paper No. 1700379

Abstract

Heat stress in swine causes decreased productivity and economic losses; hence, heat stress mitigation techniques must be developed to be economically and resource efficient. Current cooling strategies for livestock facilities, such as evaporative coolers or sprinklers, are governed by the Water Vapor Pressure (WVP) concentration gradient between the air (a function of dry-bulb temperature; t_{db}, Relative Humidity; RH, and atmospheric pressure) and the saturated WVP at the wet surface. Traditional sprinkler control systems operate at fixed 'off' intervals (i.e., drying) regardless if the thermal environment (TE) has the capacity or not to evaporate the dispersed water. Therefore, the objectives were to develop and simulate a novel Variable Interval Sprinkler Control System (VISCoS) that dynamically changes the 'off' interval based on t_{db}, RH, and airspeed feedback. A theoretical simplified pig evaporation model estimated water evaporation rate as a function of the TE, pig surface area and skin temperature, and mass of water applied. To evaluate the model in controlled conditions, a cylinder (assumed geometry of a pig) was placed inside an insulated enclosure where different combinations of t_{db}, RH, and airspeed could be simulated across the cylinder. The inside surface of the cylinder was heated and controlled to replicate the skin temperature of an animal, while the outer surface was wrapped in a thin chamois. Water was applied to the cylinder via a sprinkler where approximately 40% of the top portion of the cylinder was wetted. Comparison of modeled with measured evaporation time showed reasonable agreement with a root-mean-square error of 7.9 min for evaporation times ranging from 5 to 25 min.

Introduction

The effects of heat stress cause annual decreased productivity and economic losses in the US swine industry (Stalder, 2015). Swine are generally regarded to be poor at dissipating heat and must reduce voluntary feed intake to decrease metabolic heat production (Renaudeau, Gourdine, & St-Pierre, 2011). This feed intake reduction consequently causes decreased average daily gain, lower finishing weights, and longer time to market. Hence, heat stress abatement strategies are needed to lessen the impacts of heat stress on productivity and improve economic return for producers.

Currently, there are three common commercial cooling strategies: elevated airspeeds, evaporative pad, and low-pressure sprinkling. Elevated airspeeds increase the convective heat loss and depends on the temperature gradient between the pig's skin and the dry-bulb temperature (t_{db}) of the air. This strategy fails to be effective when skin temperature is greater than t_{db}. Alternatively, evaporative pads and sprinklers utilize the latent heat of vaporization when water evaporates. Heat can be removed from the air passing through the evaporative pad or the pad itself, or for sprinklers directly from the pig's skin once wetted. Sprinklers use less water than evaporative pads (Muhlbauer, Moody, Burns, Harmon, & Stalder, 2010) and do not cause a large increase in moisture surrounding the pigs (assuming high summertime flowrates commonly associated with heat stress conditions). Therefore, sprinklers are an effective method of reducing heat stress with minimal water.

As air moves over wetted skin, the water evaporates taking heat away from the pig. The amount of heat lost and evaporation time is dependent on t_{db} and moisture, wetted area, airspeed, and skin temperature. However, many traditional sprinkler control systems utilize a constant 'off' interval (i.e., drying time) or an 'off' interval proportional to t_{db} to allow dispersed water to evaporate. The time for complete water evaporation is substantially more complicated than solely t_{db} and needs to include the other thermal environments parameters effecting evaporation.

The goal of this study was to propose the framework for creating a novel Variable Interval Sprinkler Control System (VISCoS) with a dynamic 'off' time based on t_{db}, RH, and airspeed feedback. Therefore, the objectives were to: (1) develop an analytical evaporative transfer model and (2) compare modeled and measured evaporation time in controlled conditions on a simplified pig.

Materials and methods

An analytical evaporative transfer model was first developed to estimate evaporation time. Then, experiments were performed on a simplified pig in a controllable chamber at different TE conditions to compare the measured evaporation time with predicted.

Analytical analysis

The pig was assumed to be a cylinder in cross-flow with a 40% wetted area with length and diameter proportional to body weight. The convective heat transfer coefficient (h_c) of a cylinder was estimated from Nusselt number (Holman, 2002) and from a simplified relation using body weight and airspeed (Bruce & Clark, 1979). The ambient water vapor pressure was estimated from t_{db}, RH, and barometric pressure based on altitude (ASHRAE, 2013). The saturated water vapor pressure at the skin was estimated from skin temperature, RH = 98%, and barometric pressure. Lastly, at film conditions, moist air density, thermal conductivity, and humidity ratio were determined. Latent heat of vaporization (h_{fg}) was a function of skin temperature and the specific heat of water ($c_{p,w}$) a function of humidity ratio at film conditions. Thermal and mass diffusivity were calculated at film conditions to determine the Lewis number. The Lewis ratio (LR) was a function of film temperature and density, h_{fg}, $c_{p,w}$, and Lewis number. Although, LR is commonly assumed a constant 16.5 K kPa^{-1} (ASHRAE, 2013). Evaporative heat loss was then calculated from LR, h_c, wetted area and the water vapor pressure gradient. Division of evaporative heat loss by h_{fg} yields the evaporation rate. Finally, evaporation time is calculated from the mass water (on the object) divided by evaporation rate.

Experimental setup

A chamber (L × W × H) with dimensions of 0.89 × 0.52 × 0.52 m featured a 0.2 m diameter galvanized steel cylinder mounted at the center, spanning the width of the chamber. The cylinder was wrapped in a thin chamois and three flexible heaters were coiled on the inside such that the flexible heaters maintained contact with the interior cylinder walls. A flow straightener separated the chamber from a 0.45 × 0.52 × 0.52 m entry section, which was responsible for transitions to a 0.15 m diameter duct to the square opening of the chamber. An air handling unit provided controlled t_{db} and RH conditions through an insulted flexible duct connected the entry section. A manual damper controlled flow and subsequently airspeed across the cylinder. A tray was placed below the cylinder to collect any water that rolled off.

An custom omnidirectional thermal anemometer (Gao, Ramirez, & Hoff, 2016) was mounted above the cylinder to measure airspeed. A digital infrared thermometer was mounted slightly above the cylinder. The chamois changed color as it dried allowing this color response to be captured by a photocell mounted near the chamois. In addition, inlet and outlet t_{db} and RH were measured.

Data acquisition and procedure

A microcontroller with a time-proportioning PI control algorithm controlled surface temperature at a constant 34°C. The microcontroller was also interfaced with two 4-channel, 16-bit ADCs to collect t_{db}, RH, photocell, and airspeed analog responses.

Once the conditions in the chamber were stable, water was sprayed onto the cylinder and allowed to evaporate completely. The mass of water applied was determined as the change in mass of the spray vessel measured before and after spraying, plus the addition of any water that rolled off.

Experimental conditions included the nominal combinations of t_{db} (28°C, 33°C, and 38°C), RH (40% and 65%), and airspeeds (1 and 2 m s^{-1}).

Statistical and data analysis

Data were processed in Matlab (R2017a, The Mathworks, Inc., Natick, Massachusetts, USA). Evaporation time was determined based on the photocell analog response. Once the photocell response returned to baseline (i.e., dry) after wetting, the chamois was assumed to be dry. This was verified prior to experiment to ensure accurate results. A linear regression model was fit to the predicted and measure evaporation time to assess the accuracy of the model over the range of conditions.

Results and discussion

An example of the thermal environment conditions, cylinder surface temperature, and photocell response for one nominal treatment are shown in figure A.9. Inlet and outlet conditions are stable and surface temperature decreases once wetted. Further, the PI control increased the heater ‘on’ time (not shown) to adjust for this disturbance and had minimal overshoot. The decrease in t_{db} and RH observed in the initial minutes were attributed to the opening of the lid to the chamber for the water spraying.

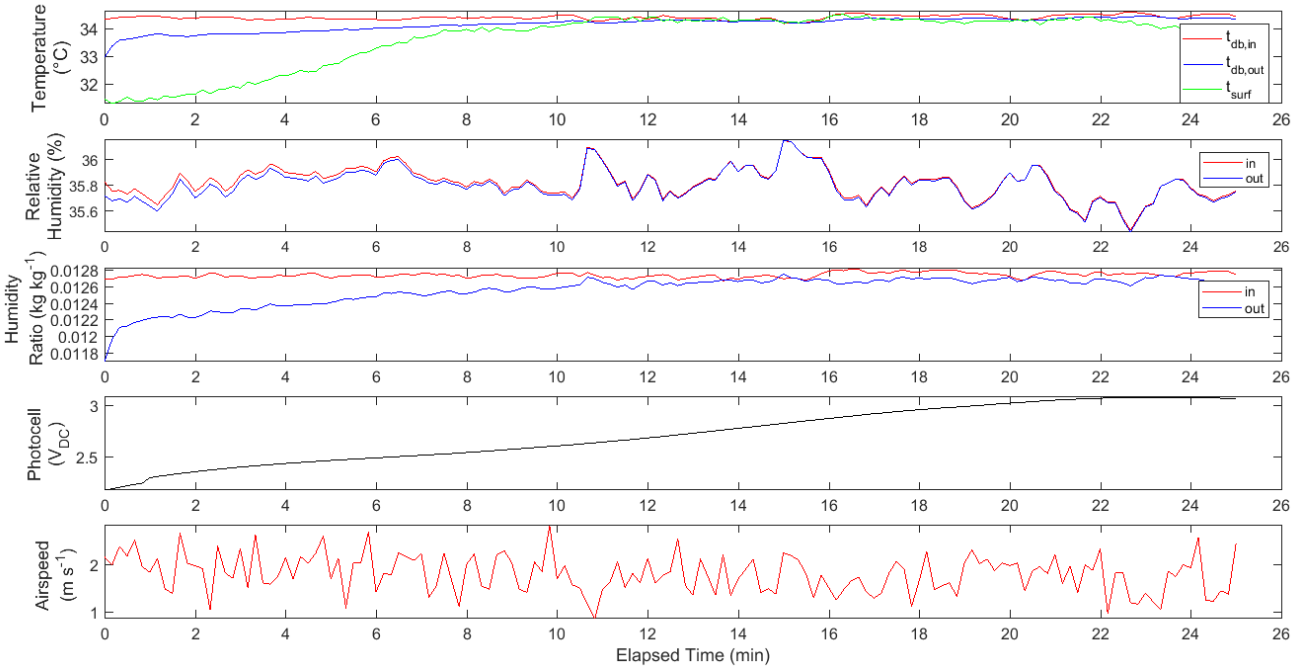

Figure A.9. Example of thermal environment conditions, cylinder surface temperature, and photocell response for one nominal treatment.

Results of the modeled and measured evaporation time are summarized in figure A.10. There was reasonable agreement with a root-mean-square error of 7.9 min over the range.

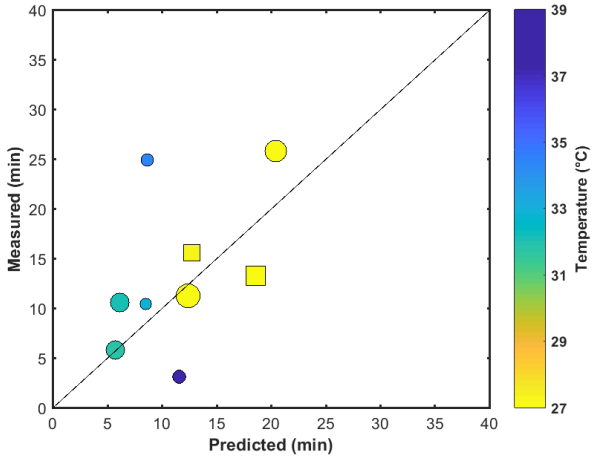

Figure A.10. Comparison of modeled with measured evaporation time. Shape size is proportional to airspeed.

Conclusions

A simplified pig evaporation model was developed to estimate water evaporation time for sprinkler "off" time control. The simplified pig evaporation model has reasonable agreement with the measured evaporation time. Since, heat stress is based on the thermal balance between animal and surrounding, the conditions for turning the sprinkler 'on' could be improved.

Acknowledgements

This research was supported with funding provided by the Iowa Pork Producers Association under NPB Project 14-242. The authors would like to acknowledge the contributions of undergraduate students Jesse Klaes and Sara Weyer.

References

ASHRAE. (2013). *Handbook of fundamentals*. Atlanta, GA: America Society of Heating, Refrigeration and Air Conditioning Engineers.

Bruce, J. M., & Clark, J. J. (1979). Models of heat production and critical temperature for growing pigs. *Animal Science*, *28*(03), 353–369. https://doi.org/10.1017/S0003356100023266

Gao, Y., Ramirez, B. C., & Hoff, S. J. (2016). Omnidirectional thermal anemometer for low airspeed and multi-point measurement applications. *Computers and Electronics in Agriculture*, *127*, 439–450. https://doi.org/10.1016/j.compag.2016.06.011

Holman, J. P. (2002). *Heat Transfer* (9th ed.). New York City, NY: McGraw-Hill.

Muhlbauer, R. V., Moody, L. B., Burns, R. T., Harmon, J. D., & Stalder, K. J. (2010). *Water Consumption and Conservation Techniques Currently Available for Swine Production* (No. NPB #09-128). Des Moines, IA: National Pork Board.

Renaudeau, D., Gourdine, J.-L., & St-Pierre, N. R. (2011). A meta-analysis of the effects of high ambient temperature on growth performance of growing-finishing pigs. *Journal of Animal Science*, *89*(7), 2220–2230.

Stalder, K. J. (2015). *Pork industry productivity analysis*. Des Moines, IA: National Pork Board.

Thermal environment performance and uniformity assessment for a novel swine breeding and gestation facility

Ramirez, B. C., Hoff, S. J., Harmon, J. D., & Stinn, J. P. (2016). *Thermal environment performance and uniformity assessment for a novel swine breeding and gestation facility*. Presented at American Society of Agricultural and Biological Engineers Annual International Meeting 2016, Orlando, FL. Paper No. 2454577.

Abstract

The Thermal Environment (TE) inside swine facilities has a substantial impact on animal performance and facility energy usage; therefore, proper control and measurement are required to maintain the optimal TE that maximizes performance and consumes minimal energy. Currently, controllers only monitor and describe the TE with dry-bulb temperature (t_{db}); however, t_{db} does not account for all the factors that influence the TE. Therefore, a novel Thermal Environment Sensor Array (TESA) network and accompanying data acquisition systems were developed for a preliminary investigation inside a commercial, ~800 hd, positive pressure ventilated, filtered breeding facility located in central Iowa. Data from the TESA network and from various ventilation system components from the installed controller would allow for control and distribution performance to be evaluated. Hence, the objectives of this research were: (1) evaluate the Thermal Environment Modification System (TEMS) controller response to seasonal and diurnal fluctuations; (2) implement and evaluate TESA and accompanying DAQ system performance; and (3) assess TE spatial uniformity across three pens. Six TESAs (two suspended per pen), each with: t_{db}, black globe temperature, airspeed, and relative humidity measurements were deployed since November 2015 to initially evaluate the performance and the robustness of this new system, as well as, explore the effectiveness and distribution of the facility's thermal environmental modification and control system. Overall, the TESAs performed well, except for some dust accumulation on the t_{db} and black globe sensors. Results showed that t_{db} inside the facility was within ±1°C and ±2°C of the set point 36.3% and 75.3% of the monitoring period, respectively. A maximum 10.6°C above the set point and 5.2°C below the set point were recorded. The preliminary findings from this study will be useful for developing functional performance tests to commission livestock and poultry facilities. These functional performance tests will analyze fan performance, heater distribution, TEMS controller abilities, spatiotemporal TE uniformity, etc. The information obtained will allow facility operators to make better management practices that ultimately decrease production costs and improve the thermal comfort for the animals.

Introduction

Thermal Environment Modification (i.e., fresh air ventilation, heating, cooling systems, etc.) and Air Distribution (i.e., inlets, baffles, side/end wall curtains, etc.) Systems (TEMADS) for

livestock and poultry production systems are designed to provide acceptable thermal comfort, fresh air, and indoor air quality inside the building for the animals. However, the implementation, operation, and control of these systems can deviate from the original design goals. This deviation between design and operation can result in poor animal growth performance, excess facility energy usage, and places the animals at an increased risk for adverse health effects (Curtis, 1983; DeShazer, 2009). Hence, throughout the operation of TEMADS, continuous monitoring and performance analysis are required to ensure that an optimum thermal environment and air quality is provided for the animal, as well as sufficiently accomplish the objectives of the operator.

Modern commercial Thermal Environment Modification System (TEMS; or more commonly known as "ventilation") controllers have extensive Data Acquisition (DAQ) and control capabilities that allow data from numerous systems, devices, sensors, etc. to be continuously monitored and recorded at user selectable frequencies during operation of the facility. For example, TEMS controllers feature analog inputs (e.g., sensors) and outputs (IOs; e.g., variable speed devices), digital IOs (e.g., relay actuation or position), frequency inputs, pulse inputs, etc. The increase in technological and DAQ capabilities has led to an increase in the amount of available data for livestock and poultry facilities. In addition, this also provides a new and unique opportunity to explore TEMS, associated controller performance, and thermal comfort spatiotemporal uniformity. Analysis of these data could help identify poorly performing system components and promote more informed management decisions.

A novel swine breeding and gestation facility was monitored over an 8-month period (November 2015 – June 2016) using the installed TEMS controller and a custom developed Thermal Environment Sensor Array (TESA) network. The commercial TEMS controller data will provide initial methods to monitor facility performance according the operator's needs. Further, this study deployed the TESA network and accompanying DAQ to collect preliminary data on the sensor network performance, as well as, analyze the spatiotemporal uniformity among three pens inside the facility. The data obtained from the TEMS controller and novel TESA network can be used to enhance the design and control of TEMADS, such that existing systems can be adjusted to enhance and maintain the optimal Thermal Environment (TE) for improved animal production efficiency and thermal comfort. Hence, the objectives of this research were: (1) evaluate the TEMS controller response to seasonal and diurnal fluctuations, and (2) implement and evaluate TESA and accompanying DAQ system performance.

Materials and methods

Facility description

The commercial swine breeding and gestation facility with interior dimensions (L by W by H) 96.9 by 15.9 by 2.4 m was located in central Iowa and housed approximately 800 sows/gilts in 54 pens (figure A.11). The facility featured a filtered, positive pressure ventilation system accomplished by a dormer extended from the side of the building (ground to roof peak), where six variable speed fans pulled fresh air through an open area controllable by a curtain, across an evaporative cooler, through a filter bank, to positively pressurize the attic; hence, continuously forcing filtered air through the ceiling inlets. Air inside the building was allowed to exhaust through shutters with an external curtain that could be adjusted to modify exhaust flow. Two of the aforementioned dormer setups (i.e., evaporative coolers, filter bank, fans, etc.) were positioned at the east and west regions on the north side of building. The interior was zoned into three regions (east, middle, and west) inside the facility for the TEMS controller. One t_{db} sensor was located in

each zone. The TEMS controller adjusted inlet open area to control for t_{db} and fan speed and exhaust curtain height for static pressure control inside the attic (with respect to ambient) and between the attic and the room. The t_{db} set point was 18.9°C for all three zones during the spring and summer monitoring months of the facility. The TEMS controller recorded t_{db}, set point t_{db}, heat run time, percent inlet open, room static pressure, attic static pressure, and variable speed output, at 2 min intervals. Data was obtained from the TEMS controller from May 9th, 2016 to June 16th, 2016.

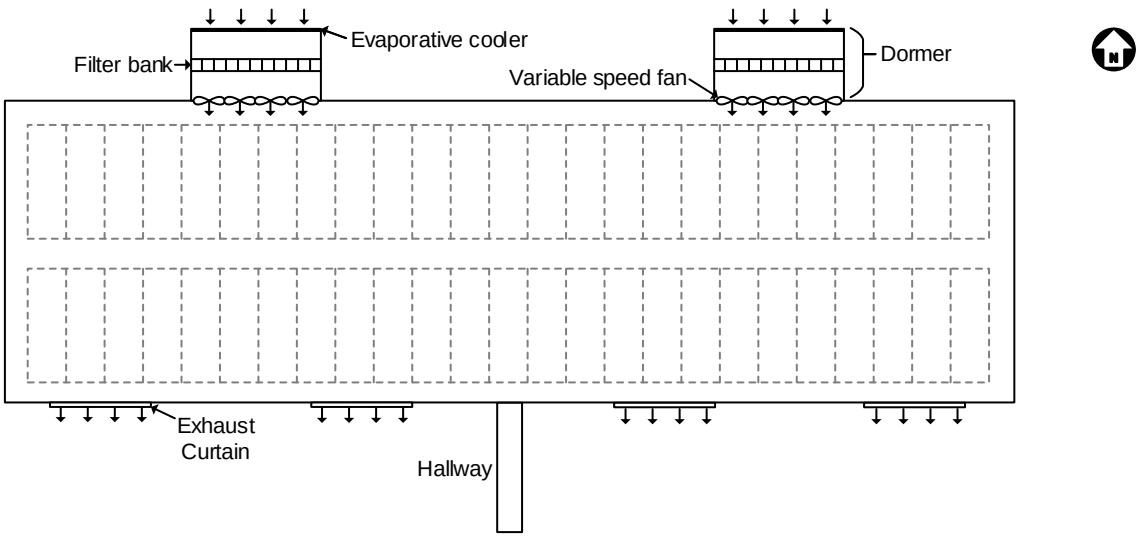

Figure A.11. Schematic of commercial swine breeding and gestation facility with interior dimensions (L by W by H) 96.9 by 15.9 by 2.4 m was located in central Iowa and housed approximately 800 sows/gilts in 54 pens.

Ambient weather data (t_{db}, t_{dp}, wind speed, and wind direction) were obtained in 1 h intervals from the Automated Surface Observing System (ASOS) located approximately 63 km from the facility at Waterloo Regional Airport (ALO).

Thermal environment sensor array

A novel thermal environment sensor array (TESA) network and DAQ system were developed and deployed in the facility to collect preliminary information on the performance and robustness of this novel network of TESAs, as well as monitor the spatiotemporal distribution of the TE (Ramirez, Gao, & Hoff, 2016). An individual TESA (figure A.12) consisted of four sensors to perform four measurements: t_{db}, relative humidity (RH), airspeed, and globe temperature ($t_{g;}$ via a black globe thermometer to calculate mean radiant temperature; t_{mr}). Sensor signals from a TESA were connected via a single, ten-conductor wire to screw terminals mounted on the TESA data acquisition, transmission, and control custom printed circuit board. The serial data communication network featured bidirectional data transfer between a notebook computer and each deployed TESA. More detailed information regarding TESA and its communication network can be found elsewhere (Gao, Ramirez, & Hoff, 2016).

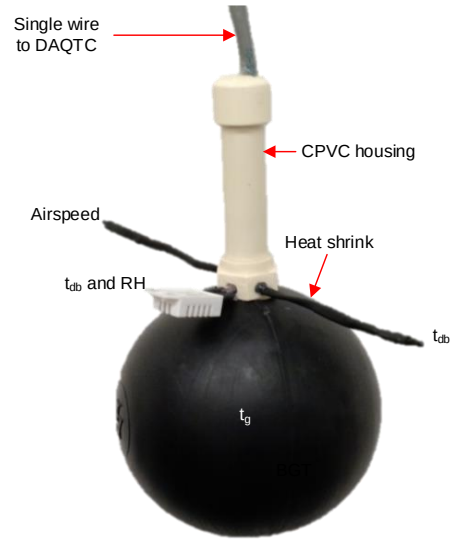

Figure A.12. Image of a Thermal Environment Sensor Array (TESA) featuring dry-bulb temperature (t_{db}), relative humidity (RH), airspeed, and black globe thermometer (BGT) sensors. Globe temperature (t_g) is obtained from a t_{db} sensor at the center of the BGT and used to calculate mean radiant temperature (t_{mr}).

Six TESAs were deployed inside the facility (figures A.13 and A.14) as a preliminary evaluation of the system, with two TESAs suspended 1.8 m above the partially slatted floor in a pen with about 15 animals housed within each pen. Sixty analog voltage measurements from aforementioned sensors were collected between 60 to 180 s intervals. Text files with the raw data were saved every hour and collected from the computer inside the facility every two to three weeks. Data from the TESAs was collected over an 8-month period from November 23rd, 2015 to June 24th, 2016.

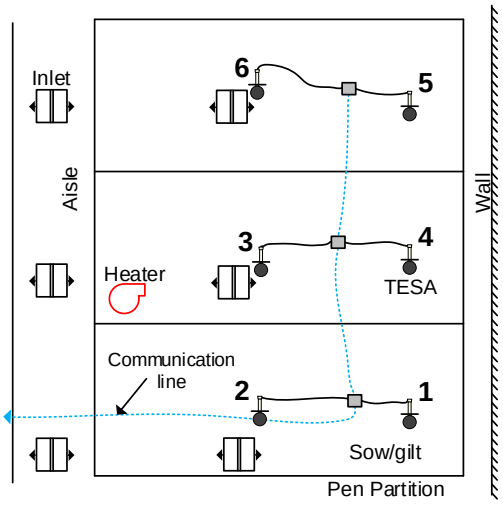

Figure A.13. Schematic of the location of the six TESAs and thermal environment modification and air distribution systems components in three pens.

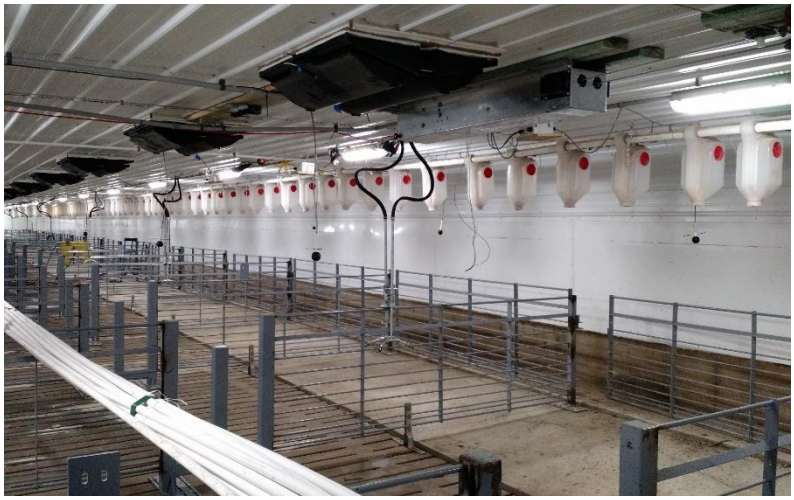

Figure A.14. Six TESAs suspended 1.8 m above the partially slatted floor in three pens with about 15 animals housed within each pen.

Data preparation and quality control

Prior to analysis, the raw voltages were verified to be within the output range of each sensor and at least two thirds of the 60 measurements collected from a TESA were recorded. Data from a sample (i.e., 60 raw measurements) were subjected to Chauvenet's criterion to remove outliers prior to taking the mean and standard deviation. Analog voltages were then transformed to their physical quantity and then verified to be within the physical limitations of the sensor.

Results and discussion

Thermal environment sensor array

Data was not recorded for about two weeks from December 20th, 2015 to January 7th, 2016 due to a hard drive failure on the notebook computer used to collect the TESA data. Three TESAs (#1, #4, and # 6) collected ~227,000 lines of the data from the five measurements, while, two TESAs (#3 and #5) collected ~216,000 lines data, and the remaining TESA (#2) only collected ~166,000 lines of data. The low amount of data collected by TESA #2, was most likely attributed to a poor sensor connection or a sensor failing. Erroneous data was most common for BGT sensor because during the assembly of a TESA, the thermistor is pulled through a rubber stopper. The leads on the t_{db} sensor are fragile and may have been severed or damaged when the BGT was assembled. A preliminary concern of TESA was the robustness of the RH sensor. The long-term suitability of RH sensors in high NH_3 and H_2S environments is questionable and exposure to these gases can lead to decreases in accuracy over time. Due to the high RH measured in the facility, for a 10 d period, eight additional t_{db}/RH sensors (HAXO-8, LogTag, Auckland, New Zealand) were attached to the TESAs for comparison. Within the stated accuracies of both sensors, there was no difference. Further, the accumulation of dust on the top half of the BGT and, also on the t_{db} sensor, required cleaning when the data was downloaded from the notebook computer. Dust was an issue in this facility, where feed was dropped from about 2 m above the floor, with no drop tube or stantion. Dust most likely did not affect the BGT and t_{db} sensor measurements, but possibly altered

the response time of the sensors and may have slightly changed the emissivity of the BGT. The airspeed sensor had less dust than the others. This was most likely due to the thermistor being maintained at 103°C, which burned off some dust over time. Overall, the TESAs performed as expected, suggesting future use in long-term TE monitoring studies are feasible.

Facility performance

Each of the four TE parameters: t_{db} (figure A.15), RH (figure A.16), airspeed (figure A.17), and t_{mr}; collected from the six TESAs over the entire monitoring period are summarized. Overall, t_{db} inside the facility was within ±1°C and ±2°C of the set point 36.3% and 75.3% of the monitoring period, respectively. Some large temperature swings are evident in figure A.15, those were attributed to operator error or an accidental change in settings. A maximum 10.6°C above the set point and 5.2°C below the set point were recorded. At the onset of the study, the RH inside the facility was relatively high until early March. By that point, the operator had been working on the issue and applying different management strategies to reduce the RH. This is shown by the declined RH and maintenance of RH at a lower level. Once the evaporative cooler was activated around mid-May, the RH in the facility increases. As expected, t_{mr} reflected t_{db} trends, but with a dampened response. Airspeeds in the facility during the winter months were low, as expected, and began to increase as the inlet gradually became more open as a higher ventilation rate was needed to maintain the set point. The omnidirectional thermal anemometer properly followed the trend of inlet percent open (figure A.18).

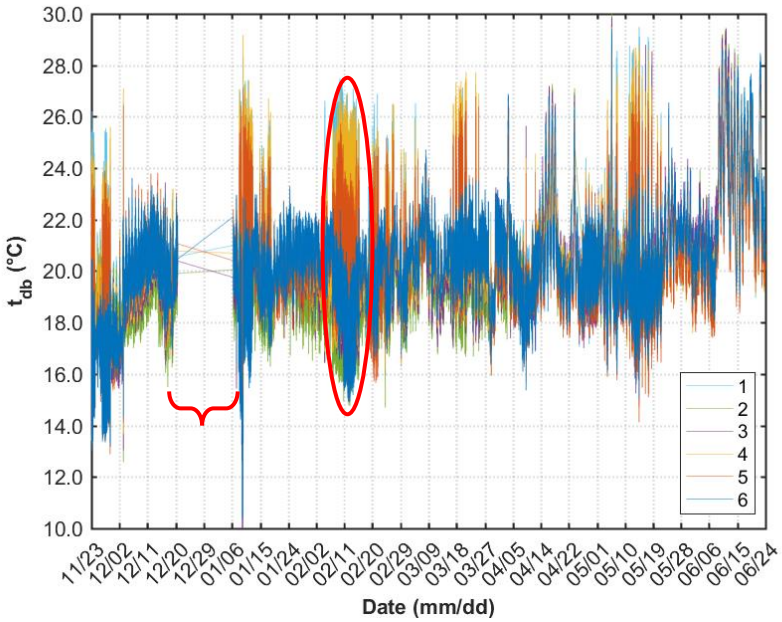

Figure A.15. Summary of t_{db} over the entire monitoring period. The bracket denotes a hard drive failure on the computer and data was not recorded during this time. The circle denotes a mechanical system failure, where the inlets were opened during winter causing a decrease in indoor t_{db}.

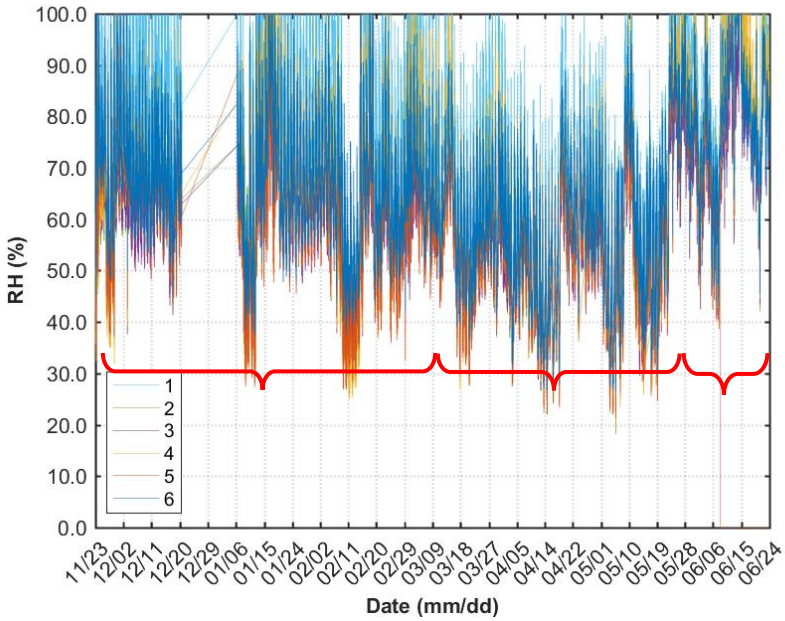

Figure A.16. Summary of RH over the entire monitoring period. The leftmost bracket (1) denotes the high RH observed in the facility, while the middle bracket (2) shows modifications by the operators to reduce the RH. The rightmost bracket (3) denotes when the evaporative cooler was activated during the late spring/summer months.

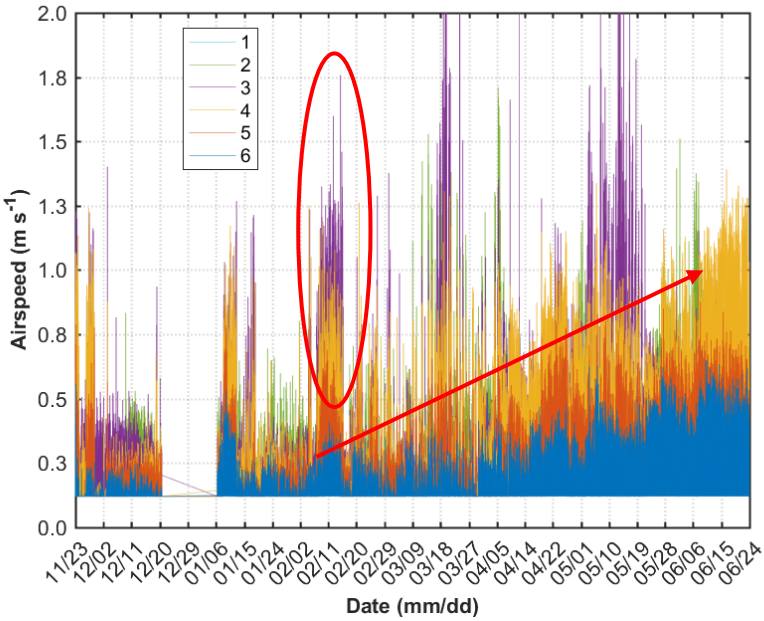

Figure A.17. Summary of airspeed over the entire monitoring period. The circle denotes the corresponding increase in airspeed when an operator error caused the inlets to open substantially during the winter. The arrow shows the increase trend of airspeed as the inlets became proportionally more open and ambient temperature increased.

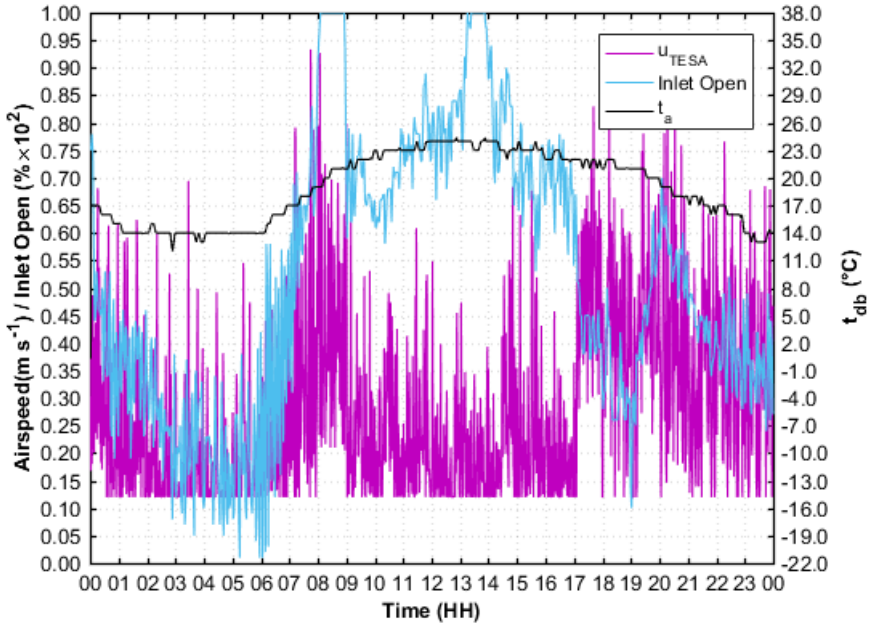

Figure A.18. Example of the relationship between airspeed and inlet open percentage. The airspeed follows the inlet open percentage trend except during the hours from 9 to 17 where the sensor may have been obstructed or an external factor caused fan speed to reduce but inlets to remain open.

Since TESA has the capability to capture all the sensible and latent modes an animal can exchange heat with its surroundings (except conduction); ultimately, the four TE parameters need to be combined into one effective index or representation of the TEMS ability to dissipate heat from the animal. For swine, that does not currently exist. However, to show the potential of monitoring the entire TE, the Temperature-Humidity Index [THI = 0.8 T_{db} + RH/100 (T_{db} – 14.4) + 46.4]; was applied. The THI only combines t_{db} and RH, but does provide some insight to the TEMS ability to maintain a thermally comfortable environment for the animals. Figure A.19 shows the inability for the TEMS to provide any reduction in THI when the ambient RH is high and ambient t_{db} is only mild. In fact, the ambient THI was lower for many hours of the day and using the evaporative cooler slight increased THI. Both inside and ambient THI were below the alert threshold of 75. On a day with much higher ambient t_{db}, the evaporative cooler was not functioning in the morning and was not activated until 15:30 (figure A.20). Once started, the evaporative cooler reduced t_{db} and increased RH, which ultimately lowered the THI inside compared to ambient. However, late into the night, operation of the evaporative cooler was probably no longer needed as the ambient THI had reduced and had become similar to inside THI.

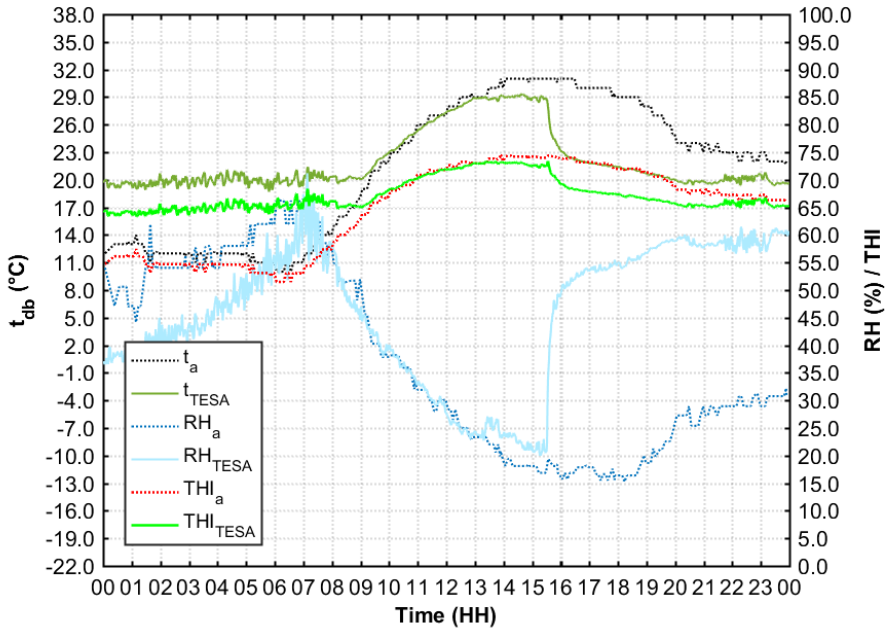

Figure A.19. Minimal reduction in THI was achieved with the evaporative cooler at mild t_{db} and high ambient RH.

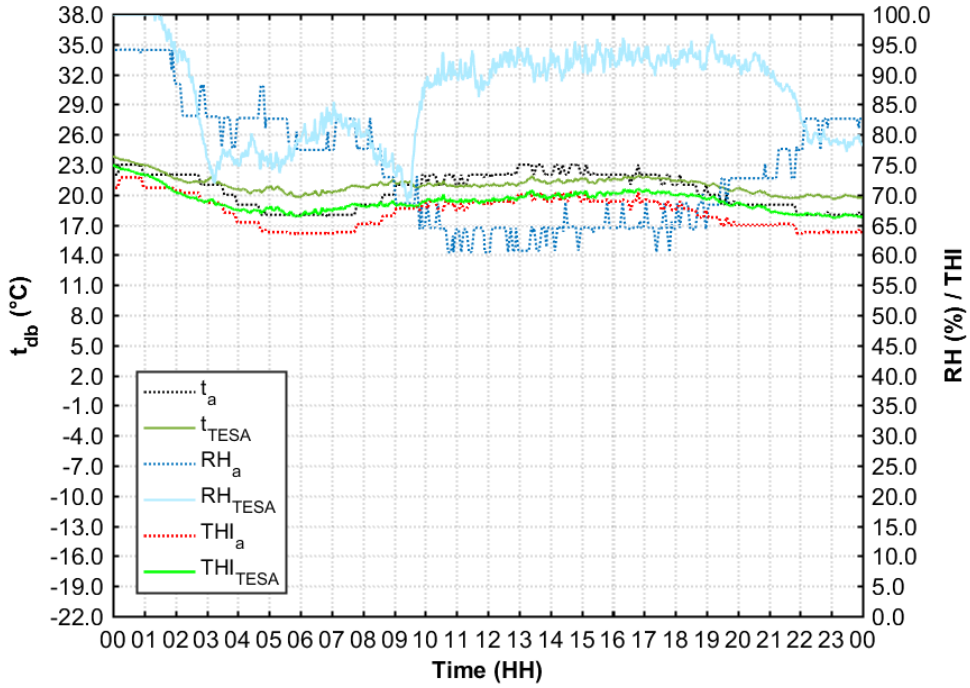

Figure A.20. There was an issue with starting the evaporative cooler in the morning; however, once started, THI was reduced from ambient and returned to the normal conditions.

Conclusions

The development and preliminary implementation of the Thermal Environment Sensor Arrays (TESAs) is the initial phase in developing a collection of functional performance tests to

commission livestock and poultry facilities. These functional performance tests will analyze fan performance, heater distribution, TEMS controller abilities, spatiotemporal TE uniformity, etc. The information obtained from these tests will allow facility operators to make better management practices that ultimately decrease production costs and improve the thermal comfort for the animals. Overall, this new positive pressure filtered facility adequately maintained the set point temperature provided by the operators.

Acknowledgements

This research was supported with funding provided by the Iowa Pork Producers Association (NPB 14-242). The authors would like to thank Ben Smith and all the employees at Iowa Select Farms and acknowledge the contributions of undergraduate student Grant Hoppes during the preparation and completion of this work.

References

Curtis, S. E. (1983). *Environmental Management in Animal Agriculture*. Ames, IA: The Iowa State University Press.

DeShazer, J. A. (2009). *Livestock Energetics and Thermal Environmental Management* (1st ed.). St. Joseph, MI: American Society of Agricultural and Biological Engineers.

Gao, Y., Ramirez, B. C., & Hoff, S. J. (2016). Omnidirectional thermal anemometer for low airspeed and multi-point measurement applications. *Computers and Electronics in Agriculture*.

Ramirez, B. C., Gao, Y., & Hoff, S. J. (2016). Development and Validation of a Spatial and Temporal Thermal Environment Sensor Array and Data Acquisition System. In *2016 ASABE Annual International Meeting*. American Society of Agricultural and Biological Engineers.